The University Of Sheffield.

Novel Methods for Interrogating Cryptic Heterogeneity in Pluripotent Stem Cells

By:

James Edward Mason

Registration Number: 110119283

A thesis submitted in partial fulfilment of the requirements for the degree of Doctor of Philosophy

The University of Sheffield
Faculty of Science
Department of Biomedical Science

29th February 2016

Acknowledgements

I would like to thank Peter for his support, encouragement and mentorship. In particular I would like to thank him for his steadfast belief in me and my data.

I would like to thank Daniel Coca and Veronica Biga for their work regarding mathematical modelling, Wei Huang for his enthusiasm and use of his Raman microscope. I would also like to thank Mark Jones for his general tuition but on flow cytometry in particular, as well as Paul Gokhale and Andrew Flemming for their guidance, lateral thinking and support. I am especially grateful for the collaborative opportunities afforded and the challenges that came with them! I would like to thank all members of the Centre for Stem Cell Biology for providing a thoroughly entertaining and thought provoking time during the course of my PhD. In particular I would like to thank Jim and Dylan for their friendship, advice and creativity.

I would like to acknowledge my friends both inside and out the academic sphere for their good humour and comradery.

I am extremely grateful to Christine, who has been unwavering in her encouragement, help and kindness. You have been a light during the last few years and I would be blind without you.

Finally, I would like to thank my parents for their faith in me. For my Dad who has been a trusty rock and, for my Mum whose compassion and sunny optimism that was so wholesome is now sorely missed.

Contents

Tables and Figures

Abstract

Human embryonic stem cells display several features of heterogeneity in culture. This heterogeneity is poorly understood and may impair differentiation protocol efficiency. There is increasing evidence that stem cell heterogeneity is dynamic and affects lineage fate decisions whilst cells are still pluripotent. The aim of this project was to develop new approaches for understanding the heterogeneity of cells within the pluripotent stem cell compartment that influences stem cell fate decisions. Understanding the rules governing stem cell heterogeneity would open up opportunities to manipulate these features for the improved application of differentiation protocols or within regular cell culture maintenance.

Two novel methods for the interrogation of pluripotent stem cell heterogeneity have been developed in this thesis. The first approach examines pluripotent stem cell dynamics by modelling the population fluctuations of the sensitive pluripotency marker SSEA3 of a pluripotent Embryonal Carcinoma (EC) cell line, NTera2. The model generated explained the heterogeneity dynamics of SSEA3 within NTera2 and in a predictive manner that also revealed candidate substate populations.

The second approach developed was the application of Raman spectroscopy for the non-invasive assessment of heterogeneity within and between stem cell populations according to biochemical signatures. These studies showed that a hyperspectral, grid based, approach proved sensitive for examination of cell biochemistry and furthermore, this approach was used to address biological questions. Raman Spectroscopy proved sensitive enough to notice differences between cell lines, between differentiated and undifferentiated cells, between intracellular compartments, and could discriminate between different pluripotent cells associated with differing lineage biases.

This work therefore represents a development in both our understanding of pluripotent stem cell dynamics and the potential for using both modelling and Raman spectroscopy to analyse this phenomenon.

Chapter 1

Introduction

1.1 Introduction

Multicellular animals demonstrate remarkable cellular specialisation, upon which their survival is dependent. However, despite the diverse array of cell types present within the body, in each case they are all the direct progeny of one cell: the zygote. All the cellular diversification in phenotype resulting in the complex organismal systems, organs and tissues of that animal are traced back to that initial, singular, cell. The feat of animal development is remarkably intricate and yet for all its complexities, it is completed with astonishing precision and accuracy. Necessarily then, the zygote represents the cell within the organism that is most plastic in terms of the range of potential cell types its progeny could become and is often therefore referred to as totipotent.

Later in development, cells of the inner cell mass of the blastocyst are restricted to progeny that can contribute to all the cells of the adult organism but not extra embryonic tissue and are thus termed pluripotent. Pluripotent cells represent a great resource for the field of regenerative medicine, where it is, in principle, possible to direct these cells *in vitro* into the formation of any cell type required for therapeutic application, including even organ formation. The understanding of how to derive cells of interest from these pluripotent cells via differentiation assays has grown immensely yet remains grossly incomplete and the processes by which pluripotent cells make cell fate decisions are not well delineated. Given the range of cell fates that a pluripotent cell may adopt, it is perhaps not surprising that not all cells in a pluripotent cell culture behave uniformly. Cryptic heterogeneity in decision making of pluripotent cells represents a problem to differentiation protocols in that the starting population of cells are liable to respond with different efficacies to the applied stimulus. Methods by which this heterogeneity can be studied and interrogated are lacking. This thesis presents two novel approaches for exploring cryptic pluripotent stem cell heterogeneity. It is anticipated that if this

heterogeneity is understood, it may be manipulated in order to improve the efficiencies of directed differentiation protocols of pluripotent stem cells.

Following a brief history of research in the pluripotent stem cell field, an introduction to current examination of stem cell identity and heterogeneity is provided. Two novel approaches to understand underlying stem cell heterogeneity are introduced via: a mathematical modelling application to the study of stem cell population dynamics is and an introduction to Raman spectroscopy.

History of Stem Cell Research

1.2 Pluripotency

The zygote would be the first specific cell ever to be termed a stem cell as coined by eminent German biologist (Haeckel, 1868). Although he originally applied the term "Stammzelle" (German for stem cell) to describe what he believed to be the first common unicellular ancestor of all multicellular organisms, Haeckel was also the first to propose applying the term to the fertilised egg (Haeckel, 1877). This term was indeed applied to early investigations into embryology, including investigations into Weissman's germ-plasm hypothesis (Weissman, 1885) where it was proposed that there were, for all intents and purposes, two types of tissue - germ cells and somatic. Under this paradigm, it was suggested that germ cells, which contained the germ-plasm that is transmitted from one generation to the next, give rise to the other cells of the body (somatic cells) and other germ cells. Somatic cells, on the other hand, are incapable of generating germ cells and therefore impotent at transferring germ-plasm from one generation to the next. In the absence of modern understanding of genetics, this idea captured the imaginations of several embryologists of the time, such as Boveri and Häcker, who sought to

isolate the earliest germ cells in developing embryos (Boveri, 1892; Häcker, 1892; Ramalho-Santos and Willenbring, 2007). From both of their studies, the term stammzelle was consequently heavily associated with what we recognise today as the germline lineage, primordial germ cells and germline stem cells. In fact, it was not until Wilson reviewed their works in English four years later that the word stem cell was popularised in the English lexicon, and he is consequently sometimes misattributed as having coined the term (Maienschein, 2003; Shostak, 2006; Wilson, 1896).

Concurrently, at around the turn of the 20th century, biologists working on the development and regeneration of the hematopoietic system postulated that there was a common precursor cell to the various cell types found in blood (reviewed by (Ramalho-Santos and Willenbring, 2007)). This common precursor of the blood cell types was also designated the title of stem cell; and this designation was popularised by Maximow (Maximow, 1908) Neumann (Neumann, 1912) and others. However, the first time the word stem cell was used in reference to the hematopoietic system was by Pappenheim in 1896 to describe the precursor cell to red and white blood cells (Pappenheim, 1896). Although it was not until much later that a common precursor cell to the entire hematopoietic system was definitively identified (Becker et al., 1963; Till and Mc, 1961; Till and McCulloch, 1964). During this time, an important clarification to stem cell identity emerged, and one integral to stem cells' relevance to regenerative medicine; a stem cell also required the capacity of self-renewal in addition to potency.

As a result of two independent fields of research we now have our modern definition of a stem cell, that is, a cell that simultaneously possesses the properties of potency and self-renewal. Under this definition, stem cells have been identified in a variety of tissues throughout the human organism such as the central nervous system, skin, intestines and so on. Although these

cells all exhibit some degree of potency, not all stem cells are equally potent with stem cells identified in the adult being generally restricted to give rise to progeny within their relevant tissue (Reviewed by (Robey, 2000)). This is not terribly surprising since as a general rule, during the process of development as the organisms grows, cells divide and gradually become more specialised; progressively losing potency as a result. Consequently, stem cells acquired from the adult have a limited capacity for regenerative medicine, whereas the pluripotent stem cells of the early embryo, still capable of producing all the cells of the adult organism do not suffer such a restriction. It is this potential that embryonic stem cells capture the imagination of researchers in the application of regenerative medicine.

1.3 Embryonal Carcinomas

Curiously enough, the origins of embryonic stem cell research begin not with the embryo but can arguably be traced back to earlier studies on teratocarcinoma in the 1950s. Teratocarcinomas are generally highly malignant tumours that tend to occur in the testis (Dixon and Moore, 1952; Mostofi and Price, 1973) . These occur rarely in the human population, although their occurrence peaks in young post-pubescent males and there has been a dramatic rise in their incidence over the last 60 years (Andrews, 2002; Moller, 1993). The peculiar property of teratocarcinomas, compared to other carcinomas and which also brought them into prominence in pluripotent cell research, was their heterogeneous histology. Teratocarcinomas have been documented to contain all manner of cells, tissues and even partially formed organs derived from all three germ layers and all completely ectopic to the testes such as; teeth, pieces of bone, nerve, muscles, skin and hair. Some tumours even contained tissue arrangements and identities that closely resembles that of the early developing embryo. This feature is in fact the root of teratocarcinoma's etymology with "teratos" being the Greek for "monster." Yet in addition to these differentiated cell types, these tumours also contained undifferentiated cell

types which were the key malignant and pluripotent stem cell of the tumour and termed embryonic carcinoma (EC) cells.

Teratocarcinoma's bizarre appearance and relative rarity meant that study of the condition was restricted to occasional spontaneous human gonadal tumours. The scarcity of sample material was compounded by the fact that teratocarcinoma is also extremely rare in mice and rats, the most common laboratory animals, and so was difficult to study experimentally. This all changed however when a particular strain of mouse, Strain 129, was reported to spontaneously develop testicular teratomas and teratocarcinomas within the seminiferous tubules of the developing gonad (Stevens and Little, 1954). Furthermore, a method by which these tumours could be induced by explanting the genital ridges of Strain 129 foetuses between 11 and 13.5 days of development indicating primordial germ cells as the source of the tumour (Stevens, 1964, 1967, 1970; Stevens and Hummel, 1957). Primordial germ cells migrate into the genital ridge at 11 days, but there is an implied change in primordial germ cell behaviour by 13.5days that precludes tumour formation, presumably attributed to these cells entering mitotic arrest (Bendel-Stenzel et al., 1998) In addition, single cells derived from a teratocarcinoma and injected intraperitoneally in mouse were shown to be capable of producing all cells within a teratocarcinoma (Kleinsmith and Pierce, 1964). This finding demonstrated that teratocarcinomas possess a unique type of cell, that has the capacity to grow indefinitely (ensuring malignancy) and whose progeny have great potency, able to differentiate into multiple adult cell types. Further experimentation on teratocarcinomas and early embryos determined great similarity in their differentiation potential by grafting early embryos onto extra-uterine sites that generated re-transplantable teratocarcinomas; suggesting that the pluripotency of cells from the early embryo and from teratocarcinomas were similar if not identical (Brinster, 1974).

Meanwhile, experiments on human teratocarcinoma were limited but there were attempts to study them via xenotransplantation into hamster cheek pouch (Pierce and Verney, 1961). The next major chapter in pluripotent cell study began with the successful *in vitro* culture of mouse embryonic carcinoma cell lines. Originally, the potency of these tumours made culturing the undifferentiated EC cells difficult and cultures typically proliferated poorly, exhibiting haphazard and unpredictable differentiation (Evans, 1972; Jakob et al., 1973; Kahan and Ephrussi, 1970; Nicolas et al., 1975; Pierce and Verney, 1961; Rosenthal et al., 1970). Eventually, culturing techniques were refined sufficiently to permit indefinite culture of mouse EC cells from teratocarcinomas that were demonstrably pluripotent as determined by teratocarcinoma formation following subcutaneous injection of these cells (Martin, 1975; Martin and Evans, 1974, 1975). Furthermore, the culture of these mouse EC on non-adherent plates resulted in the formation of cell clumps, eponymously called embryoid bodies due to their morphological similarity to the early mouse embryo (Martin, 1975; Martin and Evans, 1974, 1975).

The *in vitro* derivation of human EC cell lines followed suit with their murine counterparts; explanting teratocarcinoma tissue samples in order to permit the culture of the malignant, pluripotent, EC stem cell of the tumour. The earliest derived human cell lines established in vitro were TERA1, TERA2 and SuSa (Fogh J, 1975; Hogan et al., 1977) although these appeared to have compromised differentiation potential and it was not until about a decade later that human EC lines capable of differentiation were obtained, which remarkably included subclones from the TERA2 cell line (Andrews et al., 1984b). The cell line NTera2.D1, subcloned from a xenograft tumour of the cell line TERA2, demonstrably had the capacity to differentiate *in vitro* into several cell types, including neurons, when exposed to retinoic acid (Andrews, 1984; Andrews et al., 1984b).

1.4 Embryonic Stem Cells

Given the pluripotent properties of EC cells, and that it is possible to indirectly acquire EC cells from embryos grafted to extra-uterine sites that go on to form teratocarcinomas, the next question was whether similar cells could be derived from the embryo that had not already undergone malignant transformation. Although many attempts to culture cells from early mammalian embryos were performed prior to 1950 for the purposes of mammalian sample tissue generation none of the cultured cell lines fulfilled the modern criteria by which an embryonic stem (ES) cell is defined (Cole, 1965; Edwards, 2004). An embryonic stem cell should be capable of giving rise to all tissues in the adult organism (*i.e.* pluripotent) and this criterion may be assessed by differentiation *in vitro* and by differentiation *in vivo* within tumours caused by ES cell injection or by participation in chimeric organisms. The most stringent definition maintains that a chimeric organism, where ES cells injected into the inner cell mass of the early embryo contribute to the tissues of the adult, should develop normally and that these ES cells contribute to germ cells in the chimaera that are then able to facilitate the development of a normal, fertile adult in the next generation.

The derivation of a cell line capable of fulfilling these criteria was first performed in mouse. Since then, several attempts of deriving ES cells from other animals (including human) have been performed (reviewed in (Gardner, 2004)) and so far ES cells derived from rat are the only other capable to successfully form a germline chimaera (Buehr et al., 2008; Li et al., 2008) . It goes without saying that such experiments are not permissible in humans and so only the differentiation potential criterion is applied to human ES cells. In fact, derivation of mouse ES lines occurred independently, both employing methods to acquire cells from the inner cell mass of the embryo by explanting blastocysts on a feeder layer of mitotically inactivated mouse fibroblasts (Evans and Kaufman, 1981; Martin, 1981). The implementation of this feeder layer

was a necessary innovation for making ES line derivation permissible. Despite this success, mouse ES cell lines are prone to spontaneous differentiation in culture unless supplemented with leukaemia inhibitory factor (LIF); a discovery that was made later (Smith et al., 1988; Williams et al., 1988) but LIF now remains a standard ingredient in mouse ES cell culture.

Derivation of human ES cell lines took well over another decade to perform, despite the fact that the isolation techniques required were comparable. There are numerous reasons as to why there was such a lag behind mouse experiments, not least of which include the dissuasive legal and political dilemmas, coupled with the difficulties available with obtaining human embryonic material. The co-incidence of several factors enabled the early successful derivation of human ES cell lines including the successful technology of *in-vitro* fertilisation (IVF) which meant established IVF clinics could provide a reliable source of high-quality embryos whilst simultaneously acquiring permission from donors to utilise embryos that were superfluous to requirement for the treatment for research purposes. Furthermore, researchers had experience working with the derivation of other primate ES cell lines (Thomson et al., 1995) and private companies were willing to fund the research; circumventing the government funding in countries where public funds were prohibited for use in stem cell research, such as the USA. Once the first human ES cell lines were derived (Thomson et al., 1998) their perceived medical value quickly superseded the hesitance attributed to human ES cell research in the minds of scientists and the general public resulting with remarkable progress in human ES cell research.

Given that the assessment of pluripotency via chimaera assay is not permissible in humans, this remains unexplored. However, human ES cells display the property of pluripotency both in the contexts of both *in vitro* differentiation and *in vivo* teratocarcinoma formation when injected into immunocompromised mice; forming distinct and diverse tissues of the adult. The

teratocarcinoma assay still remains the most definitive test of human ES cell pluripotency, however improvements in *in vitro* differentiation-potential assays are providing evidence for pluripotency that is becoming more readily accepted than previously.

The derivation of human ES cells with their associated potential in regenerative medicine reignited the interest in mouse ES cells in terms of how to culture them and control of their differentiation *in vitro*. It was even considered that differentiation protocols developed in the mouse could be applied to the human. Today, derivation of mouse ES cells now no longer requires the feeder layer of mitotically inactivated fibroblasts, but can be successfully performed in the presence of LIF and bone morphogenetic proteins (Ying et al., 2003). Furthermore, in part by applying information learnt from mouse EC cell differentiation, knowledge of the differentiation of mouse ES cells down predetermined pathways by the complementary application of various chemicals, growth factors and matrices is becoming increasingly comprehensive (for example, (Kim et al., 2002; Li et al., 2003; Smith, 2001; Wichterle et al., 2002). Understanding of molecular mechanisms underlying pluripotency and differentiation has also dramatically increased in the mouse context; with *Pou5f1*, *Nanog*, *Sox2*, *Esrrb*, *Klf2*, *Klf4*, and *Tbx3* being recognised as being key pluripotency factors.

Despite the advances made in the understanding and manipulation of mouse ES cells, human ES cells do not behave in the same way as mouse and so a direct transfer of the techniques crafted in the mouse ES cell context are not applicable. One of the first and most noticeable differences is the respect to LIF in culture. When exposed to LIF, mouse ES cells tend to become more homogeneous with much reduced spontaneous differentiation mediated by activation of signal transducer and activator of transcription (STAT3) via LIF receptor (Smith et al., 1988; Williams et al., 1988). Despite the conserved STAT3 signalling pathway, and functional LIF mediated

activation of STAT3, human ES cells do not remain in an undifferentiated state in the presence of LIF (Daheron et al., 2004). Indeed, even now, despite the plethora of work gone into the development of defined culture conditions and growth matrices, there is great debate over what conditions are the best for the maintenance of human ES cells in an undifferentiated state resulting in different laboratories using their own preferred techniques.

One of the core similarities between mouse ES cells and human ES cells are those of the shared pluripotency transcription factors. In particular, the forced expression of the transcription factors *Pou5f1* (also commonly referred to as OCT4), *Klf4*, *c-MYC* and *Sox2* is capable of inducing both mouse and human terminally differentiated fibroblasts to adopt a pluripotent state resembling their respective ES cell counterpart (Takahashi and Yamanaka, 2006; Takehara et al., 2008). This breakthrough discovery, earning the Nobel Prize in Physiology and Medicine in 2012, has created a new type of pluripotent stem cell termed induced pluripotent stem (IPS) cells that can be generated from somatic cells (Nobel foundation; (Yamanaka, 2007)). The potential medical applications using patient-specific IPS cell technology are manifold and elaborated upon elsewhere (Yamanaka, 2007). Despite the febrile reception of IPS cells, it is important to recall that there are marked, albeit subtle, differences between IPS cells and their ES cell counterparts. Most notably, IPS cells often do not exhibit the same epigenetic markers as ES cells and tend to resemble, in varying degrees, the epigenetic markers of the adult somatic cell from which it was induced (Chin et al., 2009; Deng et al., 2009; Doi et al., 2009; Hawkins et al., 2010). Furthermore, with methods for generating IPS cells becoming more efficient and more accessible, there is a growing library of cell lines termed IPS cells that have not necessarily had their pluripotency tested with the same rigour expected of human or mouse ES cells.

1.5 Antigen markers for pluripotent cells:

Keeping track of the behaviours of pluripotent stem cells remains a challenge, for instance the ability to characterise whether any one particular cell in population is differentiated, differentiating or still pluripotent is crucial to understanding fate decisions a cell may make in this regard. It is clear that suitable markers are required for this purpose. Crude measures such as cell morphology are subjective and not guaranteed to be accurate in all cases. With the now developed field of immunohistochemistry, it is now possible to identify, isolate and produce antibodies to antigens specific to different cells types of interest.

The association of antigens unique to particular cell types is a phenomenon readily exploited by biologists in numerous contexts; and the field of stem cell biology is no exception. antibodies that recognise these antigens are often utilised in order to help identify cells of interest within a mixed population. Originally employed by developmental biologists, "differentiation antigens" are useful tools for examining developmental progression and multifaceted cellular systems. Examination of the development and function of the lymphoid system using antibodies to discover how different subsets of lymphocyte cells functioned and related to one another marked one particular success of these tools' application (Boyse and Old, 1978).

As early as 1969, Boyse and Old suggested that some such differentiation antigens could be recognised with regard stem cell differentiation and morphogenesis. Indeed, when the idea that teratocarcinomas provided models for early embryonic differentiation gained prominence in the 1970s, these immunological principles were applied to this new paradigm. By immunising the syngeneic mouse line 'strain 129' with the murine embryonic carcinoma line F9, polyclonal antisera were produced that defined the "F9 antigen" which became one of the most well-

known marker at that time (Artzt et al., 1973; Fenderson and Andrews, 1992). Although these sera recognised antigen(s), the F9 antigen, shared by EC cells, late morulae and inner cell mass cell types, they proved difficult to analyse due to their polyclonal nature. The development of well-defined monoclonal antibodies later in the 1970s soon replaced the use of polyclonal antisera (Kohler and Milstein, 1975)

Stage Specific Embryonic Antigen 1 (SSEA1) was one of the first embryonic antigens defined by monoclonal antibodies. SSEA1 shared similar expression patterns to the F9 antigen during development being present during late cleavage stage embryos, on ICM cells, primitive ectoderm, visceral endoderm and primordial germ cells (Fox et al., 1981; Solter and Knowles, 1978). In culture SSEA1 expression is present on mouse EC cells and absent following differentiation to parietal endoderm (Solter and Damjanov, 1979). A peculiar feature of SSEA1 and many other early embryonic antigens identified subsequently is that they possess carbohydrate structures; for example, the SSEA1 epitope is an oligosaccharide associated with lactoseries type 2 chains linked to glycosphingolipids (Gooi et al., 1981) though the epitope is also associated with high molecular weight glycoproteins (Andrews et al., 1981; Childs et al., 1983).

In contrast to mouse, studies on human EC cell lines reveal that typically SSEA1 is not expressed until the cells are induced to differentiate. Instead, in the undifferentiated state, two other globo-series glycosphingolipid antigens are expressed; SSEA3 and SSEA4 (Kannagi et al., 1983b; Shevinsky et al., 1982). Two other prominent carbohydrate antigens that have been identified on human EC cells are TRA-1-60 and TRA-1-81 (Andrews et al., 1984a). These antigens, and SSEA3 in particular, are rapidly downregulated in response to differentiation; not only in human EC cells, but also in human embryonic stem cells (Draper et al., 2002; Fenderson et al., 1987),

which in turn has led to the proposition that SSEA3 represents a sensitive marker of the human pluripotent state (Enver et al., 2005b). During human development, SSEA3 and SSEA4, but not SSEA1, are detected in the inner cell mass (ICM) with SSEA1 expression seen in the morula (Fenderson and Andrews, 1992).

Glycolipids are common cell membrane components associated primarily with the outer leaflet of the plasma membrane, all of which consist of an oligosaccharide chain linked via glucose to Ceramide. The production of glycolipids, including SSEA3 and SSEA4, occurs within the Golgi apparatus of the cell and is based upon the sequential additions of nucleotide activated sugar moieties to a ceramide backbone that are performed by several glycosyltransferases (Chen et al., 1989). Each glycosyltransferase catalyses the addition of a monosaccharide to an acceptor with precise specificity, although there are examples of glycosyltransferases that enable the transfer of multiple donors (Blixt et al., 1999; Zhou et al., 2000). There are over one hundred known glycolipid structures and this diversity is a result of the cell's use of multiple monosaccharaides (glucose, N-acetylglucosamine, galactose, N-acetyl-galactosamine, fucose, N-acetylneuraminic acid), α and β linkage arrangements as well as multiple linkage arrangements on each monosaccharide which results in a staggering number of combinatorial possibilities. The formation of globoseries glycosphingolipid antigens (such as SSEA3 and SSEA4) is dependent on the formation of lactosylceramide upon which a nucleated galactose monosaccharide is added by α1→4 galactosyltransferase (Figure 1.1). From this backbone, SSEA3 is produced by the addition of N-acetylgalactosamine followed then by galactose. The SSEA4 antigen is built upon the SSEA3 antigen by the terminal addition of N-acetylneuraminic acid by sialyl transferase (Chen et al., 1989). The precise mechanism; including the production of the relevant glycosyltransferases and the maintenance of the nucleotide activated monosaccharide pools required to generate the SSEA3 and SSEA4 moieties are not yet entirely

delineated but it remains clear that its generation is not based on a simple gene expression profile.

Despite the close association of SSEA3 and SSEA4 to pluripotency in human ES cells, it has also been demonstrated that these antigens are not necessary for pluripotency (Brimble et al., 2007). This has been demonstrated both within normal hESCs by deliberate inhibition of SSEA3 biosynthesis (Brimble et al., 2007) and within cultures of hESCs that have become adapted via selective advantage to cell culture; where the loss of SSEA3 has not necessitated differentiation (Enver et al., 2005a). The expression of SSEA3 is not limited to that of early embryonic stem cells and is also present on red blood cells, where they are part of the P blood group system (Andrews, 2011). However, a small proportion of the human population are incapable of synthesising globo-series antigens, and as a consequence have red blood cells that are SSEA3 negative, suggesting that SSEA3 expression is unnecessary for human development (Race and Sanger, 1975; Tippett et al., 1986). Indeed, individuals with the pp and p^k phenotypes are incapable of synthesising either SSEA3 or SSEA4 but appear healthy despite their lack of these strongly developmentally regulated antigens (Figure 1.1) (Tippet et al., 1986). That said, pp and p^k phenotype women have high rates of spontaneous abortion, indicating that SSEA3 and SSEA4 may be involved in immune recognition (Andrews, 2011; Tippett et al., 1986)

One feature of SSEA3 an SSEA4 expression is that the SSEA3 antibody (MC631) recognises and reacts to both glycolipids since the epitope recognised by MC631 is present in both glyoclipids (Figure 1.1) (Kannagi et al., 1983a). The SSEA4 antibody (MC813-70) recognises the terminal three sugars of the SSEA4 antigen and thus does not react with the SSEA3 antigen. During the process of differentiation, human pluripotent ES and EC cells lose the expression of both SSEA3 and SSEA4. However, paradoxically, SSEA3 expression is lost more rapidly (Fenderson et al.,

1987). Despite the fact SSEA4 expression remains detectable and high by use of the SSEA4 antibody (MC813-70), the binding of the SSEA3 antibody (MC631) remains unaccountably low despite the expected cross-reactivity to the internal trisaccharide epitope of the SSEA4 reactive glycolipid (Draper et al., 2002; Fenderson et al., 1987). This is a counter-intuitive observation since the presence of the SSEA4 antigen should permit the binding of the SSEA3 antibody. A possible explanation is that the detection of these antigens is dependent upon the manner in which they are displayed on the cell surface in addition to whether they are merely synthesised (Wright and Andrews, 2009). The mechanism governing the presentation of these antigens remains unknown and has led to the postulation that the expression of SSEA3 may integrate different information about a cell's state rather than the expression pattern of any particular gene (Wright and Andrews, 2009).

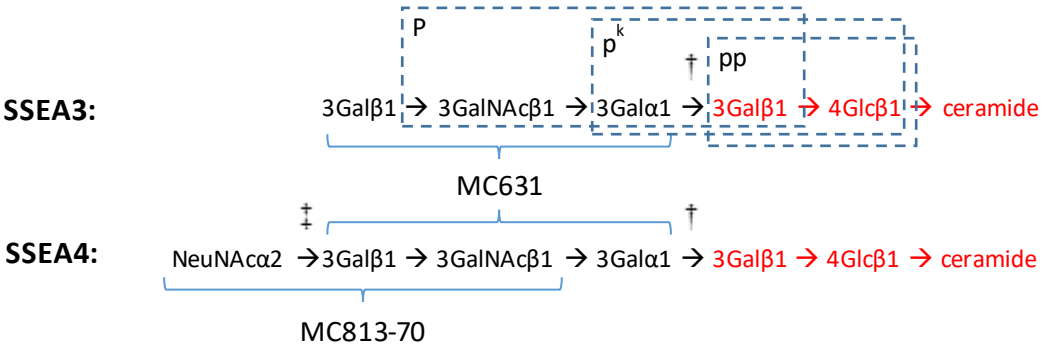

Figure 1.1 – The Carbohydrate Structures of SSEA3 and SSEA4. The globoseries structure requires the production of lactosylceramide (red), to which further sugar moieties are sequentially added. The first nucleated sugar added to lactosylceramide is Galactose and this reaction is mediated by α1→4 galactosyltransferase (†). The addition of further sugars is dependent on the action of further specific glycosyltransferases. The SSEA3 and SSEA4 moiety differ by the final addition of N-acetylneuraminic acid by sialyl-transferase (‡) to the SSEA3 moiety. These antigens are also found on red blood cells as part of the P blood group system; the P P^k and pp antigens are marked (blue dashed boxes). The epitopes recognised by the antibodies MC631 and MC813-70 are also marked.

The production of SSEA3 is not directly regulated by any one particular gene but, like with all glycosphingolipids, its manufacture is contingent on multiple factors including sufficient metabolite pools, synthesis of the relevant glycosyltransferases and the presentation of the antigen on the cell surface. As a result, SSEA3 expression is manifest by circumstantial intracellular dynamics that integrate to yield its production. The presence of SSEA3 therefore is reflective of a particular state of that cell's metabolism rather than a direct determinant of gene expression.

1.6 Pluripotent cell heterogeneity

A pluripotent cell has fundamentally three choices; the capacity to differentiate into any of the three germ layers, continue replication whilst remaining pluripotent or die, although it may exist in a state of quiescence prior to fulfilling any of those fates. While antibodies have now been generated for the identification of pluripotent stem cells, no cell surface antigens have been recognised that enable the prospective identification of cell fate choice. For instance, no cell surface antigen has been discovered that recognises pluripotent stem cells that have a bias towards endoderm differentiation. Despite the fact that pluripotent stem cell populations are clonal and that all these sister cells share the properties of self-renewal and pluripotency, it quickly becomes clear when working with these systems that not all cells in a culture behave identically. Perhaps the most obvious examples of this disparity in behaviour are the poor efficiencies of directed differentiation experiments and the phenomenon of spontaneous differentiation in culture. These alone demonstrate that not all cells within a culture behave uniformly.

There are two main, non-mutually exclusive, sources of variation that could explain such a difference. The first is that slight differences in microenvironment are responsible which ultimately manifest themselves by altering cell behaviour. For instance, cells in different locations even within the same culture vessel happen to be exposed to alternative levels of growth factors, metabolites and neighbouring cell contacts. In this case, even cells that could be considered identical in every other respect, may exhibit varied behaviours.

The second broad possibility is that the cells themselves are not identical, and this too could be the attributed to a number of factors. Examples include position in the cell cycle, transcription

factor production, alternative gene regulatory networks or stochastic alterations to any of the above. These subtle differences could easily alter a cell's propensity to react to differentiation cues, causing spontaneous or non-uniform directed differentiation. A proportion of these differences could be ascribed to cells whose fate is already determined and have committed to differentiation; thus disqualifying themselves from the pluripotent stem cell population. However, it is also conceivable that in fact these cells retain pluripotency but that their propensity to follow any particular differentiation lineage varies over time as well as in response to culture conditions, including feedback signals from cells already differentiating. In this sense, it can be argued that the outcome of a differentiation protocol is not only contingent on that protocol's conditions but also on the underlying phenotype of the starting cells.

The possibility that pluripotent stem cells could simultaneously possess the properties of self-renewal, pluripotency *and* lineage bias appears oxymoronic at first. If daughter cells have an alternative differentiation propensity to the mother, then arguably the property of self-renewal has been violated and the daughters exist in a different state to the mother. Actually, this interpretation is not necessitated. Whilst it may be true that at any given time a cell may be more likely to differentiate down one path than another, if this bias naturally fluxed and were different in a future state, then it does not exist in any one incontrovertible state. Here, that cell would be described as present within the hypothetical "stem cell compartment" (possessing the capacities of pluripotency and self-renewal) like the mother cell, but occupying a different "sub-state" within that stem cell compartment (described in Figure 1.2). Cells occupying different substates may at that point in time have differing lineage biases; being more or less probable of differentiating into Ectoderm for example. A key distinction to be drawn here is that sub-states require the property of interconversion; for if a cell entered a state where it's differentiation potential were unalterable, then it would represent a state different to that of the parental

population and at least the property of self-renewal will have been contravened. The disparity in behaviour between cells in pluripotent stem cell culture may therefore have two, non-mutually exclusive, explanations. The first is that the cause for differing behaviour between cells is that there are de facto multiple, distinct, cell populations that happen to cohabit the same culture. The second is that these cells exist within the same cell population but are occupying different, but interconvertible, substates and that these substates are responsible for the difference in behaviour.

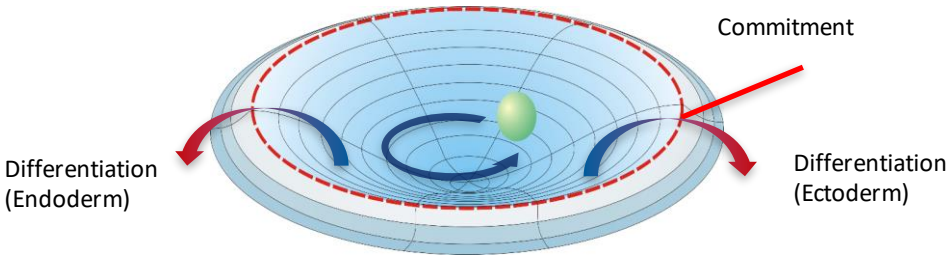

Figure 1.2 - The Stem Cell compartment hypothesis. Stem cells within the stem cell compartment retain the properties of pluripotency and self renewal, however their propensity to differentiate into a particular lineage may be encouraged or hampered depending on where within the hypothetical stem cell compartment the cell occupies at any particular time. In this illustration, the bowl represents the stem cell compartment, and the green ball represents a pluripotent stem cell. Depending upon the ball's position in the bowl alters the likelihood of which side it may leave the bowl. Currently for example, the ball is closer to committed differentiation along the Ectoderm route, however given its dynamics, it may soon occupy a pro-endoderm fate instead. In this way, it is possible for cells to express lineage bias at any particular time, yet retain the same propensity to differentiate down any other lineage pathway if considered over time.

Indeed, within mouse embryonic stem cells, it has been demonstrated that such subtle forms of heterogeneity exist. For instance, mouse ES cell cultures are heterogeneous with respect to Nanog and Stella expression. Nanog positive and negative cells are both interconvertible, however Nanog negative cells also exhibit an increased propensity to differentiate (Chambers et al., 2007). Stella, on the other hand, fluctuates within mouse ES cell cultures in a manner resembling a dynamic equilibrium where on average 20-30% of cells in a culture are positive for Stella expression despite the transitions of individual cells between Stella positive and negative states (Hayashi et al., 2008). The populations of Stella positive and negative cells may interconvert however only Stella negative, but not Stella positive, cells were permissive for trophectoderm differentiation (Hayashi et al., 2008).

In the human context, the early stages of human ES cell differentiation presents cells that co-express lineage specific transcription factors in addition to the pluripotency associated genes (Laslett et al., 2007). Although this may be reflective of functionally distinct substates, any relationship between this co-expression of lineage specific transcription factors with pluripotency genes and functional differentiation bias was not determined in this case (Laslett et al., 2007). Indeed, the idea of lineage promiscuity where progenitor cell types may simultaneously express cell surface markers that are associated with distinct differentiated cell types has existed for some time and was the subject of examination in the hematopoietic system (Greaves et al., 1986).

The paradigm that individual stem cells naturally vary in their gene expression patterns and identity in an interconvertible manner presents a challenge to stem cell biologists. Suddenly, population based transcriptome analyses represent a homogenous mixture of heterogeneous cell transcripts. The representation of distinct transcriptomes is obscured by that of the

amalgam; catapulting the importance of single cell studies to the forefront of stem cell research. Furthermore, a unique complication in the field of stem cell biology is that once a transcriptome has been identified, even peculiar to a particular cell/population, it is impossible to know what biases that cell would have in the context of differentiation lineage since determining the transcriptome necessitated that cell's destruction. This problem is compounded even further by the fact that human ES cells require intercellular cues for survival and maintaining pluripotency; which hinders functional analysis of cells in culture on a single cell basis (Fox et al., 2008).

This has led to the application of non-destructive techniques to examine the relationship between stem cell heterogeneity and cell fate such as cell surface antigen studies to determine potential substates. The cell surface antigen SSEA3 for instance has been studied closely in relation to pluripotency due to its close association to the undifferentiated state (See antigen section). A comparative clonogenic analysis of early passage and late passage, culture adapted ES cells suggested that SSEA3^{-ve} and SSEA3^{-ve} populations represent two different, interconvertible substates, where in the early passage ES cells, SSEA3^{-ve} cells had an increased propensity to differentiate similar to NANOG^{-ve} mouse ES cells. The effect of culture adaptation had selected for ES cell variants that were capable of being simultaneously SSEA3^{-ve} and undifferentiated; since ultimately normal ES cell differentiation eventually removes that cell's progeny from the reproducing population (Enver et al., 2005b). Although undesirable for any medical application, this case demonstrated a hidden value for adapted ES variants as a useful tool for exploring normal ES cell behaviour.

Indeed, study of SSEA3 in relation to pluripotency has also successfully revealed that even while in a pluripotent state, EC cells within the same population exhibit different biases with regard differentiation potential to neuronal or non-neuronal fates (Tonge et al., 2011) Furthermore, it

has been demonstrated that these biases changed over time rather than being the result of a particular EC cell that had an already determined fate (Tonge and Andrews, 2010). In this example, cultures of the EC line NTera2 were used in a differentiation assay utilising retinoic acid (Andrews, 1984) that was designed to examine cell fate decisions. Well documented, the exposure of whole NTera2 cultures to all-trans retinoic acid (10^{-5} M concentration) for 1-2 days is sufficient to irreversibly commit almost all cells to differentiation resulting in 1-5% of the population becoming neurons after around 12-14 days and the remainder of the population constituting a heterogeneous mix of other cell types (Andrews, 1984; Fenderson et al., 1987; Tonge and Andrews, 2010). However, when individual NTera2 cells (modified to constitutively express tdTomato for identification) were plated onto a bed of unlabelled NTera2 cells and immediately subject to the same retinoic acid differentiation protocol, resulting tomato-labelled NTera2 colonies did not all pertain to a single phenotype. The proportion of neurons within the colonies ranged from 0-100%; with colonies containing entirely neurons or no neurons indicating that the eventual phenotype of these differentiated cells was determined very early in response to retinoic acid exposure; denoting alternative lineage biases of the initial seeded cell. On its own, this result could just reflect two different populations with separate biases, of the labelled NTera2 cells that do not interconvert. By repeating this experiment, but waiting 24 hours or 48 hours before exposing the seeded cells to retinoic acid, the proportion of neurons present within the differentiated colonies changed; the longer exposure to retinoic acid was postponed, the closer the proportion of neurons in the colonies was to the result of global cell retinoic acid exposure of 1-5%. By postponing retinoic acid exposure, seeded cells were presented the opportunity to divide and permit the interconversion between pro-neuronal and pro-non-neuronal states. The fact that delayed exposure yielded a reduced proportion of differentiated colonies that were entirely neuronal or non-neuronal as the instant exposure treatment strongly suggests deviance from the lineage bias of the initial cell.

It has been suggested that the pluripotent stem cell represents a 'ground state', or stable attractor, and that maintenance of that ground state involves prevention of cells leaving that attractor (Ying et al., 2008). (Although mouse and human ES cell share a network of transcription factors, they respond to those factors in different ways. For instance, human ES cell pluripotency is not maintained with the introduction of LIF, whereas it is critical for the maintenance of naïve mouse ES cell pluripotency (Niwa et al., 1998). Furthermore, the action of activin/TGFβ and BMP signalling pathways act with opposite effect in the two species; with activin/TGFβ signalling maintaining human ES cell pluripotency whilst BMP signalling induces differentiation and vice versa in the mouse ES cell context. Incidentally, this evidence has been used, amongst others, to build the argument that mouse ES cells and human ES cells as maintained *in vitro* correspond to different stages of embryonic development (Brons et al., 2007; Peerani et al., 2007; Pera et al., 2004; Tesar et al., 2007).

The issue of heterogeneity with respect to pluripotent cell identity has been examined in great detail in the mouse ES cell system. At least three different types of pluripotent stem cell have been defined within the mouse ES cell context, each purported to be counterpart to an *in vivo* pluripotent cell type at different stages of development (Figure 1.3). These cell types are referred to as naïve embryonic stem cells (also known as groundstate), formative pluripotent stem cells and primed stem cells that are deemed to correspond to pluripotent cells of the preimplantation epiblast (E4.5), the formative epiblast (E5.5) and postimplantation epiblast (EpiSC) (E6.5) respectively.

Mouse ES cells were classically derived and maintained in serum-based media on a layer of mitotically inactivated mouse fibroblast "feeder" cells (Evans and Kaufman, 1981; Kalkan and Smith, 2014). Mouse ES cells cultured this way display a degree of morphological and

transcriptional heterogeneity (Tosolini and Jouneau, 2016). Progressively, the use of feeder layers was supplanted by the use of media supplemented with LIF as well as serum (Kalkan and Smith, 2014). Regardless, the individual cells within the population of mouse ES cells derived and maintained in either manner varied significantly in their expression of pluripotency genes (Chambers et al., 2007; Festuccia et al., 2012; Marks et al., 2012; Niwa et al., 2009; Toyooka et al., 2008).

The heterogeneity displayed in culture by these mouse ES cells is ascribed to sub-optimal culture conditions and the development of defined culture conditions for the maintenance of pluripotent stem cells resulted in the generation of the 2i/LIF media system. This culture media makes use of two inhibitors (2i) that block mitogen activated protein kinase and glycogen synthase kinase 3 whilst LIF activates the Stat3 pathway (Blair et al., 2011; Niwa et al., 1998; Wray et al., 2010; Ying et al., 2008). This medium not only maintains the pluripotency of cultured ES cells, but it also acts to reduce the degree of variation in the expression of pluripotency factors and upon inspection cells appear to express pluripotency factors at similar levels to the cells of the early preimplantation epiblast. The combined description of homogeneous cells representative of an extremely early point of development earnt this cell type the description of naïve stem cell. The use of the 2i/LIF media can be applied to the culture of already derived mouse ES cell lines to reduce heterogeneity in culture; with cultures resembling the naïve state. Another breakthrough in the use of the 2i/LIF media is that it permits the derivation of ES cell lines from all mouse and rat strains tested, where before ES cell cultures could only be derived from the inbred 129 mouse strain (Buehr et al., 2008; Hayashi et al., 2008; Li et al., 2008; Nichols and Smith, 2009).

The description of the formative pluripotent mouse ES cell is more recent and refers in part to the transition from naïve ES cells to primed ES cells. In mouse this transition occurs spontaneously in response to withdrawal from 2i conditions. During this transition, naïve ES cells asynchronously downregulate Rex1 expression (Betschinger et al., 2013; Boroviak et al., 2014; Marks et al., 2012). The Rex1 negative cells, termed formative ES cells, remain pluripotent and are thought to represent cells of the early post-implantation embryo. After this formative ES cell stage, cells continue down their developmental lineage and begin to resemble the primed pluripotent cell identity in culture that corresponds to that of the primitive streak postimplantation epiblast proper.

Primed pluripotent cells are termed such since they represent cells of the primitive streak that are 'primed' for lineage commitment (Nichols and Smith, 2009) . These primed pluripotent stem cells may be derived directly from the postimplantation epiblast and are thus referred to also as EpiSCs. EpiSCs may be derived from a range of postimplantation stages (E5.5 to E8) and express the pluripotency factors Oct4 and Sox2, but they do not express other factors considered necessary for naïve pluripotency except for Nanog (Kalkan and Smith, 2014). EpiSCs may be differentiated *in vitro* or in teratomas, but single cell differentiation assays have not been performed and it remains unclear whether EpiSC cultures represent mixtures of different lineage precursors with some pluripotent precursors (Tsakiridis et al., 2015).

Parallels between the primed mouse EpiSCs and that of human ES cells have been drawn before, most notably because they both exhibit heterogeneity in terms of morphology and pluripotency factor expression, as well as exhibiting similarities in energy metabolism and DNA methylation (Weinberger et al., 2016). Additionally, mouse EpiSC and human ES cells behave similarly in response to TGFβ/activin signalling and neither respond to LIF in culture. However, the nature

of human and mouse ES cell correspondence is not clear-cut. Human ES cells and mouse primed ES cells are not identical, nor do human ES cells respond to 2i/LIF in the same manner as mouse primed ES cells. In the mouse, leaving the naïve state is in part marked by loss of the expression of Rex1, with EpiSCs being negative for Rex1 expression, however the pluripotency factor Rex1 is expressed by human ES cells (Shi et al., 2006). Furthermore, one of the core pluripotency transcription factors for the maintenance of naïve mouse ES cells, Esrrb, does not possess a binding site for other key pluripotency factors in humans indicating that the pluripotency networks between these species has not been completely conserved (Takashima et al., 2014). The question remains open as to whether the equivalent of a naïve state exists in the human *in vitro* ES cell context.

Human ESCs are notorious for their heterogeneous nature, poor clonogenic potential and high rate of spontaneous differentiation in culture. Spontaneous differentiation of human ES cells in culture further complicates their maintenance since the differentiated progeny generate feedback signals that alter the growth of the parental population or even drive further differentiation of the parent population, for instance by endodermal BMP production (Enver et al., 2005a; Peerani et al., 2007). Alternatively, other differentiated cells in culture may act as a stem cell niche and help maintain proliferation of the ES cells by the production of factors such as IGF1 from fibroblast-like cells (Bendall et al., 2007).

The presence of differentiated cells in a culture of ES cells clearly presents that culture as heterogeneous, however a more cryptic form of heterogeneity may exist within the stem cell compartment itself, manifesting in different differentiation responses or protein expression. Developmentally important factors such as OCT4 and NANOG exhibit varied expression on stem cells, and may indicate the presence of interconvertible substates within that population. As

previously discussed, SSEA3 also presents itself as a cell surface marker that indicates the presence of interconvertible substates (Enver et al., 2005b). Indeed, interconvertible substates have also been demonstrated within several adult stem cell populations (Booth and Potten, 2000; Hu et al., 1997; Jones et al., 2007) as well as well as early mouse embryos and ES cells (Chambers et al., 2007; Hayashi et al., 2008).

With the growing evidence that ES cell heterogeneity impacts upon differentiation potential in culture, tools for the identification of substates within the stem cell compartment become crucial for the delineation of this effect. So far there remains no prospective marker for cells occupying different substates although there are numerous approaches that could be explored in order to uncover these cryptic behaviours including mathematical modelling of population dynamics or non-destructive methods of cell state identification.

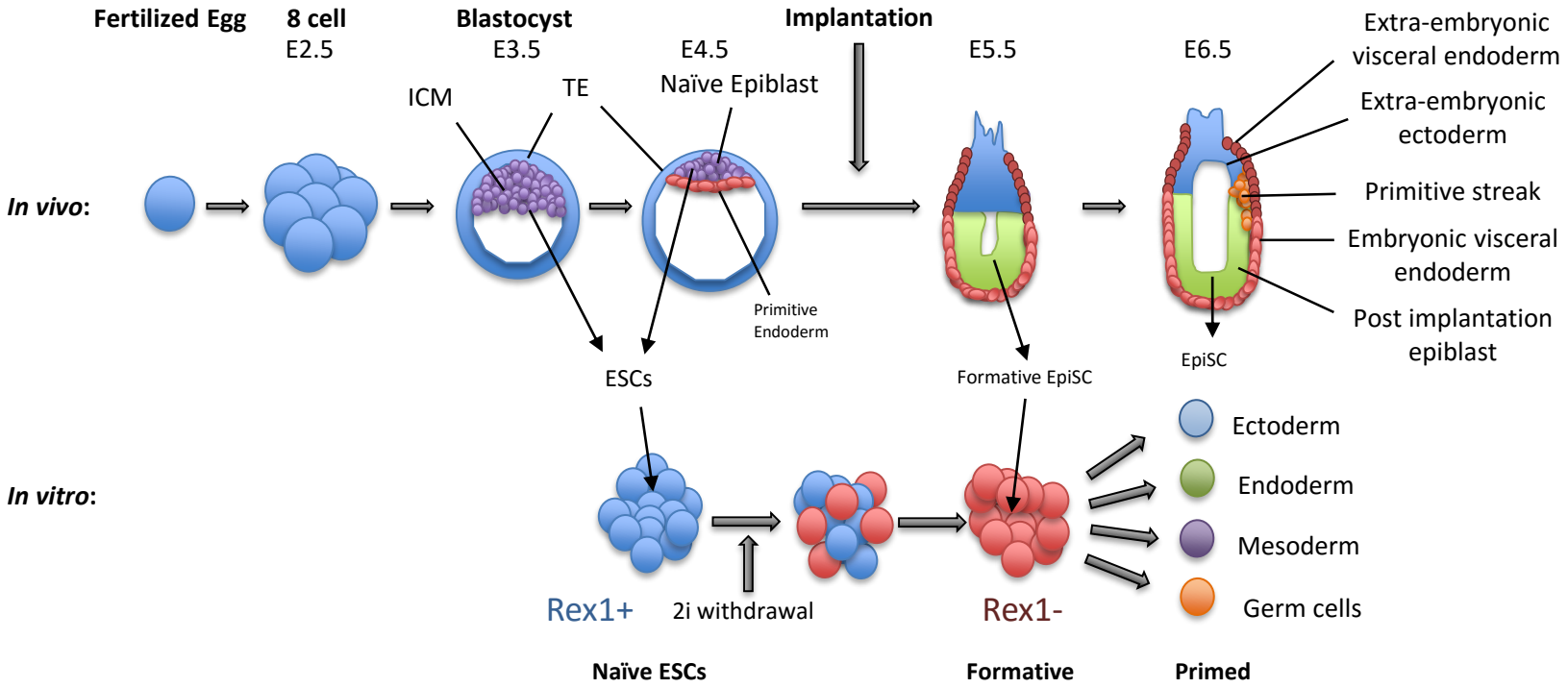

Figure 1.3 – Progression from naïve to primed pluripotency in mouse with a comparison between the *in vivo* and *in vitro* counterparts. *In vivo*: Up to the eight cell stage, blastomeres are totipotent. At embryonic day (E) 3.5, the inner cell mass (ICM) cells express both pluripotency and endoderm genes. At E4.5, the epiblast and primitive endoderm lineages separate, and the epiblast represents the naïve state of pluripotency. The E4.5 epiblast is the cell of origin of mESC, although it is possible to derive them from earlier stages, but these cells mature *in vitro* to resemble mESCs derived from the E4.5 epiblast. Naïve mESCs all express Rex1 homogeneously. The embryo implants in the womb between E4.5 and E5.5. EpiSCs are most similar to the late E6.5 epiblast, although they may be derived from E3.5 up to E6.5 and are described as being in a "primed" pluripotent state. As part of the transition from naïve to primed pluripotency upon the removal of 2i media conditions in culture, mESCs asynchronously downregulate Rex1 and being to resemble cells of the early, "formative" epiblast.

1.7 Heterogeneity and Cell Fates *In vivo*

The paradigm of cellular substates and heterogeneity is generally applied to in vitro studies since these are much easier systems to interrogate than their in vivo counterparts. With regard to pluripotent stem cells, this is probably a result of the fact that these cells are immortal in vitro, whereas their in vivo counterparts exist transiently as part of development. This short window of opportunity can make substate heterogeneity difficult to examine in vitro, especially since there is a symphony of concurrent developmental activity acting to guide cellular proliferation and differentiation. There are, however, well documented systems describing the process of spontaneous tissue patterning decisions made by equipotent cells in response to stochastic fluctuations of endogenous factors.

The Notch-Delta system, for example, comprises of the Notch family of type 1 transmembrane receptors and membrane bound ligands. This signalling pathway is activated by cell-cell interaction bringing the receptors and ligands into contact (Artavanis-Tsakonas et al., 1999). Upon ligand binding, the Notch receptors are cleaved and the intracellular domain is translocated to the nucleus, where it can influence the transcription of downstream genes, such as the Hes family (Selkoe and Kopan, 2003). The Notch-Delta system is subject to fluctuation in expression of both the receptor and ligand. Small changes in either can cause changes in either the expression or response to signalling, leading to amplified responses to signals (Artavanis-Tsakonas et al., 1999).

The Notch-Delta system is employed for specifying robust and separate cell identities in eye development in Drosophila. Neuroectodermal cells are initially equipotent and express Delta in a comparable manner. However, cells that recognise this ligand on a neighbouring cell will

downregulate its own ligand expression. Thus, small initial fluctuations in Notch/Delta expression can initiate cells to adopt a binary state. Ultimately, this leads to fate decisions, low Delta-expressing cells become epidermal, and high delta expressing cells become neural (Artavanis-Tsakonas et al., 1999; Heitzler and Simpson, 1991; Sestan et al., 1999).

Another example of the Notch-Delta system used for cell fate determination is in the nematode C. elegans with regard to anchor cell/ventral uterine cell specification. In this system, two precursor cells can adopt either identity, and the Notch-homologue (Lin-12) and its ligand (Lag-2) are expressed on both initially. The Lin-12 activation promotes its own expression and inhibits Lag-2, and thus stochastic fluctuations in signalling leads to the cells adopting a definite Lin-12 or Lag-2 expressing status, and then differentiating into the ventral uterine cell or anchor cell respectively (Christensen et al., 1996; Wilkinson et al., 1994).

An alternative paradigm whereby endogenous factor fluctuations results in distinct cell fates for participating cells is in somitogenesis where the basic helix-loop-helix (bHLH) factor Hes7, is expressed in an oscillatory manner in the presomitic mesoderm (Dequeant and Pourquie, 2008; Imayoshi et al., 2013; Kageyama et al., 2012; Oates et al., 2012). Hes7 auto-supresses by interacting with its promotor, and its mRNA and protein have a circa 20 minute halflife (Bessho et al., 2003; Bessho et al., 2001). Together this leads to 2 hour cycles of Hes7 expression that are shown to be critical in generating somites from the presomitic mesoderm. The Hes7 oscillatory clock allows genes to be activated or repressed in a synchronous manner, allowing cells within a tissue to initiate developmental processes as a defined unit. In the case of the presomitic mesoderm, two independent somites of a regular size are generated simultaneously on either side of the neural tube at a precise time. Experimental disruption of the synchronised state leads to irregular or impaired somitogenisis (Hirata et al., 2004). Additionally, dissociated cells lose

Hes7 periodicity, suggesting that cell-cell communication is important for oscillator maintenance, in this example Notch-Delta has once again been identified (Jiang et al., 2000; Maroto et al., 2005; Masamizu et al., 2006; Niwa et al., 2011; Riedel-Kruse et al., 2007).

Hes1 is another bHLH factor that oscillates during somitogenesis, in addition to other tissues (Hirata et al., 2002). Notably, fluctuating Hes1 regulates proliferation and differentiation in neural progenitor cells (Imayoshi et al., 2013; Shimojo et al., 2008). Hes1 functions to slow differentiation and ensure progeny types are distributed appropriately. Loss of this factor leads to premature differentiation that depletes the progenitor pool and produces a small and deformed brains comprising of only certain types of neurons. Hes1 fluctuates initially, but becomes stabilised when neural progenitor cells differentiate into astrocytes, and is lost in differentiating neurons. Ascl1 expression is repressed by Hes1, and the release of repression allows Ascl1 expression to induce neuronal differentiation (Imayoshi et al., 2013).

These examples above indicate that there are indeed mechanisms that occur during development that rely upon apparently stochastic processes to generate regular patterns. Therefore, it's worth noting that the behaviour cells exhibit in culture may be able to inform of processes that occur in vivo. However, especially in the case of pluripotent stem cells, in vitro cell behaviour is likely adapted to culture conditions that are not the same as those experienced by their in vivo counterparts. This is in addition to the evidence that stem cell substate heterogeneities exist in vitro in their own right (see previous). With regard application to regenerative medicine, most approaches focus on the directed differentiation of pluripotent cells in vitro, are based upon processes understood in vivo. The paradigm of stem cell substate heterogeneity is capable of influencing those differentiation decisions and by extension

differentiation efficiencies, regardless of whether there is opportunity for such a process to occur to their in vivo counterparts of the inner cell mass.

1.8 Modelling Heterogeneity

In general, there are two methods for interrogating the mode of action of an unknown system; systems identification and analytical modelling. Systems identification treats a new system as a black box type problem and will examine the system in terms of inputs and outputs; *i.e.* how information is transformed by the system. Although systems identification approaches do not purport to elucidate on the internal mechanism of this black box they instead inform on how inputs are mapped to outputs and thus have a predictive capacity. Analytical modelling, on the other hand, attempts to understand the mechanism of the black box by comprehensively dissecting all of the individual interactions that may take place within that system then fastidiously integrating all these interactions in order to describe how an input would be processed to an output.

These two methods may be investigated exclusively in their own right but a comprehensive and complete model of any particular system will include a cohesive integration of both approaches. It should be noted that an analytical modelling approach is a much more labour intensive method; and the capacity to map an input to an output using this method requires considerably more computational power than utilising a systems identification approach. Furthermore, analytical modelling can lead to a more accurate description of the relationships between mechanisms governing the system. Conversely, the model can only be as complete as the understanding of the processes that are entered into the model.

Multiple methods have been adopted in order to address features of cell heterogeneity and it is not a problem displayed only by pluripotent stem cells. Models constructed by collating existing experimental and bioinfomatic data, have been shown to have a predictive capacity: for example, the cross-antagonism of Fli-1 and EKLF at the erythroid megakaryocyte lineage branch point was predicted before it was demonstrated experimentally (Frontelo et al., 2007; Swiers et al., 2006). However, models of a network are generally a description of interrelationships of factors, rather than a true picture of the fluctuating components (i.e. proteins and mRNA levels, and the activities thereof) of that network, thus, the ability of these models to predict complex dynamics that permit a cell to enter particular differentiation lineages is limited.

In the hematopoietic field, a well-described decision point in the myeloid progenitor cell is the cross-inhibitory interaction between the transcription factors GATA-1 and PU.1 that allows the decision between erythroid/megakaryocyte and myeloid-monocytic fates by promoting lineage-specific transcription (Laiosa et al., 2006). In addition to mutual inhibition, GATA-1 and PU.1 also auto-stimulate, and modelling this simple circuit mathematically suggests three stable states (termed 'attractors'): either of the differentiation lineages, or the bi-potent progenitor state in which both transcription factors are held in balance. This model provides an explanation as to why classical 'differentiated' markers are found in combination in undifferentiated cells (Chickarmane et al., 2009; Hu et al., 1997; Huang et al., 2007). Other examples of these switches have been described for the early lineage decisions of embryonic stem cells (Boyer et al., 2005; Chambers et al., 2003; Chickarmane and Peterson, 2008; Chickarmane et al., 2006).

This example of GATA-1 and PU.1 dynamics provides a neat explanation for a simple, binary decision based upon a relatively uncomplicated model for the decision path. However, reality rarely presents itself with such simplistic decision trees. Experimental evidence of the

transcriptional response of human leukaemia cells (HL-60) differentiating down a single cell fate in response to two different inductive signals shows that although both sets arrive at the myelomonocytic fate (the attractor), different molecular pathways are utilised to do so (Huang et al., 2005).

As the stem cell state is considered an attractor, by definition a stable state, it has been suggested that the steering of a cell towards any specific differentiation state is a two-step process. The first step involves the destabilisation from the state of potency, and the second the impetus towards a secondary attractor state, or differentiated cell type (Huang et al., 2007). This model is evidenced by the multipotent cell line EML, which expresses the cell surface antigen Sca-1 at high or low levels, and experiments have shown that when sorted by expression level, either sorted population will reconstitute both high and low Sca-1 expressing cells, suggesting interconvertibility between these two states. However, Sca-1 expression levels correlate with Pu.1 and inversely with GATA-1 expression and this appears to link to lineage bias. Therefore, EML stem cells appears to exist in lineage biased, but interconvertible, substates (Chang et al., 2008b).

This is not the only evidence that cells stably within the stem cell attractor can exhibit different lineage biases. Blood stem/progenitor cells assayed by RT-PCR were found to express a mixture of lineage characteristic genes, although levels of each gene were heterogeneous within the population. Therefore, it was proposed that although each cell was multipotent, at any given point it was likely to favour one lineage over others, and that this bias was in flux (Delassus et al., 1999; Enver et al., 1998). The nature of lineage bias and lineage commitment remains unclear and it is not known whether lineage commitment is a gradual process or a discrete transition (Pina et al., 2012). Exploration of some multipotent systems has enabled the interrogation of

early stages associated with lineage affiliation that indicated an important role for transcriptional noise (Chang et al., 2008a).

In this thesis, a systems identification approach was adopted to assess whether some aspects of cell heterogeneity in a population could be modelled in a predictive manner. In this case, the feature of SSEA3 heterogeneity in culture was interrogated to help identify how substates are manifest. In keeping with the black box metaphor above, here the cell population's SSEA3 intensity distribution is considered the black box input, the cells within the population as the black box and finally the subsequent population's SSEA3 expression as the black box output. In other words, an examination of cell population SSEA3 distributions with regard their change from one day to the next. In particular, understanding how cells alter their SSEA3 expressions from one day to the next may uncover particular intensities of SSEA3 expressing cells that exhibit unique behaviours worthy of further interrogation. For instance, the identification of an attractor region where a cell's SSEA3 intensity is unlikely to change over time could be indicative of a substate population.

1.9 Raman Spectroscopy

Systems identification modelling of pluripotent stem cell dynamics is not the only method by which stem cell substates may be identified and subsequently explored. Methods that examine stem cell behaviour may also be employed in order to categorise pluripotent cell types. The most common methods by which pluripotency is interrogated *in vitro* generally fall into two main categories; destructive and non-destructive. As outlined above, almost all "omics" studies (transcriptomic, metabolomic) mandate the destruction and lysis of the cell of interest; making the future behaviour of that cell impossible to assess. The common non-destructive methods all require some degree of interference with the cell, be it by genetic alteration in the process of reporter line generation for proteins of interest or by cell surface antigen studies. Cell surface antigens are likely to have some function, and their interaction with antibodies may elicit some unknown response. In the context of substates within the stem cell compartment, where subtle behaviours are of great significance, any artefactual change to behaviour will be of consequence.

If, then, any interaction with a cell is of detriment to the effective understanding of future behaviour, the problem of stem cell substates could be deemed intractable; the act of measuring the system changing the outcome of the behaviour sought to be understood. Methods that interact minimally with the cell would be preferable to those that do not. Raman spectroscopy may provide such a method since it is capable of interrogating the biochemical compliment of a cell in a non-invasive manner.

Raman spectroscopy is a vibrational spectroscopy technique that exploits the Raman effect for the determination of chemical information. The Raman effect is the phenomenon whereby light is scattered in an inelastic manner as a direct consequence of a photon's interaction with a

molecular bond. The interaction with the molecule results in a change of energy in that photon which, since a photon's energy is a direct function of its inverse wavelength and the speed of light, corresponds directly to a change in that photon's wavelength. The change of energy that the photon is subject to is directly related to the chemical species of molecular bond with which it interacted (Figure 1.4). Using a monochromatic light source, the Raman scattering that occurs from that sample may be examined in the form of any resulting light that is of a different wavelength to the initial source. The Raman effect is a rare phenomenon and affects only about 1 in every 10 million scattered photons.

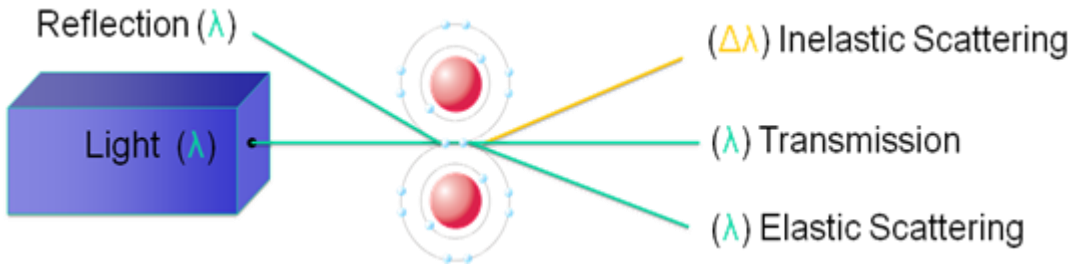

Figure 1.4 – The Raman Effect. The Raman effect is a rare phenomenon whereby photons interact with molecular bonds. Most light will transmit straight through the molecule or be reflected. Some light, however, will interact with the molecular bond and be scattered as a result. Most of this scattering will be elastic, with no transfer of energy between bond and photon; this interaction is called elastic scattering, or Rayleigh scattering. A small fraction of scattered photons (~1 in every 10^7 scattered photons) will interact with the molecular bond and an energy transfer event will occur, changing the photon's wavelength; which is known as inelastic scattering or, the Raman effect. The energy transferred relates directly with the molecular bond species, thus inelastic scattering of these photons is informative of the molecule(s) that those photons interacted with. White light contains lights of many wavelengths and so photon wavelengths associated with Raman scatter are not detectable or interpretable. Using a monochromatic light source such as a laser, enables the difference in wavelength of inelastically scattered photons to be measured; providing an indirect measure of the chemical composition with which photons interacted.

The inelastic scattering of light was first theoretically predicted in 1923 by the Austrian quantum physicist A. Smekal (Smekal, 1923). Although previously scientists had been studying light scattering in various media, no change in wavelength had been observed and thus this scattering

was deemed energetically elastic (Einstein, 1910; Strutt) with the only exception being in specific cases in the X-Ray spectrum called Compton scattering (Compton, 1923). One of the chief issues of the time was the production of a monochromatic light source and effective filters that could exclude the effects of elastic light scattering and transmission of light from the original source. The inelastic scattering of light was first observed in 1928 by Sir C. V. Raman (together with Krishnan and almost simultaneously by competing group Landsberg and Mandelstam), after whom the effect is now named, by the application of a narrow band photographic filter to generate a monochromatic light source from the Sun. Coupling this monochromatic source with the use of a "crossed filter" to subsequently block light of that wavelength, but permit the transmission of other wavelengths, resulted in the observation of light that had indeed changed wavelength. The practical discovery of the Raman effect earned him the Nobel prize in physics in 1930.

Following the discovery of the Raman effect, the systematic description of the effect and its relation to particular molecular vibrational frequencies was performed by G. Placzek between 1930 and 1934 (Placzek, 1934). Indeed, due to the low sensitivity of the technique at the time, highly concentrated samples, in large volumes were required to characterise the molecular vibrations of that sample. The advent of the laser in the 1960s provided a means of generating vast quantities of monochromatic photons that in turn boosted the sensitivity of the Raman technique.

Given the fact that the Raman effect is demonstrated by the interaction of molecular bonds with photons, which may be made interpretable by the use of a monochromatic light source, Raman spectroscopy offers a unique technique for the interrogation of chemical samples. Indeed, Raman spectroscopy has been implemented in a variety of fields, particularly in chemistry and

material sciences for the purposes of sample identification and for measures of sample purity (Eliasson and Matousek, 2007; Wolf, 1996). In a simplistic interpretation, cells exist as, albeit very complex, biochemical mixtures. The interaction of these chemicals ultimately culminates in the performance of a majority of cellular behaviours and conversely cells performing different behaviours do so as a result of differing chemical composition and interaction. Here, it is proposed that the differences in cellular behaviour may be explored in a non-destructive manner that requires little to no sample preparation. Indeed, Raman spectroscopy has gained traction in the biological sciences and has been used to discriminate between different cell types (Dochow et al., 2011; Ellis and Goodacre, 2006). Here it is proposed that Raman spectroscopy may be employed to distinguish between more cryptic cell types – possibly even different substates.

Although this application of Raman spectroscopy to that of pluripotent stem cell substates is a novel, exploratory application, it is not beyond the realm of possibility that differences are to be expected between different substates. As mentioned above, cells that exhibit different behaviours do so primarily due their chemical compliment at the time that includes transcription factors and proteins. Furthermore, pluripotent cells and their differentiated derivatives can be distinguished based upon their Raman spectra, indicating that cellular behaviours can be delineated based upon their chemical composition. Finally, there are gross changes in cellular energy metabolism that correlate with the process of transitioning from a pluripotent to differentiated state, although the exact nature of this relationship is not fully resolved (Kondoh et al., 2007; Varum et al., 2011; Zhang et al., 2015).

1.10 Technical Contributions

This thesis was built, in part, upon the work and help by others in collaboration. In terms of technical contribution for Chapter 3: Dr. Mark Jones operated the FACS machine to sort cells required for the modelling experiments; Dr. Xioakai Nie and Professor Daniel Coca for the mathematical development of the modelling process used; Dr. Xioakai Nie for modelling the experimental data. With reference to Raman spectroscopy in Chapters 4 and 5: Raman spectroscopy work outsourced to Renishaw was performed by Dr. Katherine Lau who acquired and analysed the Raman spectra (presented in Section 5.2; Figure 5.1); Professor Wei Huang provided the Raman microscope and equipment tuition used for the other Raman experiments; Dr. Veronica Biga for the development of the regional isolation tool in MATLAB (Mathworks inc.) that allowed the isolation of Raman spectra from regions of interest.

1.11 Aims and Objectives

This thesis describes the generation and optimisation of two methods for examining pluripotent stem cell heterogeneity in the stem cell compartment. The first method interrogates SSEA3 dynamics within a pluripotent cell population that are subsequently modelled in order to uncover the underlying rules that govern ES cell SSEA3 expression levels. The underlying pattern of SSEA3 dynamics within the population could be employed to identify substates within the population, especially given the close relationship between SSEA3 and pluripotency. The second method aims to optimise the non-intrusive Raman spectroscopy technique with application to ES cell research in order to uncover biochemical signatures that may belie subtle differences in ES cell behaviour. The clear advantage of Raman spectroscopy is that in principal cells may be studied in real time and future behaviours examined.

Chapter 2

Materials and Methods

2.1 Cell lines

A number of different cell lines were used and are outlined below:

Human Embryonic Stem Cell lines

Human embryonic stem cell lines used were derived previously, within ethical and legal guidelines from fully-informed, consenting patients.

H14.S9 Cell Line

The H14s9 cell line is a karyotypically normal cell sub-line of the H14 human embryonic stem cell line.

H14.BJ1 Cell Line

The H14BJ1 cell line used is a karyotypically abnormal cell line previously described (Baker et al. 2007). The H14BJ1 karyotype includes an extra copy of chromosome 17 containing an amplification of chromosomal region 17p11.2.

H7.s6 Cell line

The H7.s6 cell line is a karyotypically abnormal variant (46,XX, der(6)t(6;17)(q27;q1)) of the H7 embryonic stem cell line derived by Dr. James Thomson (University of Wisconsin). The karyotypic abnormality is considered an adaptation caused by mutation and natural selection facilitated by long term cell line culture (Draper et al., 2004).

Shef4 *Gata6*:GFP Reporter Cell line

The Shef4 line was derived using a micro-drop culture system on mitotically inactivated mouse embryonic fibroblast cells (Aflatoonian et al., 2010). A sub clone of the Shef4 embryonic stem cell line was used here that had a GFP construct knocked into the ATG site of the second exon of one allele at the *GATA6* locus. This modification was performed by Dr. Andrew Smith (University of Edinburgh) using zinc finger nucleases to cause a double stranded break at the integration site and the GFP cassette (Figure 2.1) electroporated into the Shef4 line. Cells that had undergone successful integration of the GFP cassette were clonally selected through neomycin selection and sub-clones subsequently created. The subclone Sheff4 Gata6:GFP (S4G6)/F-9 A3 was used and neomycin resistance was removed using TAT-FLP recombinase.

Hes3 *Mixl1*:GFP reporter cell line

The Hes3 human embryonic stem cell line was derived from cells isolated from the inner cell mass of the embryo. The cell line was later modified by Dr. Elefanty et al (Monash University) to include a targeted insertion of GFP into exon1 of the MIXL1 locus via electroporation (Davis et al., 2008). Successfully transfected cells were selected for through neomycin resistance. Successfully integrated cells were expanded and transiently transfected with a vector expressing Cre-recombinase in order to remove neomycin resistance (Figure 2.2).

Human Embryonic Carcinoma Cell lines

Human embryonic carcinoma cell lines used are described below.

N2102 Ep cell line

The N2102EP embryonic carcinoma cell line was derived from a primary human testicular teratocarcinoma and later sub-cloned (Andrews et al., 1982). This cell line exhibits low rates of spontaneous differentiation *in vitro*.

NTera2 Clone D1 cell line

The NTera2 cl.D1 cell line is a pluripotent human testicular embryonal carcinoma cell line sub-cloned from parental NTera2 lines established in 1984 from nude mouse xenograft of the TERA2 cell line (Andrews et al., 1984b). The TERA2 cell line was originally established from a lung metastasis of a testicular teratocarcinoma in 1975 (Fogh J, 1975).

Mouse Cell lines

Cell lines derived from mouse:

Mouse Embryonic Fibroblast (MEF) Cells

Mouse embryonic fibroblast cell lines were derived from embryonic day 13.5 embryos of the MF1 mouse strain grown in-house. Embryos were excised followed by thorough mechanical and enzymatic (trypsin) tissue/cell dissociation. Residual tissue chunks were filtered out by gravity and the remaining mixture was seeded into culture vessels and permitted to grow to 90% confluence before being harvested and cryopreserved for later use.

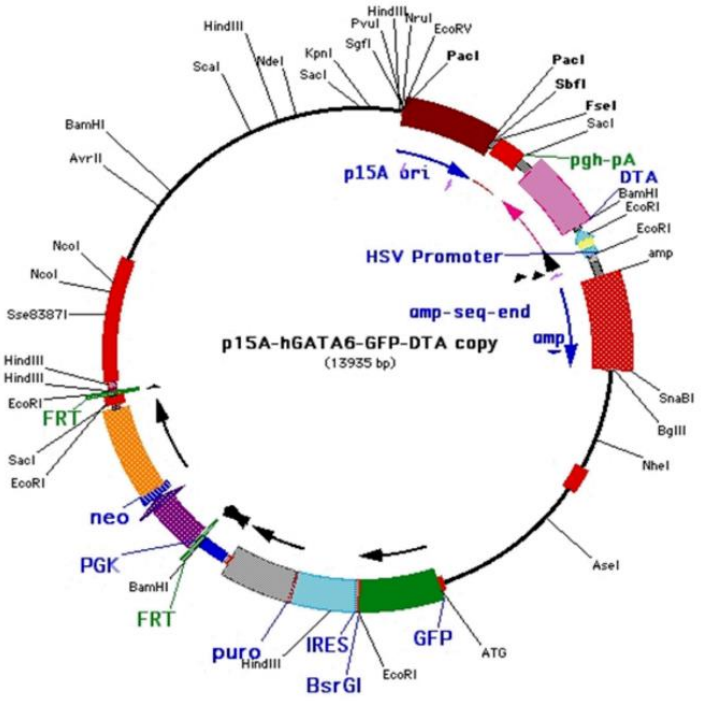

Figure 2.1- GFP transfection cassette electroporated into the Shef4 line to generate the Shef4 *GATA6*:GFP (S4G6) reporter cell line. The cassette contains the wild-type GFP gene bolted to puromycin resistance through an IRES. The GFP construct is knocked into the ATG site of the second exon of one allele for the *GATA6* locus resulting in an heterozygous *GATA6*:GFP cell line. The ATG site is targeted using zinc finger nucleases, causing a double stranded break at the integration site. Constitutive neomycin expression (via the PGK promoter) allowed for the selection of successfully transfected cells. The S4G6 4/F-9 A3 subclone used had neomycin expression removed using TAT-FLP recombinase.

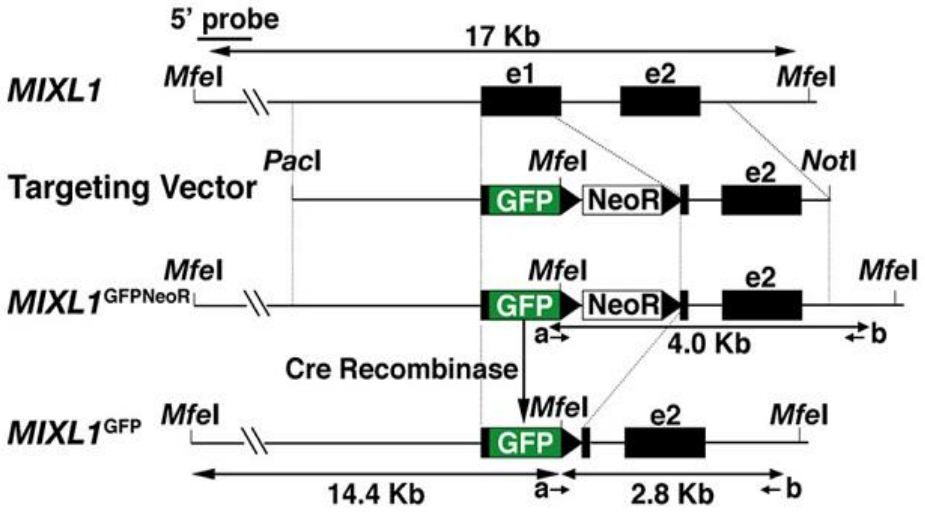

Figure 2.2 – GFP targeting to the MIXL1 locus in the Hes3 cell line (Davis et al, 2008). Gene targeting vector structure used to insert sequences of GFP into exon one of the MIXL1 locus in order to generate the MIXL1:GFP reporter cell line in human Embryonic Stem cells.

2.2 Reagents

Media & Matrices

Human Embryonic Stem Cell Culture

Human embryonic stem (hES) cells were either grown with or without mitotically inactivated mouse embryonic fibroblast (MEF) support. When grown using MEF support, culture vessels were first treated with 0.1% gelatin (Thomson and Marshall, 1998) and cell cultures were grown in hES cell media (Table 2.1). When grown in the absence of MEFs, embryonic stem cells were cultured on culture vessels treated with Vitronectin (LifeTech A14701SA) and maintained using E8 media (LifeTech A1517001).

Table 2.1 - Media composition used for human embryonic stem cell cultures when grown on mouse embryonic fibroblasts

Component	Final Volume
Knockout DMEM	800mL
Knockout Serum Replacement	200mL
1% Non-essential Amino Acids	10mL
1mM L-Glutamine	10mL
0.1mM β-mercaptoethanol	2mL
4ng/mL human bFGF	1mL

Human Embryonic Carcinoma Media

Cell culture for human embryonic carcinoma cell lines and mouse embryonic feeder cells were cultured in media containing 90% DMEM and 10% foetal calf serum (See table 2.3).

Cell staining/ Antibodies used

Cellular staining was performed using the reagents listed in Table 2.2.

Table 2.2 - List of antibodies/ cell markers used and their supplier details

Antibody	Target Antigen	Antibody species/subtype	Supplier	Cat Number
Primary Antibodies				
P3-X-63-AG8			In house	
MC631-2C2	SSEA3	Rat IgM	In house	
MC480	SSEA1	Mouse IgM	In house	
TRA-1-60s	TRA-1-60	Mouse IgM	In house	
Secondary Antibodies				
Alexa Fluor 488		Goatαmouse IgG	Thermo-Fisher	Z25002
DyLight 647		Goatαmouse IgM	Thermo-Fisher	62265
Nucleus Staining				
Hoechst 33342	DNA		Sigma	B2261

General Reagents

A list of reagents used are listed in table 2.3 below.

Table 2.3 - List of general reagents used during experiments

Reagent	Supplier	Catalogue Number
Dulbecco's Phosphate Buffered Saline (w/o Mg^{++} or Ca^{++})	Sigma-Aldrich	D1408
Paraformaldehyde	Sigma-Aldrich	441244-1KG
Gentamycin	Sigma-Aldrich	G1397-10ml
Dulbecco's Modified Eagle's Medium	Sigma-Aldrich	D5796
Dulbecco's Modified Eagle's Medium w/o Phenol Red	Sigma Aldrich	D1145
Foetal Calf Serum (EU)	HyClone	SV30143.03
Mitomycin C	Sigma-Aldrich	M-4287
Y-27632 (ROCK Inhibitor)	Sigma-Aldrich	Y0503
Sodium Hydroxide	Sigma-Aldrich	S8045-1KG
Propidium Iodide	Sigma-Aldrich	P4170-100mg
Vitronectin	Life Technologies	A14701SA
E8 Media	Life Technologies	A1517001
TrypLE	Life Technologies	12563-029
Knockout DMEM	Life Technologies	10829-018
Knockout Serum Replacement	Life Technologies	10828010
1% Non-Essential Amino Acids	Life Technologies	1140-035
1mM L-Glutamine	Life Technologies	25030-81
0.1mM β-mercaptoethanol	Life Technologies	31350-010
4ng/mL human bFGF	RnD Systems	233-FB-01M
Bovine Serum Albumin (BSA)	Sigma-Aldrich	A-1470

Methods

2.3 Cell culture

Human Embryonic Stem Cell culture

Human embryonic stem cells were cultured either with or without mouse embryonic fibroblast support as required by different experimental procedures described below. In all cases, hESCs were incubated in a humidified incubator at 37°C with 5% CO_2.

Mouse Embryonic Fibroblast dependent culture

Human ES cells were cultured on mitomycin inactivated MEFs derived in-house from the MF1 mouse strain. Stocks of these MEFs were defrosted at P0 and cultured to P4 with DMEM/10% FCS and incubated in 10% CO_2 humidified incubator at 37°C prior to inactivation treatment with mitomycin C. Mitomycin C was diluted in DMEM/FCS at 1ug/mL and added to MEFs for 2h. Cells were then washed in PBS and detached from culture vessels using trypsin:EDTA for 2minutes at 37°C. Trypsin was neutralised by the addition of DMEM/10%FCS then cells were harvested, centrifuged, supernatant aspirated, resuspended in DMEM/10%FCS and counted. On average $2x10^6$ cells were resuspended in 0.5mL of freeze media (80% DMEM, 10% FCS & 10% DMSO) and stored at -80°C.

The culture surface of T-25 Flasks was coated with 2mL of 0.1% Gelatin/PBS and incubated for 30 minutes at room temperature. Following incubation, gelatin was aspirated from the T25 flasks and MEFs were seeded at a density of 10,000 cells/cm^2 in DMEM/10%FCS and incubated in 10% CO_2 at 37°C overnight prior to use. Fresh MEFs were used for hESC culture whenever possible. In preparation for hESC culture, the media from MEF flasks was aspirated and replaced with 2mL of hESC media and incubated at 37°C with 10% CO_2 for a minimum of 30 minutes to equilibrate. Media from hESC cultures to be passaged was aspirated and replaced with 1mL/T25 of 1mg/mL collagenase IV to facilitate colony detachment. Cells were incubated for 7 minutes at 37°C after which collagenase was aspirated and removed with 3mL of fresh hESC media. Cells were gently scraped using a plastic Pasteur pipette or glass beads to detach cells from the flask surface and split into the equilibrated MEF flasks at a ratio of 1:3-1:4.

Mouse Embryonic Fibroblast independent culture

When culture on mouse embryonic fibroblasts was not used, human embryonic stem cells were cultured on a matrix of Vitronectin and with E8 media. Vitronectin was thawed on ice and diluted 1:100 with Dulbecco's Phosphate Buffered Saline (PBS see table 2.3). Culture vessels were coated with 100µL/cm^2 of diluted Vitronectin for 1 hour at room temperature, which could then be stored for up to 1 week at 4°C.

Human Embryonic Carcinoma Cell culture

Human embryonic carcinoma cell lines were cultured at 37°C in DMEM/10%FCS under a humidified atmosphere of 10% CO_2 in air. Cultures were passaged by either enzymatic or mechanical detachment. For enzymatic detachment, media was aspirated from culture and replaced with 1mL 0.25% trypsin in EDTA and incubated at 37°C for 2 minutes. Flasks were knocked to aid detachment prior to trypsin inactivation by the addition of 4mL DMEM/10% FCS and cells were rinsed with this media to aid detachment then transferred to a 15mL falcon tube and centrifuged at 1000rpm for 3 minutes. The supernatant was aspirated and the cell pellet resuspended and triturated in DMEM/10%FCS and split at a ratio of 1-3:1-4. For mechanical passage, media was aspirated from culture vessels and replaced with 1mL DMEM/10% FCS and mechanically detached using glass beads. DMEM/10% FCS was used to wash the cells off the beads and collected to be split at 1:3-1:4.

Mouse Embryonic Fibroblast Cell culture

Mouse embryonic fibroblast cells were not only used to facilitate human embryonic stem cell culture. For experiments requiring non-inactivated mouse embryonic fibroblasts, cultures were cultured at 37°C in DMEM/10%FCS under a humidified atmosphere of 10% CO_2 in air. Cultures were passaged enzymatically using 0.25% trypsin:EDTA as described for human embryonic carcinoma cell culture.

Cell Culture in preparation for Raman Spectroscopy

Cells for examination with Raman spectroscopy were grown on Raman grade CaF_2 (Crystran) discs within a petri-dish as the culture vessel. These CaF_2 discs were utilised in the same manner as regular culture plastic. Human EC cells were seeded directly onto CaF_2 slides and maintained

with 10% FCS/DMEM. Human ES cell lines were cultured in a MEF free format using vitronectin/E8 supplemented with Y-27632 as the matrix/media combination as described above (see above). In each case, cells were seeded and left to attach overnight prior to PFA fixation (See below).

Thawing Cell lines for culture

Cell vials were transported on ice when removed from liquid nitrogen facilitated cryopreservation. Cell were allowed to partially thaw in a 37°C water bath. To prevent DMSO mediated cell damage, cells were not left to thaw completely prior to further manipulation. Cells were quickly transferred into a 15ml falcon tube, diluted with 10ml of pre-warmed appropriate media; human ES cell media for human ES cell lines and DMEM/10%FCS for human EC and MEF cell lines. Cells were centrifuged at 1000rpm for 3 minutes. The supernatant was aspirated and cells were resuspended in fresh relevant media before being plated in prepared flasks. Note that human embryonic stem cell lines require inactivated mouse embryonic fibroblast culture vessels prepared in advance and when seeded, human embryonic stem cell culture media was supplemented with 10µM Y-27632 to improve cell survival.

Single cell dissociation of Human Embryonic Stem Cells

For experiments that required single cells, hESCs were dissociated using TrypLE. Media was aspirated from the cells and 100µL/cm^2 of 1X TrypLE added to the vessel. After incubating for 2 minutes at 37°C, the cells were dislodged by gently hitting the flask, and then returned for a further minute to 37°C. Two volumes of hESC media were added to neutralise the TrypLE, and the cells were transferred to a 15mL falcon tube and centrifuged at 1000rpm for 3 minutes. The supernatant was aspirated and cells were re-suspended in hESC media for further downstream application.

Single Cell Dissociation of Human Embryonic Carcinoma cells

For experiments that required single cells, hEC were dissociated using trypsin. Media was aspirated from the cells and 40µL/cm2 of 0.25%trypsin, in 1 mM EDTA in calcium and magnesium free PBS were added to the vessel. Cells were incubated for 2 minutes at 37oC, 5% CO2, the trypsin removed and cells were dislodged by gently hitting the flask. DMEM/10%FCS

(160µL/cm2) was added to inactivate the trypsin. Cells were transferred to a 15mL tube and centrifuged at 1000rpm for 3 minutes after which the supernatant were removed and cells resuspended in DMEM/10%FCS.

Cell Counting

Cells to be counted were first dissociated to single cells (see above) and resuspended into an appropriate volume of media. 10µL of cell suspension was added to an improved nebauer haemocytometer and the four corner grids were counted. Consequently, the number of cells/mL of the 10µL sample is determined:

$$Concentration\ [cell/mL] = \frac{Number\ of\ cells\ counted}{Number\ of\ grids\ counted} \times 10{,}000$$

$$Total\ cell\ number = Concentration \times Total\ volume\ (mL)$$

2.4 Flow cytometry analysis and *in situ*

Flow cytometry analysis

Cells for flow cytometry analysis were first dissociated into single cells and counted. Following centrifugation at 1000rpm for 3 minutes, supernatant was aspirated and cells resuspended in FACS buffer (10% FCS/PBS) at a cell density of $1x10^7$ cells/ml. 200µl of sample was transferred to a 5mL FACS tube, the relevant primary antibody appropriately diluted and 200 µl was added to each sample. Cells and primary antibody were incubated at 4°C for 30 minutes an occasionally disturbed to resuspend the cell pellet. Following incubation, cells were washed in 4ml FACS buffer, centrifuged and supernatant aspirated three times prior to resuspension in 200µL FACS buffer. 200µl of diluted, relevant secondary antibody was added to each sample and incubated at 4°C for a further 30 minutes with occasional disturbance to resuspend the cell pellet. After incubation in the secondary antibody, the cells were again washed three times in 3ml FACS buffer, centrifuging each time at 1000rpm for 3 minutes, and resuspended in 500µL for flow cytometry analysis using the CyAn (Beckman Coulter) flow cytometer, or for cell sorting using either a MoFlo (DakoCytomation) or FACSJAZZ (BDBiosciences) platforms.

Cell flow cytometry analyses were performed with Summit software. Events registered during flow cytometry and FACS sorting were gated in order to remove noise from the dataset such as debris or cell doublets (example in Figure 2.3). These events were excluded based upon size measures from forward scatter/side scatter measurements; where the main cell population was inferred to be the most numerous. Therefore, only events within this main size distribution were accepted. Secondly, cell doublets were excluded using the pulse width metric.

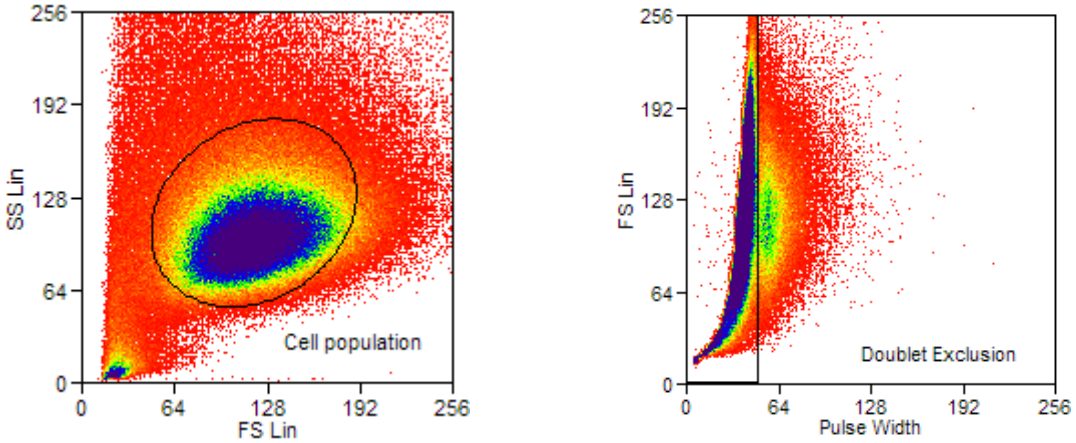

Figure 2.3 – Cell density plots to provide examples for cell gating measures undertaken during flow cytometry for the exclusion of events representative of debris and cell doublets. The FS Lin/ SS Lin measures of the population provides information on general cell size; events were gated around this density plot in order to exclude outlying events that may be more representative of debris. The Pulse width against FS Lin exclusion is used to exclude cell doublets where flow cytometry data are not acquired on a single cell basis.

Flow Automated Cell Sorting

Cells were prepared in the same manner as described above but cells were also filtered using a 70µm filter (Miltenyi Biotec 130-095-823) to ensure single cells were used, and the FACS buffer used for cell sample washes was replaced with the relevant cell media; i.e. DMEM/10% FCS for human embryonic carcinoma cells and human embryonic stem cell media for human embryonic stem cells. Additionally, cells were sorted into cell line relevant media supplemented with 50µg/mL gentamycin. To aid survival, sorted human embryonic stem cells were re-plated in media additionally supplemented with Y-27632.

Immunostaining cells *in situ*

Following fixation (see above) in PFA, the cells for *in situ* immunostaining had PBS aspirated and were incubated with a blocking solution (10% FCS/PBS 0.3M Glycine and 1% Bovine Serum Albumin) at room temperature for one hour. The blocking solution was removed from cells and replaced with relevant primary antibody that was diluted in PBS/10% FCS at an appropriate concentration. Cells were incubated with primary antibody at 4°C for one hour. Primary antibody was then removed and cells washed three times with PBS. The Cells were incubated for one hour at 4°C with relevant secondary antibody and Hoechst 33342 also dissolved in PBS/10% FCS at an appropriate concentration. Secondary antibody was aspirated away and cells washed three times in PBS. Cells could then be stored in PBS at 4°C until examined using the InCell Analyser system.

2.5 Cell Fixation

Paraformaldehyde preparation

Paraformaldehyde solution used for cell fixation was prepared using powdered paraformaldehyde dissolved in PBS heated to 65°C in a dilution of 4% paraformaldehyde in terms of weight per volume. 5M NaOH was added dropwise until solution became transparent, then filtered to remove any residual particulates and left to cool. Aliquots of PFA were either used immediately when or frozen to -20oC for storage and used within 2 weeks.

For *in situ* immunohistochemistry

Cells that were subject to immunostaining *in situ* were fixed using 4% paraformaldehyde. Media was aspirated from cell cultures, washed three times with PBS and incubated with 4% PFA for 12 minutes at 4°C. Following incubation, cells were washed three times with PBS and stored at 4°C in PBS ready for later staining.

For Raman Spectroscopy

Cells grown for Raman spectroscopy (see above) were fixed in paraformaldehyde prior to interrogation with Raman spectroscopy. Media was aspirated from the culture vessel and cells were washed with Dulbecco's phosphate buffered solution three times. PBS was aspirated off

the cells, 4% paraformaldehyde added and incubated at 4°C for 12 minutes. Following incubation, PFA was aspirated off and the cells again washed three times with PBS (w/o Ca^{++} and Mg^{++}). PBS was then aspirated off the cells replaced with dH_2O and incubated at room temperature for one minute prior to being aspirated and left to dry in a lamina flow hood.

Clonogenics

Clonogenic experiments were carried out on the NTera2 embryonic carcinoma cell line. In this context, Clonogenic assays were performed after FACS cell sorting. Sorted cells were centrifuged at 1000rpm for 3 minutes and resuspended in DMEM/ 10% FCS supplemented with 50µg/mL gentamycin. Cells were passed through a 70µm filter counted and diluted to a cell plating density of 1000 cells/cm^2. After plating in DMEM/10% FCS supplemented with 50µg/mL gentamycin, fractions were cultured for 4 days in DMEM/10%FCS under a humidified atmosphere of 10% CO_2 humidified incubators at 37°Cin air. After 4 days, cells were fixed in PFA and stained for appropriate markers.

2.6 Raman Spectroscopy Data Collection and Processing

Two Raman microscope setups were used to generate data presented in this thesis. The data discussed in Section 5.2; "Different Cell Types" were acquired using the inVia Reflex confocal Raman microscopy system, designed by Renishaw plc, that was fitted with a 532nm laser. The collection and analyses of these data were outsourced to the Raman microscopy company Renishaw plc (uksalessupport@renishaw.com) and performed by Dr. Katherine Lau.

All other Raman spectra (Chapter 4 and Section 5.3 onwards) were collected using an in-house modified HoribaLabRam HR (Wellsens Biotech. Ltd., China) that employed a 532nm Nd:YAG laser (Ventus, Laser Quantum Ltd, UK), a Newton EMCCD (DU970N-BV, Andor, UK) and integrated Olympus microscope (model BX41) for sample observation and Raman acquisition. A pinhole of 300µm and a slit size of 100µm was used enabling a spatial resolution of $1\mu m^2$ laser spot size to be obtained. The System was calibrated prior to analyses and monitored using a Silicon Raman band reference. Raman spectra were collected from cells spatially and temporally defined for specific experiments.

Spectra collected were pre-processed using Labspec software (Horiba) for spectral zeroing and normalisation by area under the curve. In the case of spectral maps, relevant spectra were selected from the acquired data by use of a tool developed in MatLab (Biga & Mason, unpublished) that was developed to group spectral data according to stored X and Y coordinates within mapping files against microscope photographs of the relevant sample. File management and spectral database compilation was performed in R Language for statistical computing (R Foundation for Statistical Computing).

2.7 Multivariate analysis

A number of multivariate analytic techniques were employed to analyse the Raman spectra collected. Multivariate analyses of spectra were performed using the Simca (version 14, UMETRICS) analysis software, unless otherwise stated. Multivariate analytic techniques are designed to address data that presents multiple measured variables as outcomes for a particular sample(s). Raman spectra contains information from multiple wavenumbers which are all measured variables and so suitable for multivariate analysis. Two multivariate analytical techniques were applied to the Raman spectra; Principal component analysis (PCA) and Partial Least Squares Regression (PLS).

Principal Component Analysis

PCA is a technique that is employed to reduce the number of dimensions present within a dataset by an orthogonal transformation of the data from a set of possibly correlated variables (e.g. wavenumbers) into a set of linearly uncorrelated principal components (PC). The PC are calculated in such a manner as to account for as much variation within the dataset as possible and are defined that the first PC accounts for the largest possible variance in the dataset with each subsequent PC accounting the most variance that is orthogonal (*i.e.* perpendicular) to the preceding component. The number of PC generated by this transformation is less than or equal to the number of original variables and each PC is linearly uncorrelated to the other PCs since they are orthogonal. PCA therefore transforms the dataset in such a way as to best explain the variation seen within the dataset on a hypothetical axis which the first principal component, whilst each subsequent PC describes the next largest axis of remaining variation.

The application of PCA presents an unbiased examination of the variables, which aims to reduce the number of dimensions in the dataset by systematically describing those variables most

responsible for differences between all samples. This calculation is performed on all samples and does not take into account any *a. priori* knowledge regarding the samples such as classification or experimental treatment. Therefore, if samples separate according to PCA in a manner that correlates with experimental treatment, then this is a correlation born out of the dataset rather than one presupposed by the PCA and so indicates a real difference between the experimental treatments.

The PC themselves do not exist directly from the variables measured in the original dataset but instead are hypothetical axes through the multidimensional dataset that best capture the remaining variance of the dataset. Each PC does however have a relationship with all the variables in the dataset, since the variation of each variable is in part responsible for the calculation of the PC. It is possible then to calculate the degree by which all variables contribute to the PC of interest (termed PC loadings) and thus enables those variables that are contribute the most for samples separating according to that PC to be determined. A sample that has a particularly large measurement (compared to the rest of the dataset) for a variable (wavenumber) that contributes to a positive separation on a PC will tend to be positive when compared against that PC in relation to other samples. However, this trend is true for all variables and so the degree to whether a sample is positive or negative on a PC axis is an integration of all variables from that sample with respect to the PC. A PC that shows a trend of separation between samples may be examined to determine what variables (or wavenumbers) contribute most heavily towards that sample separation. It is important to note that all PCs are particular to their respective PCA and so the PC data from one PCA/dataset is not directly comparable to that of any other PCA/dataset.

Partial Least Squares Regression

PLS is a multivariate technique that bears some resemblance to PCA analysis, however instead of determining the PC of maximal variance between variables in an unbiased manner, the technique also factors in *a. priori* information about the experimental treatment of samples into the analysis as predicted variables (e.g. whether sample cells have or have not been treated with RA). PLS acts to find a linear regression model that projects the predicted variables with the observed variables (wavenumber) in order to find the observed variables that are the strongest predictors of the predicted variables. This type of modelling is particularly useful for predicting the predicted variable (experimental treatment) of a novel sample, but is not suited for understanding the relationship between these variables.

2.8 Calcium Fluoride slide cleaning protocol

Raman grade Calcium Fluoride slides (Crystran; Figure 2.4) used for Raman analysis were washed after use for cell culture, prior to sterilisation and reuse for further experiments. CaF_2 slides were washed by; thorough rinsing in sequence with distilled water, tergazyme (prepared as per the manufacturer's instructions, Sigma-Aldrich), distilled water, coulter cleanser (Beckman Coulter) and distilled water. In between cleansing agent exchange, CaF_2 slides were polished with lint free cloths. After washes, CaF_2 were left to air dry until ready for use. In preparation for cell culture, CaF_2 slides were sterilised by submersion in 70% ethanol and exposed to ultra-violet radiation for one hour in a lamina flow hood. CaF_2 slides were then rinsed in filter-sterilised water and allowed to dry in the lamina-flow hood before use in cell culture.

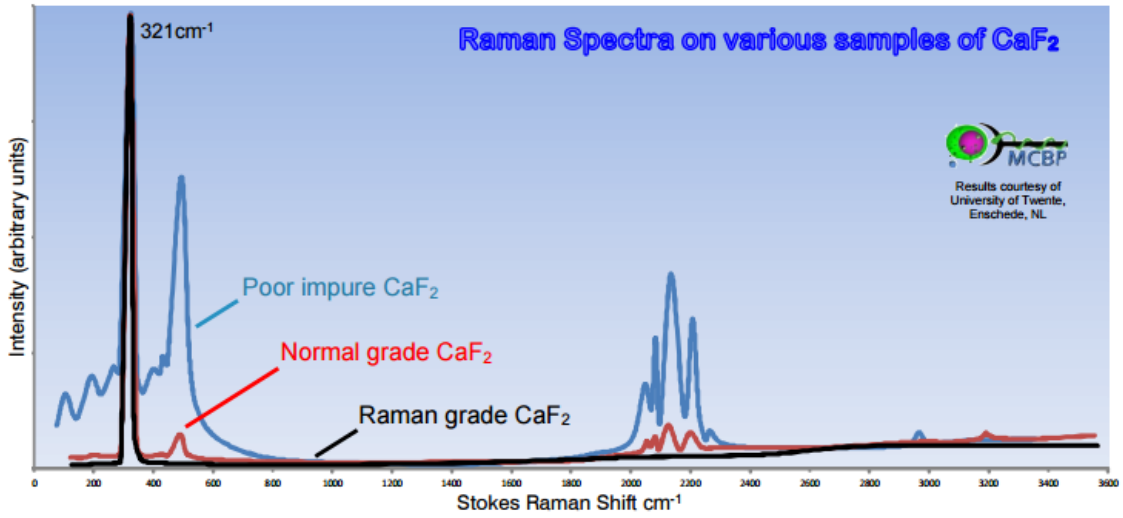

Figure 2.4 – Raman Spectra of CaF_2 slides produced by manufacturer Crystran. Raman grade CaF_2 slides (black) used in experiments here do not present a strong Raman band within the organic fingerprint region between wavenumbers 500cm^{-1} and 1800cm^{-1} and so are ideal for cell based applications

2.9 SSEA3 Dynamics Modelling

The approach adopted to model the SSEA3 intensity dynamics is based on methods developed by Nie & Coca (2015), with whom we collaborated. Nie and Coca performed the modelling using experimental data generated (see chapter 3). For more details regarding the modelling algorithms and application to other experiments please contact Professor Daniel Coca (d.coca@sheffield.ac.uk).

Chapter 3

Modelling Pluripotent Cell Heterogeneity

3.1 Introduction

Heterogeneity

The behavioural heterogeneity displayed by human ES cells during culture and differentiation remains an enigmatic problem, both conceptually and practically. Lineage biases may be inferred by observing the differentiated derivatives of a pluripotent stem cell long since left the pluripotent state (Tonge and Andrews, 2010). Alternatively, investigations into global gene expression patterns of human ES cells while maintained in a pluripotent state in culture requires the destruction of the cell of interest, so that the future behaviour of cells presenting gene expression patterns predicted to represent substates cannot be studied. All of these problems precede the conceptual issue that the definition of ES cell substates mandates the property of interconvertibility and so the substate identity of any one particular cell would be in flux preventing any "snap-shot" profiling approach of cells in culture from accurately representing this dynamic system. Currently, no established method exists by which particular substates may be prospectively identified and even less is known about the interconversion dynamics of substates within what is termed the hypothetical "stem cell compartment" (See Figure 1.2).

Although there exists functional evidence for interconvertible stem cell substates (Tonge and Andrews, 2010), there are currently no direct methods for the readout of substate status of either individual cells or of a population. Currently, different methods for the gross categorization of cells based upon marker expression are not the same as defining the position of a substate proper. However, examination of the fluctuating

expression of pertinent markers should reflect the dynamical changes of cells within the stem cell compartment.

It should be noted that the marker modelled should not be taken as a direct readout of any given substate since at the moment we have no proper marker for substates. The most appropriate marker would sensitively reflect the pluripotency of the cell, as well as having a dynamic, heterogeneous expression that has been associated with substate behaviours previously. The approach adopted here does not look for absolute marker expression, but the rather interrogates the dynamics of that marker expression with respect to a population over time. An adapted model of Waddington's canalization of development purports that cells within a specific substate are expected to be more stable than cells inter-substate (Figure 3.1, (Andrews, 2002)). Therefore, we look specifically for indications for marker expression levels that are more stable over time and that less stable marker expression levels tend towards: termed 'attractors'. Attractors represent equilibria in the stem cell substate landscape visualized as wells or depressions, where cells are liable to reflect observable behavioural phenotypes.

A dynamical model of the system would allow determining analytically the location of these equilibrium points in the state-space defined by the marker variables. Subsequently, it should be possible to isolate cells in different putative substates that can be tested further for their lineage biases or other differences in biological behaviour. If there are putative substates identified, they require investigation to see whether they are in fact representative of substates with different behaviours. Cells in a substate

should be more uniform in their behaviour than those between substates and cells in different substates should behave differently in some manner, for example with regard differentiation lineage biases. However, the way in which substates manifest differing behaviour could be varied and unexpected.

In order to address the problem of stem cell substates identification, a new method to characterize the dynamics of stem cell population was developed. This method involves measuring the marker expression patterns of distinct cell fractions within the stem cell compartment at regular time intervals over a period of time. The experimental data generated takes the form of sequences of probability density functions that reflect at population level individual state transitions for cells within the stem cell compartment. The behaviour of heterogeneous stem cell populations, as reflected by FACS measurements of a sensitive pluripotency marker, was subsequently modelled using a technique recently developed by (Nie X, 2013).The model not only predicts the evolution of the pluripotent marker distributions over time but also the location and stability of equilibrium points that are potential substates.

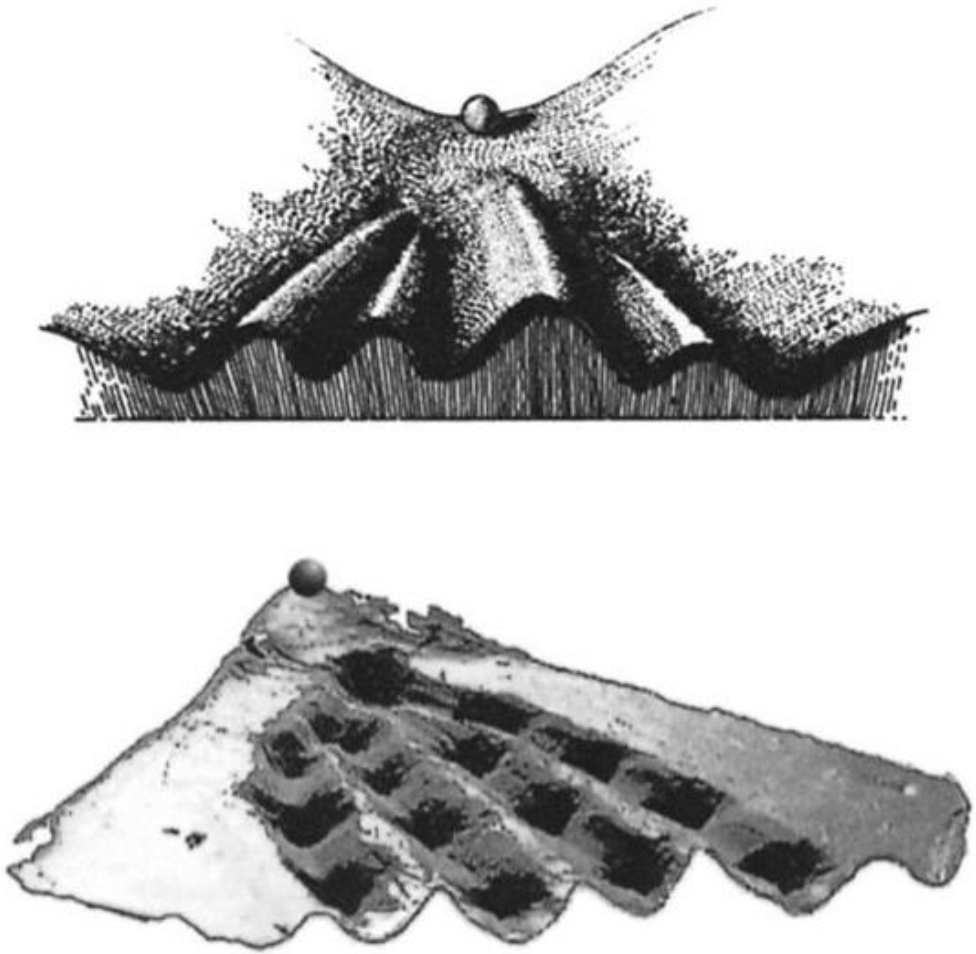

Figure 3.1 – Waddington's canalisation of development**.** Visual representation of Waddington's canalisation of development. The "ball" represents a potent cell and the valleys in the landscape represent lineage choices and differentiation along with the progressive loss of potency.

a.) Classic visualisation of Waddington's canalisation of development where the cell continues rolling through valleys until terminally differentiated.

b.) Interpretation by Andrews (2002); Valleys are nuanced with divots in which the ball (or cell) may reside during the same process of differentiation as in a.). Here the divots represent stable attractor points which manifest themselves phenotypically as cell types that are stable but not yet terminally differentiated. Regions between divots are unstable cell states in which the cell may only transiently reside until it comes to a new, stable attractor state.

Figure from Andrews, 2002

3.2 Stage Specific Embryonic Antigen 3

The ideal marker for the delineation of substates within the stem cell compartment is one that has a strong association with pluripotency, is heterogeneously expressed and whose expression is itself dynamic. The cell surface antigen Stage Specific Embryonic Antigen 3 (SSEA3) represents an ideal candidate in this case.

The expression of SSEA3 and its association with pluripotency have been studied in detail elsewhere and it is clear that with human pluripotent stem cells, SSEA3 is expressed and is one of the first known cell surface antigens to be lost from cells during differentiation (Draper et al., 2002; Enver et al., 2005a; Kannagi et al., 1983b; Shevinsky et al., 1982). Furthermore, it has been proposed that SSEA3 is lost from cells prior to differentiation commitment proper, suggesting that SSEA3 expression may be sufficient to identify a stem cell as pluripotent, but it is not necessary for pluripotent stem cell identity (Brimble et al., 2007). In normal culture, human ES cells present a very heterogeneous expression pattern of SSEA3, with cell populations occupying a broad range of expression, including cells that do not present SSEA3.

The expression of SSEA3 is also dynamic with cells being able to change their SSEA3 expression over time. For example, cells that are sorted for SSEA3 positive and negative fractions and cultured separately eventually yield an SSEA3 expression pattern just as heterogeneous as the original parental population, although the negative population reconstitutes the expression of the parent population considerably faster (Olariu et al.,

2009). That being said, the relationship between SSEA3 and pluripotency is not causal and the biological function of SSEA3 on ES cells, if any, remains enigmatic. As a globo-series glycolipid, SSEA3 expression is not the direct determinant of any particular gene but is instead the product of several glycosyltransferases and so represents the integration of several processes that culminate in the production of the SSEA3 antigen. Therefore, the extent of SSEA3 expression presents an indirect measure of cellular behaviour rather than as a direct determinant of gene expression (See Section 1.5).

Due to the heterogeneous expression of SSEA3 on human ES cells, coupled with its strong association with the pluripotent state in humans, SSEA3 represented an ideal marker to explore ES cell heterogeneity in culture.

3.3 Introduction to modelling approach

The investigation focussing on SSEA3 expression and its dynamics is predicated on the hypothesis that the heterogeneity displayed is the result of deterministic chaotic behaviour rather than a random, stochastic manifestation (See glossary table 3.1). Chaotic systems generate densities of states and can be studied using probabilistic approaches. The main difference is that in the case of chaotic systems the evolution of the system is governed by a deterministic rule rather than a stochastic process. Since embryonic stem cells are programmed to follow very precise development programs it is reasonable to assume that the deterministic rules that hESCs follow 'in vivo' may lead to chaotic behaviour under the culture conditions.

Table 3.1 – Glossary of Modelling Terms

Term	Meaning
Probability Density Function	With respect to an SSEA3 distribution; A manipulation of the raw count histogram of a population's SSEA3 distribution to reflect the likelihood of SSEA3 expression intensity. This normalisation procedure across the range of SSEA3 intensity allows for comparison of SSEA3 expression distributions taken from different cell populations that may have been acquired using different total cell numbers.
Chaotic	When used in the context of chaos theory, a chaotic behaviour refers to an apparently random but deterministically driven behaviour (Thietart and Forgues, 1993).
Determinism	A deterministic system is one in which no randomness is involved in the development of the future states of that system. A knowledge of the present allows accurate prediction of the future.
Deterministic Chaos	A deterministic system is chaotic whenever its evolution is extremely sensitive to the initial conditions; where two quite different trajectories may emerge and exponentially diverge over time starting from two different but close initial conditions (Boccaletti et al., 2000). Although Deterministic chaos is predictable since it may be described without the introduction of random variables, the quality of the prediction is dependent on precise knowledge of the initial conditions. This feature is often popularised as the butterfly effect, where slight changes in initial conditions may have very different latent effects. Edward Lorenz summarised as: "When the present determines the future, but the approximate present does not approximately determine the future." (Lorenz, 1963)
Stochastic	A Stochastic event is one that is unpredictable because it is reliant on a random variable. This differs from that of an event resulting from deterministic chaos since there is no need to use random variables in a deterministically chaotic system.
Probabilistic approaches	Considering the outcome states of a system in terms of the probability of an individual component exhibiting a particular behaviour. For instance, the probability of any given cell displaying any particular SSEA3 intensity within a defined population.
Dynamic Systems	A system whose states change with respect to time based upon its current state.

Many systems in the real world exhibit chaotic behaviour (Ott, 1993) and indeed some of the best known examples of chaotic systems were originally proposed to model population dynamics (May, 1976). Other examples of chaotic behaviour include that of predicting weather patterns, where although these may be governed by deterministic rules, prediction of future weather is confounded by imprecise knowledge of the present (Lorenz, 1963; Palmer, 2000). One of the simplest examples of a deterministic system that exhibits chaotic behaviour is the motion of a double pendulum (Shinbrot et al., 1992). The motion of a single pendulum is extremely easy to predict with approximate initial conditions, however the motion of a double pendulum is extremely sensitive to initial conditions, making its future motion difficult to predict. Two double pendula that are set in motion with a miniscule difference in initial conditions may appear in phase for some time before their trajectories exponentially deviate from each other (Shinbrot et al., 1992). An alternative simple example is that of a quincunx (or Galton Board) where a ball is dropped through a harrow of pins (Judd, 2007). Although the ball's motion may appear random, it is actually determined by a series of individual collisions with the pins, determining its velocity for the next collision and so on. Slight changes in the initial condition of the ball such as linear velocity or rotational velocity results in different trajectories (Judd, 2007) . Deterministic chaos is perhaps best distinguished from a stochastic system (*i.e.* relies upon random elements) by the phrase "When the present determines the future, but the approximate present does not approximately determine the future" as coined by Edward Lorenz who pioneered Chaos theory (Lorenz, 1963).

In many cases in which it is of interest to study chaotic systems, it is not possible, or is extremely challenging to observe individual point trajectories over time and instead the distributions of the variable of interest are measured at regular intervals. For instance, here it is very difficult to know by direct observation how any particular cell's SSEA3 expression will change over time, yet its SSEA3 expression remains observable at any discrete instant.

Recently Nie & Coca introduced a method to infer the models of discrete time chaotic dynamical systems based solely on sequences of density functions measured experimentally. Specifically focussing on one-dimensional chaotic maps described by

$$x(t_{k+1}) = S(x(t_k))$$

Where $x(t_k)$ is the variable of interest at a given moment in time (t_k), S is a non-linear function, $t_{(k+1)}=t_{(k)}+\Delta t$ is the future timepoint and Δt is a constant time increment. In the particular case here, x denotes the SSEA3 fluorescence level of a cell population as an observed probability density function and Δt is 24 hours. Thus the SSEA3 dynamics of a cell population may be explored and, given the relationship between SSEA3 expression and pluripotency employed to interrogate the stem cell substate hypothesis (Nie X, 2013).

Although simulated data have been successfully modelled with this approach, we provide here real data for the modelling procedure within the SSEA3 heterogeneity context. By taking cells from the population of SSEA3 expressing cells and following their

change in SSEA3 expression over time, a model of the rate of change between particular intensities of SSEA3 from one day to the next is made. With a comparison made with enough samples of SSEA3 expressing cells and their transition between time points, a comprehensive model explaining these transitions is constructed. Therefore, large populations of SSEA3 expressing NTera2 cells were cultured to be stained for SSEA3 and separated into different fractions of differing SSEA3 intensity by Fluorescent-Activated Cell Sorting (FACS). Following the evolution of the resulting SSEA3 fractions subsequently provides temporal information on how the SSEA3 distribution behaves depending on its initial distribution. The transition from one day to the next could be modelled by considering each SSEA3 distribution to be a probability density function of which SSEA3 intensity any cell from that population is likely to display. The probability density function redefines the initial histogram of a population's SSEA3 profile in terms of the probability of any cell expressing any particular SSEA3 intensity; essentially normalising the raw count data to a proportion that allows for SSEA3 profile comparisons having taken into account differences in the number of cells used to generate the profiles. This probability density function describes the SSEA3 distribution across the whole intensity range and thus generates vectors for each sample that may be readily compared irrespective of time point or raw count data. Following the SSEA3 evolution from any particular sorted set of cells is then described by determining the transition matrix (S) that will describe the conversion of a sample's vector from one day ($x_{t(k)}$) to the next ($x_{t(k+1)}$).

3.4 Generating and Interpreting the Model

Modelling the evolution of SSEA3 intensity within culture populations over time is performed by the examination of many independent observations of the SSEA3 intensity within populations as it changes with respect to time. The trajectories of SSEA3 intensity evolution are estimated by the examination of different populations that have been sorted by their SSEA3 expression and the way in which these sorted populations go on to generate their own SSEA3 intensity profiles. Examining the way SSEA3 intensity transitions over time (daily in this case) in these different populations provides insight of the underlying system that governs these transitions. Multiple (~35) SSEA3 intensity transitions from one day to another are used to generate an optimised model that is able to predict SSEA3 intensity transitions for any given population.

Observation of the SSEA3 profiles to be used in this modelling procedure is performed by flow cytometry that provides SSEA3 intensity information of the population in the form of a histogram with a total cell count measured. These distribution data are each transformed into that of a probability density function (x); maintaining the shape of the SSEA3 intensity distribution for each measured population and so by treating these data in a probabilistic approach enables different distributions to be compared against each other in a manner that normalises for differences in the total number of cells used to generate these distributions (Figure 3.2).

These probability density functions are then partitioned (λ) along the intensity axis (Conceptual example figure 3.2). The process of partitioning the probability density functions is described elsewhere (Nie and Coca, 2013) The probability of any particular cell occupying one of these partitions is related to the proportion of the population that exists within that segmentation.

Thus this partition may be used to convert the entire probability density function into that of a vector, with each number in the vector relating directly to its corresponding interval along the SSEA3 intensity axis.

Converting the probability density functions into their own unique vector format permits the calculation of a transition matrix (P) that describes the specific transition of a vector from one timepoint (t_k) onto the next timepoint (t_{k+1}). Where,

$$x(t_{k+1}) = P(x(t_k))$$

P is the matrix that maps this specific transition of the probability density function (x) of a temporally consecutive pair of observations of SSEA3 intensities from the population. This transition matrix (P) only describes one particular transition, albeit accurately, but it does not describe the way a population's SSEA3 dynamics behave generally. In order to generate a generalised model (S) that describes the underlying transitions of SSEA3 intensity comprehensively and generates predictions for any probability density function of SSEA3 intensity, many individual transitions (P) must be calculated. These numerous transition matrices (P) undergo together a least-squares optimisation process to culminate in a generalised model (S) that describes SSEA3 intensity dynamics (Nie and Coca, 2015). Where

$$x(t_{k+1}) = S(x(t_k))$$

The generalised model (S) may be presented graphically in order to visualise the behaviour of a given SSEA3 intensity/distribution from one timepoint to the next (conceptual example in figure 3.3). In such a graphical portrayal, the axes (grey lines) both represent the range of SSEA3 intensity (from 0 to j) on day t_k (x-axis) and day t_{k+1} (y-axis) and the dotted lines that intercept the axes correspond to the partitions (λ) used in the formulation of the model. In figure 3.3, a simple 3 partitioned ($\lambda_1 - \lambda_3$) graphical representation of a hypothetical model (S) is portrayed

(the solid black line) with three examples of what the model would predict with given SSEA3 intensities at time t_k. For the sake of simplicity, each example is only given over one partition, (λ_1, λ_2 or λ_3) however real life examples would most likely involve multiple partitions simultaneously. For a given SSEA3 intensity/distribution at time t_k the prediction for the following day's SSEA3 intensity can be found by reading where that intensity crosses the map of the model (black line) and reading across to the y-axis value to give the predicted SSEA3 intensity on t_{k+1}. The line y=x (red dashed line) is a particularly useful reference line for interpreting the graph of the model since if the model intercepts the line y=x, then a given SSEA3 intensity on that point is not expected to change, for example, an SSEA3 intensity of ½j at t_k is expected to remain at ½j at t_{k+1} (green line). Additionally, if the map of the model lies above or below the line y=x, then the predicted SSEA3 intensity on the following day is anticipated to rise or fall respectively (demonstrated particularly in Figure 3.3 c' and d').

Figure 3.3 (b-d) each show a hypothetical SSEA3 probability density distribution at time t_k with a range of intensities covering their respective partitions (λ_1, λ_2 or λ_3). In each case, the blue arrow underneath represents the application of the model (S) to those hypothetical distributions with figure 3.3 b'-d' representing the predicted probability density distributions at time t_{k+1}. In the case of b, the map of the model (S) shows that across partition λ_1, the model happens to match y=x across its entirety. In this instance, the gradient of the model is equal to 1, which means that the general shape of the distribution remains unchanged but in addition, the line lies on y=x and so the distribution is not transposed to that of a greater or lesser intensity on the following timepoint. As a result, it is predicted that that each intensity maps perfectly back onto itself and so the probability density distribution remains unchanged in b'. The lack of change in distribution from one day to the next exemplified in b - b' is interpreted that this is a stable region for SSEA3 intensity that does not readily change from one day to the next.

In the case of c, the probability density distribution of SSEA3 intensity lies across the range of the λ_2 partition. Figure 3.3 a shows that across the λ_2 partition, the gradient of the model is constant but greater than 1 and therefore the distribution is predicted to stretch across a greater range of intensities on t_{k+1}, which is demonstrated in c' since the predicted distribution can be seen also in partitions $\lambda 1$ and λ_3. Furthermore, the depiction of the model (S) shows that across partition λ_2 the model also intersects the line y=x, meaning that the intensity at that point (½j) will also be present on the following day t_{k+1}. Since these graphs are all described in terms of probability density functions, the area under the curve for the distributions are all equal to one which explains why the maxima in example c' is lower than the maxima in c as well as b'.

The final hypothetical example in figure 3.3 d and d' is the most complicated. The initial SSEA3 distribution at time t_k in d lies across the partition λ_3 and the predicted distribution for time t_{k+1} shown in d'. The model (S) in figure 3.3 a shows that across partition λ_3 three gradients are depicted; two gradients being greater than one, with one gradient being less than one. The two gradients greater than one predict that there will be a spread of SSEA3 distribution (as seen with example c and c'), however the gradient that is less than one may be interpreted to predict that SSEA3 intensities will condense around that intensity for the following timepoint. The condensation around this region of the model (S) with the gradient less than one is reflected by the large population of cells in d' λ_3 albeit across the narrow range that they are predicted to occupy in λ_3 at time t_{k+1}. This is due to the fact that approximately half of the range of SSEA3 intensity across λ_3 maps into a narrow range on λ_3 for the following timepoint. Furthermore, the model (S) predicts that d' will have an SSEA3 distribution that covers the entire range of λ_2 and some of λ_1, however it is expected that there will be a greater population in λ_1 than λ_2 given the small range of intensities from λ_3 that are predicted to enter λ_2 compared to the range of intensities predicted to enter λ_1. Indeed, this is reflected by the bi-modal distribution in d' where

there is a large area under the curve occupied in λ_1 compared to λ_2. The final point of note is that across partition λ_3, no part of the model lies on nor above the line y=x so the entire range of SSEA3 intensity is expected to be lower at timepoint t_{k+1} than at t_k if within partition λ_3 at t_k.

Finally, the predictions generated at time t_{k+1} may all be iterated against the model again if they are used as the next t_k. In this way, the distribution in b' could be used as the input for the model in order to generate a prediction for the following timepoint. Since b predicted b' at time t_{k+1} and the distribution of b' was identical to b, it is further predicted that at time t_{k+2} that the distribution will still remained unchanged from that of both b and b'. A stable, unchanging distribution for future timepoints is not predicted for the distributions from c and d since, in part, their predicted counterparts c' and d' now have intensities in other partitions. If run iteratively enough times it is likely that the SSEA3 distribution in this example will always end up approximately similar to that of b and b' since anything in partition λ_1 is not predicted to escape λ_1 and anything that ends up in the first half of the λ_3 partition will decrease, with most going into λ_1. Anything that is of particularly high intensity in λ_3 is anticipated to form a compact distribution that is in the lower intensity range of partition λ_3 which, as already mentioned, will mostly enter λ_1 from which there is little chance of escape.

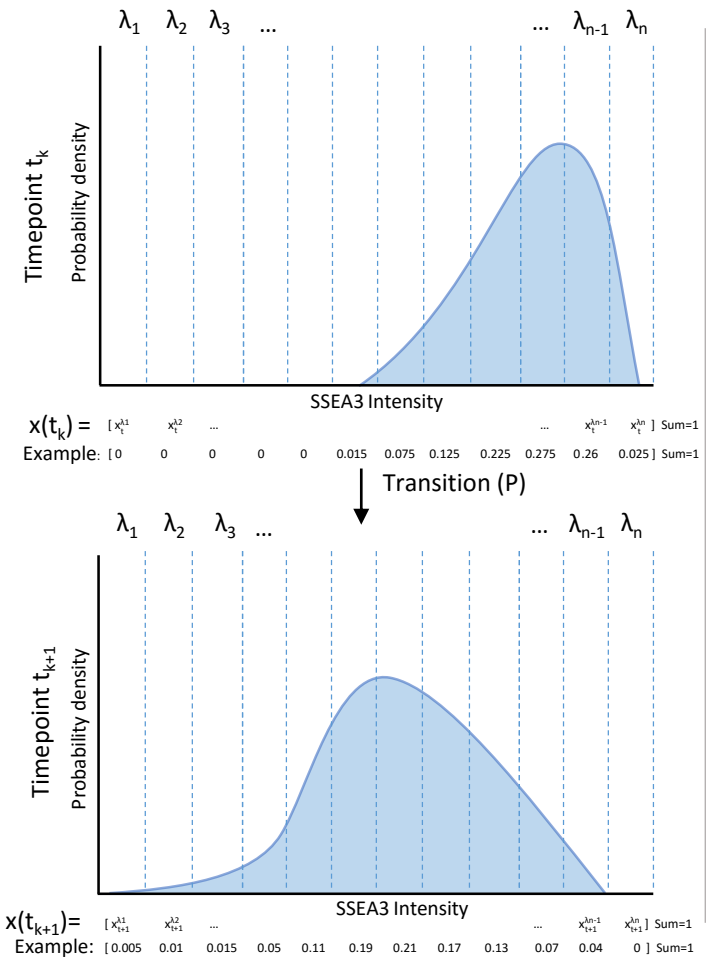

(1) $$\sum_{\lambda 1}^{\lambda n} x(t_k) = \sum_{\lambda 1}^{\lambda n} x(t_{k+1})$$

(2) $$x(t_k) = \begin{bmatrix} x_t^{\lambda 1} \\ x_t^{\lambda 2} \\ \vdots \\ x_t^{\lambda n} \end{bmatrix}$$

(3) $$x(t_{k+1}) = \begin{bmatrix} x_{t+1}^{\lambda 1} \\ x_{t+1}^{\lambda 2} \\ \vdots \\ x_{t+1}^{\lambda n} \end{bmatrix}$$

(4) $$x(t_{k+1}) = P.x(t_k)$$

Figure 3.2 – Conceptual example of the modelling procedure for one hypothetical distribution transition. The two distributions shown represent two SSEA3 distributions from one day (t_k) to the next (t_{k+1}). Both distributions are normalised by means of conversion into a probability density function and the sum of the area under each curve is equal to 1 (equation (1)) to enable a comparison of the distributions independent of the total number of cell counts used to generate the raw data. The distributions are partitioned, symbolised by the series $\lambda_1 \ldots \lambda_n$ (dashed blue lines). All distributions in the dataset are partitioned in the same way. The partitioning method and calculation is described elsewhere (Nie & Coca, 2015). The proportion of the distribution occupying each partition is calculated and converted into a vector format (Equations (2) and (3)); again the sum of the elements of these vectors are equal to one and therefore, each other (hypothetical example in figure; equation (1)). These distributions can be described as shown in equation (4), where the distribution on day t_{k+1} is equal to the distribution on day t_{k+1} multiplied by some factor, P that represents the transition matrix for these distributions between timepoints. The transition matrix, P, describes very accurately this one particular transition and is extremely unlikely to describe all the transitions of a population. To acquire a generalised model of transition dynamics (S) of the distribution in question across a population, (in this case SSEA3), many transition matrices are acquired that describes multiple types of transition (*i.e.* different starting distributions) over consecutive time points. These multiple P undergo an optimisation process to generate a generalised model (S).

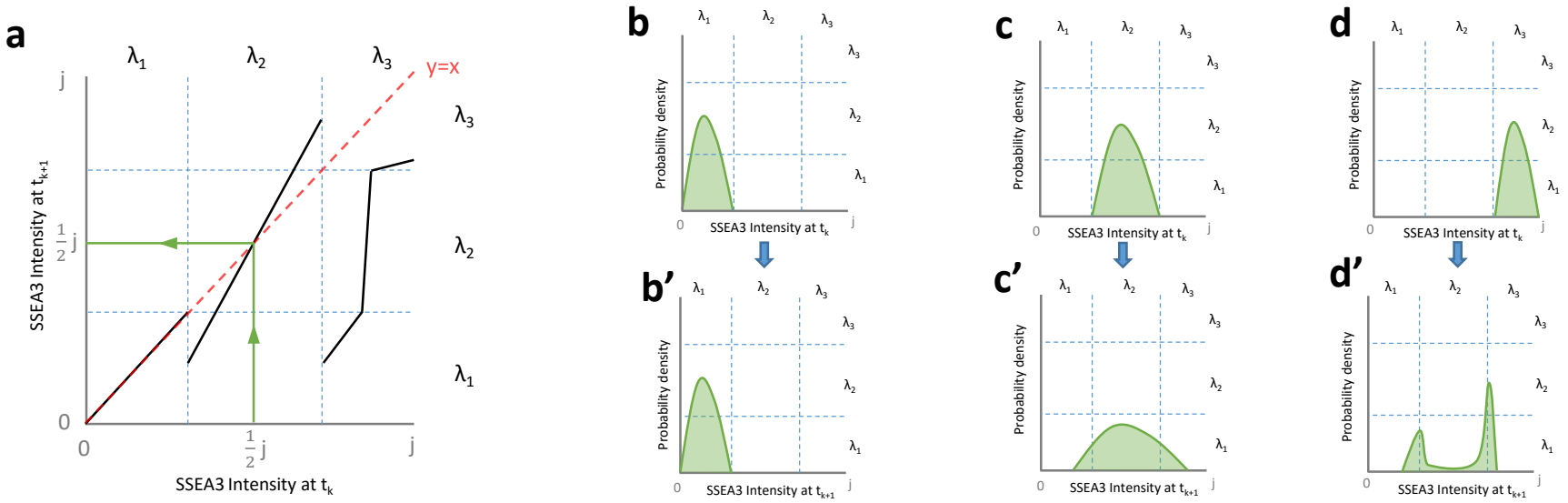

Figure 3.3 – Hypothetical map of a generalised model and transition predictions. A generalised model (S) of distribution transitions determined (as described in Figure 3.2) may be viewed graphically as a map of the model (a). Both axes represent an SSEA3 intensity distribution (from 0 to j) at time t_k (x-axis) and t_{k+1} (y-axis), with the model describing the relationship between them (black lines). The partitions used for generating the individual distribution transitions are plotted on both axes (blue dashed lines, λ_1.. λ_3), where each partition has a direct correspondence on each axis *i.e.* λ_1 on the x-axis covers the same SSEA3 intensity range on the y-axis. The map itself (black lines) describes how a given SSEA3 intensity at time t_k is predicted to transition to for time t_{k+1}. For interpreting the model, the line y=x (red dashed line) is particularly useful since whenever the map intersects the line y=x, that point is not expected to change and is termed an equilibrium point (*e.g.* ½j; green line). The relative position of the map of the model to the line y=x is also useful since where the map is above or below the line y=x, then the predicted SSEA3 distribution is more or less intense respectively. Example hypothetical distributions (b-d) and their predicted distributions (b'-d') are explored. For the sake of simplicity, the hypothetical distributions are confined to the range of individual partitions, although in reality this is rarely ever the case. Distributions are described in terms of probability density and so the area under each curve, whether original or predicted are equal to one. b) The map of λ_1 partition lies exactly on the line y=x, and so the distribution is expected to remain unchanged (b'). c) The map of λ_2 is of one gradient, greater than one, that intersects the line y=x. Therefore, the predicted distribution is covers a greater range of SSEA3 intensities (c'), but the point at ½j remains unchanged. d) The map of λ_3 partition is the most complicated; it is entirely below the line y=x and has multiple gradients. The most intense population in λ_3 is predicted to become slightly less intense and condense around the lower region of λ_3, a small proportion of the population is predicted to cover the entirety of λ_2 and the remaining, larger, portion of the population expected to occupy λ_1 which altogether results in a bimodal distribution (d').

3.5 Cell line used

Modelling the heterogeneity of human pluripotent stem cells with respect to SSEA3 expression mandates the use of a pluripotent cell line that also displays the SSEA3 epitope. As a proof of concept approach, the pluripotent EC cell line NTera2.D1 was used. NTera2 also has the advantage that it is a robust cell line that is easy to expand, which made it an ideal candidate since a large population of cells were required in the first instance. Indeed, the culture of EC lines is considerably easier than that of ES cell lines since EC cell culture requires less expensive reagents and EC cells display a "robustness" that early passage ES cell lines simply do not. The result of such robustness is the easy expansion of cell lines to achieve large cell numbers for experimentation that experience an extremely low rate of spontaneous differentiation (ISCI, 2007). NTera2 in particular is a long-standing pluripotent EC cell line that also displays heterogeneous expression of SSEA3 in culture that may be readily induced to differentiate *in vitro* in response to various differentiation cues such as induced by all-trans retinoic acid or Hexamathylene Bisacetamide (Andrews et al., 1990). As outlined previously, NTera2 has also been shown to present at least two substates within the stem cell compartment (Tonge et al., 2010). Therefore, due to its robust nature, easy expansion, pluripotency, heterogeneous expression of SSEA3 and demonstrable substates, NTera2 was a prime candidate cell line for modelling in this proof of concept approach.

3.6 Summary of introduction and main aims

Here we aim to develop a method by which the dynamics of SSEA3 within the stem cell compartment may be explored. We anticipate that, by being able to predict these dynamics and how readily cells with particular SSEA3 intensities are liable to maintain or change that level of expression, clues leading to substate identity and isolation from the stem cell compartment will be found. Pursuing these clues should help us to readily and repeatedly isolate these substates that should behave in a more uniform manner. This proof of concept approach, initially applied to SSEA3 in the NTera2 context, will open up other avenues by which heterogeneity may be explored in other cell line contexts and with other markers. Adopting a flow cytometric approach in the first instance is easier for data generation but it does require a large number of cells to complete, which is one of the reasons that the human EC cell line was chosen. Therefore, we also aim to develop a strategy that can be applied using substantially fewer cells that can be readily applied to cell lines, such as human ES cells, which are more expensive to culture and less robust. The method we exploit here is *in vitro in situ* cell culture immunofluorescence on the InCell analyser imaging platform where fewer cells are required for population analysis.

3.7 Overview of Approach

In order to model the SSEA3 dynamics within the NTera2 population, the approach adopted for interrogating this system was based upon dividing a population of NTera2 cells into sub-populations. The experiment was replicated three times, with each replicate referred to as a "Batch." Each batch underwent workflow outlined in Figure 3.4, where a number of sister flasks of NTera2 cells are expanded to provide enough cells for the experiment and represent the "parental population." The cells in these flasks were then harvested, stained and measured for SSEA3 using the MC631-2C2 antibody coupled with flow cytometry. Cells were then sorted based upon their SSEA3 expression profile by Flow Assisted Cell Sorting (FACS). Five separate culture vessels, one for each day, were used to culture samples of each sub-population (or "fraction"). In this way, samples of cells from each fraction were plated in five separate culture vessels, where each day, one of these cultures would be expended for analysis of their SSEA3 distribution. Once the SSEA3 distribution of each fraction for each day was acquired, data was sent to Dr. Xiaokai Nie for modelling the SSEA3 dynamics of the population (Materials and methods, Conceptual overview Section 3.4).

Given the replicates available, the SSEA3 distribution data from Batch 3 was used to model the SSEA3 dynamics since it was the most complete dataset (Figure 3.7). Data collected from Batch 2 was used to test against the model generated from the Batch 3 data (Figures 3.6, 3.12, 3.13). No viable data was collected from Batch 1 and so is not referred to hereafter.

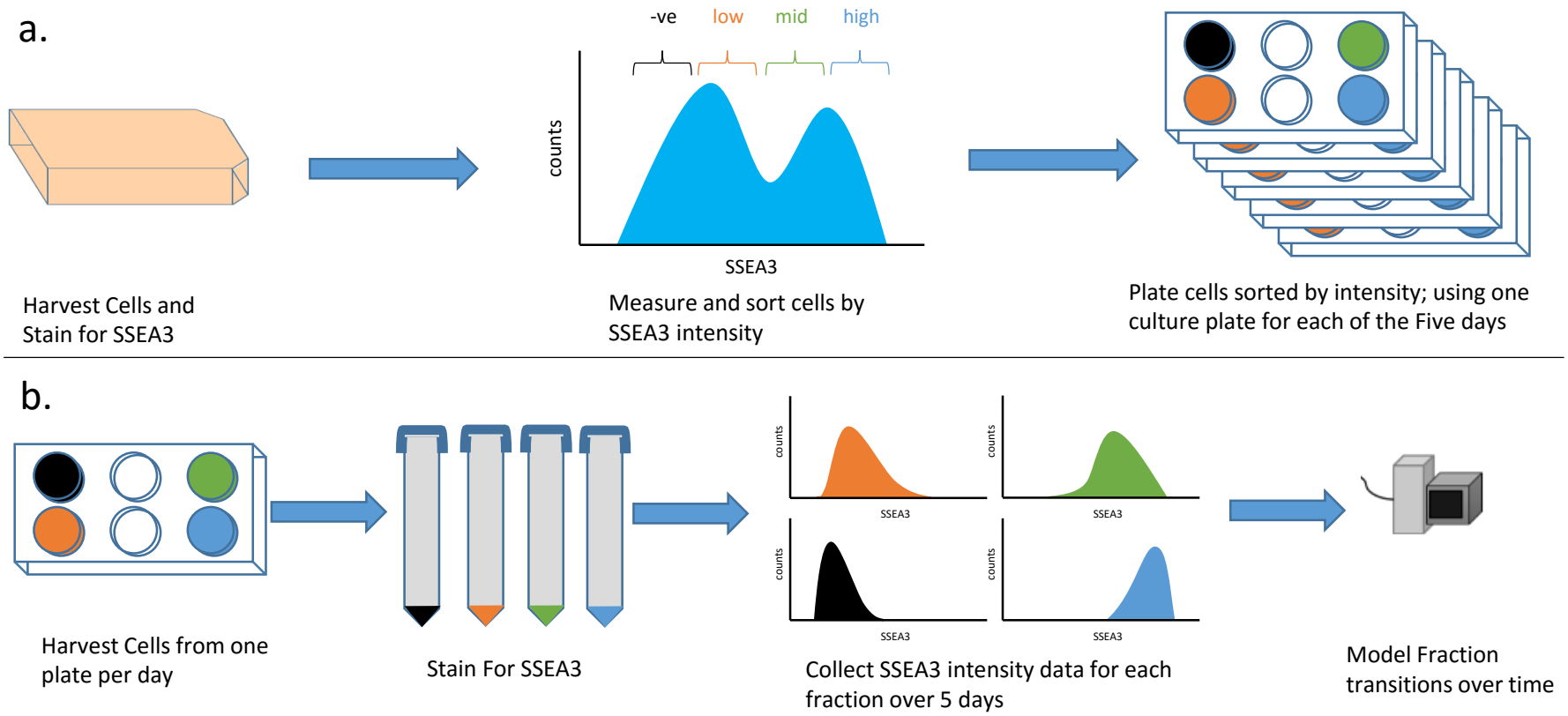

Figure 3.4 – Modelling SSEA3 Dynamics Workflow for cell sorting and modelling SSEA3 dynamics in a cell population. **a.)** Parental cell population is cultured and expanded in order to provide enough cells for the experiment. Cells are then harvested, stained for SSEA3 expression and sorted into subpopulations ("fractions"). One culture plate per day is prepared in which all fractions are represented. **b.)** The fractions from one plate for each subsequent day are harvested, stained and analysed for SSEA3 expression separately. Finally, data from all five days of the experiment are sent to model the populations' SSEA3 dynamics.

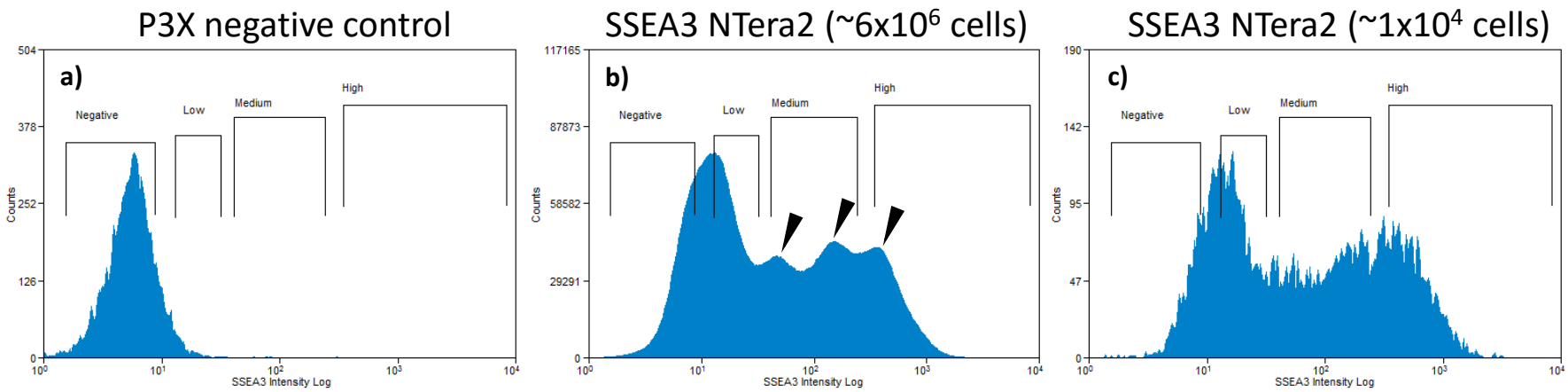

Figure 3.5 – SSEA3 Expression in NTera2 Populations. Examples of flow cytometric analysis against populations of NTera2.D1 cell line examined via indirect immunohistochemistry for expression of SSEA3 and P3X. **a.)** Negative control for off-target binding assessed using P3X primary antibody permits the designation of a baseline level of fluorescence exhibited by the sample. The baseline is set to be apparent at around 10^1 intensity. **b.)** A large population of Ntera.D1 (~$6x10^6$ cells) reveals a broad range of SSEA3 expression exhibiting multiple peaks (arrows). This particular population was used in a sorting experiment to collect Four different fractions of different, non-overlapping SSEA3 expression ("negative", "low", "medium" and "high") which are demarked accordingly. **c.)** An example of an SSEA3 stain performed on a more usual sample size of NTera2.D1 (~$1x10^4$ cells) cells from regular laboratory experiments; note that although there is a large distribution (as in a.), the lower cell count does not enable the same degree of the multimodal characteristic seen in a.) to be resolved.

Results

3.8 Parental population

Cultures of NTera2 were expanded (described in methods) in order to provide the cell number required for the experiment (100,000 cells per fraction per timepoint per rep). This equated to approximately eight T-75 flasks of NTera2 cultured per sort; containing approximately $1.2x10^8$ cells per sort. Following staining for SSEA3 (See materials and methods), samples were subject to a gating regime to exclude events that do not represent cells such as debris and cell doublets (See materials and methods). A baseline for off-target antibody binding effects was obtained as a negative control by simultaneously staining a separate randomly acquired subsample of the cell population with P3X as opposed to SSEA3 as the primary antibody.

A typical examination via flow cytometry of a large population of NTera2 cells reveals a multimodal distribution of SSEA3 intensity; with several peaks over a large range of expression (Figure 3.5b). This pattern of SSEA3 expression cannot be attributed to non-specific binding of the secondary antibody used for immunofluorescence since the P3X negative control does not also exhibit the same pattern (Figure 3.5a). It is worth noting that some of the distinct modal regions (arrows) only become clear when dealing with a large sample of Ntera2 cells (~10^6 cells) (Figure 3.5c). Thus, the heterogeneous expression of SSEA3 in the NTera2 was confirmed and a four-way sort was performed to include different, non-overlapping levels of SSEA3 intensity representing negative, low, medium and high levels of expression and dubbed eponymously (Figure3.5b). Cells from

these four fractions were collected and separately plated at a density of 10,000 cells/cm^2 in six-well plates. Five replicate wells were seeded and incubated for each fraction in order to perform further flow cytometric analysis on these samples over the subsequent five days; harvesting and exhausting one replicate per fraction per day for this purpose (Figure 3.4).

It was plausible that cell sorting and/or antibody staining could affect behaviour in the resulting cell fractions. Therefore, in order to account for any effects that cell sorting or antibody staining may have on cell behaviour, three other conditions were included: Unstained Unsorted (UU), Unstained Sorted (US) and Stained Unsorted (SU). These subsamples were from the same population of harvested cells used for the sort. The fractions UU and US were both exempt from the antibody staining protocol prior to seeding, whereas fractions UU and SU did not undergo the stressors associated with cell sorting (UU and SU conditions were plated at a lower density in order to account for anticipated lower mortality 1,000cells/cm^2). If there were any major effects caused by these processes, it was anticipated that it would be noticeable by discrepancies between the populations resulting from these conditions.

Biological replicate sorts were performed on separate days. To avoid confusion, replicates as distinguished by sort day were termed batches and numbered chronologically. In an attempt to ensure fair comparison between batches, flasks used for sorts were all cultured to have similar confluence of between 90-100% on the day of harvest for their sort. Ensuring comparable confluency between batches necessitated

staggered culture of flasks in preparation for use. This was achieved by adjusting the seeding densities of flasks several generations in advance so that the regular time for passage was offset between batches by at least one day. Once cultures for each batch were staggered, all cultures were passaged several times using the regular split ratio in order to re-establish more usual conditions for several generations prior to their use in the sorts.

3.9 Evolution of the sorted fractions

Cell fractions were plated in separate vessels for each fraction and timepoint in order to facilitate cell harvest and flow cytometric analysis of cell cultures from each fraction daily over the following five days. Cells were once again stained to elucidate SSEA3 expression via indirect immunohistochemistry. Once collated, the SSEA3 dynamics of the various sort fractions were examined using data from Batches 2 and 3 (Figures 3.6, 3.7 and 3.8).

Examination of the SSEA3 population dynamics between fractions reveals that all fractions generate cells from all other fractions by the end of the experiment and indeed from the range of the original distribution of the parental population. It is also clear that the propensity of a fraction to repopulate the parental distribution differed between fractions; for example, the High fraction took considerably longer to reach a distribution similar to the parental population than the medium and low fractions. There were no cell fractions that did not eventually re-occupy the SSEA3 expression range of the parental population, although the low and medium fractions did so at a greater rate

than the negative and high fractions. Indeed, the High fraction consistently took longer to reconstitute a distribution that looked similar to that of the starting population.

The control fractions of UU, SU, US from Batch3 revealed relatively little difference between conditions over time with regard to the SSEA3 dynamics of the population, effectively mimicking each other (Figure 3.8). In Batch2 there was some variation between the conditions, which is exemplified by the poor resolution in conditions SU and UU that was the result of low cell numbers, indicating mediocre cell growth in these conditions. Due to the complete nature of the Batch3 dataset as well as its consistent and concordant control samples Batch3 was chosen for use in the modelling procedure.

Batch 2:					
Fraction:	Negative	Low	Medium	High	Parental Population
Day 1:	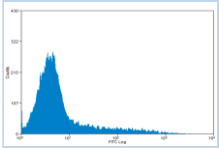	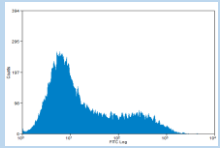	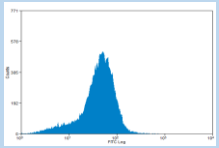	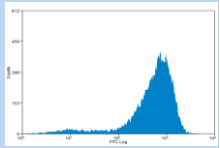	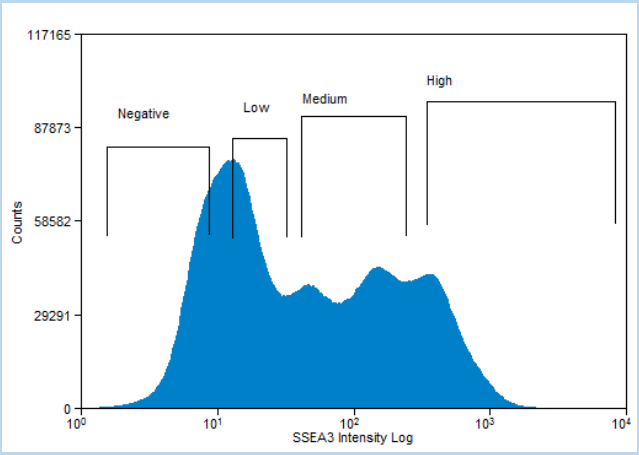
Day 2:	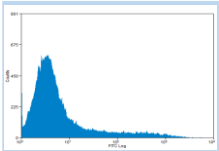	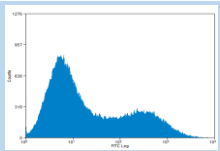	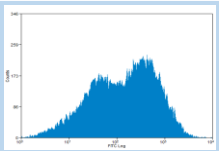	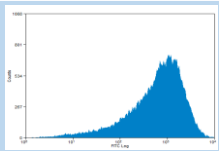	
Day 3:	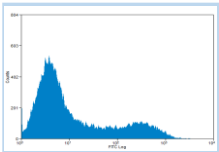	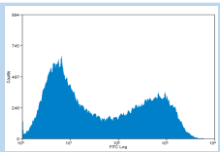	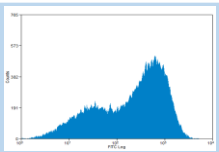	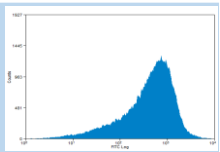	
Day 4:			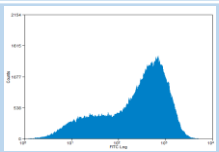	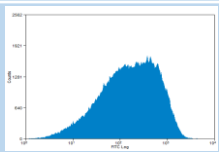	
Day 5:	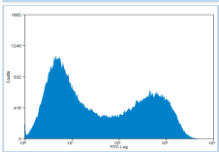	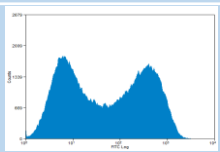	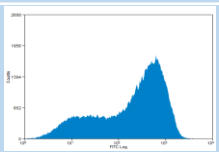	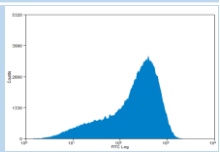	

Figure 3.6 – Evolution of SSEA3 Dynamics in Batch 2. Fractions taken from the parental population (see figure 3.3) that have been subsequently plated and analysed over the following five days. For all fractions there is a tendency towards the heterogeneous distribution as seen in figure 3.1, however some fractions acquire this heterogeneous phenotype at a greater rate than others (e.g. the "High" fraction takes longer to re-establish that distribution than the "Medium" fraction).

Batch 3:					
Fraction:	Negative	Low	Medium	High	Parental Population
Day 1:	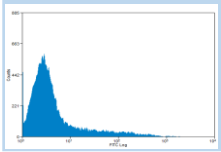	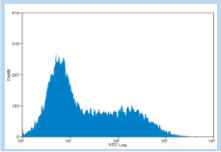	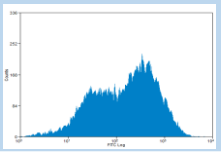	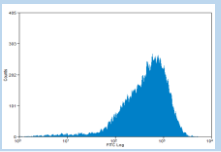	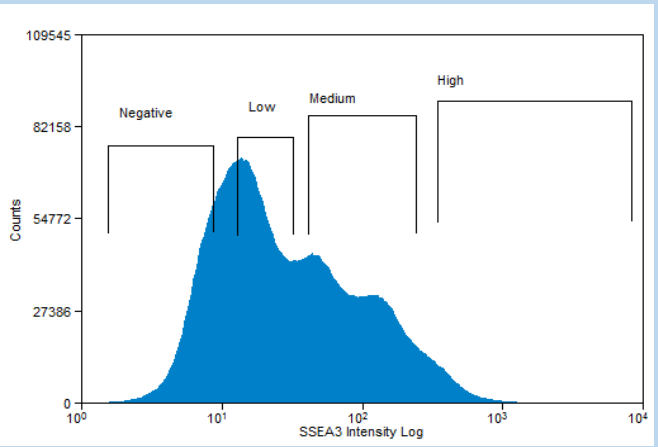
Day 2:	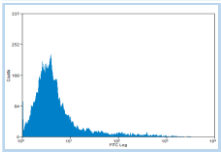	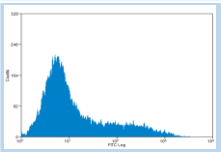	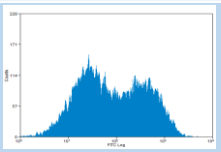	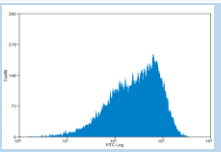	
Day 3:	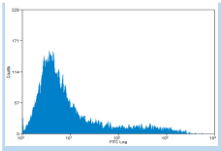	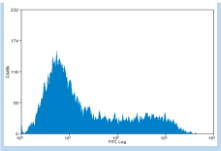	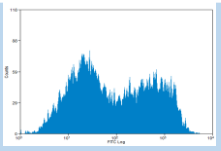	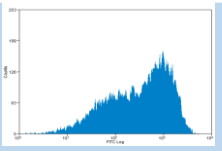	
Day 4:	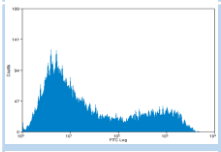	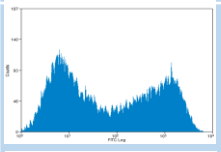	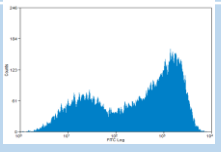	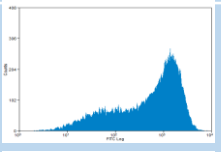	
Day 5:	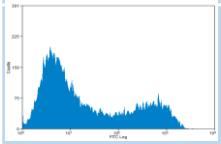	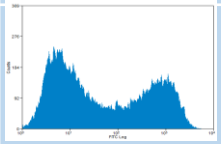	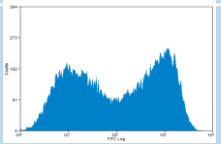	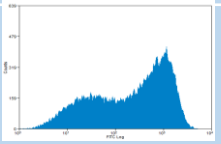	

Figure 3.7 - Evolution of SSEA3 Dynamics in Batch 3. Fractions taken from an alternative parental population to that in figure 3.3 that have been subsequently plated and analysed over the following five days. For all fractions there is a tendency towards the heterogeneous distribution of the parental population, however some fractions acquire this heterogeneous phenotype at a greater rate than others (e.g. the "High" fraction takes longer to re-establish that distribution than the "Medium" fraction).

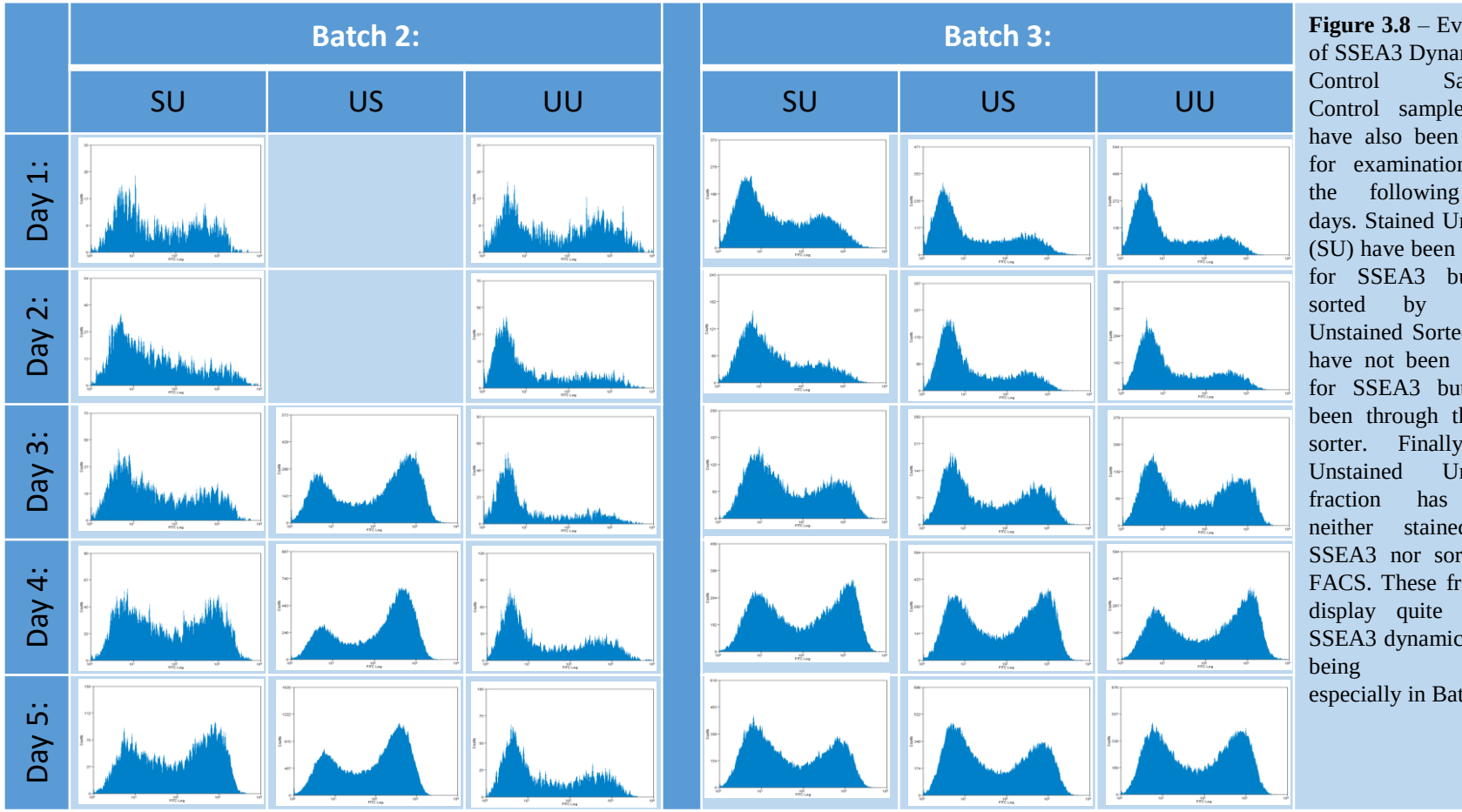

Figure 3.8 – Evolution of SSEA3 Dynamics in Control Samples. Control samples that have also been plated for examination over the following five days. Stained Unsorted (SU) have been stained for SSEA3 but not sorted by FACS. Unstained Sorted (US) have not been stained for SSEA3 but have been through the cell sorter. Finally, the Unstained Unsorted fraction has been neither stained for SSEA3 nor sorted by FACS. These fractions display quite similar SSEA3 dynamics since being plated; especially in Batch3.

3.10 Map of the model

The dataset from Batch3 (See section 3.7) was used for modelling and a map of the model is shown in Figure 3.9. Such maps depict aspects of the rules underlying chaotic systems modelled in this manner and are designed to illustrate how systems change over time (Conceptual examples in figures 3.2 and 3.3). Here for instance, SSEA3 intensity is presented on both axes; with SSEA3 intensity (x) at day "t_k" on the x-axis and at day "t_{k+1}" on the y-axis. The map of the model enables predictions of future SSEA3 intensities based upon present SSEA3 levels. For instance, cells expressing SSEA3 at $10^{2.2}$ intensity on day "t_k" are predicted to have an SSEA3 intensity of $10^{2.8}$ on day "t_{k+1}" (Shown in blue in Figure 3.9).

Any part of the slope that lies on the line y=x (superimposed on the graph) represents an SSEA3 intensity that will remain unchanged from one day to the next. These intersects are equilibrium points. If the gradient about an equilibrium point is between 1 and -1 (denoted <|1|) then it may be classified as an attractor since the adjacent intensities would condense upon that equilibrium point on the subsequent iteration (or, day). It may be useful to visualise a ball in a cup that will proceed to reach that basin (or, attractor) under gravity.

On the other hand, regions where the gradient is <|1| about an equilibrium point actually implies that surrounding intensities of SSEA3 drift away from any particular equilibrium point. In line with the previous analogy, this would be akin to a ball resting

perfectly balanced on the apex of a hill (having an unstable equilibrium point); anything adjacent to, or any perturbation of, that ball would see it accelerate away from that nearby equilibrium.

In this case, the map reveals that there no attractors relevant to NTera2 SSEA3 dynamics but there are several equilibrium points (Table 3.2). In general, the magnitude of gradients present across the map are quite large suggesting that the SSEA3 properties of individual regions are subject to change position quite substantially from one day to the next.

Table 3.2 – Calculated equilibrium points for SSEA3 expression in populations of NTera2 cells from the model trained using Batch3 data. Equilibrium points represent intensities where SSEA3 expression is predicted to remain unchanged from one day to the next

Calculated Equilibrium Points (log_{10})
0.4682
0.5667
0.6593
0.9772
1.0333
1.4815
2.9288
3.0731
3.1403
3.2442

3.11 Model Predictions and Observed Data

The model generated boasts a predictive capacity for SSEA3 distributions, enabling future SSEA3 distributions to be predicted from any given SSEA3 distribution. The simplest test of this is against the data used to train the model from Batch3 already collected above. A comparison of observed data against predicted data from Batch3 demonstrates that the model is capable of generating predictions (Figures 3.10 and 3.11). Predictions were made by computing iteratively the SSEA3 expression trajectories for individual cells using the inferred map S

$$SSEA3_{day=tk,cell=i}=S(SSEA3_{day=tk-1,cell=i})$$

given the initial (day $t_k=0$) expression level $SSEA3_{day=0,cell=i}$ where i=1,...,N and N is the total number of cells analysed. The predicted SSEA3 expression levels for the entire cell populations were subsequently used to estimate probability density functions for each time point. Figures 3.10-3.13 show the measured and the predicted density functions generated by the model.

Generally, there is a lot of overlap of predicted distributions and observed predictions for the training dataset from Batch3. Of sorted fractions, the most consistent overlap between observed and predicted data appears to be in the negative and low fractions with the greatest discrepancy being with the medium and high fractions; particularly on days two and three. The control fractions (UU, SU and US) all also exhibit consistency between predicted and observed SSEA3 distributions.

In a more quantifiable manner, Bhattacharyya distances were calculated as a measure for the degree of disparity two distributions lying on the same axes (Hazewinkel, 1994). These distances are expressed numerically, where the larger the number, the greater the disparity between the distributions. In this case, measuring the distance between the observed and predicted distributions of SSEA3 reveals that there is a substantial amount of overlap between the distributions (Table 3.3). An examination of the Bhattacharyya distances for the predictions demonstrates that the predictions tend not to deviate from the observed data. Bhattacharya distances between observed and predicted data are generally quite small, with the largest discrepancy on Day 4 for the medium fraction at 0.113. On average, Bhattacharya distances for each fraction were all less than 0.08 in size; suggesting an accurate model.

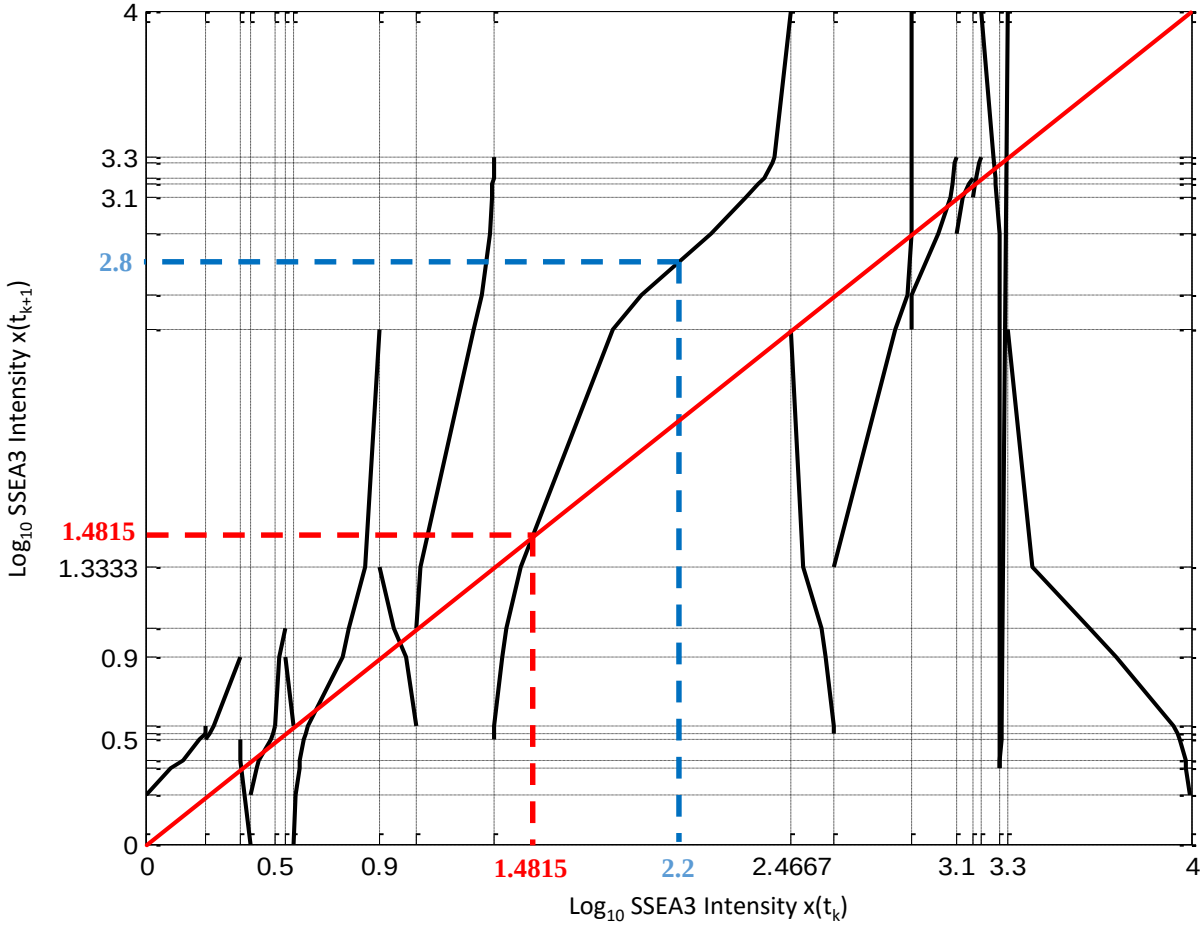

Figure 3.9 – Map of the model. A hypothetical model and explanation of interpretation/ generation are provided in figures 3.2 and 3.3.
Axes represent the Log SSEA3 intensity (X) on day "t_k" (x-axis) and one day later "t_{k+1}" (y-axis). Both axes represent the range of SSEA3 intensities measured during the experiment. Generating the model requires partitioning of the SSEA3 intensity range (figures 3.2, 3.3), and the partitions used are marked by the dotted black lines. This map represents a generalised model of SSEA3 dynamics that allows predictions of future SSEA3 intensities. For example, if a cell has an SSEA3 intensity of $10^{2.2}$ it will be expected to have an SSEA3 intensity of $10^{2.8}$ on the following day (Example in blue).
Any case where the map of the model intersects with the line y=x (solid red) represents an equilibrium point where SSEA3 intensity of a cell is predicted not to change the following day. For example, a cell with an SSEA3 intensity of $10^{1.4815}$ on day "t_k" is anticipated to have unchanged with respect to SSEA3 intensity on day "t_{k+1}" (dotted red line).
This map reveals that SSEA3 is generally not anticipated to remain unchanged between timepoints, and that SSEA3 intensity will vary between days. Finally, there are no basins of attraction. The mode reveals ten equilibrium points that are noted in Table 3.2.

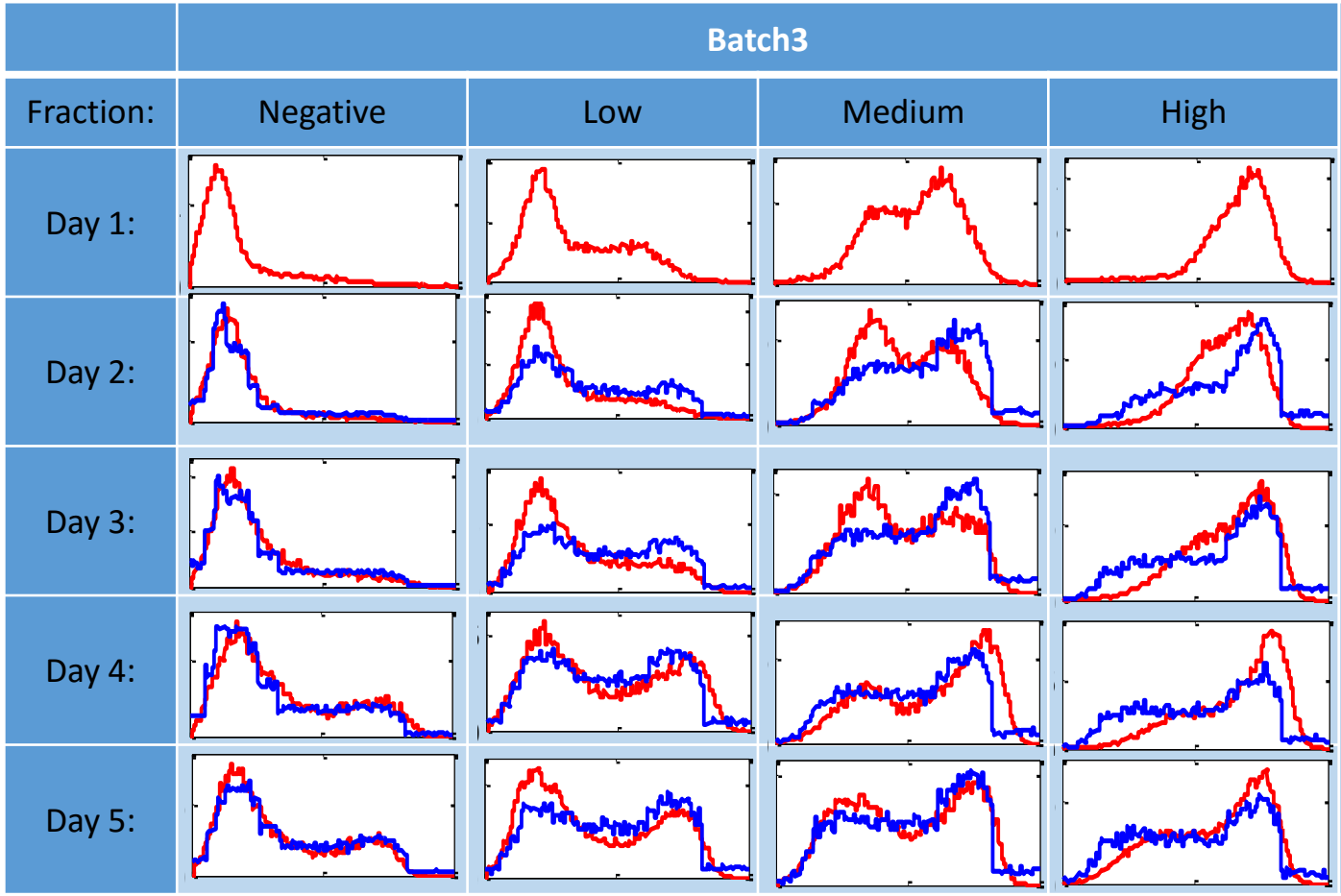

Figure 3.10 – Observed and Predicted data of Training Dataset. Predictions generated from the model using observed data from Batch3 that were used to train the model. X-axis; log SSEA3 intensity ranging from 10^0 to 10^4. Y-axis plots calculated probability density function transformations of observed data; a normalisation that allows cross comparison between data (arbitrary units).

Observed data is shown here in red, predictions in blue. Predictions are generated using the model and the observed data from the previous day. The predictions generally align closely to the observed data, with the greatest discrepancy shown in the Medium fraction on day 2.

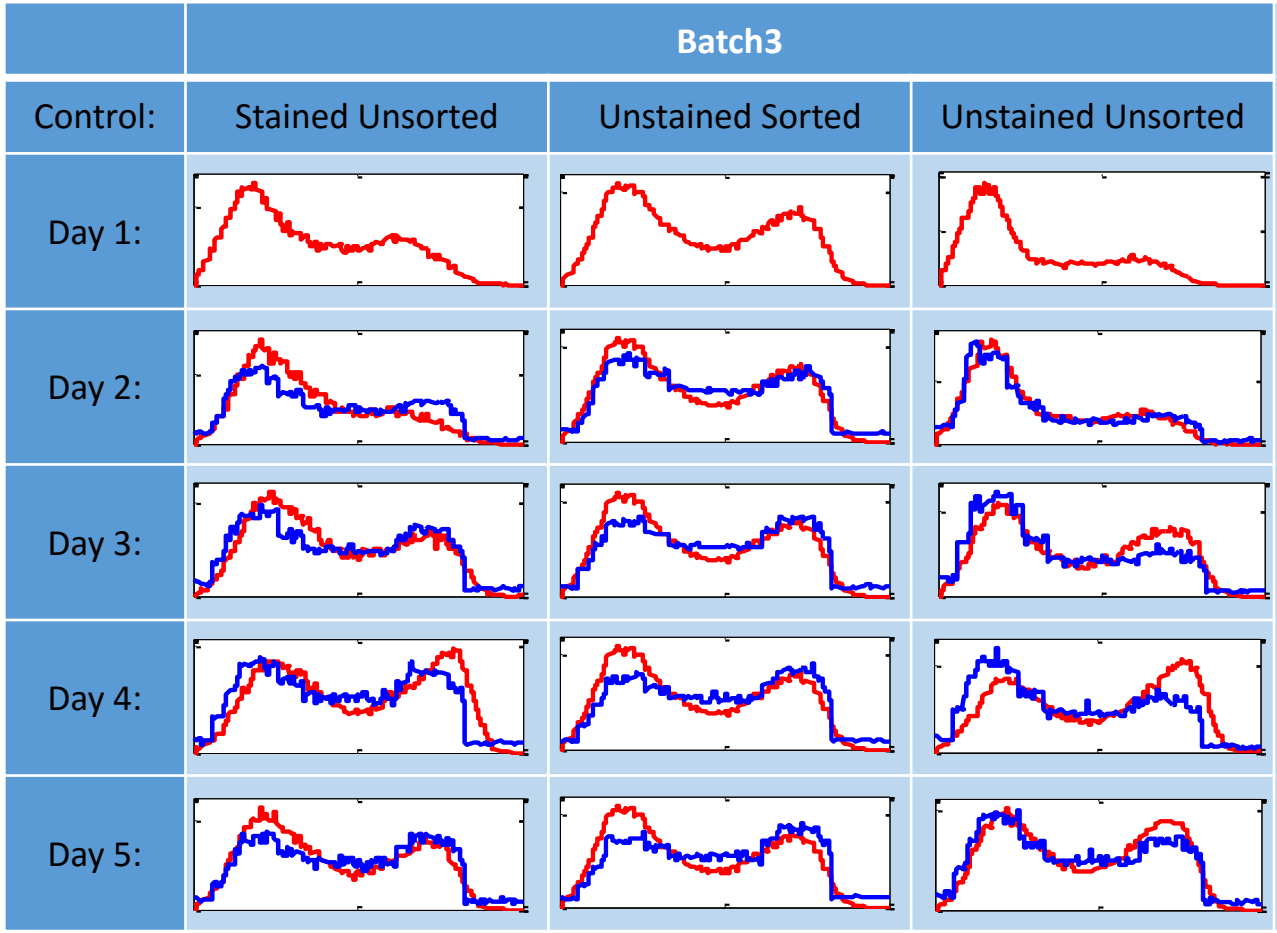

Figure 3.11 – Observed and predicted SSEA3 distributions on Training Dataset control treatments from Batch3. X-axis; log SSEA3 intensity ranging from 10^0 to 10^4. Y-axis plots probability density function transformations of observed data; a normalisation that allows cross comparison between data (arbitrary units).

Observed data is shown here in red, predictions in blue. Predictions are generated using the model and the observed data from the previous day. The control fraction SSEA3 distribution changes over time are well predicted by the model.

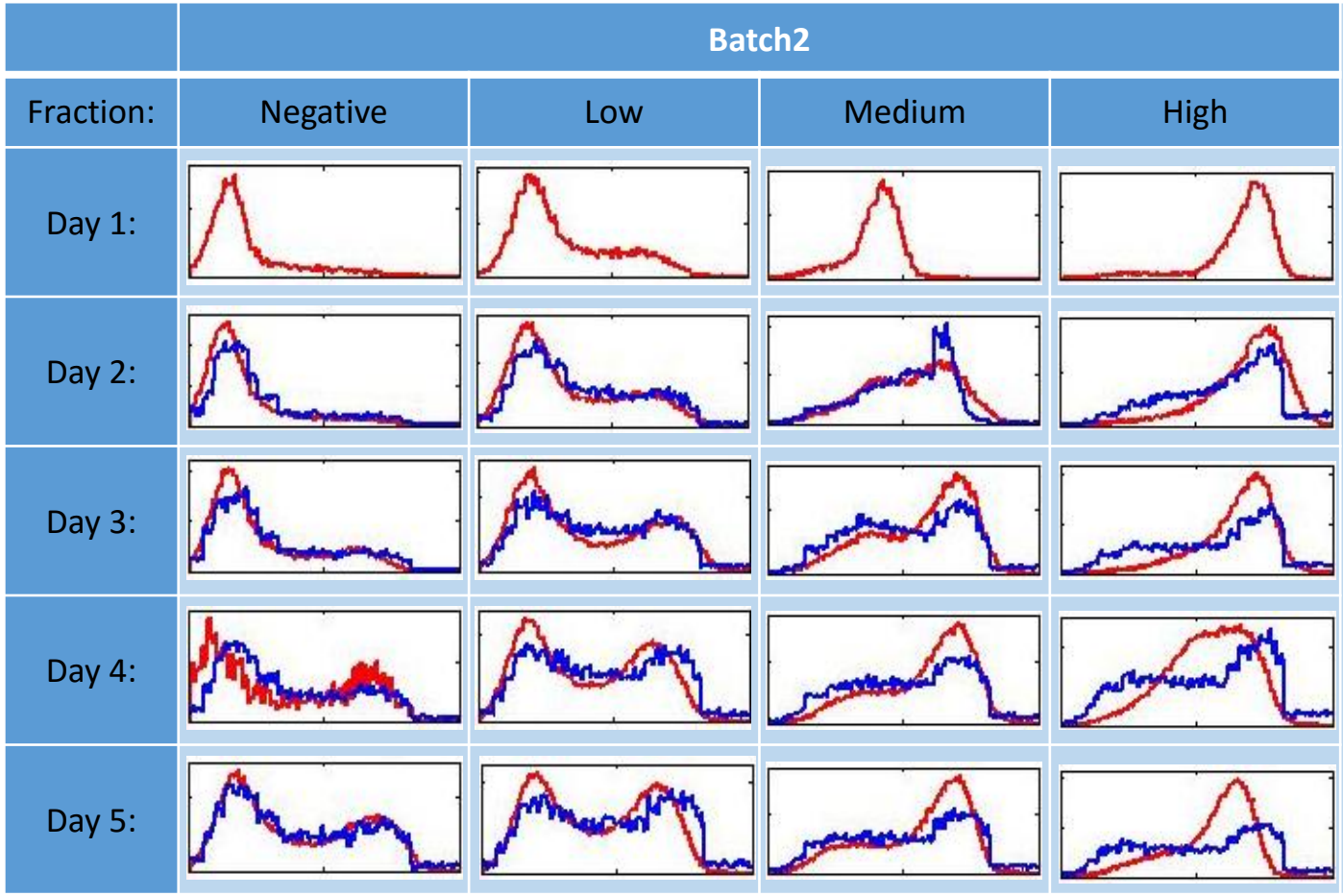

Figure 3.12 – Observed and predicted data of Test Dataset. Predictions from the model using observed data from Batch2. These data were not used to train the model and so represent a test on data independent from the model's generation.

X-axis; log SSEA3 intensity ranging from 10^0 to 10^4. Y-axis plots probability density function transformations of observed data; a normalisation that allows cross comparison between data (arbitrary units).

Observed data is shown here in red, predictions in blue. Predictions are generated using the model and the observed data from the previous day. The predicted distributions mirror closely the observed data, with the greatest discrepancy being in the High fraction on day4.

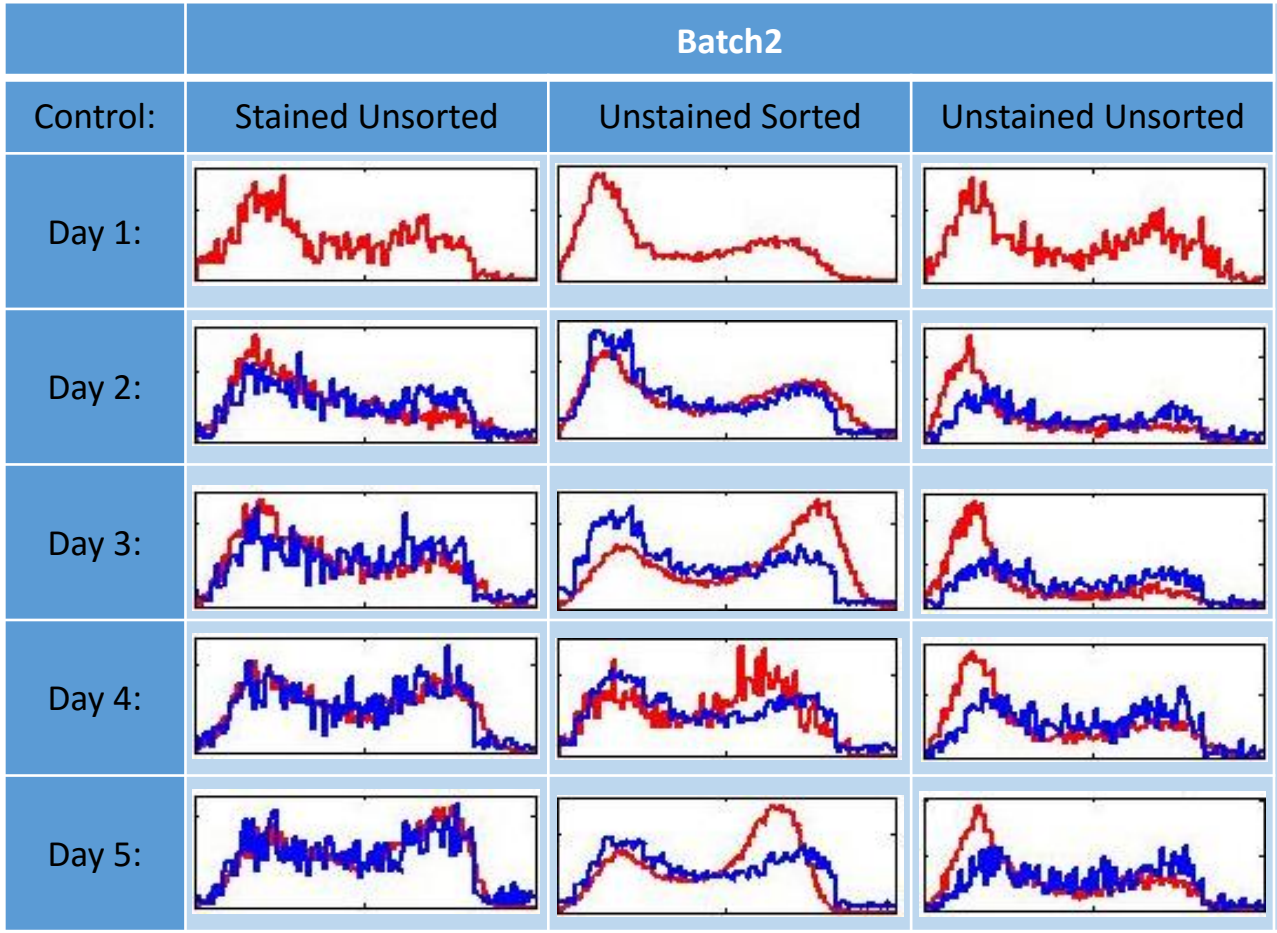

Figure 3.13 – Observed and predicted SSEA3 distributions on Test Dataset Control Treatments from Batch2. X-axis; log SSEA3 intensity ranging from 10^0 to 10^4. Y-axis plots probability density function transformations of observed data; a normalisation that allows cross comparison between data (arbitrary units).

Observed data is shown here in red, predictions in blue. Predictions are generated using the model and the observed data from the previous day. As with the training data, these control fractions are quite well predicted by the model.

Table 3.3 – Bhattacharyya Distances comparing the distribution similarities between predicted and observed SSEA3 distributions from the Batch 3 dataset (Figure 3.10) from the model of SSEA3 dynamics (Figure 3.9). Bhattacharyya distances are expressed on a scale between zero and one, where the larger the number, the less similar the distributions under comparison. All distances are relatively small (<0.1) with the exceptions of the High and Medium fractions on Day 4.

	Bhattacharya Distances				
	Day 2	Day 3	Day 4	Day 5	Mean
Negative	0.058	0.063	0.090	0.084	0.074
Low	0.045	0.050	0.054	0.065	0.054
Medium	0.065	0.059	0.106	0.050	0.070
High	0.076	0.070	0.113	0.054	0.079

An application of the model to a non-training dataset, such as the biological replicate data that is Batch 2 from the aforementioned experiment was performed to test predictions against data that was not used to train the model (Figures 3.12 and 3.13). Predictions from the model were tested against data from Batch 2; which was a dataset obtained independently from the data used to train the model (Batch3). Again these predictions were generally consistent to the observed data. The negative and low fractions also show a substantial degree of overlap between observed and predicted distributions. The High fraction displays the greatest discrepancy between observed and predicted distributions although there is still a fair degree of overlap, with Day 4 and Day 5 for the high fraction showing the greatest differences. As with the Batch 3 comparison, the control samples (UU, SU, US) all display general concordance between the predicted and observed data.

3.12 Clonogenic Analysis

With equilibrium points predicted (Figure 3.9 and Table 3.2), another sort experiment on NTera2 was performed in order to interrogate regions that contained equilibrium points for evidence of putative substates by assessment of aspects of behaviour within the confines of a clonogenic assay (see materials and methods). The assay used here provided information on the rate of colony formation of cells, the growth rate of colonies as well as cell size (see discussion).

As with the previous sort, cell culture was staggered so as to provide several batch replicates prepared for sorting on different days. Since there were more fractions taken, with each fraction representing a lower proportion of the entire population, it was necessary to increase the number of cells used in the sort; requiring approximately 24 T-75 flasks per batch (corresponding to approximately $3.6x10^8$ cells per batch). These were harvested and stained as described above and in materials and methods.

The SSEA3 distribution of the various batches were examined and an example is shown in Figure 3.14. This distribution, similar to the first experiment, covers a large range of intensities and the large number of cells used in the sort permitted sufficient resolution to identify several peaks (arrows). In contrast to the example distribution shown in the first experiment, this distribution contained a larger proportion of negative cells, yet also seems to encompass a slightly larger range of intensities.

The fractions sorted for are shown on this sample population, with fractions containing equilibrium points indicated in red. Equilibrium and non-equilibrium points were acquired from across the entire range of the SSEA3 distribution. For instance, Region R9 was deliberately chosen to represent a region where SSEA3 was of high intensity but was not predicted to contain an equilibrium point as opposed to its neighbours, (R13, R7 and R8) which either all contained, or were extremely close to, predicted equilibrium points.

The fractions described above were plated for subsequent clonogenic analysis (materials and methods). This was designed to help assess whether there were pertinent biological differences between the fractions collected and whether these had any relevance to equilibrium points. Cells were seeded in six-well plates at a density of 1,000 cells per cm^2 in order to account for the poor clonogenicity of these cells (see discussion) and fixed after 5 days of culture. Cultures were stained with Hoechst 33342 and analysed using the InCell analyser platform. Instances of Hoechst staining with an area greater than 35μm^2 were considered cells. For each nucleus identified, a mask was applied about that nucleus' perimeter of 50 µm, overlapping masks between cells were considered to be within the same colony and this combined overlap used to estimate colony area.

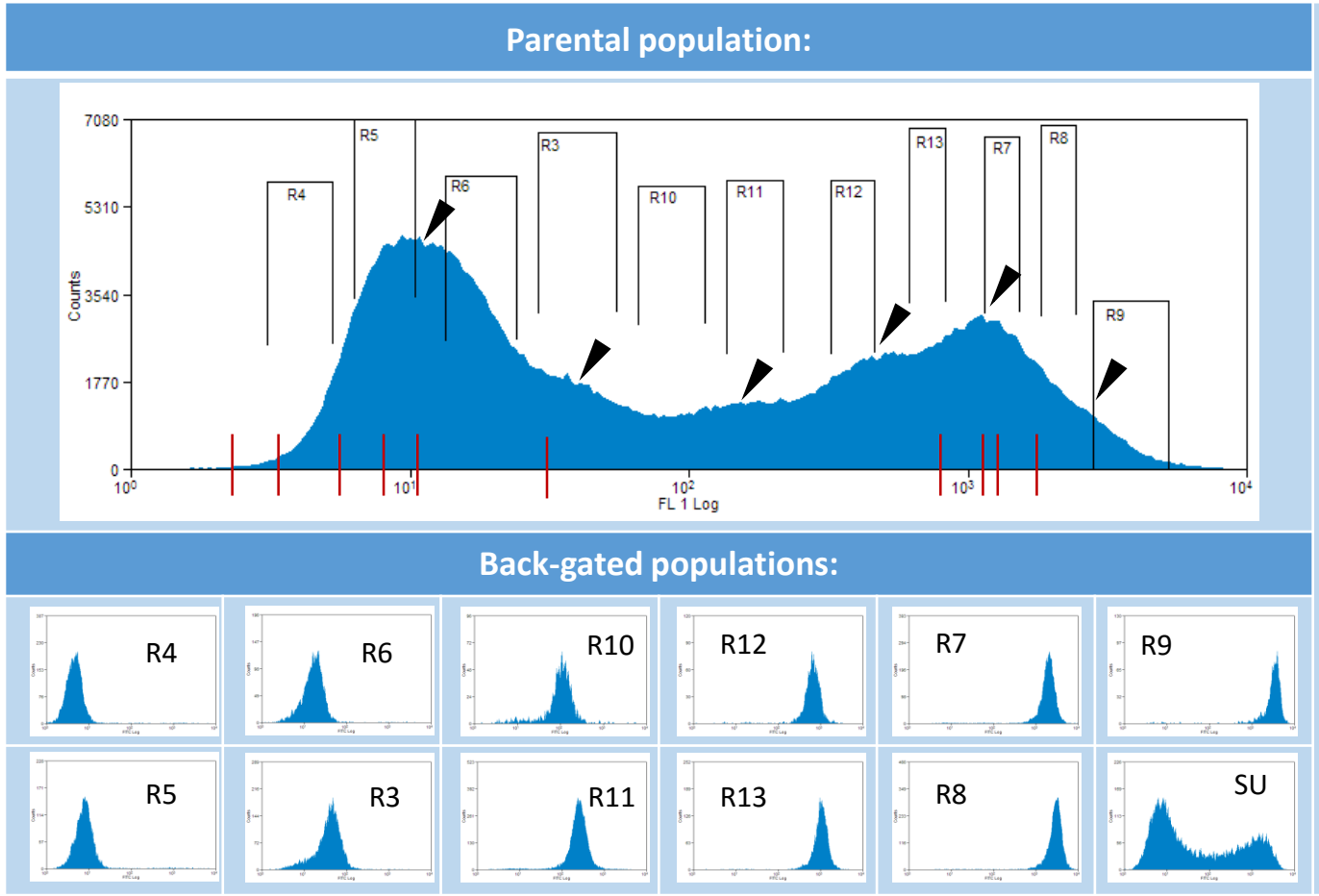

Figure 3.14 – NTera2 cells stained for and sorted according to SSEA3 expression. The parental population chart shows the original population's SSEA3 expression level, which is multimodal (Black arrows indicating multiple peaks) as well as the gates used for sorting the population into multiple fractions for further analysis. Regions R4, R5, R3, R13 and R7 are predicted to contain equilibrium points predicted by the model. Predicted equilibrium points are marked in red along the x-axis and represent those points shown in table 3.2. Samples of populations from sorted fractions were examined for their SSEA3 expression to assess sort accuracy. Sort accuracy was generally very good, with regions R10 and R3 showing the greatest inaccuracy.

All fractions taken from the original sort contained cells that could attach to the plate and proliferate (Figure 3.15). With regard only to survival and attachment of cells, generally at least 1000 cells from each fraction adhered to the plate regardless of whether they went on to proliferate; i.e. colonies of size 1 cell or greater by the end of the experiment. There were marked differences between the fractions, with R4 (negative for SSEA3) having the lowest number of adherent cells (~800), and fractions R10 and R9 tending towards the largest number of adhering cells (~3,500). Generally, fractions that were low or negative for SSEA3 expression had a low rate of adherence for cells, whereas Fractions that were most positive for SSEA3 had a greater degree of adherence. The fractions R10 and R11 appear out-of-place; representing regions where the number of adherent cells was noticeably larger than surrounding fractions.

Of those cells that attached the proportion that were proliferative are displayed in Figure 3.15b. Colonies were considered proliferative if they contained more than 3 cells. Fractions displayed similar proportions of cells (out of all adherent cells) that were proliferative. Overall, roughly 15-25% of cells that adhered to the well plates were capable of proliferating with a few exceptions. Region R4 displayed the lowest proliferative capacity with on average 15% of colonies being of a greater size than 3 cells. Regions R12 and R13 for their third replicate each showed the greatest proportion of proliferative colonies (Figure 3.15b), which also coincided with their lowest number of adhered cells (Figure 3.15a).

The number of cells per colony from each fraction was generally low, with the median number of cells being 6 ±1 across all fractions (data not shown). The frequency distributions of the number of cells per colony appear similar and were all heavily skewed (Figure 3.16). The least skewed distributions were fractions R12 and R13, which were relatively high for SSEA3 at the time of the sort, whereas the most skewed distribution was that of fraction R6. Given the timeframe of the experiment (5days/ 120 hrs) and assuming short cell cycle duration (~20hrs) (personal communication with Prof. Andrews), it would only be possible for a single cell to generate a colony of maximum size 2^6 (or 64) cells. Therefore, colonies examined in Figure 3.16 contain between 4 and 64 cells inclusive.

Colonies that contain more than 64 cells cannot be explained only by one single, proliferative cell and must have occurred by some other means which includes: multiple cells seeded together, colony merging by proximity, or colony merging caused by motility (see discussion). Regardless, colonies greater than 64 cells did occur (Figure 3.17). The formation of colonies larger than size 64 did appear to differ between colonies, with fraction R10 having the greatest spread (Figure 3.17). Fraction R4, on the other hand, was the only fraction not to have any colonies with more than 64 cells (maximum= 52 cells). Generally, fractions that were negative or low for SSEA3 did not tend to produce giant colonies.

The cell sizes within colonies, as calculated based upon colony size divided by colony area for each colony, ranged from about 500 μm^2 to 3500 μm^2 for each fraction (Figure

3.18). The control fraction, US, displayed an even distribution in cell sizes across this range, similar to region R6. Regions R9, R7, R13, R12, R11 and R10 all had fairly similar distributions with a low proportion of smaller cells. Regions R4, R5, R3 and R8 displayed an alternative distribution that appears bimodal in nature, with average cell areas of approximately 1250 (μm^2) and 3000 (μm^2) for the two modes displayed (Figure 3.18).

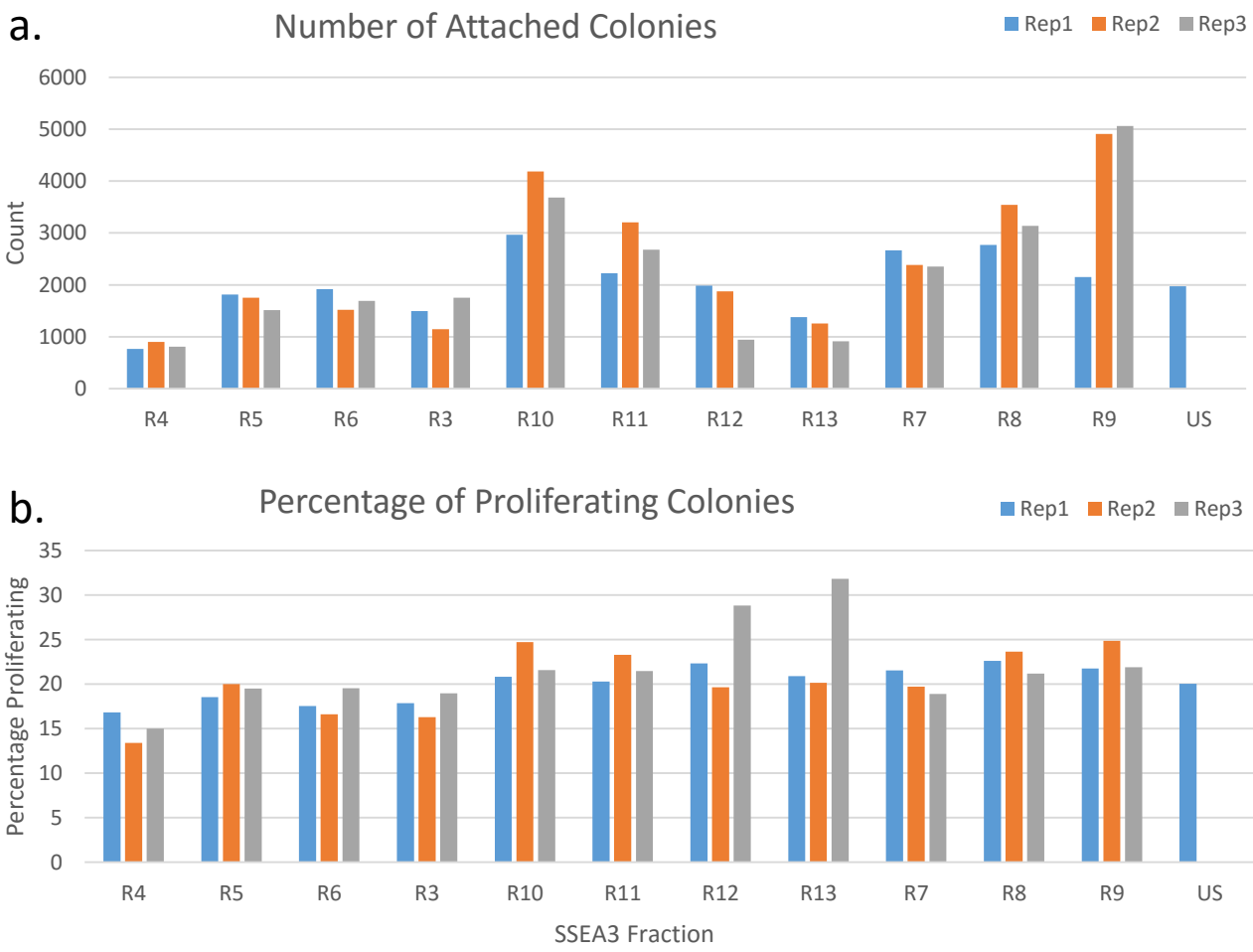

Figure 3.15 – Colony survival and Proliferation. Examination of the clonogenic data analysed using the InCell platform. All sorted fractions (according to sort parameters in fig3.10) were seeded at 1,000 cells/cm^2, and left to grow for 5 days prior to fixation, staining and analysis. **a.)** The total colony count returned for each rep in each fraction, Colonies were included of any size (>0 cells) in this analysis. The number of colonies, including single cells in this instance, is used as a metric relating to the survival rate of cells within each fraction that were able to survive long enough to attach from the initial seeding.
b.) The percentage of attached colonies (as measured in a.)) that demonstrated proliferation after attachment (i.e. colonies with a cell count>3). Overall approximately 15-25% of cells that attach display proliferated, displaying clonogenic potential of all cells regardless of parent fraction.

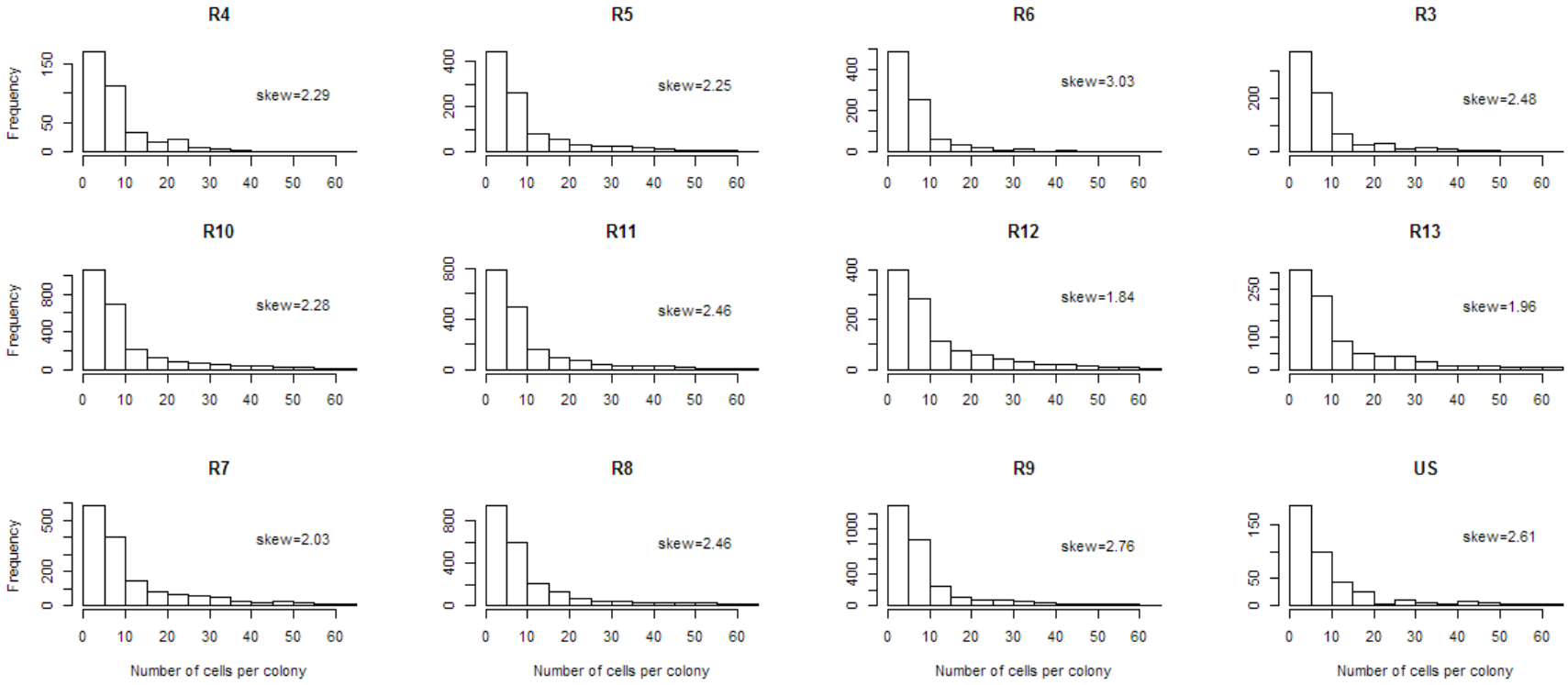

Figure 3.16 – Number of Cells per Colony Distribution. Examination of the number of cells per colony distribution from clonogenic cells from clonogenic analysis of NTera2 cells examining cell fractions initially sorted for differing levels of SSEA3. These data are calculated from cell colonies between 3 and 65 cells in size. All fractions show a similar pattern of a very skewed distribution of number of cells per colony. A measure of skew is included on for each chart.

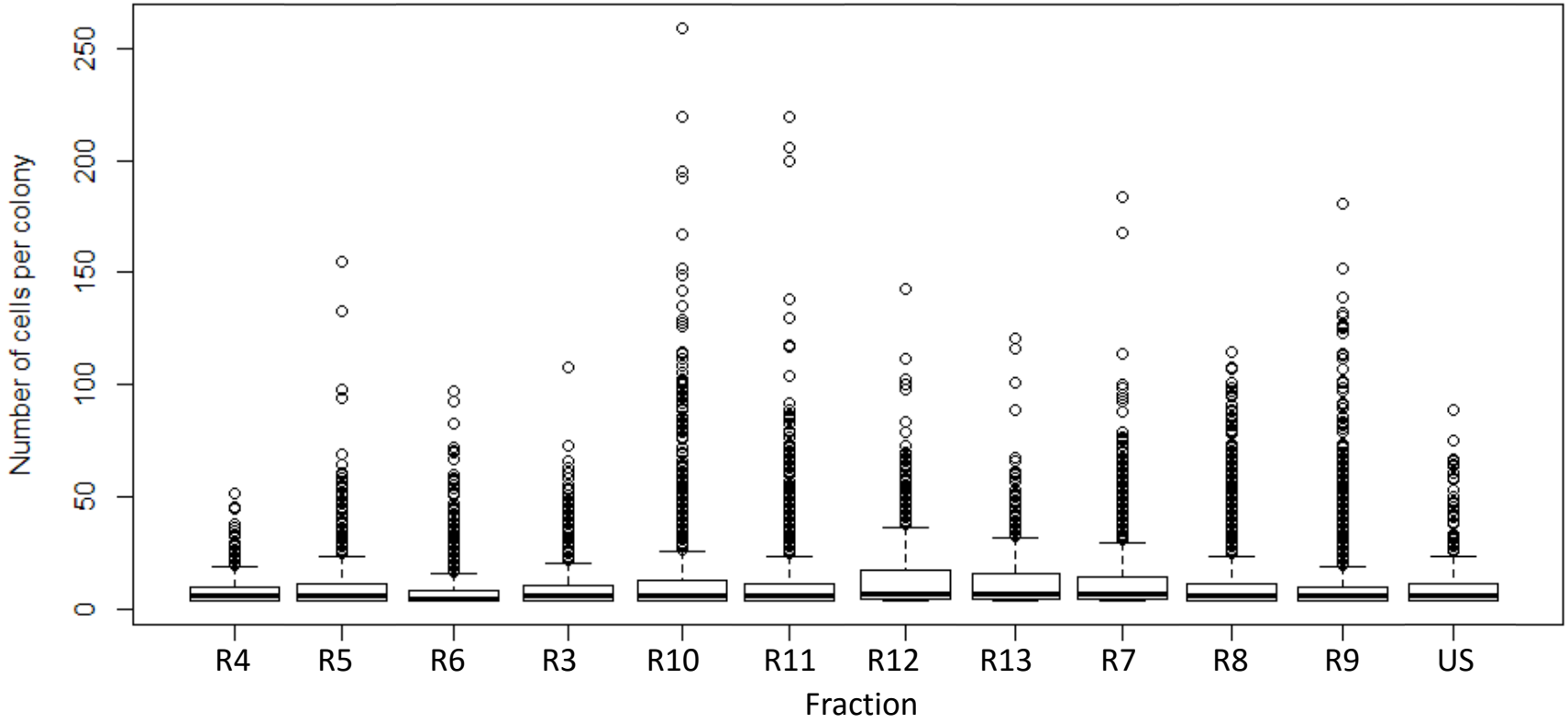

Figure 3.17 – Large Colony Formation Rates. Boxplot examining the propensity of fractions to form colonies that are larger than 65 cells in size. These colonies are too large to be caused only by regular cell division by an individual cell. Explanations for these colonies are; increased motility of cells, cell doublets at the time of seeding and/or random chance of colony distributions. Different fractions appear to have differing propensity of large colony generation, with fraction R10 being the most susceptible and fraction R4 not producing any colonies larger than 64 cells in size.

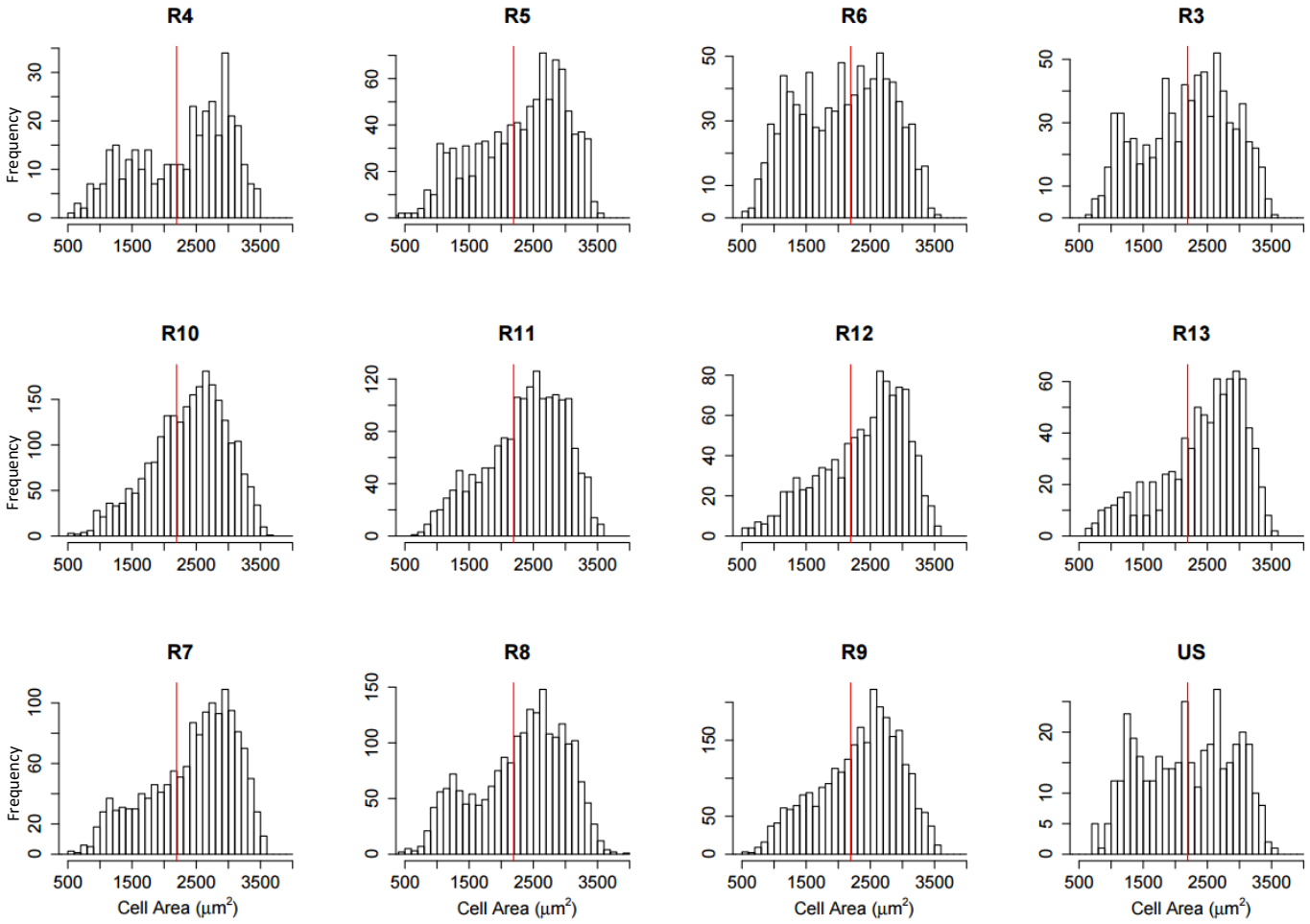

Figure 3.18 – Cell Size in Clonogenic Assay. Histograms of the average cell areas (µm²) within colonies from different populations sorted based upon SSEA3 intensity (Figure 3.14). Cell area calculated by dividing colony size by colony area as measured on the InCell analyser platform. Fractions R10, R11, R12, R13, R7 and R9 present a similar distribution of cell areas with a negative skew; generally containing cells of a modal area of approximately 2750µm². Regions R4, R5, R6, R3, R8 and US seem to display a slightly different distribution where there is a larger number of smaller cells compared to the other cell area distributions.

The red line on each plot represents the median cell area for the control group (2193µm²) and acts as a reference point for comparison between graphs.

3.13 Cell Cycle comparison and Sort duration

In addition to the previous experiment where SSEA3 fractions were sorted for (as well as the controls of UU, SU and US), these sorts afforded the opportunity to examine two other factors capable of influencing cell behaviour that may, by result of artefact, appear to be correlated with fractions taken independent of SSEA3 expression.

Firstly, if there were an increase in cell mortality over the course of a sort, then the sequential acquisition of fractions would mean that those collected later would contain a greater proportion of dead cells; which may influence the behaviour of surviving cells in that fraction. This was a particularly pertinent question considering the unusually long time these sorts required of approximately seven or eight hours. To assess this, cell samples were taken both at the start and end of the sort to be treated with propidium iodide that is normally actively exported out of cells. These samples were then examined by flow cytometry to measure the proportion of cells that contained propidium iodide at the beginning and end of the sort (Figure 3.19).

Examination of the cell mortality by propidium iodide staining revealed that on average 0.67±0.37% (n=4) of cell population were compromised prior to sorting whereas by the end of sorting, 1.00±0.25% (n=3) of the cell population were stained with propidium iodide (Figure 3.19). Overall this does not represent a significant change in mortality between the beginning and the end of the sort.

The second consideration was whether the difference in SSEA3 expression of cells in the population was in fact reflective of that cell's position in the cell cycle, which would imply that differences seen between fractions could be attributed to differences in cell cycle rather than SSEA3. This question was addressed by taking sub-samples from the parental population that, in addition to SSEA3, were co-stained with Hoechst 33342; a fluorescent dye that stains DNA (materials and methods). Dual plots showing cell SSEA3 intensity and Hoechst 33342 fluorescence reveal that there is very little to no correlation between the two factors (Figure 3.20).

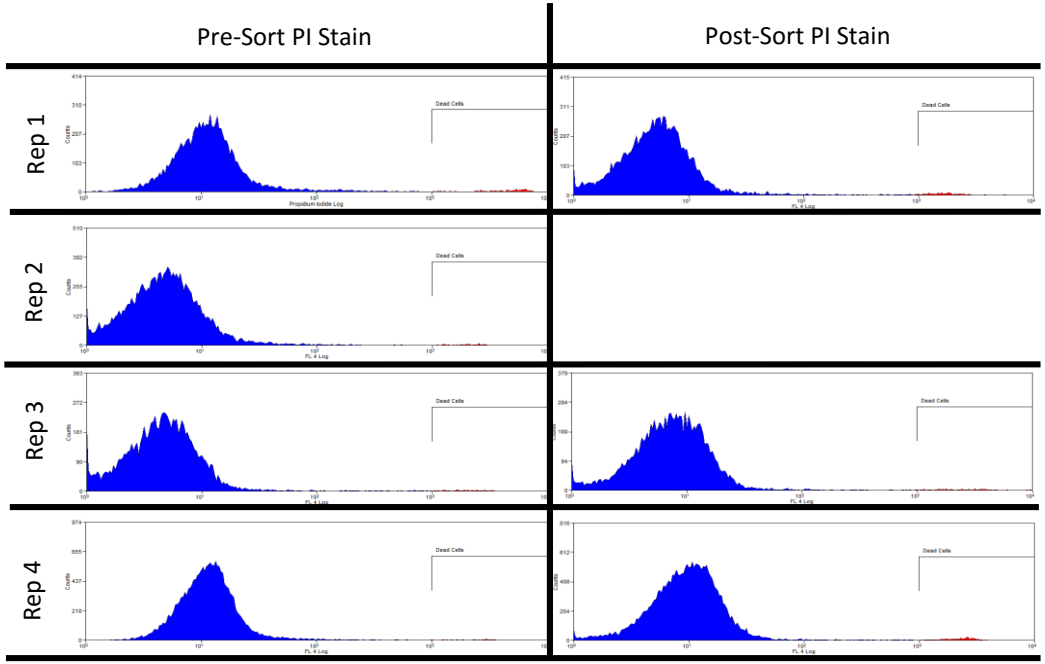

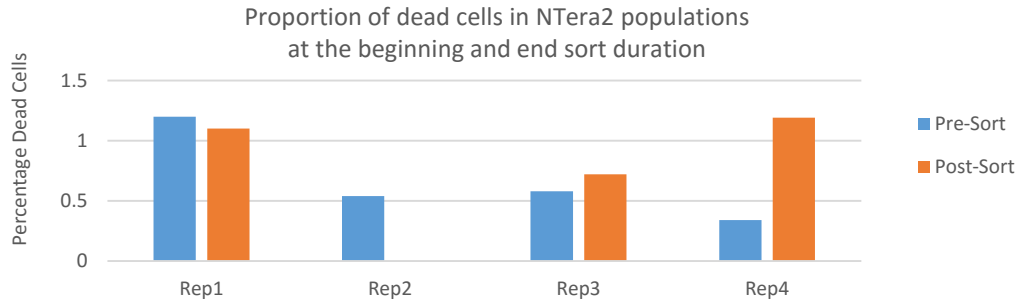

Sample	Early PI dead cell (%)	Late PI dead cell (%)	Relative change
Rep 1	1.20	1.10	0.917
Rep 2	0.54	-	-
Rep 3	0.58	0.72	1.241
Rep 4	0.34	1.19	3.500
Average	0.67 ± 0.37	1.00 ± 0.25	-

Figure 3.19 – Cell Sort Mortality. Examination of cell mortality over the duration of a sort assed via PI staining. At the start of a sort, on average, 0.67±0.37% (n=4) of the population incorporated propidium iodide, whereas by a sort's conclusion, this proportion rose to, on average, 1.00±0.25% (n=3).

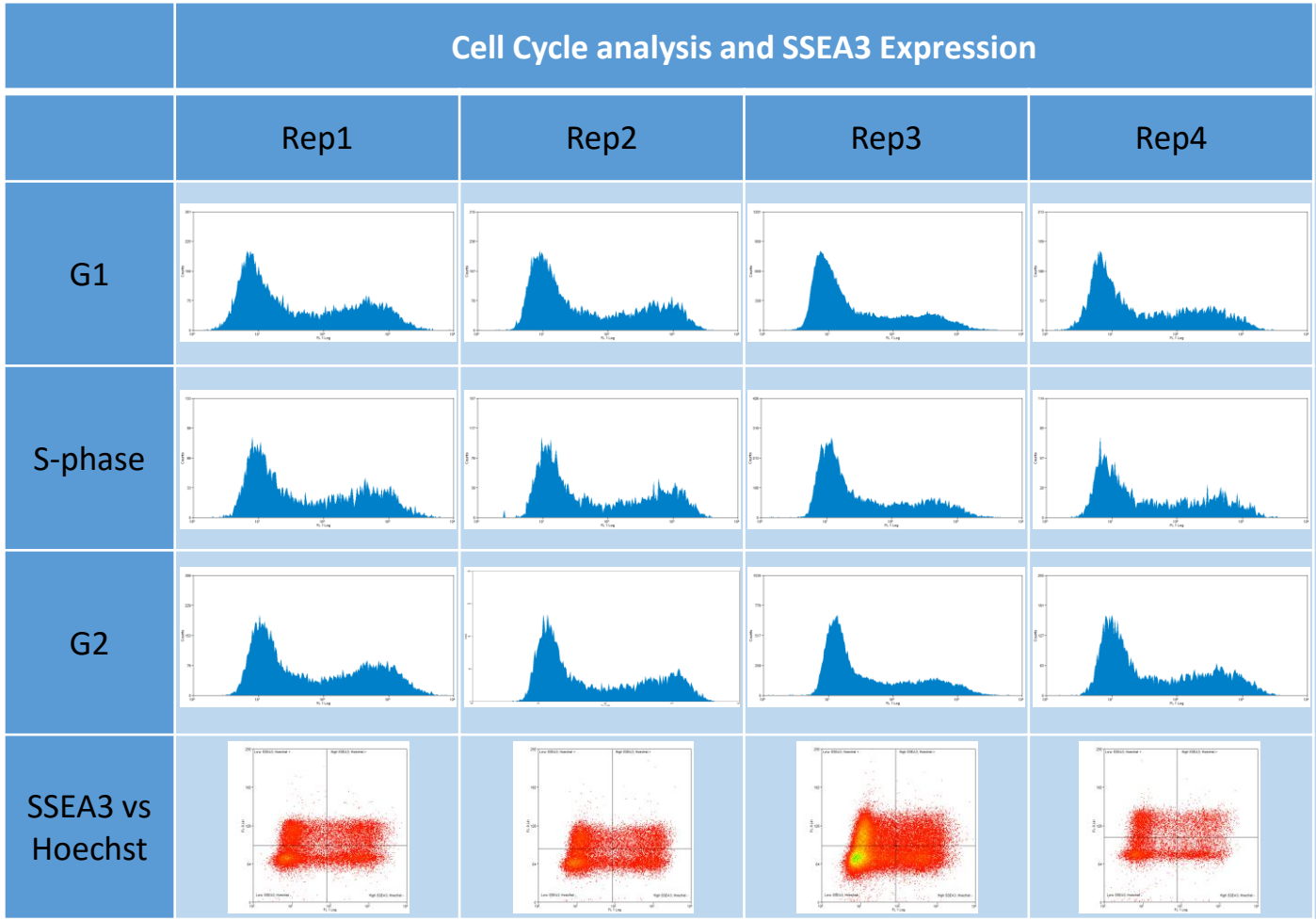

Figure 3.20 – Cell Cycle and SSEA3. A comparison of SSEA3 expression from cells in different stages of the cell cycle as determined by Hoechst33342 analysis in four replicates. There does not appear to be a marked difference in SSEA3 expression as a result of being in a different stage of the cell cycle. The dual plot of SSEA3 against Hoechst expression relays little, if any correlation. Regardless of position in the cell cycle, the complete range of SSEA3 expression is present.

3.14 Development of Modelling on the InCell Analyser Platform

The application of the modelling process currently requires a large cell number of cells seeded in order to facilitate flow cytometry analysis of sorted fractions on subsequent days. Cell preparation for flow cytometry mandates sufficient sample material for analysis but also inevitably results in cell loss during harvest and wash steps. Ntera2 cells are more robust than human ES cell lines, with a greater survival rate from the stressors associated with cell sorting. Already the current method used for Ntera2 was only just feasible to perform over 8 hours of sorting. To conduct a similar sort to acquire comparable surviving cell numbers for fractions from human ES cell lines from fractions would quickly become impractical and prohibitive.

In order to reduce cell number required for application of the modelling process, a method independent of flow cytometric analysis was proposed that exploited *in situ* methods for staining cells directly within plates. This approach, in principal, circumvents the cell loss associated with cell harvest for flow cytometry and allows for a lower number of cells required as sufficient starting material. For instance, culture vessels with lower well surface areas may be readily employed such as a 96 well plate (surface are ~0.33cm^2 per well) as opposed to a 6 well plate format (10cm^2 per well). The reduced emphasis on initial cell number could facilitate the use of culture vessels that have a reduced absolute surface are, whilst maintaining cell density; dramatically reducing the number of cells required for a sort. This reduction in cell number would relieve pressure on the cell culture and line expansion in advance of the sort, and enable the examination of less robust cell lines such as human ES cell lines.

In the first instance, a sort was performed similar to the first experiment; a four-way sort for SSEA3, plating cells in a 6-well plate format in order to compare the *in situ* method against the flow cytometry approach. Sorted fractions were plated as described above at a density of 10,000 cells/cm^2. The distribution of the parental population can be seen in Figure 3.21. Instead of harvesting cells for flow cytometric analysis of the sorted fractions on subsequent days, plates were fixed using 4% w/v paraformaldehyde (PFA) prior to staining against SSEA3 and with Hoechst 33342 (see materials and methods). Stained cells were analysed using the InCell analyser platform with measures for both SSEA3 and Hoechst 33342 fluorescence; these data were then post processed in order to generate values for cell number, SSEA3 intensity per cell and SSEA3 intensity across a cell's area (materials and methods). These data were chosen so as to provide information analogous to that generated by flow cytometry; principally enabling examination of the SSEA3 distribution across a population ready for use in the modelling process.

Once the plated cells were imaged and examined, it became apparent that some misclassification occurred as evidenced by the cell size data (Figure 3.22). Some "cells" presented in these data were evidently too small and existed outside of the relatively normal distribution of the logged (base 10) cell size data (Figure 3.22a). Closer inspection of the cell data on a linear scale, revealed a "jump" in cell size frequency between 50 µm^2 and 60 µm^2 (Figure 3.22b). These "cells" were interpreted as debris/noise from the collection procedure and were removed from subsequent analysis.

The SSEA3 expression patterns of the fractions collected on the InCell platform are non-identical, but do not display the same classic distribution as cells interrogated by flow cytometry (Figure 3.23). Despite this reduced heterogeneity, the cell populations do tend towards a norm over time, with a median log intensity vale of around 5.59 (red line, Figure 3.23) that is evidence for some SSEA3 dynamics. It is clear that this technique is not directly comparable to that of the flow cytometry counterpart, but with further development, may provide data that is amenable to similar modelling procedures described by (Nie and Coca, 2013).

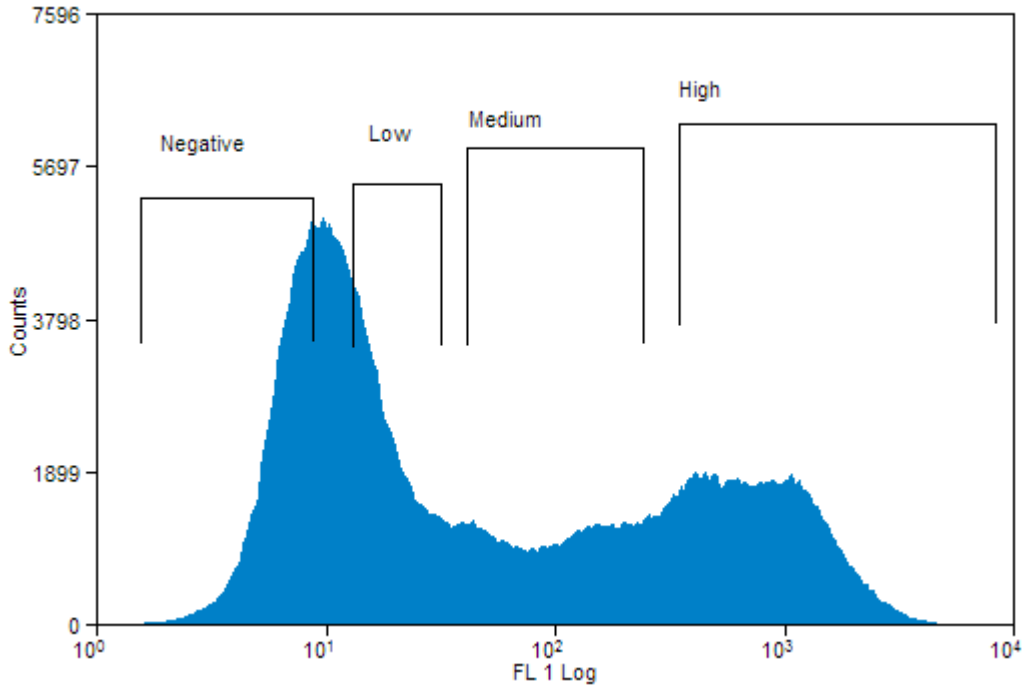

Figure 3.21 – Initial Sort for *in situ* Model Generation. Parental Population distribution of NTera2 cells stained for SSEA3. Cells from this sort were sorted according to the listed fractions (Negative, Low, Medium and High) in order to examine their future SSEA3 dynamics' behaviour within an Incell analyser *in situ* format. Sorted cell fractions were plated into 6 well plates and samples fixed daily over the following five days for examination using the Incell analyser platform.

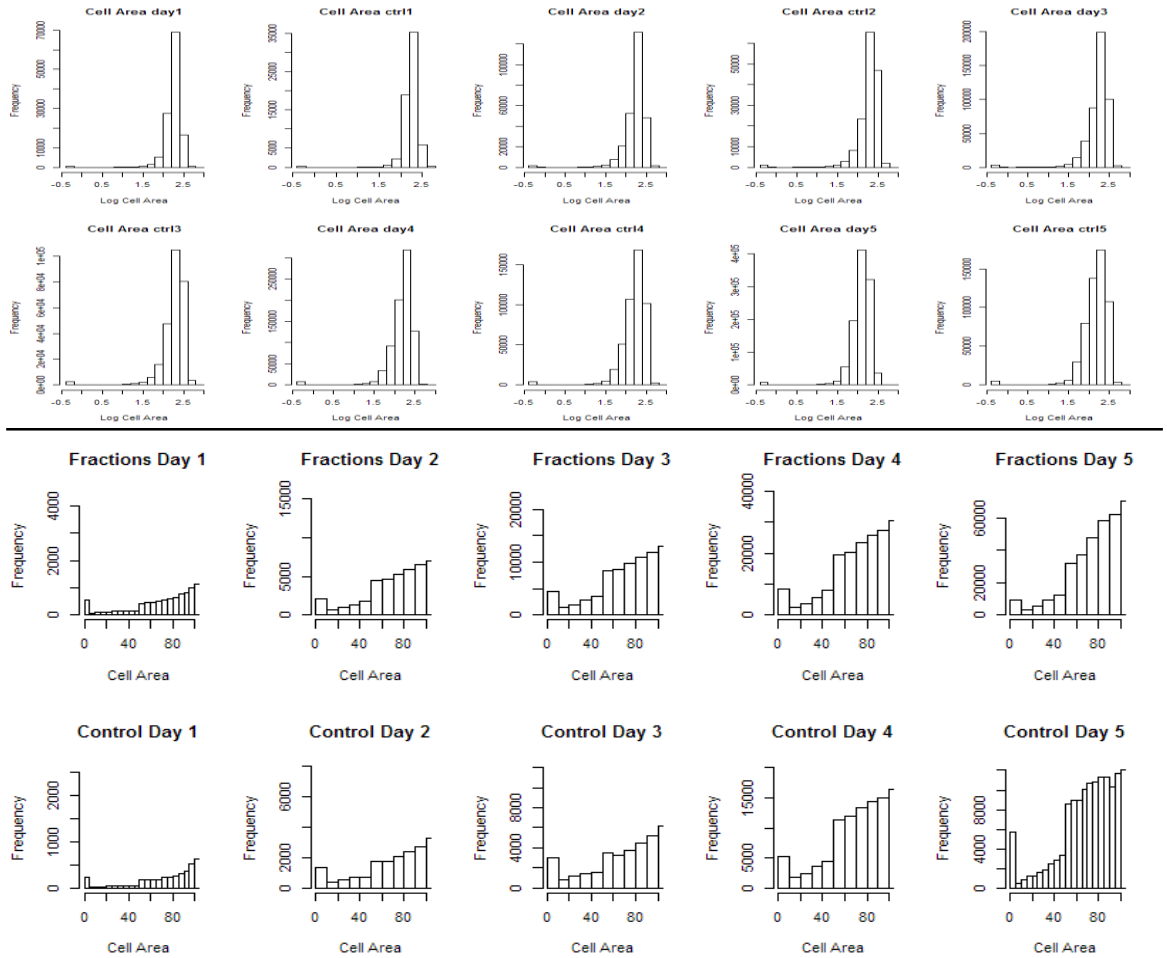

Figure 3.22 – Cell Size Exclusion. An examination of the cell size data reveals that some noise was also collected as data a.). cells which were clearly too small did not fit the normal distribution of the logged data, and the bounds of this distribution were around $10^{1.5}$. b.) An examination of the region around $10^{1.5}$ on a linear scale reveals that there is a clear change in the behaviour of the distribution around this region. These were interpreted as noise and removed from further consideration.

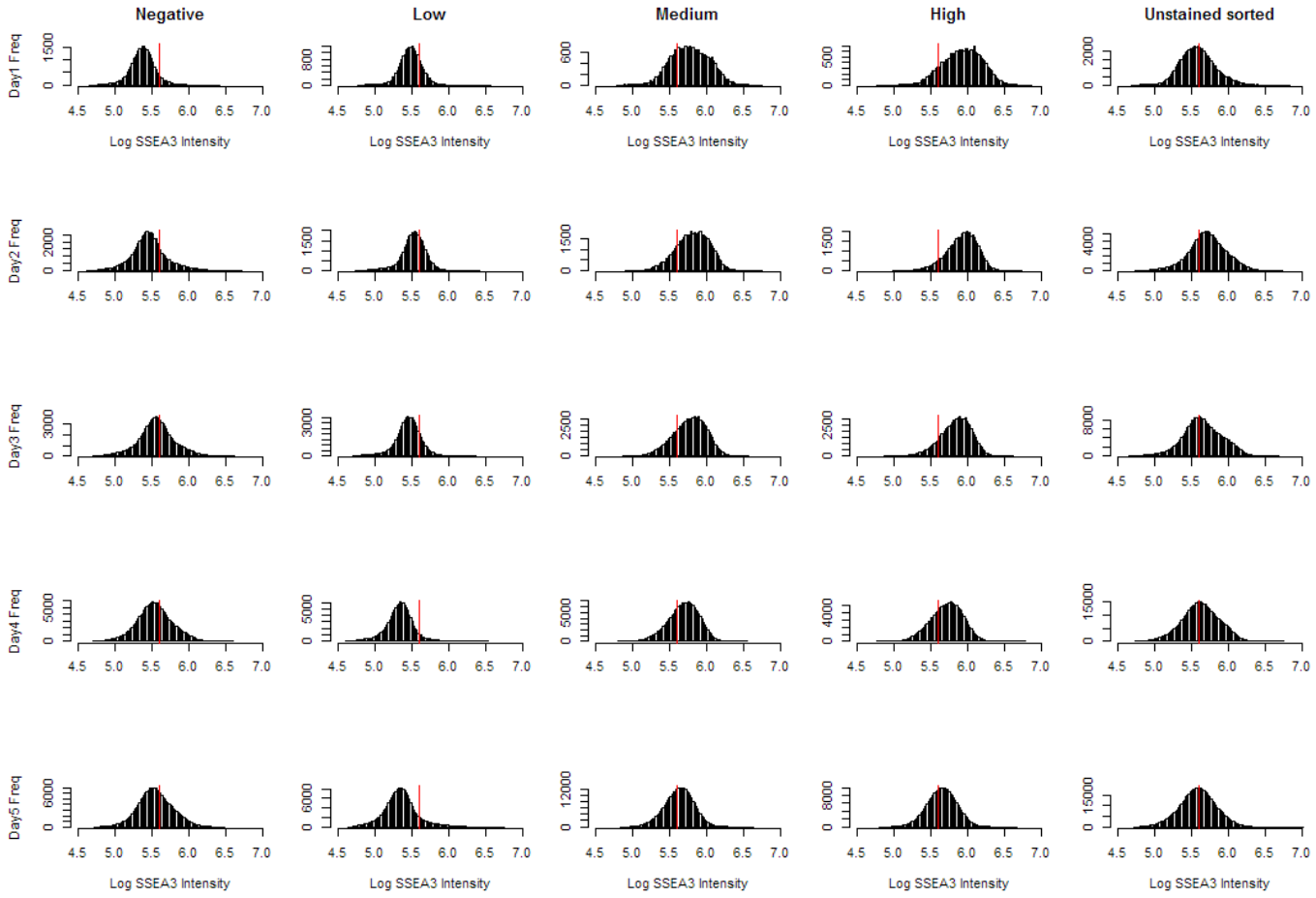

Figure 3.23 – SSEA3 Heterogeneity Analysed *in situ*. Examination of cells examined using the InCell analyser platform in a similar manner to the flow cytometry based assay, reveals that the distribution of SSEA3 is not manifest identically to the flow cytometry counterpart. Although the cells do not appear with identical distributions, the typical heterogeneous display of SSEA3 is not present. The red line on each plot represents the median intensity of the cells on Day5 for the control group and acts as a reference point for comparison between graphs. Cells do tend towards this median regardless of sorted population with the possible exception of the ”low” fraction, which appears to remain more negative than the other fractions.

3.15 Discussion

Main Conclusions

These experiments demonstrate that SSEA3 dynamics of model pluripotent cell line NTera2 can, for the first time, be effectively modelled using this approach. By observing the evolution of SSEA3 distributions over time it was possible to infer directly from data a chaotic one-dimensional map that predicts well the SSEA3 dynamics. This shows that the heterogeneity associated with SSEA3 expression across populations in standard cell culture can be the result of deterministic rules exhibiting chaotic behaviour rather than purely stochastic. In this context, given that embryo development is in essence a deterministic process, this suggests that heterogeneity reflects the transition to chaos of a deterministic system as a result of changes in the system parameters induced by the culture conditions.

One of the key features of the model is that it is capable of making predictions of future SSEA3 distributions that were generally well aligned with observed data from both the training and test data sets acquired during the first sort.

The model itself produced a non-uniform map which in itself contained several notable features. Examination of this map revealed that there are particular intensities of SSEA3 that had a higher propensity to vary over time than others. Additionally, equilibrium points were present upon this map of the model which, it was postulated, represented candidates for substates within the SSEA3 expression axis of variation. These notable

regions were sorted for in order to assess, via clonogenic analysis, whether there were any obvious biological corollaries associated with these highlighted points.

One of the fundamental findings from the clonogenic data was that there were some behavioural differences between fractions sorted by SSEA3 expression. Indeed, this was anticipated due to the already documented differences in behaviour particularly between SSEA3 positive and negative populations (Enver et al., 2005a). The most obvious differences shown were with regard the cell survival/attachment data, but there is no obvious corollary between predicted equilibrium points and observed behavioural patterns. Although cells were plated as singlet cells at a low seeding density (1,000 cells/cm^2), it is possible for individual cells to associate with each other, especially early on which could obfuscate the data. If a cell doublet were seeded at time zero, then all else being equal, it could produce a colony twice the size of a colony founded by a single cell. This is an issue that is particularly important with regard the differences seen in cell adherence to the culture vessel that may also influence/correlate with cell:cell adherence. Although efforts were taken to ensure cells remained as singlet cells by filtration prior to seeding, this does not guarantee that cells did not adhere to each other after filtration. This issue was also in part addressed by removing particularly large colonies from analysis, however this could also be erroneously disqualifying cells/ colonies that merged later due to differences in cell motility or even simple colony proximity. Strictly speaking, a clonogenic assay could be performed by the examination of a single cell isolated in culture, but human pluripotent stem cells are notorious for their poor clonogenic efficiency as well as evidence of improved survival when near

neighbours and this shortcoming usually overcome by seeding multiple cells as performed here (Enver et al., 2005a; Harrison et al., 2007; Li et al., 2010).

The final key objective was to develop a method by which data appropriate for modelling in this way could be acquired using significantly less material. Fulfilling this objective would make amenable the modelling of hESCs and other, less robust, cell lines where cell survival from sorts is low and cell line expansion is particularly impractical and expensive. The SSEA3 distributions derived from the fractions used in this analysis did display some degree of heterogeneity and indeed evidenced changing SSEA3 levels over time, although the appearance of these distributions were considerably different to that of those acquired by flow cytometry. Altogether this is not surprising since data acquired from the two different techniques are not directly analogous and it is encouraging to see the differences between fractions from the InCell-measured data. Further optimisation of the data collection approach and post-processing is clearly required to replicate the SSEA3 distribution appearance that is readily available with flow cytometric analysis. The observable SSEA3 expression differences contingent on sorted fraction and time support pursuing the development of this approach.

3.16 SSEA3 Population Distributions

Despite the fact that the SSEA3 distribution across NTera2 populations consistently displayed heterogeneity, it would be incorrect to assert that these distributions were identical. Take for example the difference between the distributions of batches 2 and 3 from the first sort; it is clear that despite some shared characteristics, they are clearly not identical. The distribution from Batch2 displays a multimodal distribution, but there are two clear larger populations representing an approximately bimodal population (Figure 3.5). The Batch3 distribution on the other hand did not present this broadly bimodal distribution; although there are multiple peaks and a broad range of intensity. There are several factors that could explain this difference; one of the main indirect corollaries of SSEA3 expression is culture confluency. From my own experience, SSEA3 expression generally appears bi-modal but expression rapidly decreases once cultures approach and surpass confluency. To counteract this, efforts were made to stagger cell culture in an attempt to perform sorts on cultures that were at approximately 90-100% confluency as a compromise between cell number and SSEA3 expression integrity. Despite this, there was in fact variation in culture confluency between these batches; with Batch3 being more confluent than that of Batch2. This difference could account for the reduced proportion of cells with high levels of SSEA3 expression. Regardless, cells from each fraction were available to sort between the batches and so could be examined. One crucial potential flaw would be if the reduction in the proportion of cells from these fractions was reflective of a global behaviour that would take time to resolve and become manifest in the behaviour of these fractions over subsequent days. In other words, if the proportion of cells of a particular fraction affects the behaviour of an

individual cell taken from within that fraction in advance of the sort, then subsequent SSEA3 dynamics observed would be contingent on the parental population and consequently altered by differences in this initial condition. An alternative interpretation is that once sorted, all cells exist, roughly, from within a fraction that is 100% reflective of itself, and so is no longer influenced by the proportion of cells occupying other fractions. A comparison of the observed and predicted data, not only of the training dataset (Batch3) but also of the test data-set from Batch2, demonstrates that the predictions were generally well reflective of the observed data. This implies that there was not a huge impact caused by the difference in the starting population SSEA3 expression patterns of these batches.

On the other hand, there were also differences between the SSEA3 distributions of the first and second major sort that are not the same as those seen between batch2 and 3 within the first sort. Firstly, the entire range of SSEA3 expression was larger in the second sort as compared to the first sort; in the first sort, SSEA3 intensity did not go much above $1x10^3$ whereas in the second sort, the maximum SSEA3 intensity was approximately $5x10^3$. There are several non-mutually-exclusive potential explanations for this. Firstly, this effect could be an artefact of some difference manifest during antibody staining resulting in a change in observed range of expression. This could be due to antibody degradation or different batches of secondary antibody resulting in a minor change in the range of expression pattern. Secondly, there could be differences in baseline as calibrated by the P3X negative control; a change here could alter the range that SSEA3 appeared to occupy. Thirdly, a change in the voltage sensitivity of the channel used to

measure SSEA3 intensity by indirect immunohistochemistry would alter the range upon which the intensities were seen. Finally, this could be a real effect, where the expression of the two populations really was different as measured.

In consideration of the aforementioned possibilities that could result in the difference seen between the SSEA3 distributions observed in the two sorts, the hypothesis with greatest power of explanation is probably a difference in the voltages associated with the channel. An offset here would change the range that the SSEA3 population appears to cover, and a comparison of the p3x medians between the two experiments reveals that they were indeed different.

Another issue to consider is that of sort accuracy. If there were significant inaccuracies in the sorting procedure, then the possibility that the dynamics we see are due to misclassified cells present by contamination during the initial sort. Considering the relationship between SSEA3 and pluripotency, where cells negative for SSEA3 are much more likely to have left the stem cell compartment whose progeny are unlikely to return and resume SSEA3 expression. A difference in classification could be particularly cumbersome for the negative/low fractions; where it could be argued that positive cells present in later fractions are the result of an inaccurate initial sort. An examination of back-gated data from the initial sorts reveals that sorts were generally accurate with distinct populations sorted from the main population (Figure 3.14).

Another consideration to the modelling approach is that samples examined between days are not directly linked, since the cells used to generate the model are discarded each day. The connecting factor between cells from the same SSEA3 fraction between days is that they were sorted for the same levels of SSEA3 expression prior to plating. Following that, the different timepoints for the sorted fractions are maintained in different cultures and thus no longer directly linked. This begs the question of whether cells examined on different days (that have been separate since the original sort) are directly comparable. One way to address this question is via technical replication, in which multiple plates are prepared for replicates of the same fraction from the same sort/Batch. Generally, due to the large cell number required to get enough cells from across the range of SSEA3 expression not enough sorted cells were available to run these technical replicates. That said, there were some occasions where multiple technical replicates of the same fraction from the same sort could be performed. Good evidence that this modelling procedure is fair is that the SSEA3 distributions from technical reps are similar for each day examined, implying that the distribution observed is representative of their behaviour. Such examples of these data are displayed in Figure 3.24, where indeed it appears that technical replicates are almost identical to each other.

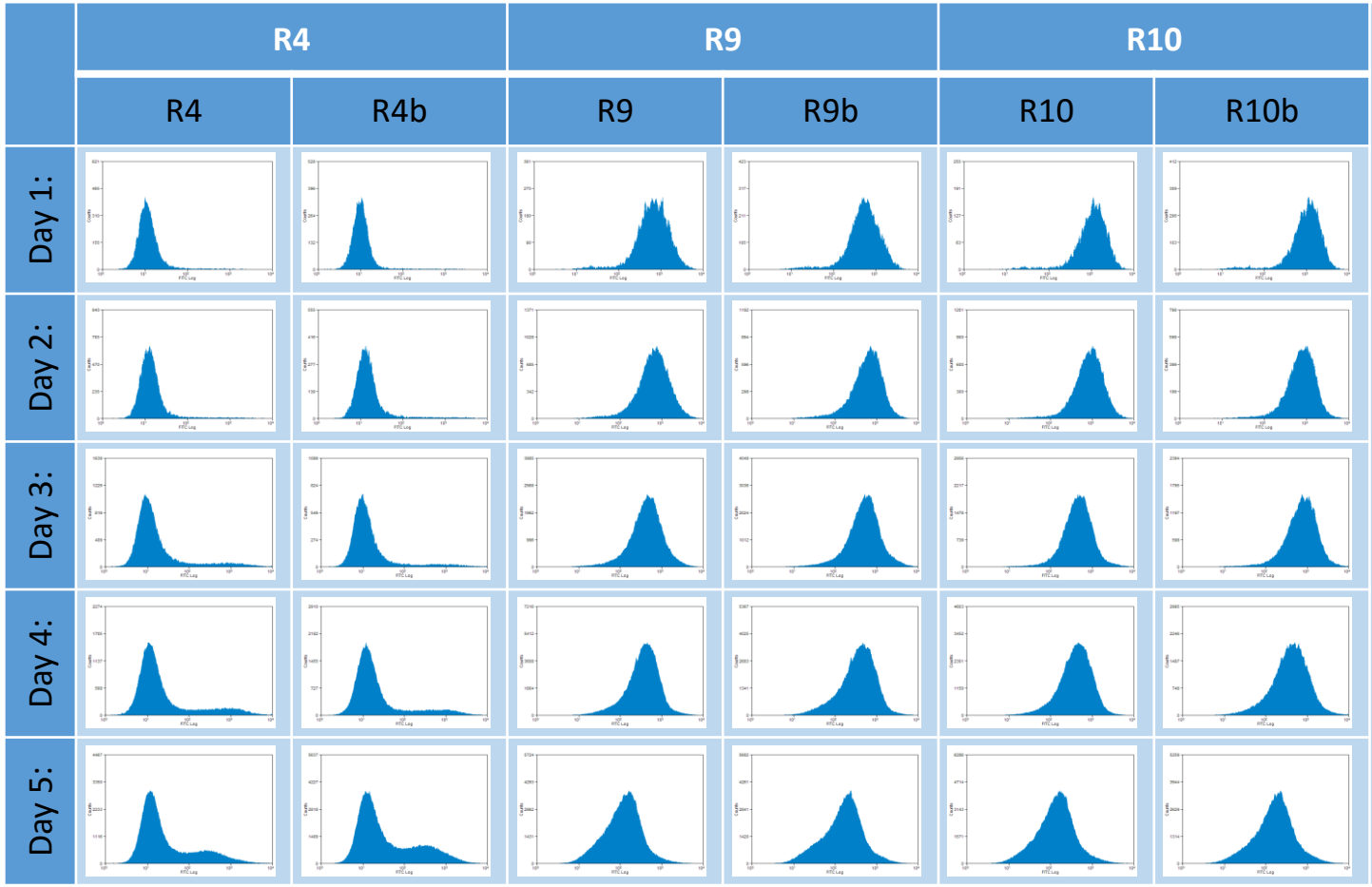

Figure 3.24 – Technical Replicate Comparison. Technical replicates performed using excess cells from sorts of these listed fractions. The evolution of the SSEA3 distributions from these fractions appear extremely similar, if not identical to each other for respective cell fractions. These data support the notion that SSEA3 changes over time are not stochastic and that the behaviour of sorted cell fractions over time is predictable

Additionally, it is quite unlikely that all negative cells have left the stem cell compartment. If that were the case, then there could not be any cells that once negative for SSEA3 then go on to express SSEA3 later. The increasing proportion of cells positive for SSEA3 within the Negative or Low fractions over time is itself evidence of this. It could, however, be argued that this is due to differential growth rates of cells that are either negative or positive for SSEA3. Taking this argument to its most extreme condition, it could be the case that no cells negative for SSEA3 ever reproduce and that all cells positive for SSEA3 reproduce and remain positive. Assuming the normal NTera2 cell cycle time of approximately one day, an estimate of the maximum proportion of expected positive cells based upon the previous day's proportion of positive cells in a population is calculable. In a hypothetical example, a population contains 5% positive cells (proportion positive= k_n), with the remaining 95% of cells being negative for SSEA3 expression (proportion negative = 1-k_n). Assuming that all positive cells replicate ($2k_n$) and none of the negative cells replicate (1-k_n), the expected maximum proportion of cells positive for SSEA3 on the following day (k_{n+1}) in the new population size ($2k_n$+(1-k_n)) is estimated by:

$$k_{n+1} = \frac{2k_n}{(1-k_n)+2k_n}$$

In this hypothetical example, the maximum proportion of positive cells possible on the following day is estimated to be 9.1% if they can only come from other positive cells. If the actual proportion of positive cells observed on the following day exceeds this proportion, then these cells must have come from an alternative population (*i.e.* negative cells). Of course, these are an extreme set of assumptions, which also includes the assumption that no cells in the population die. A comparison between the observed

proportion of positive cells and the calculated maximum on the following day is outlined in Table 3.4. Examples where the observed proportion of positive cells exceeds the predicted are highlighted in green. It is worth noting that this does not happen with all transitions and indeed for most examples that are highlighted, the predicted maximum is not exceeded by a large amount. It is worth emphasising that indeed this is the maximum proportion of cells positive for SSEA3 anticipated under a set of extreme conditions which are unlikely to all be accurate. If for instance, the criteria that negative cells never replicate and that positive cells never become negative are relaxed, then the predicted proportion of positive cells will decrease. Indeed, considering the observed cell population growth over the five-day period the replication of cells negative for SSEA3 is extremely likely (data not shown). Therefore, the fact that there are proportions of cells positive for SSEA3 that are equivalent or surpass this predicted maximum also evidences that cells negative for SSEA3 are indeed capable of giving rise to cells positive for SSEA3 and that cells positive for SSEA3 occurring within negative or low fractions cannot be merely attributed to inaccuracies in sorting.

Finally, the effects of SSEA3 staining itself and the bearing this has on the resulting behaviour of the cells examined. Cell surface antigens are likely functional to some degree and as such, the act of measuring SSEA3 expression via antibody binding is liable to elicit some change in behaviour that an untreated population of cells would not experience. In this case, it is especially true that, since we are sorting for cells based upon their expression of SSEA3, that different fractions are liable to respond differently to each other. For instance, by definition the population that is highly expressing SSEA3

will have more antibody for SSEA3 bound to it than the population that is not expressing SSEA3. Consequently, the dynamics that are witnessed are, strictly speaking, how cells that have had their SSEA3 antigen bound by antibody behave. This is not presently avoidable and is very much an inherent part of this modelling. Regardless, this model of SSEA3 dynamics can really only be used if the SSEA3 expression levels of the population of interest are known, which requires antibody interference anyway and thus remains suitable for practical purposes.

Table 3.4 – Table displaying the observed (Obs) and maximum predicted (Pred) proportion of cells positive for SSEA3 under the assumption that cells negative for SSEA3 do no produce cells positive for SSEA3 (other assumptions and calculation in the text). Predictions for any particular day are matched alongside the observed proportion and are calculated based upon the previous day's observed proportion of SSEA3 positive cells. Cells highlighted in green represent occurrences where the proportion of cells positive for SSEA3 exceeds the maximum predicted; indicating that some of these positive cells must have come from the negative cells and cannot be simply explained by positive cell reproduction.

	Percent positive (%) Using fraction: -ves						Percentage positive (%) Using Fraction: R5					
Replicate	May Batch1		May Batch2		May Batch3		Nov Batch1		Nov Batch2		Nov Batch3	
	Obs	Pred	Obs	Pred	Obs	Pred	Obs	Pred	Obs	Pred	Obs	Pred
Day0	-	-	-	-	-	-	-	-	1	-	2	-
Day1	15	-	20	-	17	-	15	-	7	3	7	4
Day2	35	27	22	33	17	30	-	26	16	13	-	13
Day3	51	52	36	36	32	29	40	-	21	28	22	-
Day4	63	67	-	53	53	48	58	57	28	34	41	36
Day5	63	77	60	-	49	69	51	73	42	44	52	58

3.17 Future directions

The modelling approach utilised here presents a completely novel way for investigating heterogeneity within the Stem cell compartment. Steps here have been made to develop the modelling procedure on the pluripotent EC line NTera2, and although the NTera2 system is not completely understood, applying this modelling to the human ES context is clearly desirable and more directly relevant in the context of regenerative medicine. Attempts to model NTera2 cells imaged in the InCell system have begun to make this setup more amenable to lower cell numbers. This work here provides the basis from which to develop a comprehensive method that would allow the analysis of heterogeneity within human ES cell lines in particular.

This modelling procedure has elucidated possible relationships between equilibrium points, which merits further investigation into how this informs our understanding of real biological behaviours. An examination of the differentiation potential of different equilibrium points will be the most likely method by which lineage bias may be assessed; this is one of the most important next steps. Alternatively, an examination of the gene regulatory networks by RNA sequencing, or examination of the pluripotency transcription network by qPCR may also draw out differences between these equilibrium points.

In this investigation, we have modelled one axis of variation (SSEA3 in these examples) but it would be exciting, and is plausible in principle, to extend the model to

simultaneously include other axes of variation. Such application could be useful in studies of cell lines using multiple markers such as the Sheff4.Gata6 cell line which has a GFP marker for Gata6 transcription. Studies performed by our group demonstrate that Sheff4.Gata6 exhibits multiple populations when its SSEA3 expression is compared against Gata6 (Figure 5.15a and personal communication with Dr. Thomas Allison). Sorting based upon these markers alone reveals that these different populations have different lineage biases.

Furthermore, it is possible to use this modelling procedure to examine how different environments affect the behaviour of cells with respect to a modelled marker. For example, the role of different culture media in ES culture is a heavily discussed feature of ES cell work, with many competing formulations generated and marketed frequently. The effect that different formulations on ES cell culture, in terms of ease of culture and spontaneous differentiation varies between users and laboratories. The effect that these media have on stem cell dynamics or substates within the stem cell compartment remains unknown but using this modelling technique provides a method by which to examine this problem. In a similar way, modelling of this kind could highlight how dynamics within the stem cell compartment differ between normal and culture adapted variants of ES cell lines.

This represents a promising new method by which to interrogate cell population heterogeneity dynamics that can be applied to the examination of substates within the stem cell compartment. Although this is a potentially powerful technique, it requires

labelling cells in some way, which may have unexpected consequences on cell behaviour, especially when dealing with subtle behaviours. In the next chapter a complementary method for analysing stem cell behaviour without the use of markers is explored.

Chapter 4

Raman Spectroscopy Use and Optimisation

4.1 Introduction

Techniques that permit the effective tracking and isolation of particular cells from within a much larger population such as cell surface antigen binding or the generation of fluorescent marker cell lines have been of great assistance for the interrogation of human ES cell biology. However, both of these approaches mandate some degree of interference with the cells of interest. Furthermore, there are very few approaches that provide a global readout of a cell's phenotype without requiring the destruction of that cell, particularly in the fields of transcriptomic and most metabolomic techniques such as mass spectrometry.

A technique that is steadily gaining traction in the biological sciences is Raman spectroscopy. Raman spectroscopy is a vibrational light spectroscopic technique that is capable of providing a plethora of information on the types of chemical bonds present within a sample. Although this technique has been traditionally used in the chemical and material sciences for sample identification and verification of sample chemical purity, it is being utilised steadily more frequently for biological research. Furthermore, it is also emerging as a technique applied to the field of pluripotent stem cell research. In effect, Raman spectroscopy represents a minimally invasive method for the examination of the biochemical state of a cell which may be readily compared against its neighbours or, indeed, other cell types.

Raman spectroscopy has a twofold advantage when it comes to biological research. It can be used for the generation of "spectral signatures" reflective of particular cell types, but it also contains biological information that is directly pertinent to the cell's biochemical composition. An example Raman spectrum typical of a cell is presented in Figure 4.1. The x-axis represents the Raman shift that is a measure of the inelastic scatter of the photons that interacted with the

sample. Raman shift is typically presented in wavenumber format ($\Delta\omega$ (cm^{-1})) and is calculated by

$$\Delta\omega\ (cm^{-1}) = \left(\frac{1}{\lambda_0} - \frac{1}{\lambda_1}\right) \times 10^7$$

Where λ_0 is the excitation wavelength (*i.e.* of the incident photon) and λ_1 is the Raman spectrum wavelength, with both λ_0 and λ_1 measured in nanometres. The y-axis represents relative intensity in arbitrary units. Since the Raman shift any incident photon experiences is as a result of its interaction with particular molecular bonds, it is possible to identify particular peaks and patterns that are attributable to different classes of molecule or even of specific candidates. For instance, phenylalanine typically has an extremely sharp peak at 1000.3 cm^{-1} that is readily identifiable and is evidence that a biological sample is under consideration (Krafft et al., 2006) In addition, there are particular regions in the Raman spectra that are attributable to nucleic acids, proteins as well as saturated and unsaturated fatty acids (Figure 4.1; (De Gelder, 2007; Harz et al., 2009; Kneipp et al., 2006; Maquelin et al., 2002; van Manen et al., 2005). Organic molecules have Raman shifts that are typically in the region of 500-1800cm^{-1} and is termed the "fingerprint" region (De Gelder, 2007).

Raman spectroscopy has been used in a variety of biomedical research and the scope of its use has developed in line with the technology around it. The earliest applications of Raman spectroscopy were of large volumes of highly concentrated biomolecules, with spectra collected over a long time-frame owing to the weak Raman effect (Krafft et al., 2006). However, the advent of several key technologies has significantly reduced the acquisition time of Raman spectra. Indeed, the availability of modern commercial benchtop Raman spectroscopy systems was only made possible with the development of the air-cooled LASER, Charge coupled device (CCD) multi-channel detectors, the desktop computer and holographic notch filters for Rayleigh

scattered photon suppression (Adar, 2007). The feature of high powered lasers for maximal signal generation and sensitive CCDs for efficient collection have facilitated the use of Raman spectroscopy within the single cell context (Excellently reviewed in Smith et al, 2016).

With regard to pluripotent stem cell heterogeneity, the ideal scenario would be the live, real-time acquisition of Raman spectra where cells are maintained in a healthy environment, i.e. aseptic, 37°C in appropriately buffered cell culture media. Raman spectroscopy has been applied in a number of ways to interrogate cellular systems and has been used to examine cells in suspension (Crow et al., 2005; Krishna et al., 2006; Mourant et al., 2005; Short et al., 2005), live cells in a standard culture monolayer format (Notingher, 2002), as well as chemically fixed (Krafft et al., 2006; Swain and Stevens, 2007) and dried cells (Crow et al., 2005; Krafft et al., 2006; Krishna et al., 2006; Mourant et al., 2005; Notingher, 2002; Schuster et al., 2000; Short et al., 2005; Swain and Stevens, 2007). These different approaches come with their own sets of considerations, of which the most notable is the difference between fixed and live cells (Swain and Stevens, 2007). Fixed cells are killed and preserved by chemical means, which translate to an altered chemical composition compared to living cells that is certainly reflected in the Raman spectra (Meade et al., 2010). However, this does not preclude the examination of biochemical information from fixed cells in comparison to each other.

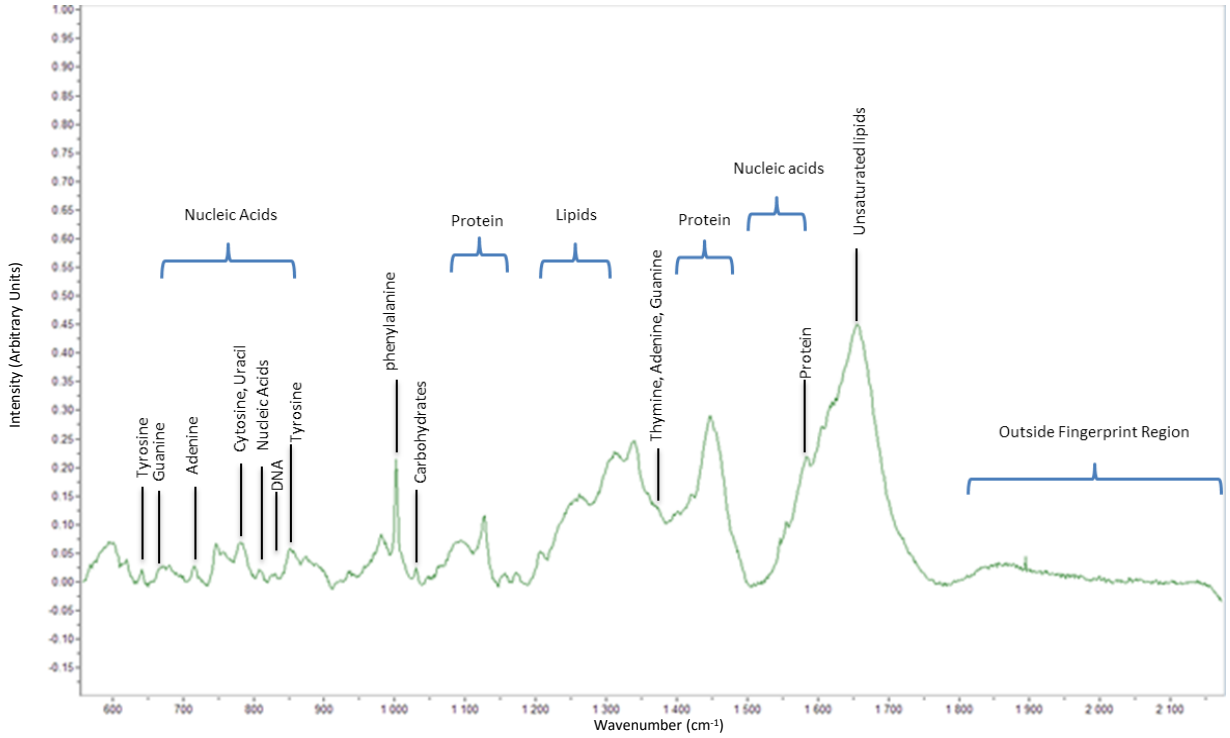

Figure 4.1 – A typical Raman spectrum of a live pluripotent embryonic carcinoma cell, NTera2. Raman spectra are information rich and provide substantial information about the biochemical state of the cell. Almost all Raman scatter related to organic molecules occur in the region 500-1800cm^{-1} wavenumbers and is thus termed the fingerprint region. Raman spectra of cells generate a plethora of Raman bands reflecting the degree of complexity biochemical complexity of the cell. The Raman spectra of many organic molecules have been determined elsewhere which allows the tentative identification of molecules represented in the biochemical mixture. For instance, there are several bands associated with proteins, lipids and nucleic acids of both RNA and DNA. The association of particular Raman bands to organic molecules has been studied elsewhere and these examples are compiled from the literature (De Gelder, 2007; Harz et al., 2009; Kneipp et al., 2006; Maquelin et al., 2002; van Manen et al., 2005)

The application of Raman spectroscopy to cell culture is still a developing technique and there currently exists no standardised method. One of the key differences among existing methods is the time required to acquire Raman spectra from cells of interest, which is also affected by the format in which the cells are presented; for example, live/fixed or suspension/monolayer. If Raman bands of interest are known *a priori* then the collection time required for suitable comparison between particular samples is considerably shorter than holistic approaches to examine general cellular "signatures" since only a direct comparison between known bands of interest is required. For instance, a technique, using culture media containing metabolites labelled with alternative radioisotopes (such as ^{13}C rather than ^{12}C) can be used to readily identify microbes that metabolise the labelled metabolite with extremely short acquisition times (100ms) since the differences of interest are already known (Huang et al., 2004b; Li et al., 2013) ; Radioisotope labelling is effective in Raman spectroscopy since the altered mass of the labelled nuclei causes a change in the vibrational frequency of that molecule and this difference may be calculated *a priori* (Huang et al., 2004b; Li et al., 2013).

Different Raman techniques also contribute to the manner in which Raman spectra are collected in terms of acquisition time and spectral information. Spontaneous Raman imaging, which is used here, acquires Raman spectra from individual points from the sample of interest using a single laser for the generation of Raman scattered photons. Alternatively, coherent anti-Stokes Raman spectroscopy (CARS) utilises a multiple photon approach using tuneable lasers that produces a signal where emitted waves are coherent to each other. Coherent radiation emitted is greatly enhanced when the difference between the laser pulse frequencies match that of the Raman frequency of the molecule of interest. As a result, CARS signals are approximately 10^5 times stronger than that of spontaneous Raman spectroscopy and CARS has been used to examine the differences between differentiated and undifferentiated mouse ES cells with

acquisition times of 0.3s per spectrum (Konorov et al., 2007). CARS remains in its infancy, although several successful proof-of-concept approaches have been demonstrated in a biomedical context (Keren et al., 2008; Qian and Nie, 2008; Ryder, 2005). Another common Raman technique is surface enhanced Raman spectroscopy (SERS) that typically employs the use of metal nanoparticles that when adsorbed by sample molecules generate high Raman scattering intensities by a plasmonic effect (Nie and Emory, 1997; Qian and Nie, 2008; Schlucker, 2009). Although SERS can increase the Raman effect 10^{14} or 10^{15} fold (Nie and Emory, 1997) it necessitates sample interference that can alter cell behaviour which is undesirable in this case (Kneipp et al., 2005).

One major prerequisite for the application of Raman spectroscopy to biological samples is that the Raman effect reflects the chemical composition of the sample in a quantitative manner. However, this quantitative aspect is readily obscured by various experimental factors that influence the raw intensity of Raman signal acquired since the emission of Raman scattered light depends on multiple factors including the intensity and frequency of the excitation laser, the number of molecules (Rea, 1959) and in some instances with sample temperature, although usually associated with inorganic compounds (Chattopadhyay et al., 1982; Xie et al., 2001). Raman spectroscopy can however be used to infer relative concentrations of particular molecules within a sample which, when compared against a calibrated concentration curve for that molecule can be used to calculate absolute concentration within solid (Araiza-Reyna et al., 2013) and liquid samples (Sato-Berru et al., 2016) .

Furthermore, noise is introduced into Raman spectra acquisition from surrounding light and cosmic radiation in addition to sensitivity to instrumental parameters that may reduce the efficiency of photon flow between sample and instrument. Finally, fluorescence is an especially

powerful source of noise in the collection of Raman spectra. Raman scattering is a rare event, with only about one in every ten million scattered photons undergoing this process (Ellis and Goodacre, 2006). On the other hand, fluorescence is a much stronger effect by several orders of magnitude and Raman spectra are easily obfuscated by broad bands of fluorescence. Utilising lasers with frequencies in the near infrared or ultraviolet regions. However, the low energy infrared laser approach necessitates longer acquisition times, whereas high energy UV lasers risk sample heating and destruction (Afseth et al., 2006). Therefore, here, a 532.32nm excitation laser was employed which was also found to generate the best single cell Raman spectra in the context of bacteria examined with the same system (Huang et al., 2004a). In order to acquire a meaningful interpretation of Raman spectra, mathematical correction methods are applied in order to remove the unwanted aspects of variation described above.

Raman spectroscopy, like other light vibrational techniques, offers unique insight into the biology of the cell, and may be used to identify signatures pertinent to particular cell types (See chapter 1). This capacity to distinguish cell phenotype based upon signals generated endemically from the cells of interest presents an opportunity to interrogate stem cell substates in a manner that is minimally invasive. This is appealing both as a research tool, as the cells can be measured and then used experimentally, and later as a tool to identify particular cells pertinent to an e.g. medical application by sorting for cell with a particular lineage bias for a differentiation protocol. Ultimately, the development of Raman signature-based based method for live cell type recognition and sorting for cells of interest, similar to that of flow cytometry, that requires very little physical interaction with the cells under consideration. Alternatively, the combination of Raman spectroscopy with time-lapse studies on pluripotent cell behaviour could prove extremely informative.

Raman spectroscopy is not a technique already utilised by the Centre for Stem Cell Biology and thus needed to be introduced, developed and optimised for data collection from pluripotent stem cells. This chapter deals with the optimisation of Raman spectra collection and data processing for use in addressing the biological questions raised in Chapter 5 although this optimisation was a lengthy and iterative process meaning that several experiments in Chapter 5 that were performed in parallel are not addressed using the final methodology. An outline of the Raman spectra collection and spectral treatment process is shown in Figure 4.2. Here, a proof of concept approach is adopted for the application of Raman to stem cell substate analysis that uses NTera2 as a model cell line in the development of the Raman spectroscopy technique.

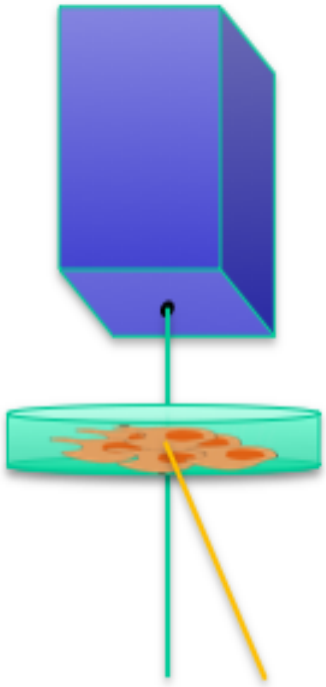

Acquisition

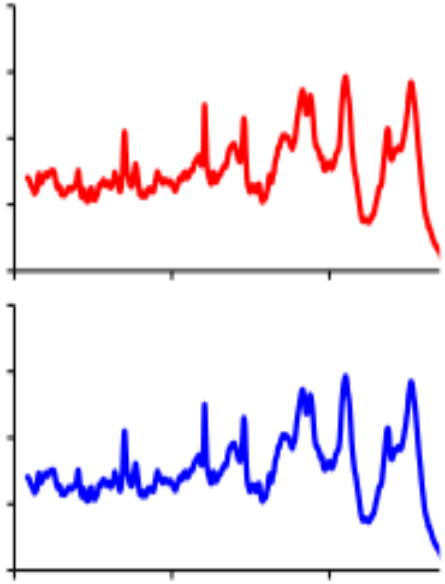

Normalisation

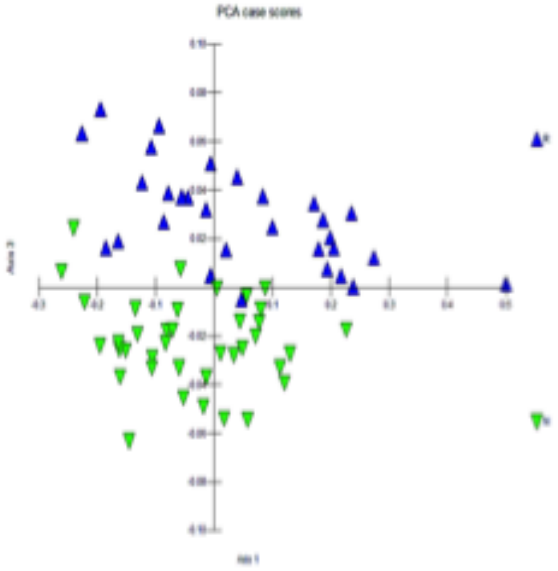

Clustering Analysis

Fig 4.2 – Typical process of Raman Spectrum acquisition and analysis. Raman spectral data is acquired from cell sample of interest, then normalised in order to remove undesirable variation in Raman spectrum collection. Normalised data are then compared against each other in a using multivariate statistical techniques such as principal component analysis (See materials and methods).

4.2 Results

Initial studies were conducted using the human EC cell line NTera2. Given the desire to utilise Raman as a cell sorting technique, similar to flow cytometry, cells were trypsinised and harvested prior to analysis as is usual for flow cytometric analysis (See materials and methods). Cells were aliquoted in PBS onto CaF_2 slides, a Raman inactive substrate, and analysed by Raman spectroscopy. It became immediately apparent that the Raman spectra acquisition time was considerably longer than that required for flow cytometry, requiring at least 30 to 60 seconds acquisition time per cell. For comparison, flow cytometry systems are capable of examining thousands of cell per second. Suspension-based acquisition methods were at this stage disqualified from further experiments since this time-scale permits too much cell movement; often causing cells to move out of focus during acquisition time.

It quickly became apparent that the substrate on which cells were grown required careful consideration when adopting a monolayer approach. The traditional adherent culture plastic on which most cell culture is performed in our laboratory transpired to be extremely Raman-active, producing a strong background (Figure 4.3a) that appeared significantly different to cells analysed on CaF_2 (Figure 4.3b in red). The common alternative to culture plastic, glass slides, also produced some background (Figure 4.3c), although not to the same extent as culture plastic as evidenced by the raw intensity data, especially when compared to the same spectrum of a cell analysed on CaF_2 (Figure 4.3d). A Raman-inactive substrate as a potential culture substrate such as CaF_2, was trialled and indeed did not produce any significant background. NTera2 cells readily adhered to this substrate and appeared to grow normally (Materials and methods). CaF_2 Is relatively expensive and so we developed a cleaning protocol for the slides so that they could be reused (see Materials and Methods).

4.3 Media

Examination of NTera2 cells grown on CaF_2 prepared for live single cell Raman spectroscopy revealed that the standard culture media for routine NTera2 maintenance was itself Raman-active, which was attributed to the presence of phenol red (Figure 4.4a). The background interference caused by phenol red was significant and saturated the detector. Only by reducing the laser power and acquisition time was it possible to acquire spectra that did not saturate the detector. Furthermore, attempts at normalising the data in an attempt to remove this background interference were not able to produce spectra comparable to that of a cell (Figure 4.4b). An alternative DMEM formulation that did not use phenol red as a buffer was trialled for the maintenance of NTera2 cells (materials and methods). The cells grew readily on CaF_2 using this media and the high background associated with phenol red was not present in cells examined (Figure 4.4a).

When spectra that were previously acquired from cells in suspension in PBS were compared against data acquired from cells grown in a monolayer format in phenol free media, a couple of things became apparent (Figure 4.5a). Firstly, although spectra presented expected regions of biochemical markers (such as protein bands, nucleic acid bands etc…), their pattern differed between the two categories. Secondly, the acquisition time required was considerably increased in the monolayer format in order to acquire spectra that were comparable in the first place (an increase from 10 seconds to 30 seconds). Finally, an examination of the phenol free media itself also revealed a similar pattern to that of the cells grown in this media (Figure 4.5b). This observation leads to the conclusion that an increased data acquisition time would be required in order to obtain Raman spectra from cells of interest that could be distinguished suitably from their background media.

4.4 Cell Fixation

The above results so far, in combination, began to indicate that with the present arrangement live cell analysis would not be feasible. The data acquisition time for samples far exceeded initial expectations that could not be considered comparable to those of a flow cytometry assay. Additionally, acquisition time would be compounded further in order to acquire cellular data that would overcome noise generated from background media (Figure 4.5). Finally, facilities designed to maintain cells within normal homeostatic bounds were not present on the current set up, which led to sample infection as well as presumed stress on the sample cells. Although 30 seconds is not a long period of time for each sample, it still took several hours to collect Raman spectra from each treatment. The Raman microscope laboratory did not have any available incubator facilities, meaning that all samples were subject to sub-optimal conditions during spectral acquisition, being at ambient temperature whilst the treatment being sampled was not maintained in aseptic conditions. At this point, it was not financially viable nor practical to alter the Raman microscope with an environment chamber therefore the decision was made that live cell analysis was not an appropriate avenue to pursue at that time but that a proof of concept approach using fixed cells was justifiable (see discussion). The chosen method of cell fixation adopted was by paraformaldehyde (PFA) as described in the materials and methods section. To prevent the issues associated with infection of fixed samples stored in phosphate buffered saline (PBS), after cells were rinsed with PBS after fixation they were washed with distilled water for two minutes to remove residual salt that would otherwise crystallise and interfere with analysis before the water was removed and fixed cells left to dry.

A comparison between Raman spectra acquired from cells that have been first fixed by paraformaldehyde and initial Raman spectra acquired from the cell suspension treatment is displayed in Figure 4.6. The spectra share several similarities, with representation from all gross

types of organic molecule highlighted in Figure 4.1. There are of course several differences between these spectra that is probably attributable to the PFA fixation process. The most obvious difference between these spectra is the exaggerated peak at 1003 cm^{-1} in the PFA fixed cells.

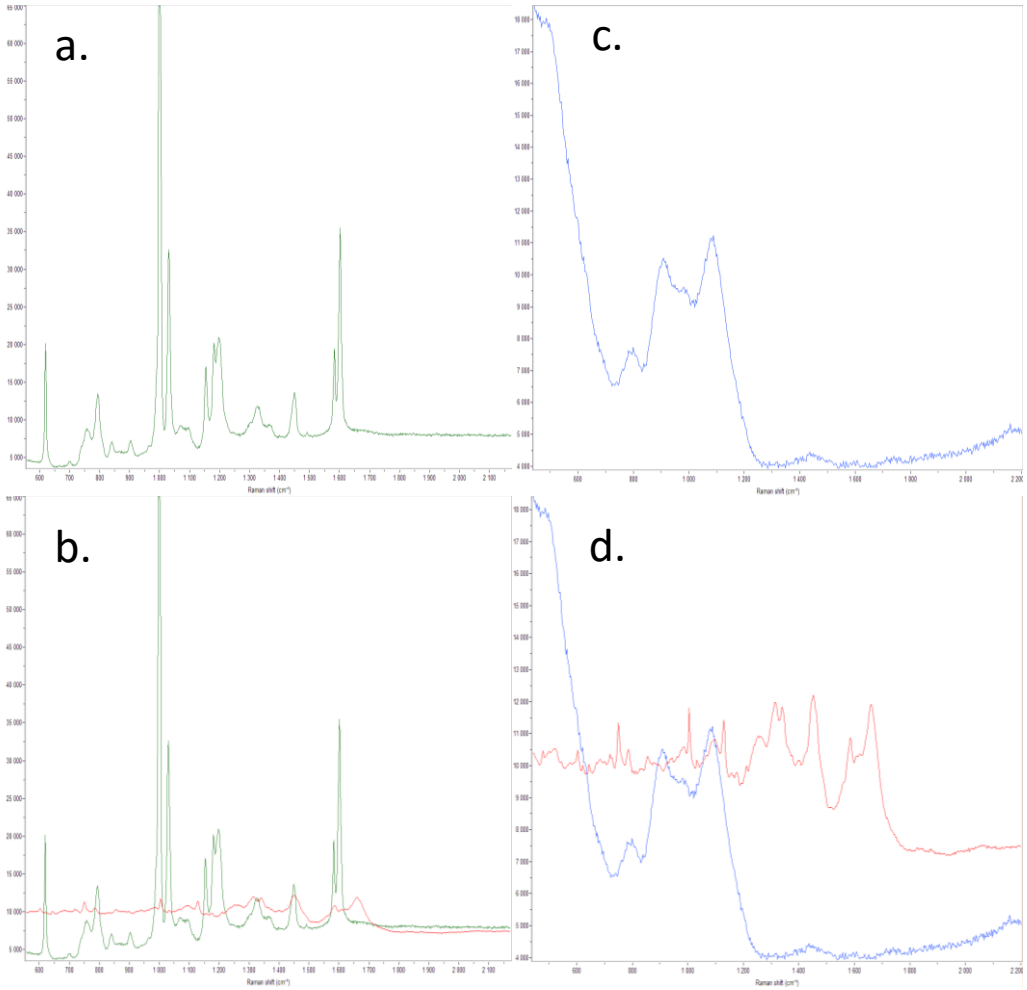

Figure 4.3 – Culture Surface and Raman Background. A comparison of Raman spectra collected from cells grown on different culture substrates. All spectra were collected for a 10 second period using the 532nm wavelength laser at 100% capacity. **a)** shows the spectral background typical of adherent culture plastic (green). **b)** The same plastic spectrum compared against Raman data collected from a cell in suspension, aliquoted onto a CaF_2 slide (red). The plastic spectrum is clearly more Raman active than the cell, producing spectra that are significantly more intense. **c)** Shows the spectral background as a result of glass microscope slides (blue). **d)** a comparison made between the same glass spectrum in c and the same Raman data collected from a cell in suspension, aliquoted onto a CaF_2 slide as in b (red). The glass slides are also Raman active, but considerably less so than culture plastic.

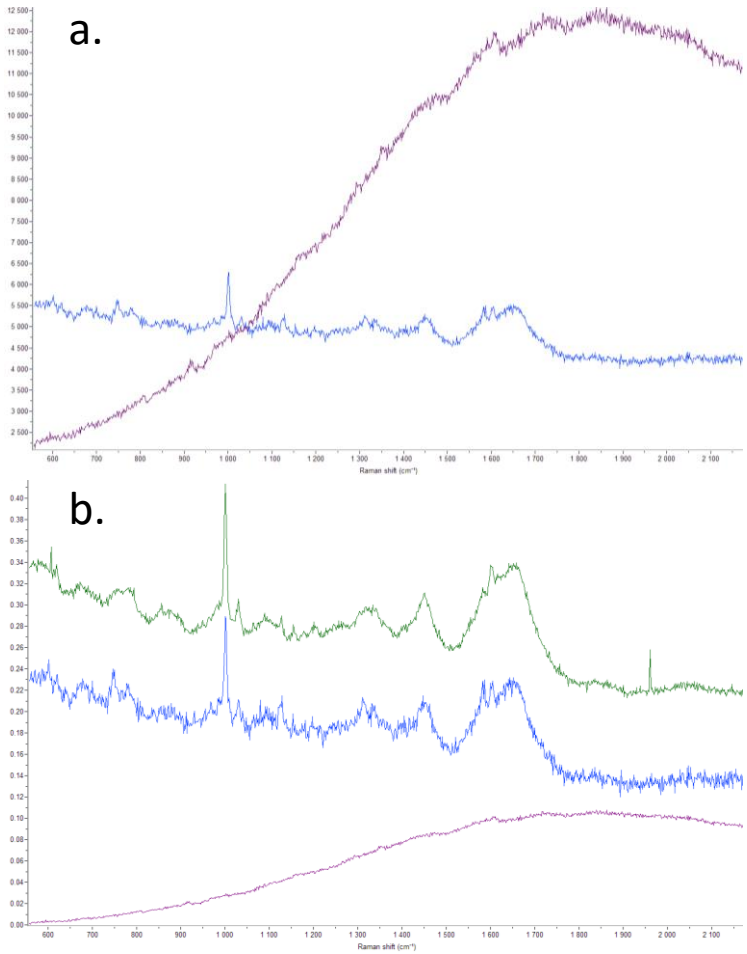

Figure 4.4 – Phenol Red Media Interference. A comparison between Raman spectra collected from cells in different culture media at the time of acquisition. **a)** Raw Raman intensity count data from a cell grown in phenol red free media (blue); Raman data was acquired over a 30second period using the laser at full power. In purple, a Raman spectrum acquired from a cell in media containing phenol-red; Raman data was collected over a 20 second period with 99% of the excitation laser radiation filtered out. The broad increase in Raman intensity in the later wavenumbers is reflective of phenol red mediated fluorescence. **b)** All spectra are normalised by area under the curve which is not able to generate a spectrum from cells grown in media containing phenol red that is comparable to spectra from media that does not contain phenol red. Blue and purple spectra are the same as in a, except normalised by area under the curve. The green spectrum is also from a cell grown in media that does not contain phenol red, however the Raman data was acquired over a 200 second timeframe (laser unfiltered). The shape of the green and blue spectra are very similar despite the change in collection time. Spectra are vertically shifted so that a comparison between spectral shape can be made.

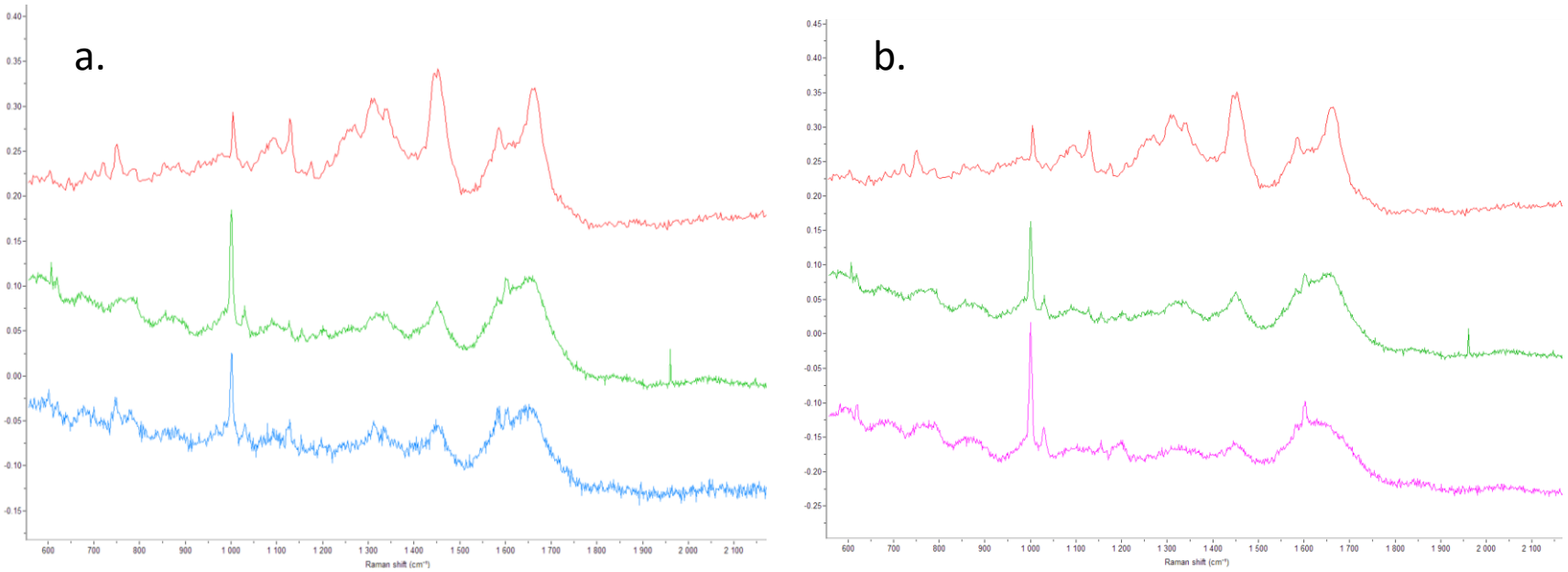

Figure 4.5 – Comparison of Suspension and Monolayer Spectral Acquisition Formats. Comparison of Raman spectra acquired from cells in a suspension or monolayer format. Spectra are vertically transposed in order to facilitate visual comparison. **a)** Comparison between normalised data collected from cells in suspension in PBS (Red, 10 second acquisition time) and Raman spectra collected from cells grown in a monolayer format on CaF_2 slides using phenol free media (Blue, 30 second acquisition time; Green, 200 second acquisition time). There are differences in the spectra between cells cultured in a monolayer format (Blue and Green) when compared to that of cells suspended in PBS however there are comparable regions, with respect to wavenumbers associated with fatty acids, amides, and nucleic acids. **b)** Comparison between the normalised Raman spectra collected from cells suspended in PBS (Red, 10 second acquisition time), cells cultured with phenol free media in a monolayer format on CaF_2 slides (Green, 200 second acquisition time) and of the phenol free media on its own (pink; 60 second acquisition time). The extreme similarity between spectra acquired from cells in the phenol free media and of the media itself suggests that there is a large contribution to spectra from the organic components of the media alone, making it difficult to determine whether the spectra acquired from the cell is actually noise from its media.

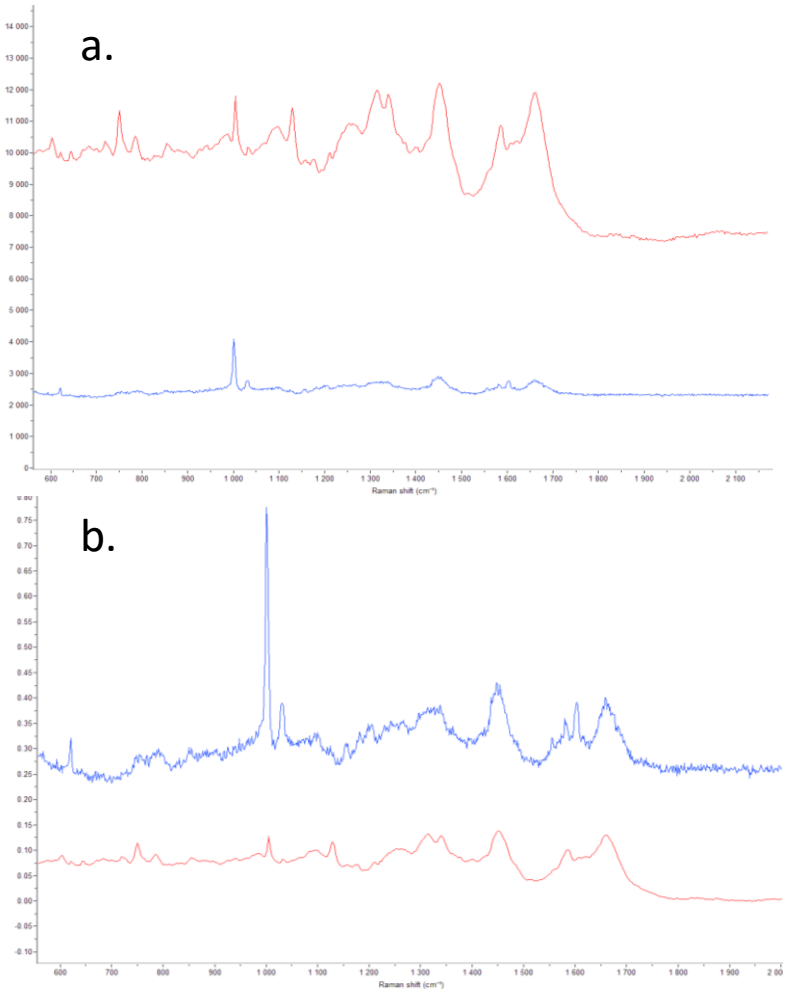

Figure 4.6 - Comparison of Raman spectra from cells that are live or fixed. Live cell Raman spectra (red; 10 second acquisition time) were collected from cells suspended in PBS, whereas fixed cells (blue; 60 second acquisition time) were cultured directly onto CaF_2 slides prior to paraformaldehyde mediated cell fixation and drying. **a)** Raw intensity data demonstrates that despite the six-fold increased acquisition time afforded to PFA treated cells, signal from this cell is approximately four-fold weaker. **b)** Normalised spectra of the data shown in a) for examination in terms of spectral pattern. Spectra are vertically transposed to permit comparison of spectral pattern. There are clear similarities and differences between the spectra, the most notable being the exaggerated peak at approximately $1000cm^{-1}$ in the fixed cell format. Regardless, Biochemical information can be acquired from fixed cells.

4.5 Intracellular considerations

Preliminary data obtained from cells were collected using an arbitrary single point to be representative of that cell. Although this meant that the sample acquisition time for each cell was less than one minute or less (depending on the experiment), it would not be appropriate to presume that a fair comparison between cells could be performed with such data. This is principally due to the fact that cells do not exist as a homogeneous collection of their biochemical components but instead exist as highly structured and compartmentalised entities. Therefore, it is quite plausible that such a comparison may be distinguishing between intra-cellular components of the cells in question rather than being reflective of those cells' biochemistry in general. For example, the arbitrary sampling of one cell may be acquiring biochemical data pertinent to the endoplasmic reticulum whereas the arbitrary sampling of another cell may be examining a mitochondrion.

In response to anticipated intra-cell biochemical heterogeneity, two approaches to address this issue were developed. The first approach posited that a more appropriate comparison would be of specific organelles between each sample cell (Chapter 5). The alternative approach proposed that the average spectrum derived from the whole area over the cell would capture the range of intra-cellular biochemical variation within that cell. Thus the average Raman spectrum across that cell would be a suitable measure by which to compare different cells.

The approach of capturing as much biochemical data from across the cell as possible was employed by systematically acquiring data across the cell in the pattern of a square grid, a process termed hyperspectral imaging. However, a compromise needed to be made between the spatial resolution of data acquired from across the cell and the analysis duration. In the initial

preliminary experiments described above, approximately sixty seconds per point were required which would be impractical to perform on a large number of points from an individual cell. Therefore, a study was conducted whereby the number of data acquisition points from a cell was altered in conjunction with the spectral acquisition time per point in order to establish a compromise between spatial resolution, signal intensity and time taken per sample (Figure 4.7; table 4.1). From this approach, it soon became apparent that the region identified as nuclear returned a much stronger signal than the surrounding cytoplasm. For the sake of brevity, the scope of these analyses changed to the collection of data from this region only; permitting improved spatial resolution from this region. Ultimately, a 2µm by 2µm grid with an acquisition time of ten seconds per point represented the compromise by which as much spatial information across the cell/nucleus could be acquired whilst maintaining a reasonable collection time of about 40 minutes to two hours per cell, which varied according to cell size and whether the cytoplasmic component was also included. A typical acquisition across a cell yields approximately 100-200 spectra of the cell's nucleus, and a larger range of spectra for the cell's cytoplasmic compartment.

Table 4.1 - Examination of the spectral acquisition time required to analyse a square grid of 40µm by 40µm according to differing acquisition times and spatial resolutions. 40µm by 40µm represents a typical grid size used for Raman spectral acquisition across a cell area, although of course the actual grid size varied according to cell analysed. Times given in the cells are presented in minutes. The 2µm by 2µm spatial resolution was chosen as a practical compromise between spatial resolution and acquisition time.

Acquisition Time per Point	Spatial Resolution				
	1µm by 1µm	2µm by 2µm	4µm by 4µm	5µm by 5µm	10µm by 10µm
1s	27	7	2	1	0.3
10s	267	67	16	11	3
30s	800	200	50	32	8
60s	1600	400	100	64	16
120s	3200	800	200	128	32

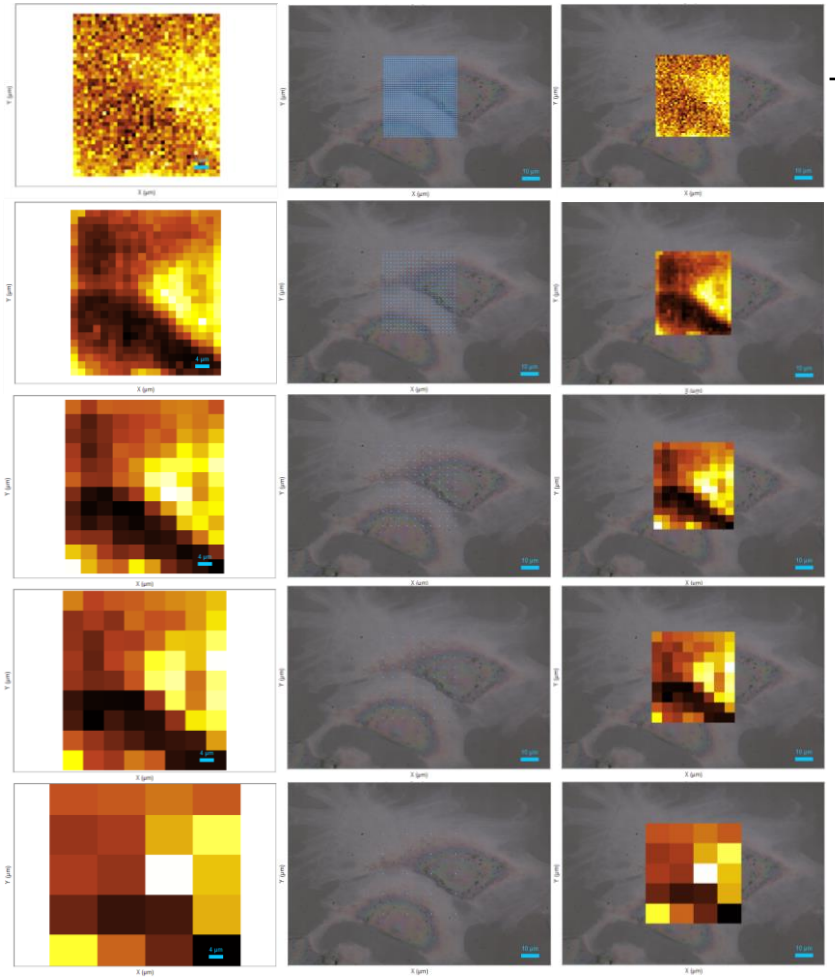

Spatial resolution	Acquisition time (s)
1µm x 1µm	1
2µm x 2µm	10
4µm x 4µm	30
5µm x 5µm	60
10µm x 10µm	120

Pixel signal intensity

High

Low

Figure 4.7 – Compromise between Acquisition time and Spatial Resoluation. A study comparing Raman spectrum acquisition time and spatial resolution, in order to determine the optimal acquisition time vs grid density. The top row represents a high spatial resolution and low acquisition time, the bottom row represents the lowest spatial resolution and highest acquisition time per point. Pixels are pseudocoloured according to signal intensity relative to other spectra from that same map. White/yellow is the highest intensity and black is the lowest.

4.6 Antibody staining

The capacity to couple Raman spectroscopy to other techniques used within the laboratory permits an increased scope in the range of questions that Raman could be used to address. Indirect immunofluorescence is one such technique that is used frequently to identify and sort for, by fluorescence activated cell sorting (FACS), particular cell populations of interest to the researcher. The capacity to acquire Raman data on these cells is another measure by which particular cell populations, determined by their marker expression, could be compared. It is important to consider then, that Raman spectroscopy is dependent on the rare proportion of photons that undergo the Raman effect; and that fluorescence is a much more frequent phenomenon. Fluorescent molecules that have excitation and emission wavelengths similar to the photons produced by the laser can cause significant and overwhelming background interference making Raman spectra almost impossible to interpret without significant alteration to spectral pre-processing (Figure 4.8). Therefore, it is important to ensure that any secondary antibodies used, or other fluorescent markers are appropriate for the laser used in the Raman analysis. The 532.32nm laser used in this system precluded the use of FITC, for example, as secondary antibody fluorophore but Cy5 (or Alexa 647) proved to present negligible background interference. Consequently, these antibodies were used in experiments that included both indirect immunofluorescence and Raman analysis.

4.7 Matrigel

Cultures of NTera2 and 2102EP EC cells grew readily on CaF_2 slides. However, these represent particularly robust cell lines and readily attached. Cultures of ES cells did not attach with the same ease and, considering that some form of matrix is usually required for their growth and maintenance even on adherent cell culture plastics, an approach by which CaF_2 slides were first treated with Matrigel was adopted. An examination of NTera2 cells that were cultured with or

without Matrigel revealed that there was no obvious background interference cause by the use of Matrigel and did not obscure the data collection, certainly not in the same manner as phenol red if at all (Figure 4.9). Therefore, Matrigel is a suitable substrate for use with ES cell lines cultured for Raman analysis on CaF_2 and was the technique adopted here. In order to accommodate for any systematic effect of Matrigel treatment of cells on Raman spectral data, one should be careful to ensure that only cells treated with Matrigel are compared against each other in analysis.

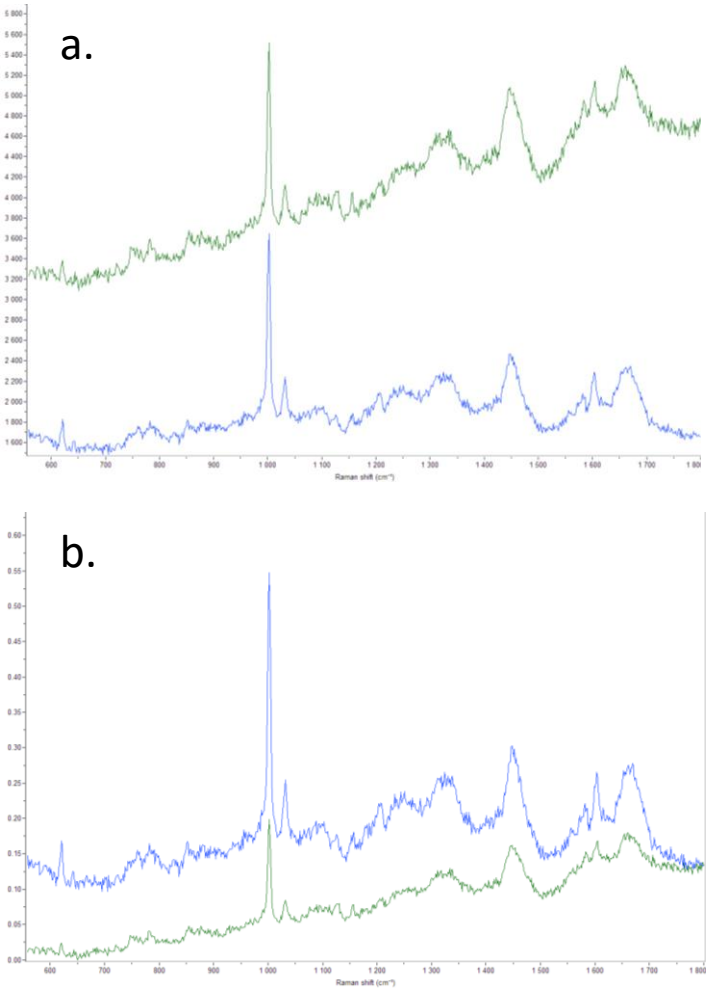

Figure 4.8 – Examining the effect of fluorophore interference. a) and b) are of the same spectra, however **a)** is the raw intensity and **b)** shows the normalised spectra. The green spectrum is contaminated with fluorescence, generating a larger tail with relatively larger intensities for larger wavenumbers than the uncontaminated blue spectrum. The effect of this fluorescence is very clear in the normalised spectra, despite their visual similarity when considering the raw spectra.

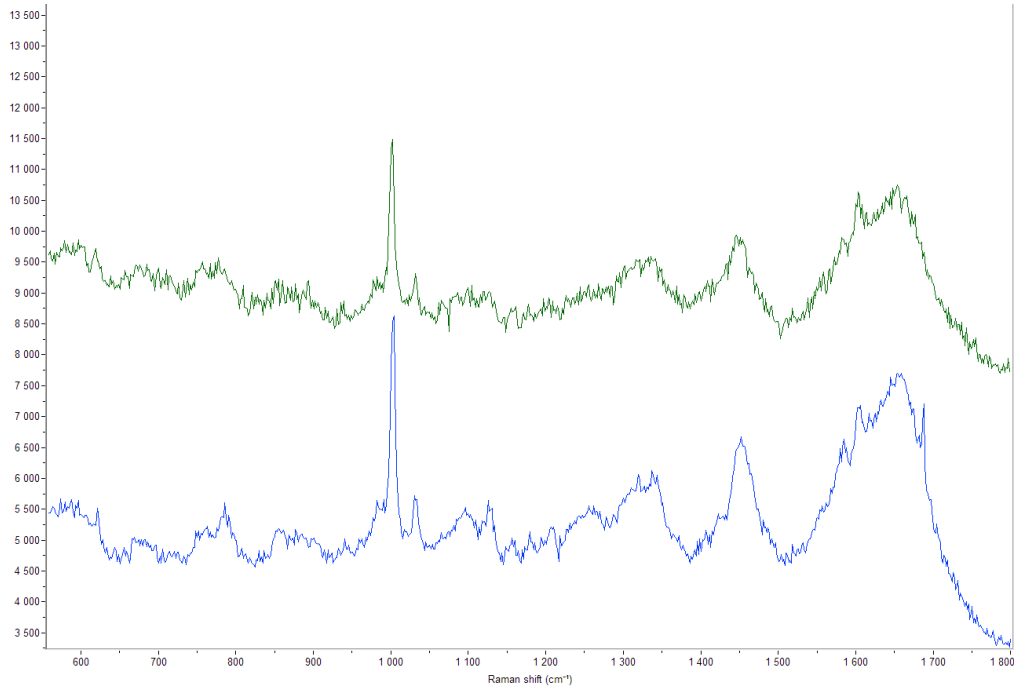

Figure 4.9 – Matrigel Shows no Obvious Raman Background. A comparison of Raman spectra between NTera2 cells grown directly on CaF_2 slides (blue) or on CaF_2 slides that were pre-treated with Matrigel. No obvious background effects were present such as that introduced by media containing phenol red.

4.8 Data processing

Once Raman spectra were collected, a number of post-processing steps were required to make data comparable for analysis. The "fingerprint" region, as it's called, from Raman spectra on biological samples is present between wavenumbers 500 and 1800 (cm^{-1}). Data from these regions specifically were extracted for use in further analysis.

Since Raman is only a semi-quantifiable technique, direct comparison of intensities from one sample and another is inappropriate. Therefore, the data are then "zeroed" by which each spectrum's intensities are linearly transposed so that its minimum intensity is equal to zero. Spectra are then normalised so that the area under the curve of each spectrum is equal to some constant (in this case, 1) so that the relative shape of the spectra may be compared. This approach removes problems associated with raw intensity values that may fluctuate according to environmental conditions at the time of collection such as temperature.

The Raman microscope requires daily calibration which is achieved by testing against a silicone sample (wavenumber should be 520.2 cm^{-1}). However, it is practically impossible to calibrate in such a way that the binning strategy for wavenumbers is identical between different days. As a result, comparison of data between different days requires further normalisation since the differing bin labels between days means that these would be viewed as separate, non-overlapping variables in the context of multivariate analyses without some standardisation. Since the silicone calibration is the standard by which the Raman microscope was attuned each day, the main difference between bin labelling on different days was negligible and nominal rather than functional. Therefore, data from different days were coerced into the same wavenumber bin-labels based around the shared prominent, sharp peak at ~1003cm^{-1}.

Finally, with regards the spatial resolution data and the generation of other Raman maps, where spatial information is present, a method by which spectra from particular regions could be extracted from the rest of the dataset was necessary. This was achieved in a collaborative effort with the department of Automatic Control and Systems Engineering at the University of Sheffield where a tool was developed in MatLab (Mathworks inc.) for the precise extraction of spectra within spatial bounds that could be isolated as specified manually by the user (Biga, 2014, unpublished; Section 1.10). In addition to comparison of intra-cellular regions, this tool could be applied to enable the examination of multiple cells from across a monolayer from the same Raman sample collection procedure.

4.9 Data analysis

The most frequently used test to determine whether there was a difference in Raman spectra from different cell types or intra-cellular region is by the use of an unsupervised multivariate clustering technique such as principal component analysis (PCA; See Materials and Methods). PCA is the most commonly used statistical tool for analysing spectral data. Spectra consist of many variables (wavenumbers), of which some contain variation that is pertinent to differences between samples, whereas variation in other variables reflects information that is not relevant to sampled spectra. PCA analysis acts to reduce the multitude of variables into a small number of linear combinations or, Principal components (PC). The goal of PCA analysis therefore, is to reduce the number of dimensions (variables) to a few PC that describe the main variation across the dataset. The application of PCA presents an unbiased examination of the spectra provided and aims to reduce the variation of the dataset down to a hypothetical integration of those variates that provide the greatest explanatory power for the differences seen between the samples. Although the calculation does not account for presupposed differences in the categories of the samples provided (e.g. nucleus or cytoplasm), the segregation of samples by

such a qualifier indicates a real difference between these categories. Finally, although the principal components upon which samples are plotted do not directly relate to any one variate, or in this case wavenumber, it is possible to identify the degree of contribution a variate has to those components by examination of the variable loadings on these PC. Therefore, the wavenumbers that are most responsible for any sample segregation that occurs according to principal components are identified and present themselves as probable candidates for the main biological differences between samples.

4.10 Discussion

Raman spectroscopy is a powerful tool for non-invasive cell analysis. Ultimately, we want to develop a platform by which to assay heterogeneity of live human ES cells in a way that allows further examination of future behaviour as a research or even medical diagnostic tool. Here, this work has demonstrated that Raman can be used for the examination of pluripotent stem cell profiles, and provides a basis by upon which to further develop this technique.

This work has demonstrated technical considerations, such as the importance of Raman-inactive culture media and substrates on which to grow cells, differences in growth formats, fixation, acquisition time and appropriate fluorophores for antibody staining.

Although live cell analysis clearly is the ideal, there are a number of factors which led to the use of a mainly fixed cell approach in this work. The Raman effect is particularly weak and requires long acquisition times that are not comparable to that of flow cytometry. This meant that cells were maintained in a monolayer format in order that they were immobile long enough to acquire the data. Early attempts to analyse cells in suspension were hampered by cells moving

away from the laser spot. However, it was noted that the acquisition time to gain comparable intensity counts to the monolayer format cells was much shorter. This is possibly a reflection of cell shape (i.e. the cell is spherical in suspension and flat in monolayer) and therefore should be considered as a superior format should lower acquisitions times become technically feasible, or if immobilisation with optical tweezers/microfluidics are an option. It should be noted that spatial resolution, i.e. the distinction between nucleus and cytoplasm is obfuscated in this approach, and so would be better suited for whole cell analysis than the spatial mapping of cellular processes.

Practically, the Raman microscope used in this analysis did not have an aseptic environmentally controlled chamber and that lead to live cells becoming infected and dying during the day-long analysis period. Clearly this provided a separate, but related issue to the long acquisition times. That is, given the long acquisition times live cell analysis was not feasible with the technical setup available. As a result of this, a fixation approach was pursued.

A fixation approach mitigates the chemical changes within dying/stressed cells that could present temporal artefactual changes within the data collected. Fixation approaches to Raman spectroscopy have been implemented before (Christoph Kraffta, 2005) Our results mirror that of other groups in that fixation causes a shift in the spectra collected. However, this change does not negate the use of fixed cell spectra, since fixed cells are reflective of heterogeneity at the point of fixation. Therefore, it remained rational to continue with fixed cells rather than introduce noise associated with cell stress, infection and death.

We analysed several different culturing conditions for monolayer-grown cells, including culture surface and culture media. It became readily apparent that plastic was highly Raman-active and obscured any cell-relevant data. Glass was less Raman active, and could be used, but interference was seen in the fingerprint region. This could be mitigated with careful post-processing, but makes data interpretation more difficult. The best option tested was CaF_2 slides that are Raman-inactive. Additionally, NTera2 cells readily attach to this substrate, and appeared normal in line with reports from other groups (Notingher, 2002). Therefore, it was used throughout much of the data collection. CaF_2 slides are expensive, so a cleaning protocol was developed so that slides could be reused (see methods). Additionally, cell grown on Matrigel were tested for Raman activity and spectra did not contain any obvious artefacts, as reported elsewhere (Schulze et al., 2010b).

Standard culture media used in our lab (DMEM, 10% FCS) contains phenol red which proved to be highly Raman active, generating a broad band of fluorescence that obscured cell relevant data. Therefore, a switch was made to an alternative DMEM formulation that did not contain phenol red, and this indeed proved not to generate fluorescence that interfered with data collection. However, all media are themselves a combination of proteins and other metabolites that of course contribute to the Raman spectra. This effect is further complicated by the use of FCS that is not chemically defined and varies between batches. Therefore, Raman comparison of cells in media containing different batches of FCS could reflect this difference. Ideally, for live cell analysis cells would be immersed in chemically defined media during that does not contain phenol red during analysis. The use of chemically defined media would facilitate baseline Raman subtraction of this media. Our analysis merited the use of fixed, rather than live cells that were not immersed in media during analysis. However, these cells were grown in phenol red

containing media. We demonstrated that the interference caused by phenol red could be removed from fixed cells by thorough washing with PBS.

As already mentioned, cells in monolayer format took longer to analyse than cells in suspension, and also occupy a greater area in which clear cellular compartments are observed. This provides both an opportunity and a problem. This allows us to associate different sub-cellular regions with different Raman spectra associated with their biochemical profile. Conversely, the problem is that given that the cell is compartmentalised, from where can representative spectra of the cell be acquired? For the purposes of examining intercellular heterogeneity, the acquisition of spectra representative of individual cells is required. Therefore, a hyperspectral imaging approach was used here, in which a grid defined on the microscope over the cell is analysed acquiring one spectra per point. After the spectra are acquired an average spectrum representative of the cell is calculated. This approach is heavily time consuming and can take between 40-180 minutes per cell, which is in line with the work of other groups (Krafft et al., 2006; Matthaus et al., 2006). One way of overcoming this issue is to utilise equipment where a larger laser spot size is generated (Notingher, 2002). This approach reduces the acquisition time required for the collection of Raman spectra from a cell of interest, but at the cost of spatial resolution. Regardless, this technology was not available for this work (Figure 4.10). The hyperspectral imaging approach revealed that the region identified as the nucleus generated the largest signal, and was therefore used in later analyses (chapter 5). The reason for this increased signal relative to the rest of the cell could be reflective of either extra out-of-plane light, or a higher biochemical density resulting in more scattering. One issue that could be associated with the low signal intensity is that the excitation laser became gradually misaligned over the course of this project; therefore it may be technically possible to have shorter acquisition times with this setup.

The development of Raman spectroscopy for the examination of cellular behaviour is a non-trivial task and is still under development in laboratories across the world. With the equipment to hand, this fixed cell, hyperspectral imaging approach to Raman spectroscopy provides a robust, albeit time-consuming method by which to interrogate the biochemistry of these cells. The development of this method does not reveal whether Raman spectroscopy can be used for the examination of cells in different, cryptic, substates; which is the substance of Chapter 5. This method was developed iteratively over the course of this thesis and so many of the experiments performed in Chapter 5 do not in fact employ this final methodology as these questions were addressed concurrently.

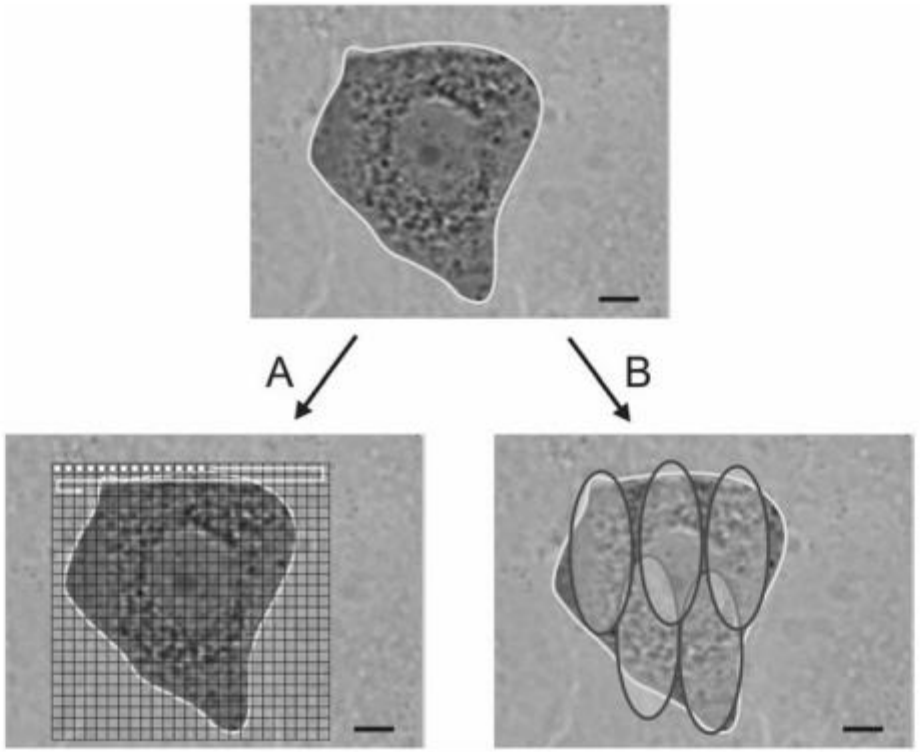

Figure 4.10 – Sacrificing Spatial Resolution for Improved Acquisition Time. From Stevens and Swain, 2007. A comparison of Raman spectroscopy carried out with a small spot size, A) or a large spot size, B). In this example, in A) a 1um by 1um laser spot was moved in 1um increments across the sample, collecting thousands of spectra. The approach with a larger laser spot shown in B) uses a 10um to 20 um spot that requires very few spectra to map the cell, which much reduces the sampling time.

Chapter 5

Application of Raman Spectroscopy to Pluripotent cell heterogeneity

5.1 Introduction

Optical microscopy has long proven itself invaluable to biomedical research. White light microscopy can be utilised to examine refractive indexes of cells and tissues, but it can only be used for thin sample sections or cell monolayers and does not yield information on sample biochemistry. Fluorescence imaging has also demonstrated itself as a revolutionary technique that enables enquiries into biochemical molecular behaviour that were previously intractable. Fluorescence imaging is not without its drawbacks such as sample modification in order to introduce the fluorescent molecule, interference of an antibody-bound fluorophore with the normal action of the tagged molecule and issues of photo bleaching that limit observation times and long term studies. Furthermore, in the case of long term studies, the degradation rates of fluorescent molecules, particularly for protein or mRNA tags, results in residual fluorescence after the tagged molecule has degraded and no longer relevant.

Raman spectroscopy is a non-invasive, label free technique for the analysis of chemical samples by the vibrational excitement of molecular bonds and has had some application already in the pluripotent stem cell field. Most studies using Raman on ES cells have been examining differences between undifferentiated ES cells and their differentiated progeny, whether directed or not. These studies have pulled out differences between undifferentiated and differentiated cell types according to Raman spectrum. A study examining CA1 hESCs and their undirected differentiated progeny after three weeks demonstrated that Raman spectrum differences between these populations predominantly correspond to nucleic acids (both DNA and RNA) and protein associated wavenumbers with lipids and carbohydrates also playing a role (Schulze et al., 2010a). An alternative study examining differences in Raman spectra between the HES2 human ES cell line and their differentiated progeny that had been directed to a cardiomyocyte fate also found the two cell types could be distinguished, with the human ES cells

displaying Raman spectra that contained peaks associated with DNA/RNA at a higher intensity than the cardiomyocytes (Chan et al., 2009a). The association of Raman bands corresponding to DNA/RNA molecules and the undifferentiated state of pluripotent cells is a common theme, and has been applied to examine the differentiation of mouse ES cell lines in comparison to their differentiating progeny as early as four days into differentiation (Notingher et al., 2004a). Coherent anti-Stokes Raman spectroscopy has also been used to demonstrate a detectable increase in protein:RNA ratio of differentiated cells compared to their undifferentiated parent at 3.5 days post directed differentiation (Konorov et al., 2007). These experiments provide promising evidence that Raman spectroscopy could have useful application in the identification of differentiated cells, but has not been used to examine how early differences between differentiating cells and their pluripotent parent can be seen. Indeed, no investigation to date has tried to determine the earliest time at which difference can be detected.

All of the above examples demonstrate that there are measurable differences with respect to biochemical cellular composition during the process of differentiation, however this is a relatively large phenotypic change experienced by cells in comparison to the stem cell substate hypothesis. Cells occupying different substates are anticipated to have differing phenotypic characteristics that inform lineage bias, however what these are remains unknown. Raman spectroscopy offers a unique tool for interrogating this heterogeneity in a non-invasive manner, and given that cells occupy substates in a cryptic manner, the sensitivity of Raman to this question needed to be addressed. In this thesis therefore, the capacity for Raman to distinguish between varying degrees of inter and intra cellular heterogeneity was tested.

The sensitivity of Raman spectroscopy to cellular heterogeneity was tested in four different ways. Firstly, the capacity to distinguish between different cell lines was tested using two

embryonic carcinoma cell lines and two human ES cell lines, one of which is culture adapted subline of the other in which an altered karyotype is associated with enhanced growth characteristics (Enver et al., 2005b). As demonstrated in other reports (Harkness et al., 2012), it was here anticipated that Raman spectroscopy would be able to distinguish between these cell lines and even the culture adapted variant from its "normal" counterpart. Here, an initial study was outsourced to the Raman spectroscopy company "Renishaw" (Renishaw plc, See Section 2.6) for analysis and is the subject of Section 5.2; "Different Cell Types." All other Raman spectroscopy experiments were performed using the setup described in Chapter 2 and a similar comparison between mouse Embryonic Fibroblasts (MEFs) and two other human ES cell lines was also made. Secondly, the effect of differentiation on pluripotent cell lines has been examined using Raman as described above, however all published studies are comparing cells that have been differentiating for some time (usually weeks) against the undifferentiated cells (Chan et al., 2009b; Notingher et al., 2004b). Consequently, the question of whether Raman spectroscopy is sensitive enough to detect early biochemical changes associated with differentiation was addressed in this thesis and addressed here by several differentiation studies using the pluripotent EC line NTera2. Thirdly, the capacity of Raman to recognise differences within cells was explored here with a comparison between spectra obtained from the nucleus and cytoplasmic regions of NTera2 cells. Indeed, it was anticipated that Raman would detect differences between these regions given that they perform different functions and in particular it is expected that the Nucleus region will contain a greater compliment of DNA related Raman bands.

Finally, the association of Raman profile with particular pluripotent cell populations was addressed in three different ways. The pluripotent cell surface marker SSEA3 was utilised to sort NTera2 population, with Raman spectroscopy performed on different fractions of NTera2

according to SSEA3 expression. The human ES cell reporter lines, Shef4 GATA6 and Hes3 MIXL1, were also examined (Materials and Methods). Both of these cell lines are currently under examination for expressions of lineage biases in other experiments within the laboratory, and there is strong indication that lineage biases correlate with fractions defined by the expression of their respective reporter and SSEA3 (Mr. Dylan Stavish, personal communication; Dr. Thomas Alison, Personal Communication, Thesis). The Gata6 and MIXL1 transcription factors are lineage transcription factors for Endoderm and Mesoderm respectively. Therefore, these markers have been used in conjunction with markers for pluripotency (such as SSEA3) to examine subtle lineage biases within the Stem cell compartment (Mr. Dylan Stavish, Dr. Thomas Alison; Personal Communication). Given differences in lineage biases exhibited by cells within these populations the question of whether these differences were reflected in the biochemistry of these cells was asked by analysis of the Raman profiles.

The development of an optimal methodology for acquiring Raman spectroscopy given available equipment is the subject of Chapter 4 however this was a lengthy and iterative process before a final approach was adopted. As a consequence, many of the questions asked in this chapter, which were addressed in parallel to the development of an optimal method, use slightly different data collection procedures to that finally described in Chapter 4 and where relevant these differences are stated.

5.2 Results

Different cell types

One of the first differences we tested was whether different cell lines displayed differences in their Raman spectra and this experiment was outsourced to Renishaw PLC, a company that specialises in Raman spectroscopy. All subsequent experiments (Sections 5.3 onwards) were performed using the Raman microscope described in Materials and Methods. The cell lines H14.BJ1, H14.s9, 2102EP and NTera2 were used. Cell lines were cultured on CaF_2 slides for 5 days prior to PFA fixation. Fixed cultures were dried (described in materials and methods) before transportation to Renishaw for analysis (performed by Dr. Katherine Lau; Section 1.10). A total of 5,200 spectra were collected with between 1-2,000 spectra collected over multiple cells per cell line.

A PCA analysis of the Raman spectra displays that the different cell types are readily distinguishable (Section 2.9; Figure 5.1a). H14BJ1 and NTera2 cell lines are clearly discriminated according to principal component one whereas H14S9 and n2102EP are separated according to principal component two. The two H14 cell lines do overlap slightly and of the cell groupings, they are the most similar. An examination of the average Raman spectra from the analysis reveals that the average NTera2 Raman spectrum is very dissimilar from the other spectra and this difference is reflected in the first principal component (Figure 5.1b). The second principal component is primarily responsible for separating the other three cell lines. Note that principal components are specific to each PCA performed and principal components are not relevant to other datasets or PCA analyses.

Raman spectroscopy distinguishes between embryonic stem and embryonic carcinoma cell lines. The H14BJ1 cell line is a culture adapted variant of the H14 cell line whereas the H14S9 cell line is a karyotypically normal variant. H14BJ1's adaptation to culture has resulted in a reduced rate of spontaneous differentiation and altered differentiation dynamics. NTera2 and the 2102 cell lines are both EC cell lines, however the 2102 EP cell line is a nullipotent EC cell line, which does not differentiate in xenograft tumours nor in culture unless seeded at particularly low densities. Principal component two therefore appears to separate cell lines according to their differentiation potential. An examination of the wavenumber loadings positive for PC2 indicates that wavenumbers associated with proteins and amino acids, whereas wavenumbers negative for PC2 are predominantly associated with glucose and lipids (Table 5.1).

Table 5.1 – Wavenumbers Relating to Differences Between EC and ES Cell lines. Examination of wavenumber loadings for Principal Component 2 (PC2) of cell lines sent to Renishaw and molecules associated with highlighted wavenumbers (e.g. Figure 4.1). Cell lines positive according to PC2 tend to have spectra associated with proteins and amino acids, whereas cells negative for PC2 tend to be associated with glucose and lipid molecules.

PC2 positive	Candidate molecule(s)	PC2 negative	Candidate molecule(s)
954	Hydroxyproline	846	Glucose
1004	Phenylalanine	870	Proline
1034	Phenylalanine	939	C-C-N stretch (peptide)
1125	Glucose, C-N protein	1062	Lipid skeletal C-C stretch
1234	Amide III, beta sheet	1264	Amide Iii and =C-H lipid, glucose
1338	Tryptophan	1295	CH_2 lipid
1574	Amide II, guanine, adenine, Tryptophan	1437	CH_2 lipid
1667	Amide I beta sheet	1656	Amide I disordered/ collagen, C=C unsaturated fat

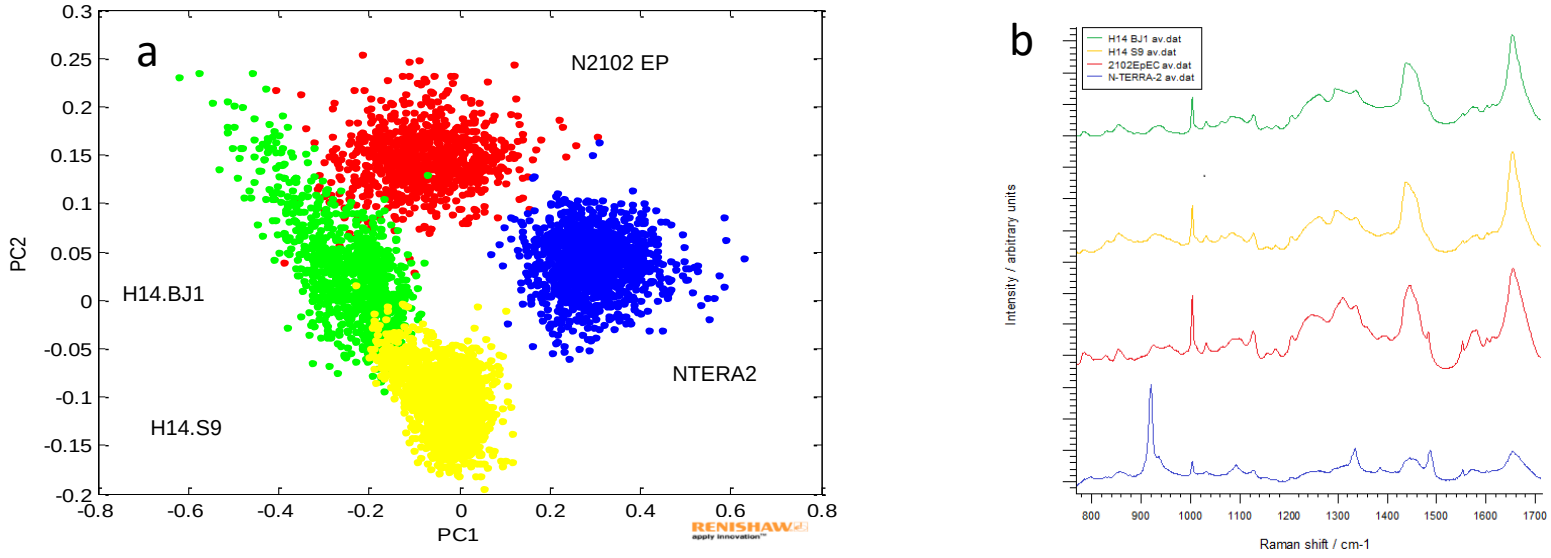

Figure 5.1 – Raman Spectroscopy Distinguishes Between Cell Lines. Four different cell lines were cultured on CaF_2 slides prior to fixation and analysis by Raman spectroscopy outsourced to Renishaw. Cell lines include two human embryonic carcinoma cell lines ; pluripotent NTera2 and the nullipotent n2102 EP cell lines. The other two cell lines were embryonic stem cell lines; H14.S9 and the karyotypically abnormal, culture adapted variant, H14.BJ1. **a)** PCA analysis performed on Raman spectra gathered for this analysis demonstrated clear separation between cell lines. **b)** Average Raman spectra collected from the cell lines; average spectra are comparable with the exception of the NTera2 spectrum which is markedly different from the others.

5.3 Retinoic acid differentiation

From here onwards, all Raman microscopy was performed using the in-house microscope and multivariate analyses performed using Simca 14 (Umetrics) as described in the Materials and Methods. An initial experiment examining the change of Raman spectrum of cells in response to a differentiation protocol was conducted and was performed prior to the final optimised method of Raman spectrum collection described in Chapter 4. Cells that had been grown on culture plastic and then treated with all-trans Retinoic acid (RA), or a culture media control were cultured for five days in these conditions, including a full media change (including re-dosing with RA) after three days. On the day of the Raman Spectroscopy analysis, cells were harvested using trypsin, and washed with FACS buffer three times to remove any residual retinoic acid in solution. The cells were then transported for Raman Analysis at ambient temperature. Immediately before analysis, aliquots of cells were resuspended in PBS then transferred onto CaF_2 slides. Ten cells from each treatment (exposed to RA or not) were analysed by Raman Spectroscopy collecting one spectra from an arbitrary intracellular location within each cell for sixty seconds with unfiltered laser power (examples in Figure 5.2a). Additionally, spectra of PBS containing trans-retinoic acid was also collected (Figure 5.2a; green Raman spectrum). PCA analysis here was performed using Multivariate statistical package (MSVP version 3.1, Kovach computing services). PCA analysis on the post-normalised spectra reveals that the treated and untreated cell populations segregate by Raman spectra, and that this is not explained purely by the chemical signature of Retinoic Acid. The Raman bands primarily responsible for this difference were Guanine (669-687 cm^{-1}), Adenine (711-722 cm^{-1}) and unsaturated lipids (1654-1660 cm^{-1}). This preliminary finding warranted further investigation. It was determined that the acquisition time required to analyse cells in suspension was too long for sustained analysis.

We determined that cells cultured on a monolayer were more suitable for analysis than cells in suspension (as described in chapter 4). Therefore, the second experiment to analyse the effects of RA was performed on cells grown on CaF_2 slides directly. This time, the experiment was replicated three times; with six separate cell cultures where three were treated with RA and three were not. For each RA exposed replicate, 10 cells were analysed (30 cells total), whereas the three replicate cultures that were not exposed to RA had 15, 10 and 13 cells analysed by Raman spectroscopy. Analysis was performed combining data from all three replicates together (Figure 5.3) and separately by replicate (Figure 5.4) and again cells separated according to treatment as demonstrated by PCA analysis, primarily separating by the third principal component. Figures 5.3a and 5.4 display the average Raman spectra of RA treated and control cells with each average spectrum flanked by one standard deviation of the relevant sample.

An examination of the wavenumber loadings for PC3 for those wavenumbers primarily responsible for the separation of RA treated and control cells shows that wave numbers corresponding to proteins and to some extent lipids associate with RA-treated cells, whereas control cells tend to be associated with wavenumbers corresponding to nucleic acids primarily (Figure 5.3, Table 5.2). This trend is also corroborated by the comparison between RA treated and control cells when separated by replicate (Figure 5.4). Each replicate was separately analysed by PCA analysis and in each case, the third principal component could act to discriminate between the treatments. Further examination of the third principal component loadings indicates that the wavenumbers responsible for the separation are similar in each separate PCA analysis (Figure 5.4). The relatively low standard deviations, as well as consistency in wavenumbers responsible for treatment separation indicate that Raman spectroscopy is able to distinguish reproducibly between these treatments.

Given the separation shown by PCA analysis a predictive model using a supervised clustering method, Partial Least Squares (PLS), was generated using replicates 1 and 2 of the dataset to train the model that also showed separation according to treatment (See Materials and Methods). This model also successfully categorised the remaining data points that were from the third replicate into the correct treatment class (Figure 5.5b).

The fact that Raman Spectroscopy appeared to discriminate between cells that were and were not exposed to RA after five days testified to the sensitivity of this technique, and justified a more iterative approach to determine the earliest time point at which a difference could be distinguished by this technique.

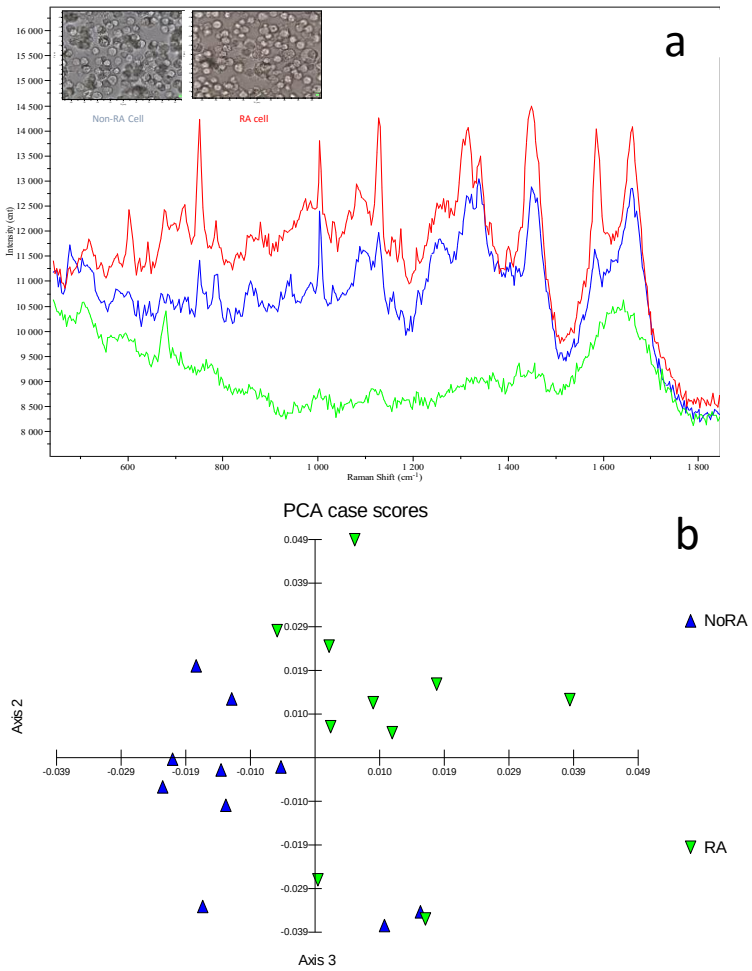

Figure 5.2 – Initial Retinoic Acid Differentiation and Raman Analysis. Raman analysis performed on NTera2 cells in suspension with a comparison of NTera2 cells that have or have not been exposed to a retinoic acid differentiation assay. Cells exposed to retinoic acid produced Raman spectra that were different to their undifferentiated counterparts and this difference was demonstrated by PCA analysis.

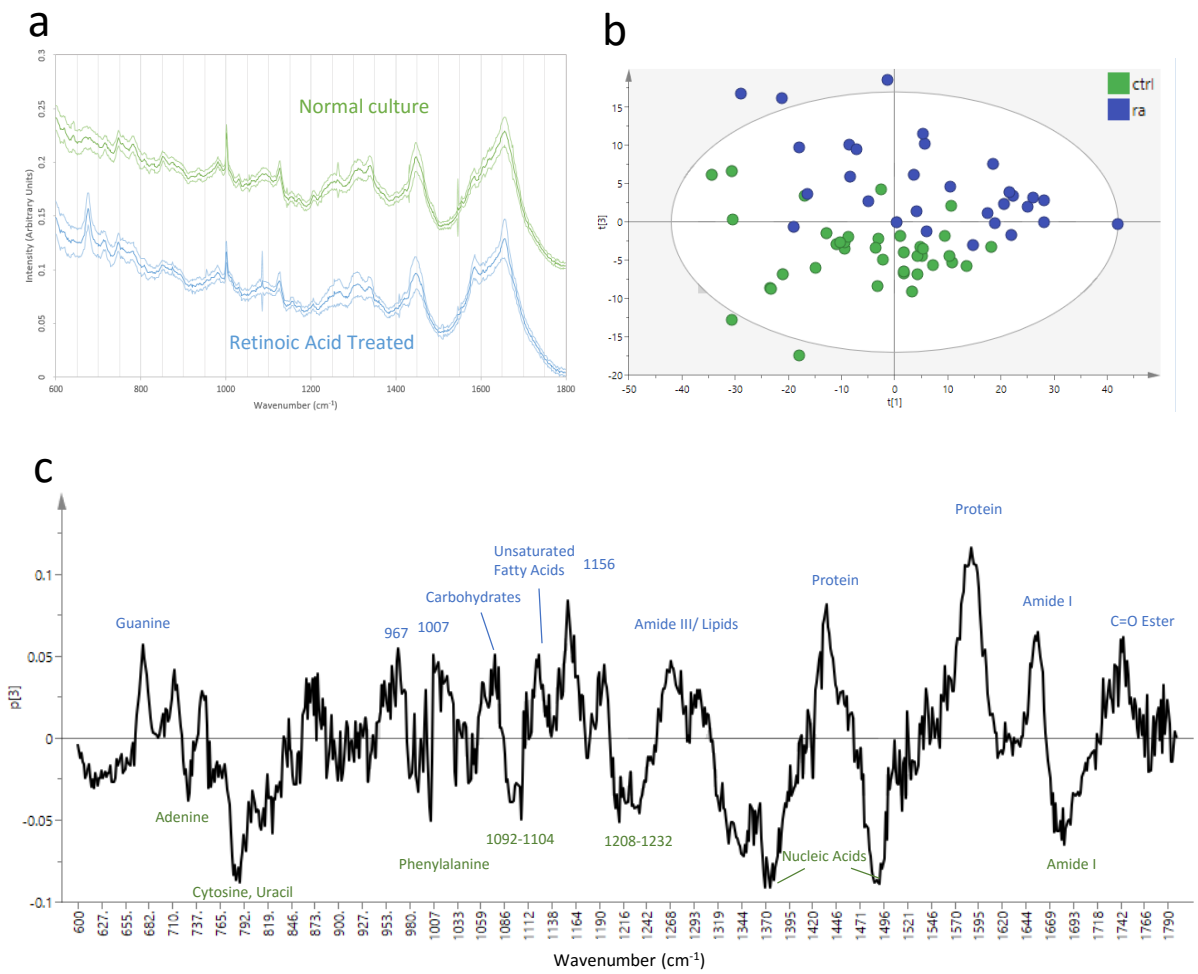

Figure 5.3 – Differences in Raman Spectrum caused by Retinoic Acid Differentiation. Comparison of NTera2 cells that have (blue) or have not (green) been exposed to a retinoic acid differentiation assay for 7 days in culture. **a)** Average Raman spectra (dark lines) gathered across all cells separated by treatment (green, not exposed to RA; blue, Exposed to RA). Pale lines show the Standard deviation about the mean. The x-axis is the wavenumber (cm^{-1}) and the y-axis is the spectral intensity in arbitrary units. The graphs have been vertically offset (green+0.1 arbitrary units) from each other to enable visual comparison. **b)** PCA analysis of these data displaying principal components one and three. Sample separation in PCA analysis primarily according to principal component (PC) three. **c)** An examination of the wavenumber loadings on PC three reveals candidate organic groups responsible for the separation along PC three (see table 5.2). This comparison describes the relative weighting each wavenumber has with regard sample separation according to PC three. A sample that tends to have relatively high values for wavenumbers with a positive loading in PC3 will be plotted more positively on the PC3 axis (b) and vice versa for wavenumbers with a negative loading on PC3.

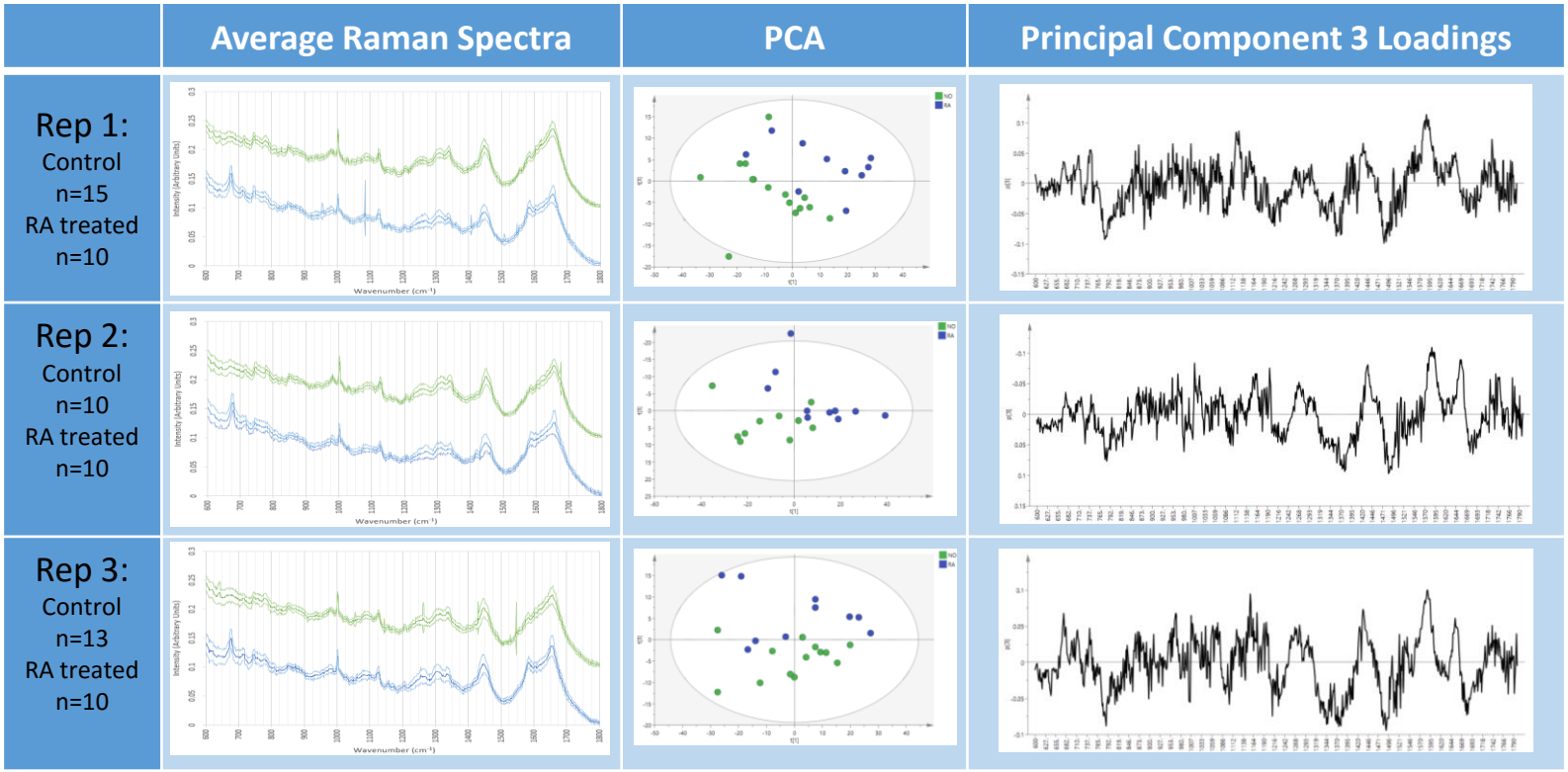

Figure 5.4 – Differences in Raman Spectrum caused by Retinoic Acid differentiation across three replicate experiments. Each experiment examined the Raman spectra from NTera2 cells that had been treated with RA (blue) for five days compared to control cells that were left untreated (green). The average Raman spectrum for each treatment and replicate is displayed (dark lines), and bounded by ± 1 standard deviation (pale lines). The average spectra are vertically offset from each other in order to facilitate visual comparison (green+0.1 arbitrary units). Principal component analyses of the individual replicates demonstrates that there does tend to be a separation between the treatments, each showing a degree of separation along principal component (PC) three. An examination of the wavenumber coefficient loadings for PC three in each replicate shows a similar pattern with each other and Fig5.3c indicating similar biochemical causes for sample separation by PCA.

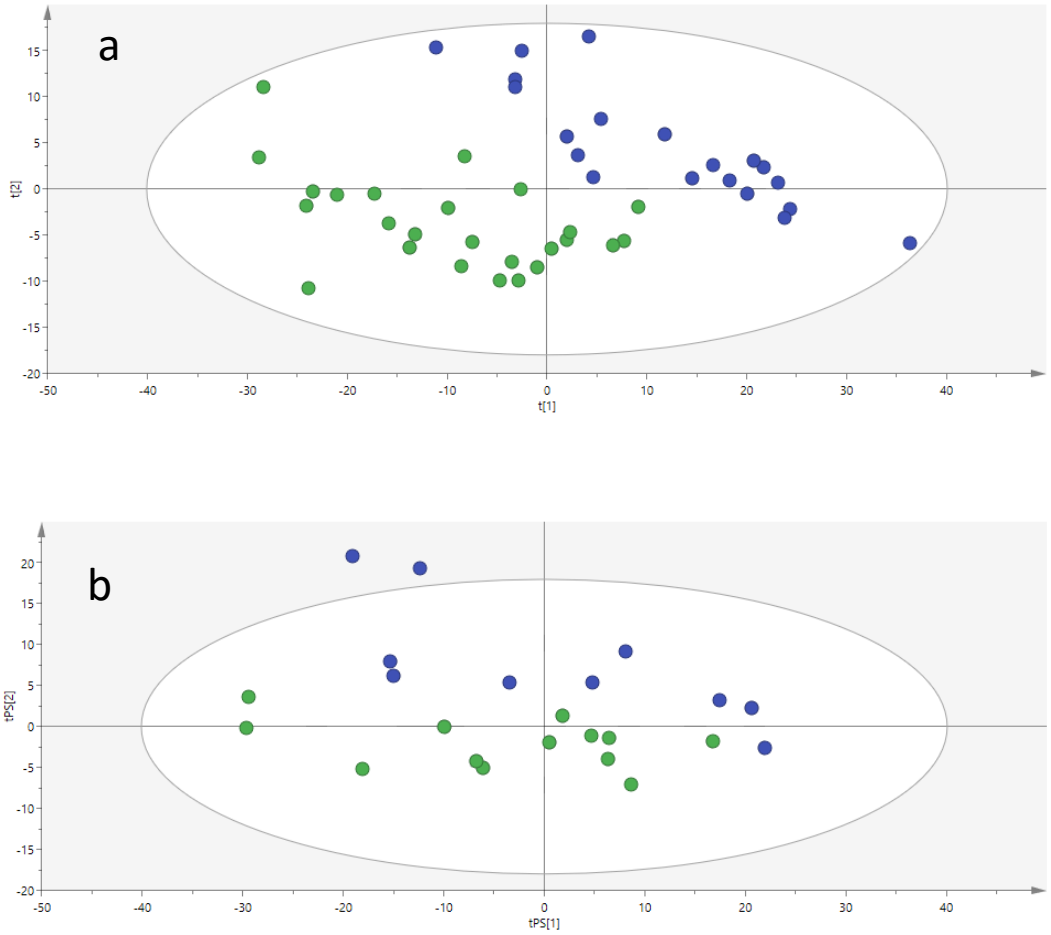

Figure 5.5 – Predictive Model Classification of cells into Differentiating or Undifferentiated Phenotype. A supervised partial least squares model was constructed to test whether the difference between the RA treated and undifferentiated samples had predictive capacity (Figure 5.3). **a)** 45 spectra of the 68 available were used to train the model and their separation is clear. **b)** The remaining 23 spectra (10 RA treated; 13 control) that were not used to train the model are plotted according the model fitted using the other 45 spectra and show extremely similar separation as to that shown by the training data in a). The model was then tasked with classification of the 23 spectra not used for training the model which it did so with a 100% success rate (table).

Observed	Members	Correct	Control	RA
Control	25	100%	25	0
RA	20	100%	0	20
Test	23		13	10
Total	68	100%	38	30
Fishers prob.	3.2×10^{-13}			

Table 5.2 – Wavenumbers Related to Differences Between Undifferentiated and RA Mediated Differentiating Cells. Examination of wavenumber loadings for Principal component 3 (PC3) of PCA plot for NTera2 cells that have or have not been exposed to retinoic acid (RA) differentiation. Cells positive for PC3 tend to be RA differentiated cells, whereas cells negative for PC3 are generally the undifferentiated control. Wavenumbers loadings for PC3 reveal that RA treated cells tend to have Raman spectra that have a higher compliment of proteins and amino acids whereas the undifferentiated cells tend to have Raman spectra associated with Nucleic acids. "?" Refers to a band that is prominent for separation but is not associated with a known molecule/group.

PC3 positive	Candidate Molecule(s)	PC3 negative	Candidate Molecule(s)
1587	Protein	1486	Nucleic Acids
1156	C-C, C-O ring breathe	1490	Nucleic Acids
1435	Protein	1488	Nucleic Acids
1657	Amide I	783	Cytosine, Uracil
1654	Amide I	1373	Thymine, adenine, guanine
1742	C=O ester	1346	Thymine, adenine, guanine, tryptophan
676	Guanine	1344	Thymine, adenine, guanine, tryptophan
967	?	1681	Amide I
1074	Carbohydrates	1003	Phenylalanine
1007	Phenylalanine, substituted benzene derivatives	1208	Tyrosine, phenylalanine, protein, amide III
1120	Unsaturated Fatty acids	1232	Amide III random, Lipids
1268	Lipids/Amide III	1092	?
1195	?	729	Adenine ring stretch
712	?		
1297	Amide III		
870	C-O-C glycosidic link/ CC stretch		
744	O-P-O/ Tyrosine		

5.4 Retinoic Acid Differentiation Time course

We then performed a RA time-course differentiation experiment in order to determine the earliest time point at which Raman Spectroscopy could distinguish between treated and untreated cell populations. Cells were cultured in culture dishes containing a CaF_2 slide, with or without Retinoic Acid. At the timepoint the cultures were to be analysed, the slides were removed from their respective media and placed into a separate petri dish then rinsed and stored in FACS buffer for transportation. Remaining cells in the original petri-dish were harvested for flow cytometric analysis and did not show any obvious morphological difference to cells cultured on CaF_2. Cultures on CaF_2 slides were rinsed three times with PBS immediately before Raman analysis where one spectrum was collected from an arbitrary intracellular location per cell with an acquisition time of 60 seconds at 100% laser power. The three-hour timepoint was the earliest time in order to permit sufficient time for cells to attach after seeding. A total of five timepoints were included in this experiment (3, 24, 48, 72 and 144 hrs post RA exposure), with 50 replicate cells analysed per treatment per timepoint (500 cells total).

To determine whether cells were responding to the retinoic acid treatment, antibody profiles of pluripotency and differentiation markers were analysed concomitantly by flow cytometry. An examination of the antibody profiles of the cell cultures shows that the retinoic acid treated cells are noticeably reduced in SSEA3 expression after 48 hours of treatment, and Tra-1-60s expression is reduced after 6 days of culture (Figure 5.6). The control cells have reduced SSEA3 expression by 6 days of culture, but Tra-1-60s was only mildly reduced by the end of the analysis period (9 days). SSEA1 expression does not show a great increase in either culture, however the RA treated cells seem to show a relatively larger increase than the untreated.

PCA analyses of the Raman Spectra between control and RA treated cells at each respective timepoint show signs of clustering as early as three hours post-treatment (Figure 5.7). PCA analyses were conducted separately between the spectra collected at each time point, thus the analysis only examines differences between the cells collected at each timepoint independent of the other time points. Figure 5.7 displays the results of these separate PCA analyses and in each case, principal components one and two are shown. Generally, as the time course proceeds the more obvious the clustering, with the exception of the 72-hour timepoint, regardless of principal component examined. The average Raman spectrum for each treatment is also displayed in Figure 5.7 with all spectra offset from each other to allow a visual comparison (a greater offset is displayed to distinguish between timepoints).

A PCA analysis was also carried out to compare RA treated cells at each timepoint against the 3-hour control timepoint since it could be argued that the earliest control timepoint is most representative of the original cell biochemistry (Figure 5.8). To perform this analysis, the control treatment cells from the three hour timepoint was compared against the RA treated cells at each timepoint, with each comparison analysed separately and independently by PCA. Figure 5.8 displays the results of these independent analyses, displaying principal components one and two in each case. At each timepoint cells tend to cluster along the first principal component. The three-hour and seventy two-hour Retinoic acid timepoints also seem to show some discrimination along the second principal component. That being said, these two timepoints also show the most overlap between control and RA treated cells.

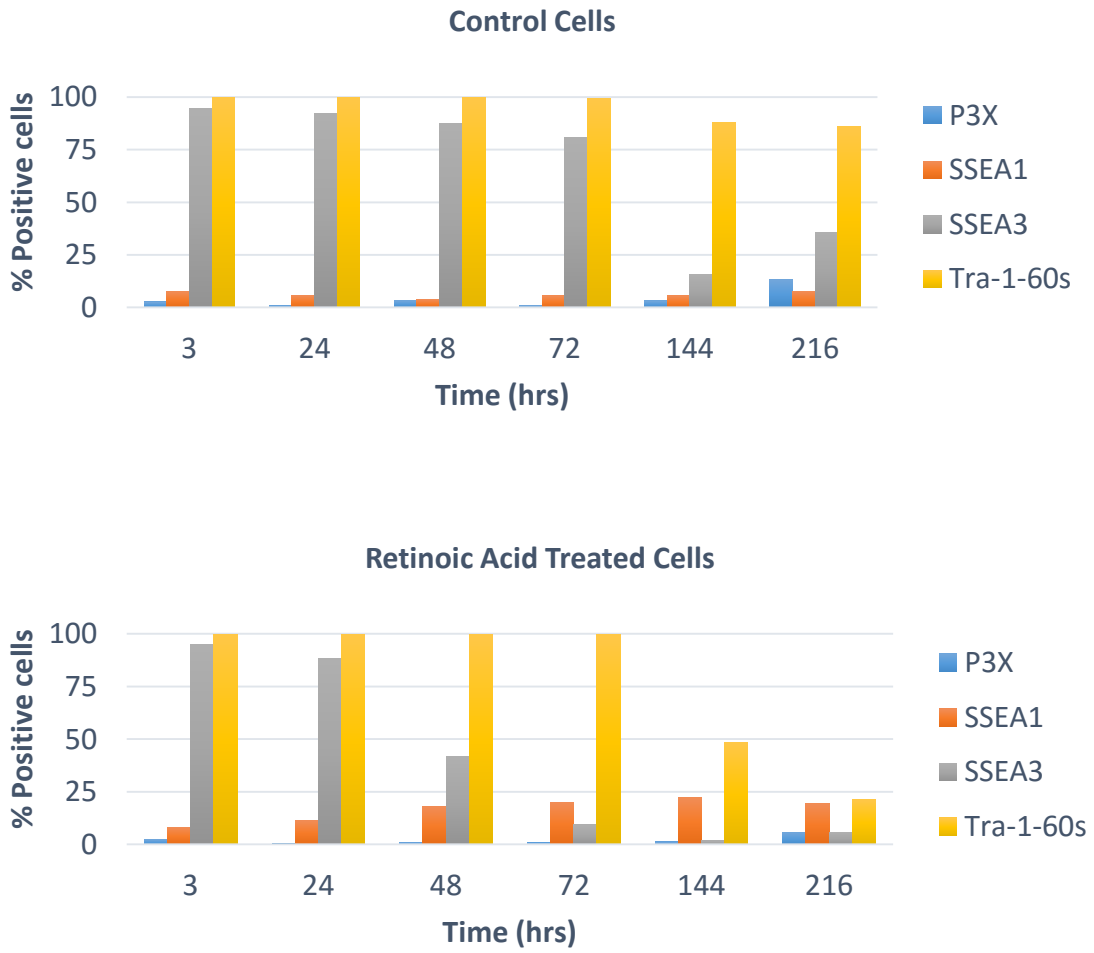

Figure 5.6 – Cell surface antigen Expression Changes During Retinoic Acid (RA) Differentiation Time-course Assay. Cell surface antigen expression of sister NTera2 cells from a Retinoic Acid (RA) mediated differentiation time-course assay in terms of the percentage of the population positive for these antigens, baselined against a P3X negative control . Control cells were not exposed to RA. The Markers for pluripotency, SSEA3 and Tra-1-60s downregulate in the RA treated cells faster than in the control cell line, with almost no cells being positive for SSEA3 3 days post RA exposure. The cell surface marker SSEA1which is associated with human pluripotent cell differentiation does not show much of an increase in the retinoic acid treated cells, but does not increase at all in the control cells.

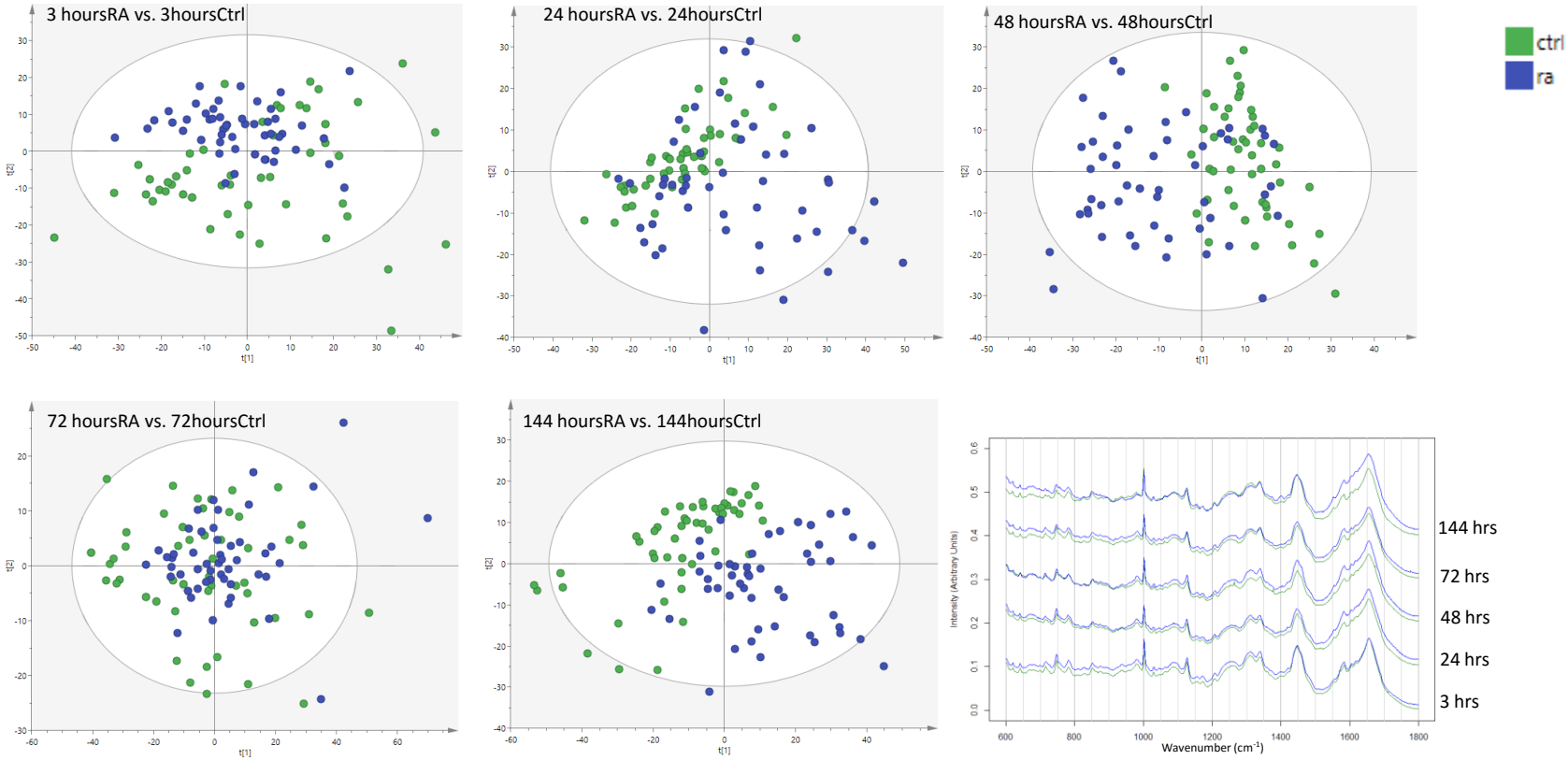

Figure 5.7 – PCA analyses performed on Raman spectra collected from NTera2 cells undergoing an RA mediated differentiation time course assay. Five separate PCA analyses are shown, each comparing 100 cells (50 treated with RA, blue; 50 untreated, green) after different RA exposure times. Samples are plotted against principal components one and two from each PCA analysis. RA exposed cells (blue) and untreated cells (green) appear to differ in most PCA analyses, excepting the 72hr timepoint and this sample separation appears as soon as 3hrs post RA induction. In addition, the average spectra of cells at each timepoint, and by treatment, are also displayed.

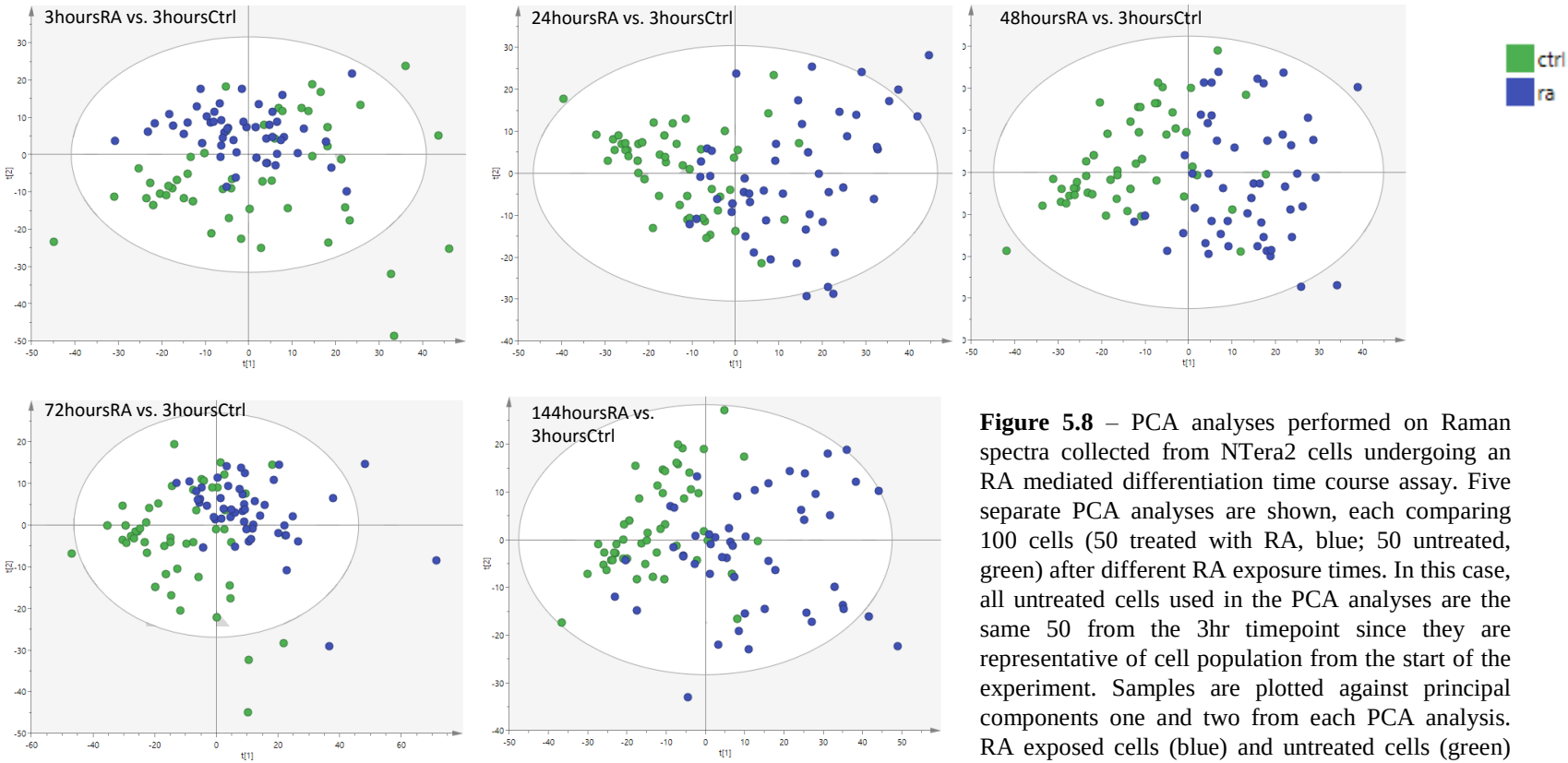

Figure 5.8 – PCA analyses performed on Raman spectra collected from NTera2 cells undergoing an RA mediated differentiation time course assay. Five separate PCA analyses are shown, each comparing 100 cells (50 treated with RA, blue; 50 untreated, green) after different RA exposure times. In this case, all untreated cells used in the PCA analyses are the same 50 from the 3hr timepoint since they are representative of cell population from the start of the experiment. Samples are plotted against principal components one and two from each PCA analysis. RA exposed cells (blue) and untreated cells (green) appear to differ in most PCA analyses and this sample separation appears as soon as 3hrs post RA induction.

5.5 Intracellular heterogeneity

As described in Chapter 4, intracellular variation could explain differences seen by PCA analysis in previous experiments where data were collected from arbitrary points within analysed cells and thus left intracellular variation unaccounted. Therefore, an experiment was conducted to examine whether subcellular regions were discriminated by Raman spectroscopy. Visual inspection on the Raman microscope revealed three readily identifiable regions within most NTera2 cells examined. Each cell exhibited its total perimeter whose area was primarily pale, within which a darker but sizable ovate would be present. This distinction was the easiest to make and this led to the inference that this dark ovate was the cell's nucleus and everything outside it, but within the cell's perimeter represented the cell's cytoplasmic component. Within the Nucleus smaller, pale ellipsoids with a "raised" appearance would often be present and were in turn inferred to represent nucleoli within the nucleus (Figure 5.9a). Although these regions were identified as cytoplasmic, nuclear and nucleolar in nature, this was not formally confirmed.

Following identification, a comparison between these regions was performed by collecting five arbitrary points for each region from multiple cells of the same NTera2 population (Figure 5.9b). In total, 645 spectra were collected of which 409 were collected from the Nucleus, 129 from Nucleoli and 37 from Cytoplasmic regions. Spectra from these regions were normalised and the average spectra are displayed in Figure 5.9c&d. It is clear from the averaged spectra that spectra collected from cytoplasmic regions were considerably different to that of both the average spectra for the Nucleus and Nucleolus regions.

A PCA analysis examining the spectra from these regions reveals that there was not much difference in general between the Nucleus and Nucleolus categories, whereas the majority of

Cytoplasm spectra were not in that same shared cluster (Figure 5.10a). All Cytoplasm spectra were positive for principal component one (Figure 510a), which also seemed to be the main discriminant. Most Nuclei spectra were negative for principal component one (Figure 5.10a). The Wavenumber loadings for principal component one reveal that known Raman bands associated with cytoplasm tend to be associated with protein and phenylalanine although there are many unknown bands (Figure 5.10b). Raman bands that cytoplasmic spectra clustered away from were generally associated with nucleic acids, although there are also bands associate with lipids, Amide I groups and C-H_2 (Table 5.3).

Table 5.3 – Wavenumbers relating to differences between cell cytoplasm and Nucleus. Cytoplasm Spectra were primarily positive for PC1 in the PCA analysis (Figure 5.10) whereas spectra from the Nucleus tended to be negative for PC1. "?" Refers to a band that is prominent for separation but is not associated with a known molecule/group

Not Cytoplasm (PC1 Negative)	Candidate Molecule(s)	cytoplasm	Candidate Molecule(s)
1241	Thymine, Cytosine, adenine ring v	1722+	Marker
1269	Lipids	1555	?
849	Buried Tyrosine	1598	?
1336	Adenine, Guanine, tyrosine, Tryptophan	1601	Protein
829	Exposed Tyrosine/DNA	1599	Phenylalanine
928	?	1506	Protein
1103	$>PO_2^-$ Stretch	1497	Adenine?
956	?	622	?
725	Adenine	1001	Phenylalanine
780	Cytosine, Uracil	1000	Phenylalanine
1464	$C\text{-}H_2$	1034	Carbohydrates, mainly C-C- skeletal, C-O
1664	Amide I	1185	?
1444	$C\text{-}H_2$	1154	C-C stretch

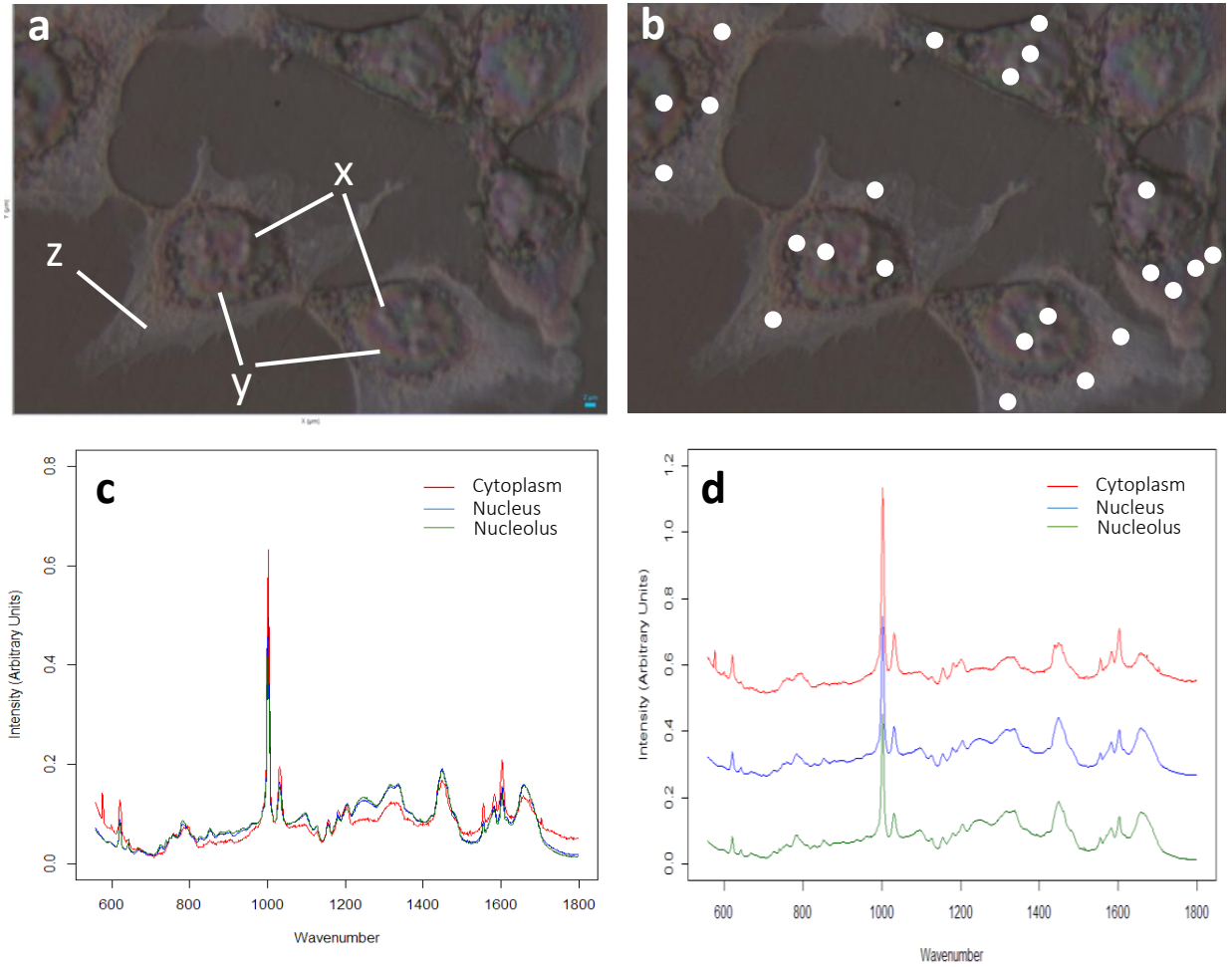

Figure 5.9 - Intracellular points Raman acquisition. Examples of examination of differing Raman spectra from identifiable intracellular regions. Data were collected according to **a.)** Different regions classified based upon morphology were; nucleolus (x), Nucleus (y) and cytoplasm (z). **b.)** Five Raman spectra were taken from each cell with an acquisition time of 60 seconds (full power laser). **c.)** Average spectra coloured according to classification. Data were collected from 115 cells; with 5 data points each; representing nucleolar (n=129), nuclear (n=409) and cytoplasmic (n=37) regions. **d.)** Average Raman spectra **g**raphs are offset vertically for comparison.

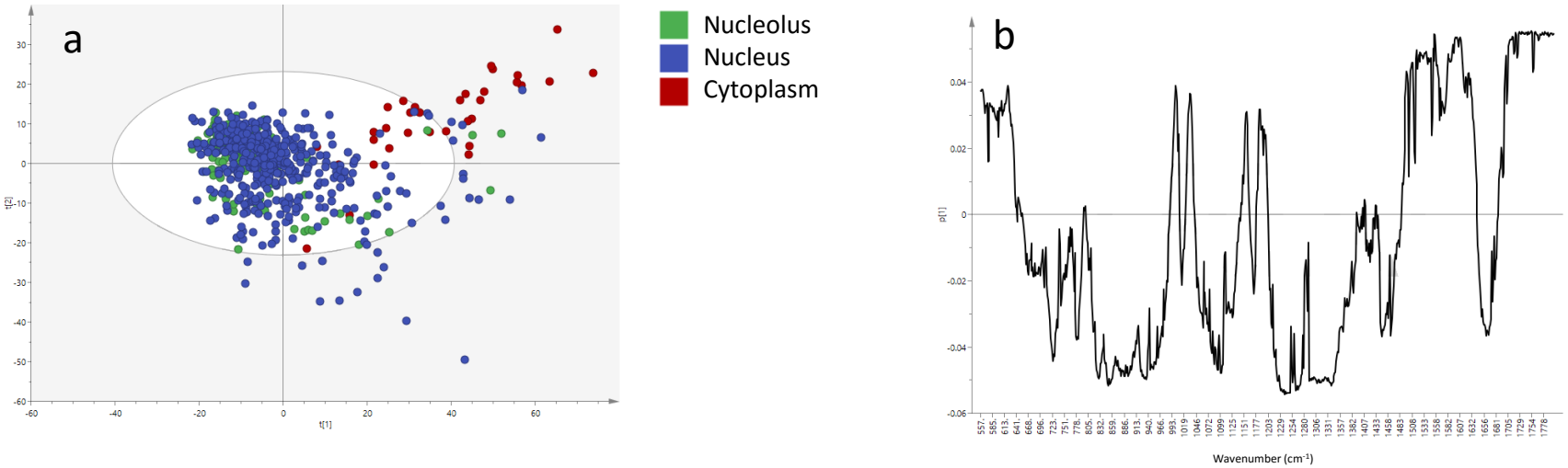

Figure 5.10 – PCA Analysis on Intracellular Raman Data. PCA analysis performed on the intracellular points acquisition experiment (figure 5.8). **a)** Data were collected according to different regions classified based upon morphology were; nucleolus (green, n=129), Nucleus (blue, n=409) and cytoplasm (red, n=39). The Cytoplasmic spectra cluster away from the nucleus and nucleolus spectra according to principal component 1. **b)** Wavenumber loadings for principal component 1.

5.6 Substates

NTera2 cells were stained for SSEA3 using the MC631-2C2 primary antibody and FITC secondary antibody, and then sorted according to intensity by flow cytometry (as described in Materials and Methods). The resulting negative, medium and high fractions were then plated onto CaF_2 slides and allowed to attach. An unstained/unsorted control was also plated. Three hours after plating the cell cultures were fixed and subsequently analysed by Raman microscopy. Five spectra per cell were acquired, all from the nuclear region and analysed by PCA (n=1378 total spectra, Figure 5.11b). A total of 276 cells were examined in this manner across all treatments, of which 89 cells were sorted from the high fraction (n=444 spectra), 40 cells from the medium fraction (n=200 spectra), 88 cells from the negative fraction (n=440 spectra) and 59 cells from the unstained/unsorted treatment (n=294 spectra). All cells were acquired from one FACS experiment.

Although high, medium and negative fractions have a degree of overlap, it is clear that the groupings are not identical (Figure 5.11b). The high fraction especially separates from the other fractions, due to being especially negative for PC1 (Figure 5.11b). The unstained/unsorted fraction lies opposite to the high fraction, being positive for PC1 (Figure 5.11b). The negative and medium fractions also appear to lie along this gradient, although the negative fraction appears slightly more positive for PC1 than the medium fraction (Figure 5.11b).

The loadings for PC1 show that the major difference between samples positive for PC1 is broadly due to spectral intensity at wavenumbers within the first two thirds of the fingerprint region, from approximately 550 to 1400 cm^{-1}, whereas samples negative from PC1 are due to relatively higher intensities at wavenumbers 1400 to 1800cm^{-1} (Figure 5.11c). Indeed, this pattern is

reflected in the average Raman spectra from each fraction, where the fractions that expressed more SSEA3 tend to have an increased proportion of intensity in the latter half of the spectra (Figure 5.11a).

It was surprising that the unstained/unsorted fraction, that should have represented unsorted heterogeneity bias, did not present spectra across the entire range, especially that of the high fraction spectra (Figure 5.11b). In conjunction with the sample gradient along PC1 that correlates with SSEA3 intensity it appears that the main differences are most likely attributable to residual FITC fluorescence.

Given the presumed interference of FITC fluorescence to these spectra a baseline correction algorithm was employed to try and mitigate the effects of this fluorophore using the LabSpec Raman analysis platform (Horiba). The resulting average Raman spectra for each fraction is displayed in Figure 5.12b. The previously described effects of the fluorescence baseline (Figure 4.8) seemed to have been removed by visual inspection and the spectra appear more similar to each other than the spectra that were not baseline corrected (Figure 5.11b). Again these spectra show a separation pattern by PCA, although this time according to PC2 and PC3 (Figure 5.12a). However, as with the previous analysis the groupings correlate with the SSEA3 gradient from unstained/unsorted to high (Figure 5.12a). That said, the loads for PC2 and PC3 responsible for the separation (Figure 5.12c and d) do so according to a different pattern to each other and respectively to PC1 for the non-baseline corrected spectra (Figure 5.11c).

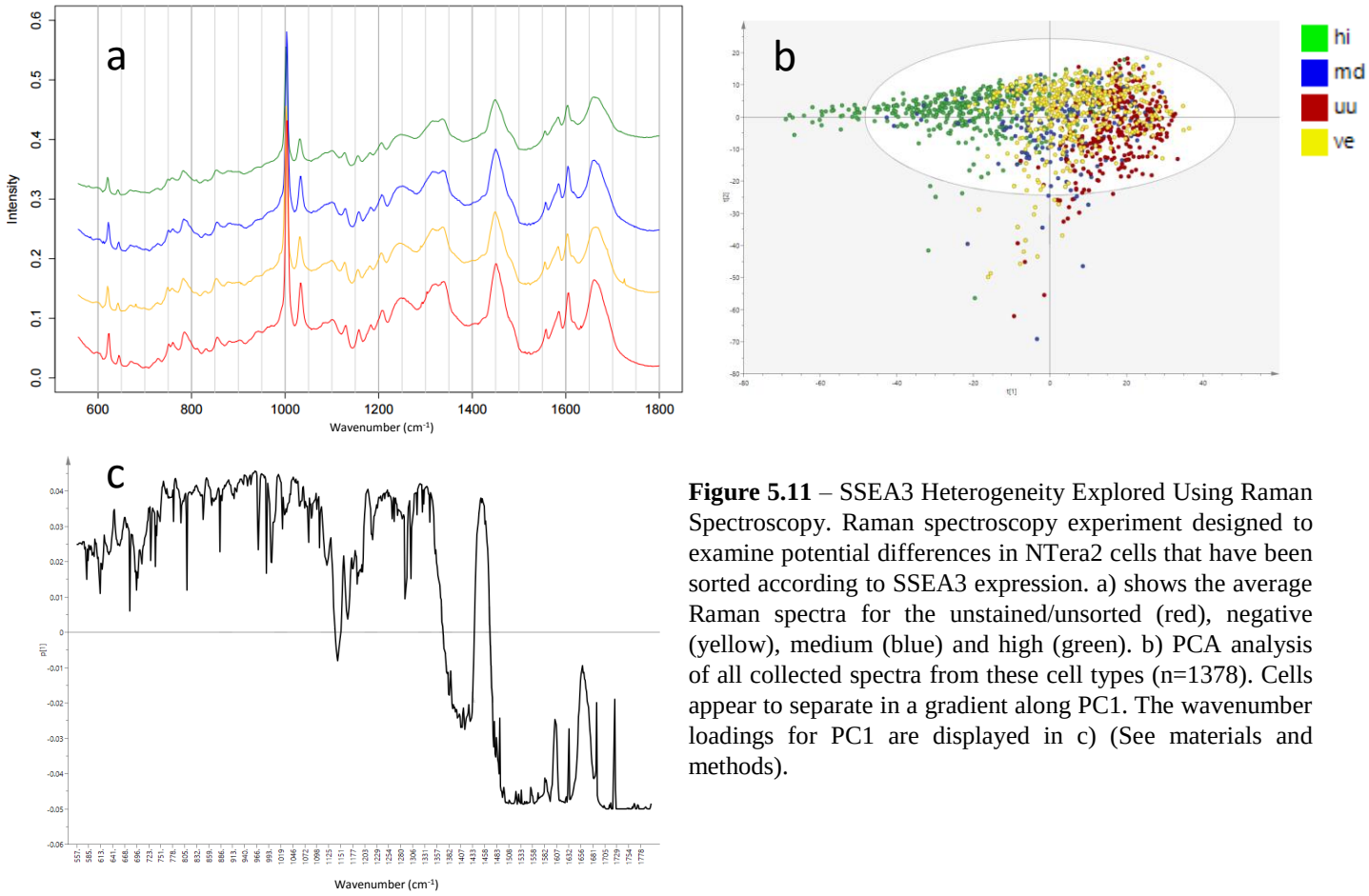

Figure 5.11 – SSEA3 Heterogeneity Explored Using Raman Spectroscopy. Raman spectroscopy experiment designed to examine potential differences in NTera2 cells that have been sorted according to SSEA3 expression. a) shows the average Raman spectra for the unstained/unsorted (red), negative (yellow), medium (blue) and high (green). b) PCA analysis of all collected spectra from these cell types (n=1378). Cells appear to separate in a gradient along PC1. The wavenumber loadings for PC1 are displayed in c) (See materials and methods).

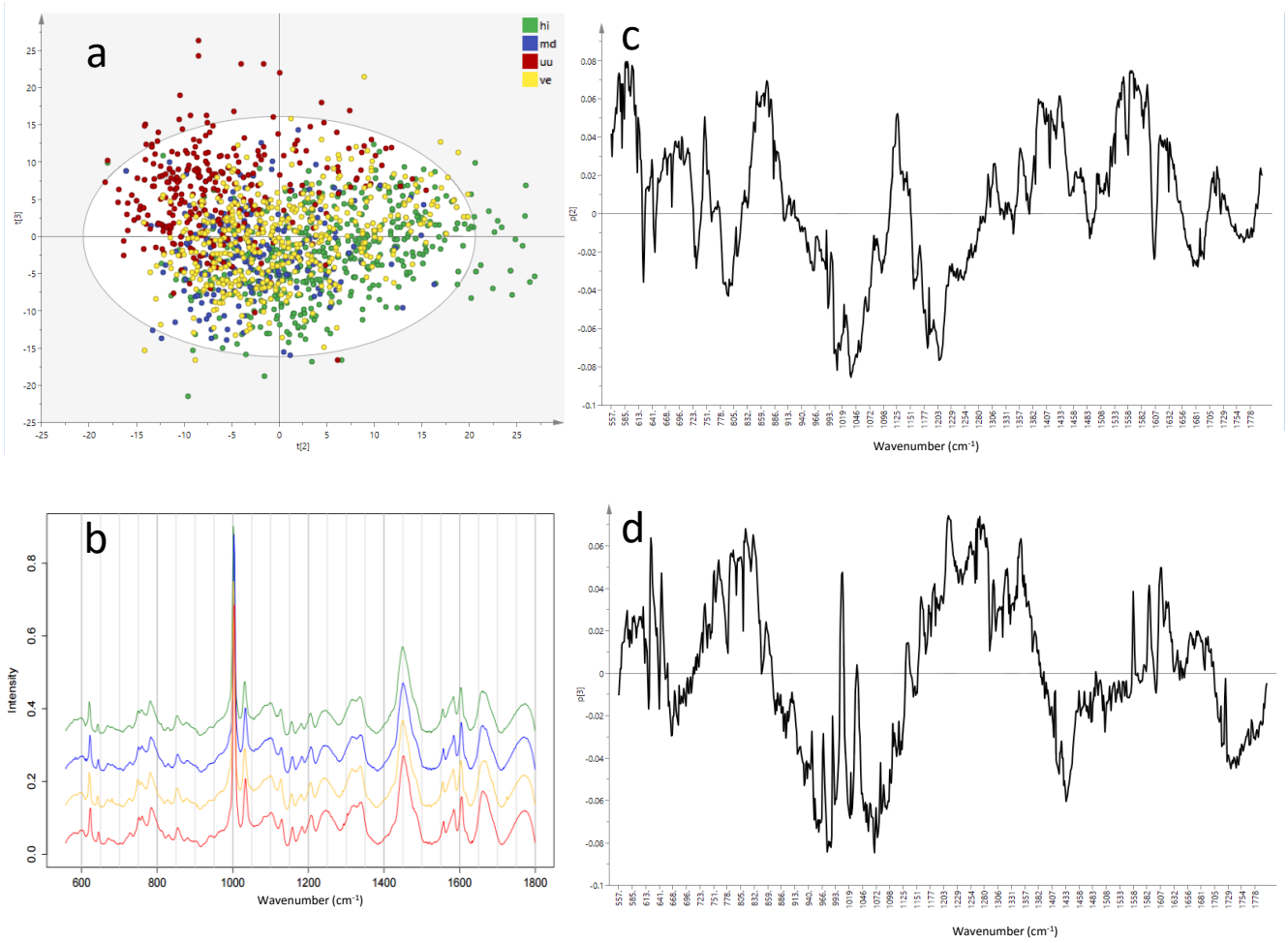

Figure 5.12 – Advanced Pre-Processing for the Raman Analysis of SSEA3 based Heterogeneity. This is the same experiment as in figure 5.10, however spectra have undergone additional pre-processing in order to remove baseline effects associated with fluorescence. **a)** shows PCA analysis performed on transformed data, and this shows a separation along PC2 and PC3 in conjunction. **b)** Average spectra for the fractions following the additional pre-processing. **c)** Wavenumber loadings for PC2, **d)** Wavenumber loadings for PC3.

5.7 Lineage Reporter Human ES Cell Lines

Previous work in the lab has shown that the Shef4 GATA6 and Hes3 MIXL1 reporter cell lines appear to show lineage bias within the stem cell compartment (personal communication with Dr. Thomas Allison and Mr. Dylan Stavish respectively). Further to this, in order to test whether the Raman spectroscopy hyperspectral imaging technique developed in chapter 4 was able to distinguish between different cell lines, Raman spectra collected from these cells were compared against each-other and against mouse embryonic fibroblast cells. All cell lines were seeded on Matrigel coated CaF_2 slides and allowed to attach overnight before they were fixed with PFA as described in the materials and methods. All the Raman data acquired from cells sorted by FACS were collected from one culture vessel each of the relevant sorted fraction and the mouse embryonic fibroblasts (MEFs) analysed were all from one culture also.

First, both hES cell reporter lines and mouse embryonic fibroblasts were analysed by hyperspectral Raman imaging. A 2D PCA plot reveals that there is some degree of clustering primarily along PC1 (Figure 5.13). This seems to delineate between MEF and ES cells, whereas PC3 seems to separate the ES cell lines. The clustering is very close; however, it appears that there are differences between these cell lines that Raman can detect. These PCA analyses, unlike others presented previously, were performed in MATLAB (Mathworks inc.). In this analysis, each point on the PCA plot is representative of the average spectra from the nucleus of each cell, each comprising of around 50 to 350 spectra. More specifically, there are average nuclear spectra calculated for; 21 MEF cells (between 29 and 321 spectra collected per nucleus), 38 Shef4 GATA6 cells (between 36 and 365 spectra collected per nucleus), and 25 Hes3 MIXL1 cells (between 43 and 215 spectra collected per nucleus). The comparison of Raman spectra from the two reporter cell lines are the data collected from the sorted cell fractions examined in more detail below; i.e. all Shef4 GATA6 and Hes3 MIXL1 data regardless of marker expression.

We took advantage of the opportunity afforded by the reporter cell lines to sort cell populations into different categories based upon dual analysis of their marker and SSEA3 to see if there were differences between cells based upon these categories that may indicate state differences. Cells were labelled for SSEA3 with the MC631-2C2 and a DyLight 647 secondary antibody and cells positive for SSEA3 were sorted into MIXL1 positive or negative fractions by virtue of MIXL1-GFP expression before plating onto Matrigel coated CaF_2 slides as per materials and methods. Cells were allowed to attach overnight prior to PFA fixation and subsequent Raman analysis. Raman spectra were collected from both fractions; SSEA3+/MIXL1-negative (12 nuclei; 49 to 175 spectra per nucleus) and SSEA3+/MIXL1-postive (13 nuclei; 43 to 215 spectra per nucleus). PCA analysis of the resulting spectra shows that although the two populations do not entirely separate, the SSEA3+MIXL1-negative population appears to cluster more tightly, and is generally excluded from the PC3 negative domain.

A similar experiment was conducted using a different reporter cell line, Shef4 GATA6. Cells were labelled for SSEA3 with the MC631-2C2 and a 647 secondary antibody and cells positive for SSEA3 were sorted four ways into SSEA3+/GATA6-High, SSEA3+/GATA6-Low, SSEA3+/GATA6-negative and SSEA3-negative/GATA6-positive fractions. Again, cells were plated onto Matrigel coated CaF_2 slides, allowed to attach overnight and PFA fixed as per materials and methods. Raman spectra were collected from cells of these fractions; SSEA3+/GATA6-High positive (13 nuclei; 36 to 189 spectra per nucleus), SSEA3+/GATA6-Low (8 nuclei; 62 to 173 spectra per nucleus), SSEA3+/GATA6-negative (10 nuclei; 48 to 365 spectra per nucleus) and SSEA3-negative/GATA6- (7 nuclei; 67 to 131 spectra per nucleus). PCA analysis on Raman spectra collected from these fractions reveal that the SSEA3-negative/GATA6-positive fraction separates out from the other spectra most readily according to as negative for PC2. On the other hand,

the SSEA3-postive/ GATA6-negative fraction groups in the PC2 positive domain. Most other cells, representing the SSEA3+/GATA6-High and SSEA3+/GATA6-Low fractions lie in a band between the 0.5 and -0.5 value for PCA2. The SSEA3+/GATA6-High fraction has the greatest degree of spread of any of the fractions, with cells lying both very negative and very positive for PC2.

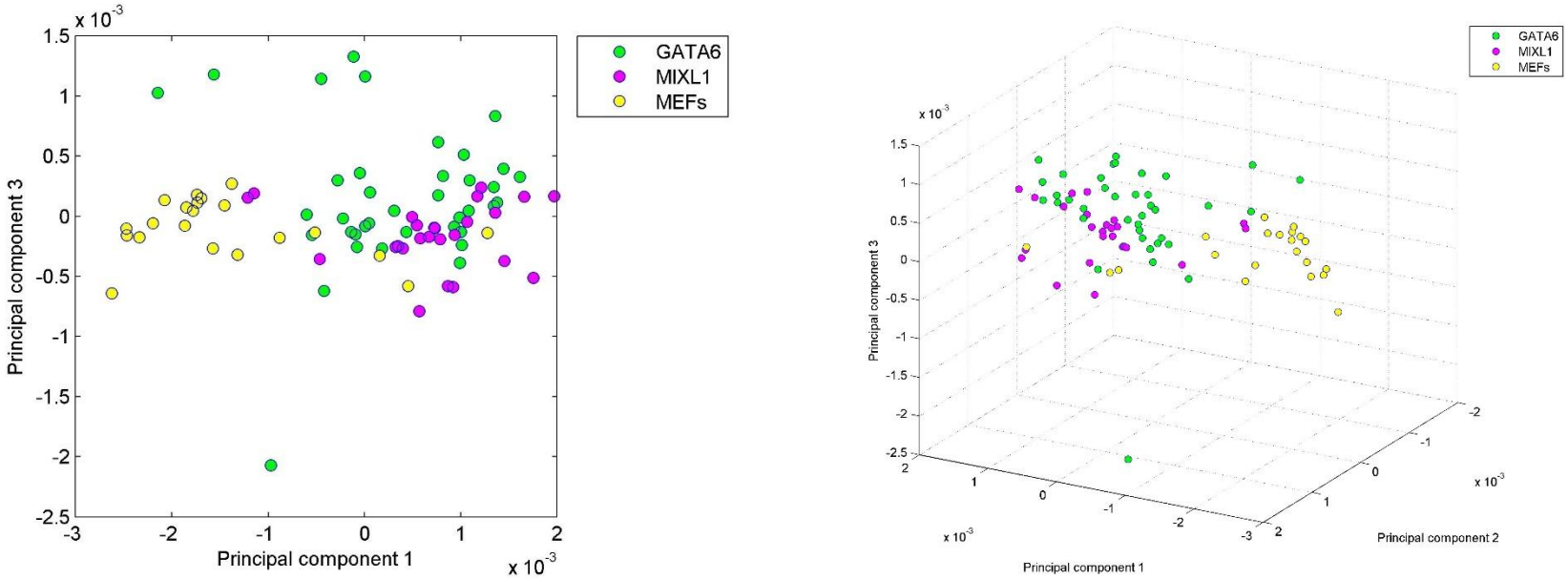

Figure 5.13 – A Hyperspectral imaging comparison between Raman spectra collected from multiple different cell lines. Spectra were acquired using a hyperspectral approach, where each point represents the average of between approximately 50 -350 spectra collected from within an individual cell. Cell lines examined were mouse embryonic fibroblasts (MEFs, yellow, n=21), and two human embryonic stem cell lines, shef4 Gata6 (green, n=38) and Hes3 MIXL1 (pink, n=25). Two PCA plots are shown showing a comparison between PC1 and PC3 as well as a 3D plot examining PC1, PC2 and PC3. Cell lines begin to cluster according to species along PC1 and the two different human ES cell lines appear to differ according to PC3.

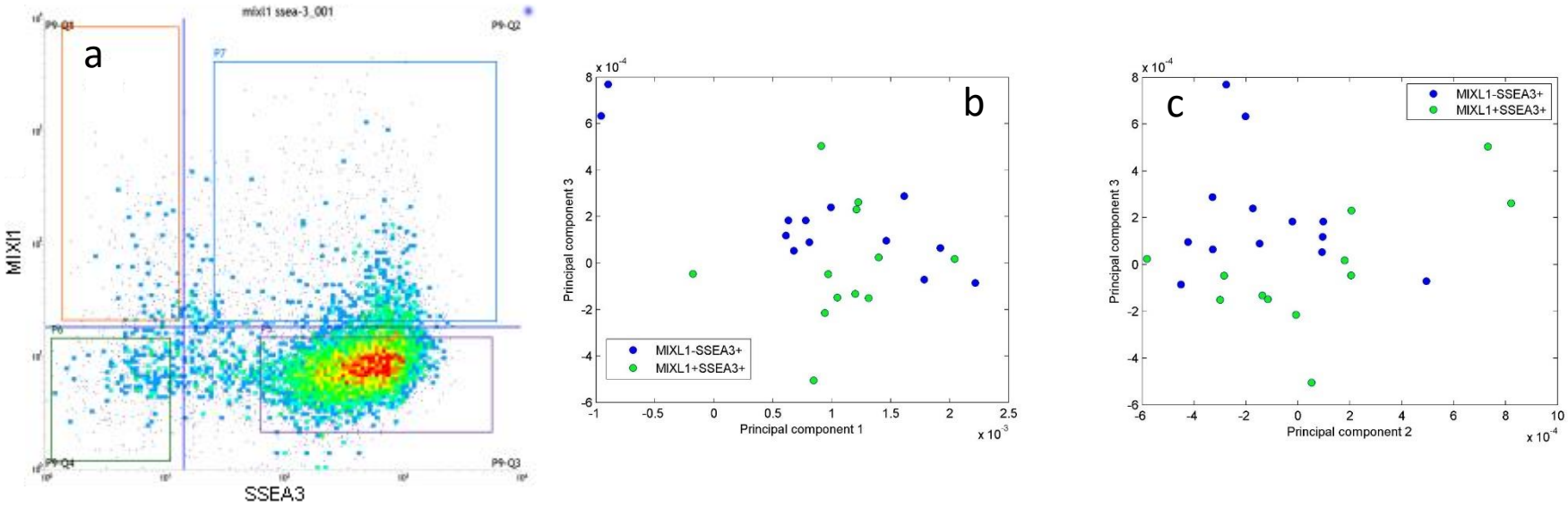

Figure 5.14 – Mesoderm Lineage Reporter MIXL1 and Raman spectroscopy. To examine whether Raman Spectroscopy could distinguish between cells based upon associations with lineage markers in the pluripotent stem cell state, Hes3 MIXL1 cells underwent a dual sort for SSEA3 and MIXL1. **a)** shows the FACS plot by which cells were sorted. Cells from regions P5 and P7 were sorted and plated on CaF_2 slides, allowed to attach and then fixed for subsequent hyperspectral Raman imaging. Raman analysis was performed on one culture each of sorted cells, MIXL1+SSEA3+ (green, n=12 nuclei) and MIXL1-SSEA3+ (blue, n=13 nuclei). Each point on the PCA plots **b)** and **c)** represents the average of between 43 and 215 spectra obtained from the nucleus of an individual cell. PCA analysis shows that there are slight differences between the cell classifications with the SSEA3-positive MIXL1-negative fraction being generally positive for PC3 and vice-versa for the SSEA3-positive MIXL1-positive cells. There is no obvious separation associated with either PC1 or PC2.

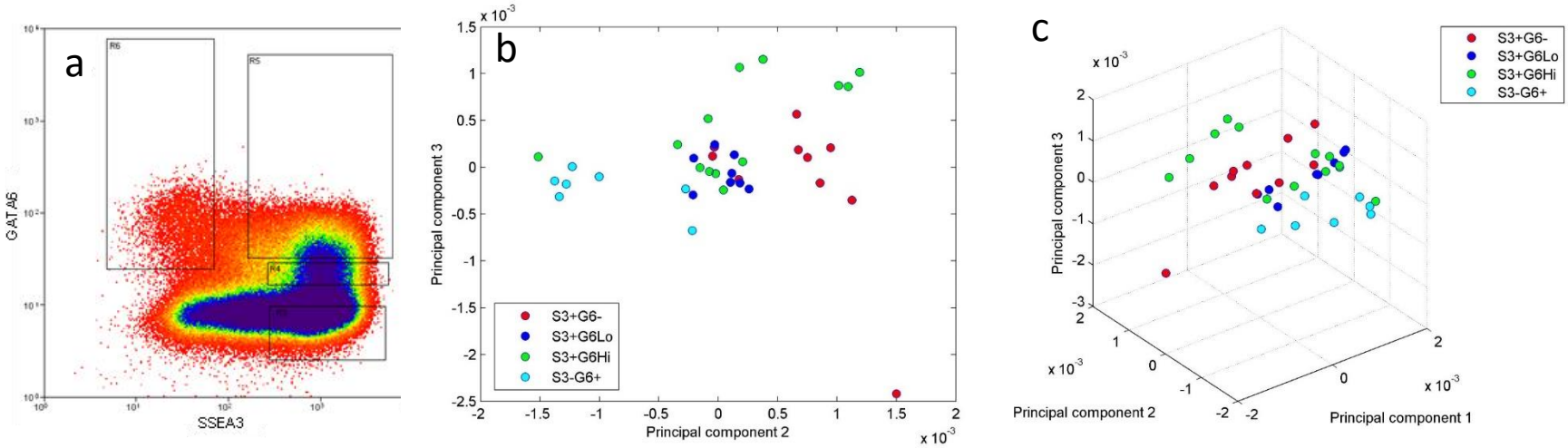

Figure 5.15 – Endoderm Lineage Reporter Gata6 and Raman Spectroscopy. To examine whether Raman Spectroscopy could distinguish between cells based upon associations with lineage markers in the pluripotent stem cell state, Shef4 GATA6 cells underwent a dual sort for SSEA3 and GATA6. **a)** shows the FACS plot by which cells were sorted. Cells from regions R3, R4, R5 and R6 were sorted and plated on CaF_2 slides, allowed to attach and then fixed for subsequent hyperspectral Raman imaging. Raman analysis was performed on one culture each of sorted cells, SSEA3+GATA6- (red, n=10 nuclei), SSEA3+GATA6lo (dark blue, n=8 nuclei), SSEA3+GATA6hi (green, n=13 nuclei) and SSEA3-GATA6+ (light blue, n=7 nuclei). Each point on the PCA plots **b)** and **c)** represents the average of between 36 and 365 spectra obtained from the nucleus of an individual cell. Cell clustering seemed to occur primarily along PC2 for the SSEA3-negative GATA6-positive, SSEA3-positive GATA6 low and SSEA3-positive GATA6-negative fractions. The SSEA3-positive GATA6-high fraction did not associate with any one particular region along PC2, and could be found associated with all other fractions.

5.8 Discussion

Here the sensitivity of Raman Spectroscopy to detect different cell types was explored with four different conceptual approaches, representing varying degrees of heterogeneity within and between cells. This examination of heterogeneity by Raman spectroscopy occurred in concurrence with the development of the final, optimal method described in Chapter 4 and thus the methods employed changed over the course of this Chapter.

The first conceptual approach was the examination of differences in cell lines, which was addressed in two different experiments. The first experiment, which was outsourced to Renishaw, revealed that Raman Spectroscopy spectra could distinguish between different cell lines (Figure 5.1). NTera2 grouped furthest away from the other samples according to PC1, although this is most likely due to artefacts in its spectra not shared by the spectra of other cell lines (Figure 5.1a). Therefore, it appears that PC1 explains most of the variation caused by these artefacts. This spectrum also looks notably different from other NTera2 spectra collected from other experiments. The remaining cell lines all separated by PC2, irrespective of PC1, so an examination of wavenumber loadings responsible for PC2 was carried out. The differences in PC2 therefore likely reflects biochemical differences between these cell populations. Although it is impossible to rule out the contribution of artefacts from NTera2 spectra, NTera2 is relatively neutral for PC2 so it is likely not to be primarily responsible for the separation of cell lines along this component. Wavenumbers that had the greatest weighting in PC2 tended to associate with proteins/amino acids when positive and glucose and lipids when negative. This association implies that the culture-adapted nullipotent embryonic carcinoma cell line N2102 EP is relatively more protein rich and lipid-poor than the normal human ES cell line H14.S9.

The two human ES cell lines H14.BJ1 and H14.S9 represent culture adapted and karyotypically normal variants of the H14 cell line respectively. These cell lines were grouped closer together than the other cells lines, however, they could still be distinguished. The main difference again lies along PC2 where the H14.S9 Raman spectra have a greater complement of lipid and glucose-associated peaks. This is not the first study to have examined human ES cells and their karyotypically abnormal variants. For example, Raman analysis of the normal cell line Hues9 and a karyotypically abnormal variant of Hues9 (47,XX,+20) show that the abnormal variant had greater peak intensities for wavenumbers corresponding to cytochrome C, and to a lesser extent increased nucleotide, protein and lipid associated wavenumbers (Harkness et al., 2012). The results here do not exactly mirror that found by Harkness, et al., and this could be for a few reasons. Differences in culture technique, for instance, could be responsible such as batch variation in the sera used between our experiments and Harkness et al. In addition, other factors such as cellular confluency and differentiation status of the cultures examined remain uncontrolled variables between these experiments. However, these results could reflect real biochemical differences between unrelated culture adapted cell lines, whereby the biochemical phenotypic manifestation of culture adaptation in these systems are metabolically different. This interpretation presents the idea that culture adapted cell lines may achieve adaptation entering different, stable biochemical states. Furthermore, the addition of N2102EP in this analysis may obscure specific differences between H14.S9 and H14.BJ1 that would be otherwise elucidated along PC2. Although it is the case that these Human ES cell lines differ along PC2, this is really a function of greater difference between N2102EP and H14.S9. Thus, the difference between the EC cell line and the ES cell line H14.S9 in PC2 explains a greater proportion of variation in the dataset than between the two human ES cell lines, where the difference between these two ES cell lines specifically could be more powerfully explained by the same biochemical markers highlighted by Harkness et al.

In our experiment, thousands of spectra were collected from each cell line, across multiple cells and collectively these replicate spectra led to the conclusions discussed above. That said, these data were collected from one sample of cultured, and then fixed, cells for each cell line without further experimental replication. It is therefore formally possible that the differences observed could be the result of differences reflective of these particular samples rather than as a complete biological representation of these cell lines. One of the major limitations with this approach is that although many spectra are generated, this is across a comparatively small number of cells (~10) per cell line. Therefore, these handful of cells are extremely well characterised by Raman spectroscopy, however it begs the question as to whether this small number of cells is a fair representation of the rest of their cell line, or even their respective sister cells in culture (See Section 5.9). Further sampling with this methodology, across multiple cultures would be required to make the claim certain that Raman spectroscopy was discriminating between inherent differences in the cell line rather than some aspect of sampling error.

Raman spectra collected using the hyperspectral imaging technique developed in chapter 4 was also capable of distinguishing between different cell lines (Figure 5.13). In this case the cell lines used were mouse embryonic fibroblasts (MEFs) and two human ES cell lines Shef4 GATA6 and Hes3 MIXL1. The technique developed here could indeed demonstrate differences between these cell lines with PC1 primarily responsible for separation of cell line by species, and PC2 began to separate the two human ES cells from each other. These results are encouraging however, the separation is not as clear cut as other papers have reported for differences between somatic and pluripotent cell phenotypes.

The sensitivity of Raman was also tested in the context of Retinoic Acid (RA) mediated differentiation of the pluripotent human EC cell line NTera2. Indeed, preliminary data on live

Ntera2 cells examined in suspension presented differences after 5 days of exposure to RA (n=10 for both treated and control cell types) (Figure 5.2). These differences were associated with differences in nucleic acids, protein and unsaturated lipids. These encouraging results warranted further investigation, however, the suspension format of the initial experiment presented its own problems (see chapter 4). Therefore, a modified version of the experiment was performed using cells grown in a monolayer format on CaF_2 slides and PFA fixed prior to Raman analysis (Figure 5.3, 5.4). Three experimental replicates were conducted for these data, where six sister culture vessels of NTera2 cells were analysed (three exposed to RA and three acting as control samples) (Figure 5.4). When these replicates were independently analysed by PCA, they demonstrated similar separation each coincidentally by PC3, and indeed the wavenumbers associated with PC3 separation were similar for all replicates (Figure 5.4). This experiment also demonstrated that differences in Raman spectra between differentiated and undifferentiated could be detected using Raman microscopy and that the main differences were primarily due to increased protein levels in the differentiating cells, and increased nucleic acid levels in the undifferentiated cells (Figure 5.3), which is concordant with other studies examining differentiation with Raman spectroscopy over similar timescales (Notingher et al., 2004a). A predictive model from our data using a supervised clustering analysis was generated that could accurately predict whether cells that were not used for training the model had been treated or not with RA (Figure 5.5).

A time-course RA differentiation assay was performed in order to assess how early during the process of differentiation Raman spectroscopy could distinguish between treated and untreated cells. Concomitant FACS analyses of sister cells confirmed that cultures treated with retinoic acid lost SSEA3 and Tra-1-60s faster than untreated cultures, and thus interpreted to be losing pluripotency and undergoing differentiation (Figure 5.6). Raman analyses of these cultures

generated spectra that showed signs of separation as early as three hours into the time-course assay according to PCA analysis, representing a method that is more sensitive to the induction of differentiation than traditional FACS analyses of markers sensitive to pluripotency such as SSEA3. PCA analyses of treated cells against their untreated counterparts at each timepoint show the greatest separation at the 2day and 6 day timepoints, whereas there appears little separation after three days (Figure 5.7).

Since it is the case that the untreated cells will also be changing over the time course, it is debatable as to how representative these cells are of the undifferentiated state as time progresses. This is evidenced by a change, albeit much more slowly, in the untreated cultures. Therefore, it could be argued that the earliest untreated timepoint is the most representative of the undifferentiated state. Indeed, PCA analyses of differentiating cells against this initial untreated timepoint show greater separation than even at the treated 3 day timepoint samples, which did not show great separation when compared against the 3 day untreated timepoint (Figure 5.8). However, a comparison of the mean spectra even at 6 days (144 hours) RA treated cells do not show the same differences in their spectra as in the previous retinoic acid differentiation experiment.

The reason for the difference between experiments was unclear and the similar mean spectra of the time course experiment was a puzzle. This experiment took considerably longer to collect data from live cells, in the order of about 4 hours per timepoint, during which time cells were not maintained in normal culture conditions. At the time of examination, cells were maintained in PBS only in order to exclude artefacts from contaminates such as foetal calf serum. This is a considerable period of time, over which cells will become progressively more stressed. The similar mean spectra could be a function of biochemistry associated with stress that may

supersede differences resulting from differentiation. However, that in itself does not explain why the populations separate according to PCA analysis and this separation could be due to tiny differences associated with the differentiation of the cell as a real biological phenomenon. Alternatively, an artefact of spectra pre-processing could be responsible. Both of these explanations could adequately account for PCA separation from populations whose main spectra appear very similar. Further investigation into this effect is warranted, especially if this effect is due to problems with pre-processing which would need addressed. There is no reason to presume that there are problems with the pre-processing approach adopted, and that has been used elsewhere, therefore its appears that Raman spectroscopy can distinguish between cells as early as three hours into a differentiation protocol, although repeats of this experiment would be required before this could be stated with utmost confidence.

Independent of the issues discussed above, only one single spectrum was acquired from each cell examined. The cells were grown in a monolayer format that means the point acquisition represents only a small area of the total cell size. Cells are not homogenous and so it would be premature to assume that only one spectrum is truly representative of the biochemical state of that entire cell. Therefore, anew experiment was designed in order to examine different regions within the cell, identified as the nucleus, nucleolus and cytoplasm was performed, in part to address whether this Raman system could detect differences between these regions as demonstrated in other studies. Additionally, cells used for these comparisons were fixed in order to reduce artefacts associated with cell stress. PCA analysis revealed Raman could distinguish between cytoplasmic regions from the nucleus and nucleolus along PC1, whereas the difference between nucleus and nucleolus was not clear. The spectra of the nucleolus grouped within the broader grouping of nucleus, suggesting that these regions are less varied. The reason for this difference along PC1 seemed primarily associated with phenylalanine and protein as

positive for PC1 and associated with the cytoplasm whereas DNA/RNA nucleotides were the most prominent group negative for PC1. Spectra from the nucleus and nucleolar regions were mostly negative for PC1 and this association with nucleotides was anticipated. Also responsible for separation along PC1 were several highly weighted bands with unknown association. Not every biomolecule, nor their combinatorial effects, have been analysed for their Raman profile, and so these regions could be reflective of this. Alternatively, this could reflect a noisy dataset, which considering the low number of cytoplasm samples analysed, cannot be excluded as a possibility. These data were acquired from monolayer cultures of NTera2 cells which were generally dense in appearance, with a high nucleus:cytoplasm ratio. This made accurate selection of cytoplasmic regions difficult to achieve. Repeating this experiment using cells in a lower density may help to address this issue.

Given that heterogeneity between cytoplasm and nuclear regions was established here and elsewhere (Notingher et al, 2002) point spectra analyses of cell nuclei were adopted in an initial study looking at SSEA3-based heterogeneity in NTera2. Although the PCA analyses of cells sorted for SSEA3 did reveal a difference between fractions, in the main it appeared that the separation appeared to correlate with SSEA3 intensity with the unstained/unsorted population lying directly opposed to the high fraction. Since the unstained/unsorted fraction should contain cells from all other fractions, this difference appears to be due to the effect of the staining itself. Indeed, this difference was most likely caused by fluorescence of the fluorophore where there was still residual fluorophore despite multiple washes as part of PFA fixation prior to analysis. That said, not all high fraction cells exhibited obvious fluorescent background, indicating that fluorescence could be from an alternative source not associated with the staining or the cell wash steps successfully removed residual fluorophore unevenly from the populations. The final

explanation is of inaccurate sort; however this is unlikely given experience with back-gating (see Chapter 3; Figure3.14).

Regardless of the source of the background interference, a polynomial baseline correction method was utilised prior to regular spectral normalisation. This correction method applies a polynomial baseline correction that is calculated for each individual spectrum. The resulting average spectra no longer exhibited the increasing baseline tail associated with fluorescence, however, the PCA analysis again seemed to show correlation with SSEA3 intensity with the high and unstained/unsorted fractions lying opposite each other. In this case it appears that the baseline correction method employed was not able to eradicate the artefactual effect of the SSEA3 stain and associated fluorophore. Therefore, further antibody studies will require the selection of a fluorophore whose excitation and emission spectra do not interfere. Consequently, further antibody studies used Dylight 647 fluorophores that were predicted not to interfere with the Raman spectroscopy.

An alternative approach to addressing the problems associated with intracellular heterogeneity was adopted by using hyperspectral imaging. This technique collects many spectra per cell that can also be coupled to spatial information across the sample/cell (see chapter 4). A method by which spectra specific to spatial regions of interest could be extracted from datafiiles was developed in Matlab in collaboration with Dr. Veronica Biga. This tool was used to compare many average spectra from across the nucleus from multiple cells with regard to the MEF, Shef4-GATA6 and Hes3-MIXL1 cell lines.

Analyses using hyperspectral profiling are incredibly time consuming, taking up to several hours to analyse individual cells. As a result, analysis on a cell by cell basis is performed using many spectra that are descriptive of few cells. This approach probably provides the most comprehensive description of the biochemistry within the nucleus and therefore is arguably the most representative of that cells' nuclear state. For the examination of stem cell heterogeneity this approach was adopted and a comparison of different states of the Sef4-GATA6 and Hes3-MIXl1 cell lines was made according to marker expression. In the case of Shef4-GATA6 there appeared definite grouping effects according to marker expression with the SSEA3-positive GATA6-high fraction capable of association with any of the other fractions including the differentiated SSEA3-negative GATA6-positive cells as a well as the 'pristine' SSEA3-postive GATA6-negative population. Similarly, there appear to be differences in the SSEA3 positive Hes3-MIXL1 populations according to MIXL1 expression. These results indicate that Raman spectroscopy seems capable of detecting differences in nucleus biochemistry of cells, depending upon the expression of particular lineage markers.

5.9 Replication and Sampling

Several experiments have been described over the course of this chapter, including the collection of thousands of spectra. A common theme through all of the experiments is a comparatively low number of cells analysed by Raman spectroscopy. The largest number of cells analysed from any of these experiments was the NTera2 retinoic acid differentiation assay that analysed 500 cells across all timepoints and treatments (Table 5.4). In this case, 50 cells were analysed by Raman spectroscopy per timepoint for each treatment, meaning that these ten total cell cultures are each represented in this data by 50 cells each. Each Cell culture may easily contain many millions of cells and it is unlikely that the Raman spectra of tens or even a few

hundred cells accurately represents this sample. This is an alternative form of the question regarding the best way of gathering Raman spectra that represents the cell of interest except extended to ask about the number of cells needed to represent its culture.

As part of developing the Raman spectroscopy technique, it was decided that it would be better to capture more information from across the cell in the form of hyperspectral mapping of the nucleus since it would provide a better means of comparison between different cells as opposed to arbitrary point location (discussed further in Chapters 4 and 6). Hyperspectral mapping by Raman spectroscopy is the more time consuming process since it requires the acquisition of more spectra per cell. The consequence of this was a reduction in the number of cells analysed per experiment. This is also reflected in the low number of experimental replicates; acquisition of hyperspectral Raman data could take weeks per condition. Given the problem that hyperspectral imaging is time intensive and that a tiny proportion of cells in the culture can be analysed for any experiment, the approach adopted to provide better sampling across the whole population was to collect more data from an individual replicate that could provide better sampling across the whole population rather than a reduced sampling proportion across more samples.

Table 5.4 – Replication Details for experiments in Chapter 5. The number of cells and spectra used for each experiment, coupled with information on the pertinent figures and experimental replication. Abbreviations: G6, GATA6; Hi, High; lo, low; M, MIXL1; MEF, Mouse Embryonic Fibroblasts; Md, Medium; RA, Retinoic acid; S3, SSEA3; -ve, negative. "?" symbolises that these data were not collected by cell number, but over an area of the dish.

Experiment	Results Figures	Nº of cells	Nº of spectra collected	Experimental replicates
Cell Line differences	5.1	?	1,000-2,000 /cell line Total: 5,200	1
Retinoic Acid differentiation I	5.2	10 per treatment Total: 20	1 per cell Total: 20	1
Retinoic Acid differentiation II	5.3, 5.4, 5.5	RA treated: (10,10,10) by rep Control: (15,10,13) by rep Total: 68	1 per cell Total: 68	3
Retinoic Acid differentiation time course	5.6, 5.7, 5.8	50 cells per condition per timepoint Total: 500 cells	1 per cell 500 total	1
Intracellular heterogeneity	5.9, 5.10	Nucleus: 115 Nucleolus: 100 Cytoplasm: 12 Total: 115	Nucleus: 409 Nucleolus: 129 Cytoplasm: 39 Total: 645	1
Substates I NTera2/SSEA3	5.11, 5.12	Hi: 89 Md: 40 -ve: 88 UU: 59 Total: 276	Hi: 444 Md: 200 -ve: 440 UU: 294 Total: 1378	1
Substates II Reporter line/MEF	5.13	MEF: 21 Hes3 MIXL1: 25 Shef4 GATA6: 38 Total: 84	Approx. per nucleus: MEF: 29-321 (~3,000 Total) Hes3 MIXL1: 43-215 (~3,750 Total) Shef4 GATA6: 36-365 (~5,500) Total: ~12,250	1
Substates III Hes3 MIXL1	5.14	S3+M-: 13 S3+M+: 12 Total: 25	Approx. per nucleus: S3+M-: 49-175 (~2,000 Total) S3+M+: 43-215 (~1,750 Total) Total: ~3,750	1
Substates IV Shef4 GATA6	5.15	S3+G6-: 10 S3+G6lo: 8 S3+G6hi: 13 S3-G6+: 7 Total: 38	Approx. per nucleus: S3+G6-: 48-365 (~1,500) S3+G6lo: 62-173 (~1,200) S3+G6hi: 36-189 (~1,800) S3-G6+: 67-131 (~1,000) Total: ~5,500	1

Where experimental replication did occur, during one of the earlier Retinoic acid differentiation experiments (Table 5.4, Figures 5.3, 5.4), the replicate experiments all produced quite similar results. The average spectra shared similar patterns and the graphed standard deviation across normalised data indicates that the standard deviation rarely exceeds 10% of the mean. Although it is expected that different cells may be performing different biochemical functions that would be reflected in differences in Raman spectra, the fact that the variance is low supports the idea that Raman spectroscopy is collecting accurate data from the cells. Retinoic acid treated cells did tend to separate by PCA from their control counterparts, and the wavenumbers associated with this separation appeared quite similar by examination of the third principal component loadings. Furthermore, the spectra from the first two replicates, when modelled by Partial least squares (PLS) regression were then able to accurately predict which treatment novel spectra (those from the third replicate) belonged to. Finally, it is worth describing that although these replicates were cultured separately, they were all daughter cells of a shared ancestral flask. In this sense they represent a pseudoreplication of the experiment, although this is an unavoidable consequence of working with a clonal cell line.

Finally, the nature of replication is one often confounded by the use of cell line-based experiments. It is clear for one thing that omniscience with regard to any particular cell line still provides no form of biological replication, which necessitates the examination of behaviours from independent biological entities. For example, absolute knowledge about the behaviour of one single person is not a reliable basis for knowledge on the behaviour of people since the subject could easily be an outlier. In order to understand the behaviour of people with regard a particular behaviour, study of multiple independent people would be required to accurately identify a trend.

Cell lines present themselves as a problem in this regard. Although there may be much to learn about the behaviour of an individual cell line, no amount of experimentation could confirm that the behaviour of that cell line is representative of all cell lines derived in the same manner. Such a confirmation requires experimentation on independently derived cell lines. That said, a robust knowledge of a cell line's behaviour has its own merit, such as understanding that of substate heterogeneity as a paradigm already identified in NTera2 with respect to SSEA3 expression.

Indeed, this work was conducted in order to develop Raman spectroscopy as a viable tool for interrogating cell behaviour and in order to practically facilitate this task, the behaviours of select few cell lines were examined by this system. Raman spectroscopy could be used as a holistic interrogator of cell behaviour between cell lines in order to draw more general biological trends. Here, the question was over whether Raman spectroscopy was sensitive enough to examine substate heterogeneities and so was developed to examine the paradigm as seen in the context of NTera2 and the reporter cell lines Shef4 GATA6 and Hes3 MIXL1. This approach could indeed be applied to other contexts; however, this would not have been practical within the scope of this Thesis.

Altogether this work demonstrates that Raman spectroscopy is a viable tool for examining cellular behaviour that is particularly sensitive to experimental design. Nevertheless, these proof-of-concept experiments highlight the potential of Raman spectroscopy. These experiment have perhaps demonstrated the earliest known timepoints at which changes associated with cellular differentiation can be detected, and also possibly demonstrated detectable biochemical associations of lineage bias within the stem cell compartment. Excitingly, this provides a non-invasive platform that can be further developed to elucidate more clearly the role of subtle biochemical variation in addressing questions of stem cell fate.

Chapter 6

Discussion

6.1 Summary of aims

The aim of this project was to develop new approaches for understanding the cryptic heterogeneity of cells within the pluripotent stem cell compartment that belies stem cell fate decisions. Understanding of the rules governing stem cell heterogeneity opens up opportunities to manipulate these features for the improved application of differentiation protocols or even regular cell culture maintenance.

To address this, two approaches were developed in the scope of this thesis. One approach examined the population dynamics of pluripotent stem cells whilst within the stem cell compartment (chapter3). Delineating the rules by which cells change their behaviours over time provides a unique insight into cellular behaviour and the location of potential substate positions that can be determined by examination of a particular marker's expression within an axis of variation.

The alternative approach adopted was the exploitation of Raman spectroscopy in order to examine cryptic stem cell heterogeneity in terms of their biochemical phenotype or "fingerprint." Given that a cell's function and phenotype is ultimately governed by biochemical reactions that occur within the cell, along with all associated variations, it is not unreasonable to anticipate that a cell's behaviour is intrinsically linked to its metabolic state. The advantage of Raman spectroscopy is that it is a non-invasive technique that exploits the physical properties of photon/molecule interactions which means that in principal no sample preparation is required to acquire this information. Indeed, it is possible to collect data from live cells in real time that can then be examined to ascertain future behaviour. The capacity to simultaneously acquire metabolomic data non-invasively as well as examine a cell's future behaviour is a novel

prospect in the field of stem cell biology since cell destruction is not necessitated. Therefore, this approach if implemented to its full potential, should be a revolutionary technique in the analysis of single cell behaviour, where metabolomic similarity no longer need be inferred by proxy between living and destroyed cells used for metabolomic analysis.

6.2 Summary of Results

Two novel methods for the interrogation of cryptic aspects of pluripotent stem cell heterogeneity have been described, developed and implemented in this thesis. In Chapter 3, the first method adopted successfully managed to model SSEA3 dynamics within the model pluripotent Embryonic Carcinoma (EC) cell line, NTera2. The model generated described the heterogeneity dynamics of SSEA3 expression in NTera2 pluripotent stem cells and in a predictive manner. The resulting model also provided candidate identifiers of substate locations according to the SSEA3 axis of variation.

The second approach developed was the application of Raman spectroscopy for the assessment of varying degrees of heterogeneity within the stem cell context. Chapter 4 is a description of the ongoing iterative optimisation of the Raman Spectroscopy technique. These studies showed that a hyperspectral approach proved sensitive for information-rich holistic examination of cell biochemistry. Additionally, this study identified that the signal intensity from the nucleus was stronger than that of the cytoplasm, narrowing the target for further studies. Chapter 5 utilised the Raman Spectroscopy techniques to attempt to answer biological questions. Raman Spectroscopy proved sensitive enough to notice differences between the cell lines Ntera2, N2102EP, the human ES cell line H14.S9 and the karyotypically abnormal variant of that line, H14.BJ1. Separately, mouse embryonic fibroblasts (MEFs) and the human embryonic reporter

lines Shef GATA6 and Hes3 MIXL1 were able to be primarily separated by species and secondarily by cell line. The differentiation of Ntera2 cells by exposure to Retinoic Acid (RA) was analysed. Clear differences were seen between cultures that were and were not treated with RA in both suspension and monolayer formats. Additionally, differences appeared to be detectable as early as three hours post RA exposure. Raman Spectroscopy appears to be able to differentiate between nucleus/nucleolus and cytoplasm. Additionally, spectra from the nucleolus appear to vary less than spectra from the whole nucleus, identifying a potential less noisy target for further studies.

These studies with both of these techniques represent the cornerstone for further development, the full realisation of which could prove revolutionary for stem cell research and future medical applications.

6.3 Further experiments

This thesis describes an ongoing and iterative body of work that has been continuously tested and refined as it progressed. Thus, the results presented here are still undergoing analysis and refinement, and are subject to further studies presented below. Technical considerations are also discussed, as a tailored and refined Raman microscope built to facilitate biological samples would extend the range of questions that could be addressed.

6.4 Heterogeneity modelling

The modelling of cryptic aspects of pluripotent stem cell heterogeneity though SSEA3 dynamics has been successful. However, the major limitation of this approach is the large number of cells required for this flow cytometry based approach, and this makes it impractical for use with human ES cells. Currently an in situ method using the InCell analyser platform is in development, and this has the potential to drastically reduce cell number required and this could make this technique applicable for stem cell applications. Presently, analysis of SSEA3 staining does not reveal the same heterogeneous expression of SSEA3 in cultured cells as revealed by flow cytometry. However, more rigorous image post-processing could be developed to reveal analogous SSEA3 distributions. It is not anticipated that models generated using different instrumentation will be directly comparable, however, development on the Incell not only enables the use of the technique with less robust cell lines, but it is also easier to examine multiple markers simultaneously, including for example, intracellular staining of transcription factors. The mathematical model could also be extended to include description of the dynamics of multiple markers for heterogeneity simultaneously. This extension of the modelling process to additional dimensions of heterogeneity is possible in principle but is yet to have ever been attempted (Coca, personal communication). Analysis on the Incell analyser platform also opens up opportunities to examine spatial arrangement of cell heterogeneity; information that is lost with a flow cytometry approach.

Examination of biological behaviours associated with equilibrium points was preformed using a clonogenic assay. This assay showed that there were differences between different sorted fractions. However, it provides no information on differentiation lineage biases. Additional experiments that examined directed differentiation efficiencies would be key to elucidating the relationship of equilibrium points to lineage biased substates, if at all. Alternatively,

transcriptomic analysis in particular of pluripotency factors and lineage transcription factors provides an additional approach whereby any association of equilibrium points to lineage biased substate could be addressed.

6.5 Raman spectroscopy

Given the groundwork already laid out, and the iterative optimisation that occurred throughout this body of work, repeating the earliest experiments with the refined technique would be informative. For instance, the Retinoic Acid differentiation time course experiment, which appeared to show differences between differentiating and undifferentiated cells as soon as three hours post induction. This potentially important result was obscured in the original experiment by problems associated with cell stress and point acquisition. Repeating this experiment using the hyperspectral imaging approach on fixed cells would be a more accurate experiment and provide a more definitive result.

The NTera2 SSEA3-based heterogeneity similarly would benefit from reanalysis in the light of more sophisticated spectral collection techniques. In particular, the use of a fluorophore that is not excited by the laser is paramount to an effective interpretation of biochemical heterogeneity associated with SSEA3 expression.

The experiments described about could be extended to include an examination of SSEA3 heterogeneity with predicted equilibrium points. If for instance, a particular equilibrium point was primed to differentiate it may present Raman spectra with the increased protein to nucleotide ratio that is the common difference between differentiating and undifferentiated

cells. Alternatively, other spectral fingerprints could become apparent that are reflective of particular substates or equilibrium points.

One aspect of the hyperspectral Raman imaging approach adopted is that of special considerations with regard to biochemistry within the cell. In a crude manner, an examination was made between nuclear and non-nuclear regions. However, a converse approach could be useful for identifying particular organelles or processes within the cell. For instance, the location of mitochondria could be identified by the presence of cytochrome c-specific wavenumbers at 751cm^{-1}, 1128cm^{-1}, 1314cm^{-1} and 1583cm^{-1}. Alternatively, spatial association of wound and unwound chromatin to different regions of the nucleus could be tracked with minimal interference.

6.6 Raman spectra normalisation

Although we have gone some way towards optimising our approach for data collection, the analysis of spectra collected remains challenging. Currently, there exists several approaches for normalising and subsequent analysis of spectra. The approach we use here was that suggested by the owner of the Raman microscope used in this study, although it has become apparent, however that this manipulation of the data is heavily distorted by baseline effects. This could itself be the cause of separation in PCA analysis. It is therefore worth exploring other normalisation techniques in order to acquire comparable spectra that are representative of real biochemical differences, rather than influenced by the baseline. This issue has been explored somewhat in in an excellent review by (Afseth et al., 2006) who provided in-depth analysis of techniques used in the pre-processing of Raman spectra.

6.7 Raman microscope instrumentation for stem cell applications

The system used in these experiments was ill-equipped for analysis of sensitive live human embryonic stem cells. However, with a few modifications suitable system for the analysis of live embryonic stem cells in a monolayer format could be easily achieved. First and foremost, the capacity to maintain healthy cells is paramount, and the installation of an aseptic, heated environment chamber would allow the acquisition of Raman spectra of cells maintained in a healthy state. This capacity would simultaneously bypass problems associated with chemical alteration caused by chemical fixation as well utilising Raman to its fullest potential as a non-invasive metabolomic profiling technique. Although this will also be associated with its own problems, such as media interference that could be overcome with effective protocols such as standardised chemically defined media and effective pre-processing to remove media baseline. However, it is likely that an increase in acquisition time will be necessary to ensure a good signal to noise ratio. This leads to the prime limitation of this technique, the long acquisition time needed to acquire spectra from individual cells. With regards acquiring informative spectra representative of individual cells, and increased laser spot size could be utilised that would cover a larger area of the cell and consequently reduce acquisition time at the expense of special resolution. This technique of increased laser spot size has been used by several groups effectively to reduce Raman spectra acquisition time. In addition, examining cells in a monolayer format could easily be coupled with time lapse experiments tracking the behaviour of cells over time as well as in comparison to its neighbours.

An alternative approach altogether is the use of Raman spectroscopy in conjunction with microfluidics for the examination of cells in suspension and can be coupled readily with cell sorting based upon Raman spectroscopy. This technique has been recently developed and termed Raman Activated Cell Sorting (RACS) (Zhang et al., 2015). This approach collects the

Raman spectrum of cells in suspension, which based upon the data collected in this thesis, generates a signal that is approximately six times stronger than the cells in monolayer. This effect in itself would act to drastically reduce acquisition time per cell. RACS could also be coupled with other single cell analyses on sorted cells of interest that could provide a link between metabolomic profiles and transcriptomic, genetic or epigenetic profiles.

Alternative ways of boosting Raman signal includes employing techniques such as coherent anti-stokes Raman spectroscopy (CARS) and surface-enhanced Raman spectroscopy (SERS) (described in chapter 1). The former technique is preferable because SERS requires that the sample be treated with metallic nanoparticles, that may introduce additional and unexpected behavioural effects of the living cells. Although CARS does produce an increased signal generation the spectral range that can be acquired is generally reduced to a couple of hundred wavenumbers, and requires a tuneable laser. However, this technique is extremely high throughput and capable of obtaining spectra from whole cells with collection times of 300ms (Konorov et al., 2007).

Within the context of pluripotent stem cell heterogeneity, it would be important to know whether heterogeneity observed is due to actual behavioural differences or whether it more closely reflects other known cell dynamics. For instance, the difference between heterogeneous cell populations may be better explained by their position in the cell cycle rather than an independent source of heterogeneity, although it is plausible that cell behaviour and other macrodynamics such as cell cycle may be related to some extent. Other groups have already examined changes in Raman spectra with changes in cell cycle position and so this may provide an angle by which sub state heterogeneity and cell cycle heterogeneity may be untangled. Finally, Raman spectroscopy does not have direct explanatory power of the differences between

samples of different spectra. The association of particular wavenumbers with biomolecules inferred here were collated from various databases in the literature. However, these associations are inferred, although probable. Candidate molecules inferred to be responsible for differences in Raman spectra would need to be measured by other means in order to categorically demonstrate that the concentration of these molecules different between samples.

This body of work has developed both novel exploratory techniques and provided a basis for understanding heterogeneity within the stem cell compartment. This thesis has laid the groundwork necessary for expanding both the dynamical modelling and Raman spectroscopy application to pluripotent stem cell biology.

Bibliography

Adar, F., 2007. Evolution of Instrumentation for Detection of the Raman Effect as Driven by Available Technologies and by Developing Applications. J. Chem. Edu J. Chem. Edu.

Aflatoonian, B., Ruban, L., Shamsuddin, S., Baker, D., Andrews, P., Moore, H., 2010. Generation of Sheffield (Shef) human embryonic stem cell lines using a microdrop culture system. In Vitro Cell Dev Biol Anim 46, 236-241.

Afseth, N.K., Segtnan, V.H., Wold, J.P., 2006. Raman spectra of biological samples: A study of preprocessing methods. Appl Spectrosc 60, 1358-1367.

Andrews, P.W., 1984. Retinoic acid induces neuronal differentiation of a cloned human embryonal carcinoma cell line in vitro. Developmental biology 103, 285-293.

Andrews, P.W., 2002. From teratocarcinomas to embryonic stem cells. Philosophical transactions of the Royal Society of London. Series B, Biological sciences 357, 405-417.

Andrews, P.W., 2011. Toward safer regenerative medicine. Nature biotechnology 29, 803-805.

Andrews, P.W., Banting, G., Damjanov, I., Arnaud, D., Avner, P., 1984a. Three monoclonal antibodies defining distinct differentiation antigens associated with different high molecular weight polypeptides on the surface of human embryonal carcinoma cells. Hybridoma 3, 347-361.

Andrews, P.W., Damjanov, I., Simon, D., Banting, G.S., Carlin, C., Dracopoli, N.C., Fogh, J., 1984b. Pluripotent embryonal carcinoma clones derived from the human teratocarcinoma cell line Tera-2. Differentiation in vivo and in vitro. Lab Invest 50, 147-162.

Andrews, P.W., Goodfellow, P.N., Shevinsky, L.H., Bronson, D.L., Knowles, B.B., 1982. Cell-surface antigens of a clonal human embryonal carcinoma cell line: morphological and antigenic differentiation in culture. Int J Cancer 29, 523-531.

Andrews, P.W., Knowles, B.B., Goodfellow, P.N., 1981. A human cell-surface antigen defined by a monoclonal antibody and controlled by a gene on chromosome 12. Somatic Cell Genet 7, 435-443.

Andrews, P.W., Nudelman, E., Hakomori, S., Fenderson, B.A., 1990. Different patterns of glycolipid antigens are expressed following differentiation of TERA-2 human embryonal carcinoma cells induced by retinoic acid, hexamethylene bisacetamide (HMBA) or bromodeoxyuridine (BUdR). Differentiation 43, 131-138.

Artavanis-Tsakonas, S., Rand, M.D., Lake, R.J., 1999. Notch signaling: Cell fate control and signal integration in development. Science 284, 770-776.

Artzt, K., Dubois, P., Bennett, D., Condamine, H., Babinet, C., Jacob, F., 1973. Surface antigens common to mouse cleavage embryos and primitive teratocarcinoma cells in culture. P Natl Acad Sci USA 70, 2988-2992.

Becker, A.J., Mc, C.E., Till, J.E., 1963. Cytological demonstration of the clonal nature of spleen colonies derived from transplanted mouse marrow cells. Nature 197, 452-454.

Bendall, S.C., Stewart, M.H., Menendez, P., George, D., Vijayaragavan, K., Werbowetski-Ogilvie, T., Ramos-Mejia, V., Rouleau, A., Yang, J., Bosse, M., Lajoie, G., Bhatia, M., 2007. IGF and FGF

cooperatively establish the regulatory stem cell niche of pluripotent human cells in vitro. Nature 448, 1015-1021.

Bendel-Stenzel, M., Anderson, R., Heasman, J., Wylie, C., 1998. The origin and migration of primordial germ cells in the mouse. Semin Cell Dev Biol 9, 393-400.

Bessho, Y., Hirata, H., Masamizu, Y., Kageyama, R., 2003. Periodic repression by the bHLH factor Hes7 is an essential mechanism for the somite segmentation clock. Genes & development 17, 1451-1456.

Bessho, Y., Sakata, R., Komatsu, S., Shiota, K., Yamada, S., Kageyama, R., 2001. Dynamic expression and essential functions of Hes7 in somite segmentation. Genes & development 15, 2642-2647.

Betschinger, J., Nichols, J., Dietmann, S., Corrin, P.D., Paddison, P.J., Smith, A., 2013. Exit from pluripotency is gated by intracellular redistribution of the bHLH transcription factor Tfe3. Cell 153, 335-347.

Blair, K., Wray, J., Smith, A., 2011. The liberation of embryonic stem cells. PLoS genetics 7, e1002019.

Blixt, O., van Die, I., Norberg, T., van den Eijnden, D.H., 1999. High-level expression of the Neisseria meningitidis lgtA gene in Escherichia coli and characterization of the encoded N-acetylglucosaminyltransferase as a useful catalyst in the synthesis of GlcNAc beta 1-->3Gal and GalNAc beta 1-->3Gal linkages. Glycobiology 9, 1061-1071.

Boccaletti, S., Grebogi, C., Lai, Y.C., Mancini, H., Maza, D., 2000. The control of chaos: theory and applications. Phys Rep 329, 103-197.

Booth, C., Potten, C.S., 2000. Gut instincts: thoughts on intestinal epithelial stem cells. J Clin Invest 105, 1493-1499.

Boroviak, T., Loos, R., Bertone, P., Smith, A., Nichols, J., 2014. The ability of inner-cell-mass cells to self-renew as embryonic stem cells is acquired following epiblast specification. Nature cell biology 16, 516-528.

Boveri, T., 1892. Sitzungsber. d. Gesellschaft f. . Morphologie und Physiologie, pp. 114-225.

Boyer, L.A., Lee, T.I., Cole, M.F., Johnstone, S.E., Levine, S.S., Zucker, J.P., Guenther, M.G., Kumar, R.M., Murray, H.L., Jenner, R.G., Gifford, D.K., Melton, D.A., Jaenisch, R., Young, R.A., 2005. Core transcriptional regulatory circuitry in human embryonic stem cells. Cell 122, 947-956.

Boyse, E.A., Old, L.J., 1978. The immunogenetics of differentiation in the mouse. Harvey Lect 71, 23-53.

Brimble, S.N., Sherrer, E.S., Uhl, E.W., Wang, E., Kelly, S., Merrill, A.H., Jr., Robins, A.J., Schulz, T.C., 2007. The cell surface glycosphingolipids SSEA-3 and SSEA-4 are not essential for human ESC pluripotency. Stem Cells 25, 54-62.

Brinster, R.L., 1974. The effect of cells transferred into the mouse blastocyst on subsequent development. J Exp Med 140, 1049-1056.

Brons, I.G., Smithers, L.E., Trotter, M.W., Rugg-Gunn, P., Sun, B., Chuva de Sousa Lopes, S.M., Howlett, S.K., Clarkson, A., Ahrlund-Richter, L., Pedersen, R.A., Vallier, L., 2007. Derivation of pluripotent epiblast stem cells from mammalian embryos. Nature 448, 191-195.

Buehr, M., Meek, S., Blair, K., Yang, J., Ure, J., Silva, J., McLay, R., Hall, J., Ying, Q.L., Smith, A., 2008. Capture of authentic embryonic stem cells from rat blastocysts. Cell 135, 1287-1298.

Chambers, I., Colby, D., Robertson, M., Nichols, J., Lee, S., Tweedie, S., Smith, A., 2003. Functional expression cloning of Nanog, a pluripotency sustaining factor in embryonic stem cells. Cell 113, 643-655.

Chambers, I., Silva, J., Colby, D., Nichols, J., Nijmeijer, B., Robertson, M., Vrana, J., Jones, K., Grotewold, L., Smith, A., 2007. Nanog safeguards pluripotency and mediates germline development. Nature 450, 1230-1234.

Chan, J.W., Lieu, D.K., Huser, T., Li, R.A., 2009a. Label-free separation of human embryonic stem cells and their cardiac derivatives using Raman spectroscopy. Anal Chem 81, 1324-1331.

Chan, J.W., Lieu, D.K., Huser, T., Li, R.A., 2009b. Label-Free Separation of Human Embryonic Stem Cells and Their Cardiac Derivatives Using Raman Spectroscopy. Anal Chem 81, 1324-1331.

Chang, H.H., Hemberg, M., Barahona, M., Ingber, D.E., Huang, S., 2008a. Transcriptome-wide noise controls lineage choice in mammalian progenitor cells. Nature 453, 544-U510.

Chang, H.H., Hemberg, M., Barahona, M., Ingber, D.E., Huang, S., 2008b. Transcriptome-wide noise controls lineage choice in mammalian progenitor cells. Nature 453, 544-547.

Chattopadhyay, T., Carlone, C., Jayaraman, A., Vonschnering, H.G., 1982. Effect of Temperature and Pressure on the Raman-Spectrum of As4s3. J Phys Chem Solids 43, 277-284.

Chen, C., Fenderson, B.A., Andrews, P.W., Hakomori, S., 1989. Glycolipid glycosyltransferases in human embryonal carcinoma cells during retinoic acid induced differentiation. Biochemistry 28, 2229-2238.

Chickarmane, V., Enver, T., Peterson, C., 2009. Computational modeling of the hematopoietic erythroid-myeloid switch reveals insights into cooperativity, priming, and irreversibility. PLoS Comput Biol 5, e1000268.

Chickarmane, V., Peterson, C., 2008. A computational model for understanding stem cell, trophectoderm and endoderm lineage determination. PloS one 3, e3478.

Chickarmane, V., Troein, C., Nuber, U.A., Sauro, H.M., Peterson, C., 2006. Transcriptional dynamics of the embryonic stem cell switch. PLoS Comput Biol 2, e123.

Childs, R.A., Pennington, J., Uemura, K., Scudder, P., Goodfellow, P.N., Evans, M.J., Feizi, T., 1983. High-molecular-weight glycoproteins are the major carriers of the carbohydrate differentiation antigens I, i and SSEA-1 of mouse teratocarcinoma cells. Biochem J 215, 491-503.

Chin, M.H., Mason, M.J., Xie, W., Volinia, S., Singer, M., Peterson, C., Ambartsumyan, G., Aimiuwu, O., Richter, L., Zhang, J., Khvorostov, I., Ott, V., Grunstein, M., Lavon, N., Benvenisty, N., Croce, C.M., Clark, A.T., Baxter, T., Pyle, A.D., Teitell, M.A., Pelegrini, M., Plath, K., Lowry, W.E., 2009. Induced pluripotent stem cells and embryonic stem cells are distinguished by gene expression signatures. Cell stem cell 5, 111-123.

Christensen, S., Kodoyianni, V., Bosenberg, M., Friedman, L., Kimble, J., 1996. lag-1, a gene required for lin-12 and glp-1 signaling in Caenorhabditis elegans, is homologous to human CBF1 and Drosophila Su(H). Development 122, 1373-1383.

Christoph Kraffta, Thomas Knetschkeb, Richard H.W. Funkb, Reiner Salzera, 2005. Identification of organelles and vesicles in single cells by Raman microspectroscopic mapping. Vibrational Spectroscopy Volume 38, , 85-93.

Cole, R.J.P., J, 1965. in Ciba Foundation Symposium on Preimplantation Stages of Pregnancy (eds Wolstenholme, G. E. W. & O'Conner, M.) , . 82-122 J. & A. Churchill Ltd.

Compton, A.H., 1923. A Quantum Theory of the Scattering of X-rays by Light Elements. Phys. Rev. 21, 483

Crow, P., Barrass, B., Kendall, C., Hart-Prieto, M., Wright, M., Persad, R., Stone, N., 2005. The use of Raman spectroscopy to differentiate between different prostatic adenocarcinoma cell lines. Br J Cancer 92, 2166-2170.

Daheron, L., Opitz, S.L., Zaehres, H., Lensch, M.W., Andrews, P.W., Itskovitz-Eldor, J., Daley, G.Q., 2004. LIF/STAT3 signaling fails to maintain self-renewal of human embryonic stem cells. Stem Cells 22, 770-778.

Davis, R.P., Ng, E.S., Costa, M., Mossman, A.K., Sourris, K., Elefanty, A.G., Stanley, E.G., 2008. Targeting a GFP reporter gene to the MIXL1 locus of human embryonic stem cells identifies human primitive streak-like cells and enables isolation of primitive hematopoietic precursors. Blood 111, 1876-1884.

De Gelder, J., De Gussem, K., Vandenabeele, P. and Moens, L, 2007. Reference database of Raman spectra of biological molecules. J. Raman Spectrosc., 38: 1133–1147. doi: 10.1002/jrs.1734.

Delassus, S., Titley, I., Enver, T., 1999. Functional and molecular analysis of hematopoietic progenitors derived from the aorta-gonad-mesonephros region of the mouse embryo. Blood 94, 1495-1503.

Deng, J., Shoemaker, R., Xie, B., Gore, A., LeProust, E.M., Antosiewicz-Bourget, J., Egli, D., Maherali, N., Park, I.H., Yu, J., Daley, G.Q., Eggan, K., Hochedlinger, K., Thomson, J., Wang, W., Gao, Y., Zhang, K., 2009. Targeted bisulfite sequencing reveals changes in DNA methylation associated with nuclear reprogramming. Nature biotechnology 27, 353-360.

Dequeant, M.L., Pourquie, O., 2008. Segmental patterning of the vertebrate embryonic axis. Nat Rev Genet 9, 370-382.

Dixon, F.J., Moore, R.A., 1952. Tumors of the testicle. Acta Unio Int Contra Cancrum 8, 310-315.

Dochow, S., Krafft, C., Neugebauer, U., Bocklitz, T., Henkel, T., Mayer, G., Albert, J., Popp, J., 2011. Tumour cell identification by means of Raman spectroscopy in combination with optical traps and microfluidic environments. Lab Chip 11, 1484-1490.

Doi, A., Park, I.H., Wen, B., Murakami, P., Aryee, M.J., Irizarry, R., Herb, B., Ladd-Acosta, C., Rho, J., Loewer, S., Miller, J., Schlaeger, T., Daley, G.Q., Feinberg, A.P., 2009. Differential methylation of tissue- and cancer-specific CpG island shores distinguishes human induced pluripotent stem cells, embryonic stem cells and fibroblasts. Nat Genet 41, 1350-1353.

Draper, J.S., Pigott, C., Thomson, J.A., Andrews, P.W., 2002. Surface antigens of human embryonic stem cells: changes upon differentiation in culture. J Anat 200, 249-258.

Draper, J.S., Smith, K., Gokhale, P., Moore, H.D., Maltby, E., Johnson, J., Meisner, L., Zwaka, T.P., Thomson, J.A., Andrews, P.W., 2004. Recurrent gain of chromosomes 17q and 12 in cultured human embryonic stem cells. Nature biotechnology 22, 53-54.

Edwards, R.G., 2004. Handbook of Stem Cells (eds Lanza, R. et al.) 1-14 (Elsevier Academic Press, Burlington, Massachusetts).

Einstein, 1910. Statistische Untersuchung der Bewegung eines Resonators in einem Strahlungsfeld. Annalen der Physik.

Eliasson, C., Matousek, P., 2007. Noninvasive authentication of pharmaceutical products through packaging using spatially offset Raman spectroscopy. Anal Chem 79, 1696-1701.

Ellis, D.I., Goodacre, R., 2006. Metabolic fingerprinting in disease diagnosis: biomedical applications of infrared and Raman spectroscopy. Analyst 131, 875-885.

Enver, T., Heyworth, C.M., Dexter, T.M., 1998. Do stem cells play dice? Blood 92, 348-351; discussion 352.

Enver, T., Soneji, S., Joshi, C., Brown, J., Iborra, F., Orntoft, T., Thykjaer, T., Maltby, E., Smith, K., Abu Dawud, R., Jones, M., Matin, M., Gokhale, P., Draper, J., Andrews, P.W., 2005a. Cellular differentiation hierarchies in normal and culture-adapted human embryonic stem cells. Hum Mol Genet 14, 3129-3140.

Enver, T., Tsuzuki, S., Brown, J., Hong, D., Gupta, R., Ford, T., Egucchi, M.I., Egucchi, M., Greaves, M., 2005b. Developmental impact of leukemic fusion genes on stem cell fate. Ann N Y Acad Sci 1044, 16-23.

Evans, M.J., 1972. The isolation and properties of a clonal tissue culture strain of pluripotent mouse teratoma cells. J Embryol Exp Morphol 28, 163-176.

Evans, M.J., Kaufman, M.H., 1981. Establishment in culture of pluripotential cells from mouse embryos. Nature 292, 154-156.

Fenderson, B.A., Andrews, P.W., 1992. Carbohydrate antigens of embryonal carcinoma cells: changes upon differentiation. APMIS Suppl 27, 109-118.

Fenderson, B.A., Andrews, P.W., Nudelman, E., Clausen, H., Hakomori, S., 1987. Glycolipid core structure switching from globo- to lacto- and ganglio-series during retinoic acid-induced differentiation of TERA-2-derived human embryonal carcinoma cells. Developmental biology 122, 21-34.

Festuccia, N., Osorno, R., Halbritter, F., Karwacki-Neisius, V., Navarro, P., Colby, D., Wong, F., Yates, A., Tomlinson, S.R., Chambers, I., 2012. Esrrb is a direct Nanog target gene that can substitute for Nanog function in pluripotent cells. Cell stem cell 11, 477-490.

Fogh J, T.G., 1975. New human tumor cell lines. Human Tumor Cells in Vitro J Plenum Press: New York, pp 115–159.

Fox, N., Damjanov, I., Martinez-Hernandez, A., Knowles, B.B., Solter, D., 1981. Immunohistochemical localization of the early embryonic antigen (SSEA-1) in postimplantation mouse embryos and fetal and adult tissues. Developmental biology 83, 391-398.

Fox, V., Gokhale, P.J., Walsh, J.R., Matin, M., Jones, M., Andrews, P.W., 2008. Cell-cell signaling through NOTCH regulates human embryonic stem cell proliferation. Stem Cells 26, 715-723.

Frontelo, P., Manwani, D., Galdass, M., Karsunky, H., Lohmann, F., Gallagher, P.G., Bieker, J.J., 2007. Novel role for EKLF in megakaryocyte lineage commitment. Blood 110, 3871-3880.

Gardner, 2004. Handbook of Stem Cells

.

Gooi, H.C., Feizi, T., Kapadia, A., Knowles, B.B., Solter, D., Evans, M.J., 1981. Stage-specific embryonic antigen involves alpha 1 goes to 3 fucosylated type 2 blood group chains. Nature 292, 156-158.

Greaves, M.F., Chan, L.C., Furley, A.J., Watt, S.M., Molgaard, H.V., 1986. Lineage promiscuity in hemopoietic differentiation and leukemia. Blood 67, 1-11.

Häcker, 1892. Archiv f. mikr. Anat., pp. 556–581.

Haeckel, 1877. Anthropogenie oder Entwickelungsgeschichte des Menschen, 3rd Edn. P144.

Haeckel, E., 1868. Natürliche Schöpfungsgeschichte. Georg Reimer, Berlin

Harkness, L., Novikov, S.M., Beermann, J., Bozhevolnyi, S.I., Kassem, M., 2012. Identification of abnormal stem cells using Raman spectroscopy. Stem Cells Dev 21, 2152-2159.

Harrison, N.J., Baker, D., Andrews, P.W., 2007. Culture adaptation of embryonic stem cells echoes germ cell malignancy. Int J Androl 30, 275-281; discussion 281.

Harz, M., Rosch, P., Popp, J., 2009. Vibrational spectroscopy--a powerful tool for the rapid identification of microbial cells at the single-cell level. Cytometry A 75, 104-113.

Hawkins, R.D., Hon, G.C., Lee, L.K., Ngo, Q., Lister, R., Pelizzola, M., Edsall, L.E., Kuan, S., Luu, Y., Klugman, S., Antosiewicz-Bourget, J., Ye, Z., Espinoza, C., Agarwahl, S., Shen, L., Ruotti, V., Wang, W., Stewart, R., Thomson, J.A., Ecker, J.R., Ren, B., 2010. Distinct epigenomic landscapes of pluripotent and lineage-committed human cells. Cell stem cell 6, 479-491.

Hayashi, K., Lopes, S.M., Tang, F., Surani, M.A., 2008. Dynamic equilibrium and heterogeneity of mouse pluripotent stem cells with distinct functional and epigenetic states. Cell stem cell 3, 391-401.

Hazewinkel, M., 1994. Encyclopaedia of mathematics. Kluwer Academic, Dordrecht ; London.

Heitzler, P., Simpson, P., 1991. The Choice between Epidermal or Neural Cell Fate in the Epidermis of Drosophila. J Neurogenet 7, 126-126.

Hirata, H., Bessho, Y., Kokubu, H., Masamizu, Y., Yamada, S., Lewis, J., Kageyama, R., 2004. Instability of Hes7 protein is crucial for the somite segmentation clock. Nat Genet 36, 750-754.

Hogan, B., Fellous, M., Avner, P., Jacob, F., 1977. Isolation of a human teratoma cell line which expresses F9 antigen. Nature 270, 515-518.

Hu, M., Krause, D., Greaves, M., Sharkis, S., Dexter, M., Heyworth, C., Enver, T., 1997. Multilineage gene expression precedes commitment in the hemopoietic system. Genes & development 11, 774-785.

Huang, S., Eichler, G., Bar-Yam, Y., Ingber, D.E., 2005. Cell fates as high-dimensional attractor states of a complex gene regulatory network. Phys Rev Lett 94, 128701.

Huang, S., Guo, Y.P., May, G., Enver, T., 2007. Bifurcation dynamics in lineage-commitment in bipotent progenitor cells. Developmental biology 305, 695-713.

Huang, W.E., Griffiths, R.I., Thompson, I.P., Bailey, M.J., Whiteley, A.S., 2004a. Raman microscopic analysis of single microbial cells. Anal Chem 76, 4452-4458.

Huang, W.E., Griffiths, R.I., Thompson, I.P., Bailey, M.J., Whiteley, A.S., 2004b. Raman microscopic analysis of single microbial cells. Anal Chem 76, 4452-4458.

Imayoshi, I., Isomura, A., Harima, Y., Kawaguchi, K., Kori, H., Miyachi, H., Fujiwara, T., Ishidate, F., Kageyama, R., 2013. Oscillatory Control of Factors Determining Multipotency and Fate in Mouse Neural Progenitors. Science 342, 1203-1208.

Jakob, H., Boon, T., Gaillard, J., Nicolas, J., Jacob, F., 1973. [Teratocarcinoma of the mouse: isolation, culture and properties of pluripotential cells]. Ann Microbiol (Paris) 124, 269-282.

Jiang, Y.J., Aerne, B.L., Smithers, L., Haddon, C., Ish-Horowicz, D., Lewis, J., 2000. Notch signalling and the synchronization of the somite segmentation clock. Nature 408, 475-479.

Jones, P.H., Simons, B.D., Watt, F.M., 2007. Sic transit gloria: farewell to the epidermal transit amplifying cell? Cell stem cell 1, 371-381.

Judd, K., 2007. Galton's quincunx: Random walk or chaos? Int J Bifurcat Chaos 17, 4463-4469.

Kageyama, R., Niwa, Y., Isomura, A., Gonzalez, A., Harima, Y., 2012. Oscillatory gene expression and somitogenesis. Wires Dev Biol 1, 629-641.

Kahan, B.W., Ephrussi, B., 1970. Developmental potentialities of clonal in vitro cultures of mouse testicular teratoma. J Natl Cancer Inst 44, 1015-1036.

Kalkan, T., Smith, A., 2014. Mapping the route from naive pluripotency to lineage specification. Philosophical transactions of the Royal Society of London. Series B, Biological sciences 369.

Kannagi, R., Cochran, N.A., Ishigami, F., Hakomori, S., Andrews, P.W., Knowles, B.B., Solter, D., 1983a. Stage-specific embryonic antigens (SSEA-3 and -4) are epitopes of a unique globo-series ganglioside isolated from human teratocarcinoma cells. The EMBO journal 2, 2355-2361.

Kannagi, R., Levery, S.B., Ishigami, F., Hakomori, S., Shevinsky, L.H., Knowles, B.B., Solter, D., 1983b. New globoseries glycosphingolipids in human teratocarcinoma reactive with the monoclonal antibody directed to a developmentally regulated antigen, stage-specific embryonic antigen 3. The Journal of biological chemistry 258, 8934-8942.

Keren, S., Zavaleta, C., Cheng, Z., de la Zerda, A., Gheysens, O., Gambhir, S.S., 2008. Noninvasive molecular imaging of small living subjects using Raman spectroscopy. Proc Natl Acad Sci U S A 105, 5844-5849.

Kim, J.H., Auerbach, J.M., Rodriguez-Gomez, J.A., Velasco, I., Gavin, D., Lumelsky, N., Lee, S.H., Nguyen, J., Sanchez-Pernaute, R., Bankiewicz, K., McKay, R., 2002. Dopamine neurons derived from embryonic stem cells function in an animal model of Parkinson's disease. Nature 418, 50-56.

Kleinsmith, L.J., Pierce, G.B., Jr., 1964. Multipotentiality of Single Embryonal Carcinoma Cells. Cancer Res 24, 1544-1551.

Kneipp, J., Kneipp, H., Rice, W.L., Kneipp, K., 2005. Optical probes for biological applications based on surface-enhanced Raman scattering from indocyanine green on gold nanoparticles. Anal Chem 77, 2381-2385.

Kneipp, K., Kneipp, H., Kneipp, J., 2006. Surface-enhanced Raman scattering in local optical fields of silver and gold nanoaggregates-from single-molecule Raman spectroscopy to ultrasensitive probing in live cells. Acc Chem Res 39, 443-450.

Kohler, G., Milstein, C., 1975. Continuous cultures of fused cells secreting antibody of predefined specificity. Nature 256, 495-497.

Kondoh, H., Lleonart, M.E., Nakashima, Y., Yokode, M., Tanaka, M., Bernard, D., Gil, J., Beach, D., 2007. A high glycolytic flux supports the proliferative potential of murine embryonic stem cells. Antioxidants & redox signaling 9, 293-299.

Konorov, S.O., Glover, C.H., Piret, J.M., Bryan, J., Schulze, H.G., Blades, M.W., Turner, R.F., 2007. In situ analysis of living embryonic stem cells by coherent anti-stokes Raman microscopy. Anal Chem 79, 7221-7225.

Krafft, C., Knetschke, T., Funk, R.H., Salzer, R., 2006. Studies on stress-induced changes at the subcellular level by Raman microspectroscopic mapping. Anal Chem 78, 4424-4429.

Krishna, C.M., Kegelaer, G., Adt, I., Rubin, S., Kartha, V.B., Manfait, M., Sockalingum, G.D., 2006. Combined Fourier transform infrared and Raman spectroscopic approach for identification of multidrug resistance phenotype in cancer cell lines. Biopolymers 82, 462-470.

Laiosa, C.V., Stadtfeld, M., Graf, T., 2006. Determinants of lymphoid-myeloid lineage diversification. Annu Rev Immunol 24, 705-738.

Laslett, A.L., Grimmond, S., Gardiner, B., Stamp, L., Lin, A., Hawes, S.M., Wormald, S., Nikolic-Paterson, D., Haylock, D., Pera, M.F., 2007. Transcriptional analysis of early lineage commitment in human embryonic stem cells. BMC Dev Biol 7, 12.

Li, L., Wang, B.H., Wang, S.A., Moalim-Nour, L., Mohib, K., Lohnes, D., Wang, L.S., 2010. Individual Cell Movement, Asymmetric Colony Expansion, Rho-Associated Kinase, and E-Cadherin Impact the Clonogenicity of Human Embryonic Stem Cells. Biophys J 98, 2442-2451.

Li, M., Zhang, D., Hou, Y., Jiao, L., Zheng, X., Wang, W.H., 2003. Isolation and culture of embryonic stem cells from porcine blastocysts. Molecular reproduction and development 65, 429-434.

Li, M.Q., Huang, W.E., Gibson, C.M., Fowler, P.W., Jousset, A., 2013. Stable Isotope Probing and Raman Spectroscopy for Monitoring Carbon Flow in a Food Chain and Revealing Metabolic Pathway. Anal Chem 85, 1642-1649.

Li, P., Tong, C., Mehrian-Shai, R., Jia, L., Wu, N., Yan, Y., Maxson, R.E., Schulze, E.N., Song, H., Hsieh, C.L., Pera, M.F., Ying, Q.L., 2008. Germline competent embryonic stem cells derived from rat blastocysts. Cell 135, 1299-1310.

Lorenz, E.N., 1963. Deterministic Nonperiodic Flow. J Atmos Sci 20, 130-141.

Maienschein, J., 2003. Whose view of life? : embryos, cloning, and stem cells. Harvard University Press, Cambridge, Mass ; London.

Maquelin, K., Kirschner, C., Choo-Smith, L.P., van den Braak, N., Endtz, H.P., Naumann, D., Puppels, G.J., 2002. Identification of medically relevant microorganisms by vibrational spectroscopy. J Microbiol Methods 51, 255-271.

Marks, H., Kalkan, T., Menafra, R., Denissov, S., Jones, K., Hofemeister, H., Nichols, J., Kranz, A., Stewart, A.F., Smith, A., Stunnenberg, H.G., 2012. The transcriptional and epigenomic foundations of ground state pluripotency. Cell 149, 590-604.

Maroto, M., Dale, J.K., Dequeant, M.L., Petit, A.C., Pourquie, O., 2005. Synchronised cycling gene oscillations in presomitic mesoderm cells require cell-cell contact. Int J Dev Biol 49, 309-315.

Martin, G.R., 1975. Teratocarcinomas as a model system for the study of embryogenesis and neoplasia. Cell 5, 229-243.

Martin, G.R., 1981. Isolation of a pluripotent cell line from early mouse embryos cultured in medium conditioned by teratocarcinoma stem cells. P Natl Acad Sci USA 78, 7634-7638.

Martin, G.R., Evans, M.J., 1974. The morphology and growth of a pluripotent teratocarcinoma cell line and its derivatives in tissue culture. Cell 2, 163-172.

Martin, G.R., Evans, M.J., 1975. Differentiation of clonal lines of teratocarcinoma cells: formation of embryoid bodies in vitro. P Natl Acad Sci USA 72, 1441-1445.

Masamizu, Y., Ohtsuka, T., Takashima, Y., Nagahara, H., Takenaka, Y., Yoshikawa, K., Okamura, H., Kageyama, R., 2006. Real-time imaging of the somite segmentation clock: Revelation of unstable oscillators in the individual presomitic mesoderm cells. P Natl Acad Sci USA 103, 1313-1318.

Matthaus, C., Boydston-White, S., Miljkovic, M., Romeo, M., Diem, M., 2006. Raman and infrared microspectral imaging of mitotic cells. Appl Spectrosc 60, 1-8.

Maximow, A., 1908. Anat. Anz., pp. 65–72.

May, R.M., 1976. Simple mathematical models with very complicated dynamics. Nature 261, 459-467.

Meade, A.D., Clarke, C., Draux, F., Sockalingum, G.D., Manfait, M., Lyng, F.M., Byrne, H.J., 2010. Studies of chemical fixation effects in human cell lines using Raman microspectroscopy. Anal Bioanal Chem 396, 1781-1791.

Moller, H., 1993. Clues to the aetiology of testicular germ cell tumours from descriptive epidemiology. Eur Urol 23, 8-13; discussion 14-15.

Mostofi, F.K., Price, E.B., 1973. Tumors of the male genital system. Armed Forces Institute of Pathology, Washington, D.C.

Mourant, J., Kunapareddy, P., Carpenter, S., Freyer, J.P., 2005. Vibrational spectroscopy for identification of biochemical changes accompanying carcinogenesis and the formation of necrosis. Gynecol Oncol 99, S58-60.

Neumann, E., 1912. Arch. f. Mikrosk. Anatomie und Entwicklungsgeschicht 207, pp. 480–520.

Nichols, J., Smith, A., 2009. Naive and primed pluripotent states. Cell stem cell 4, 487-492.

Nicolas, J.F., Dubois, P., Jakob, H., Gaillard, J., Jacob, F., 1975. [Mouse teratocarcinoma: differentiation in cultures of a multipotential primitive cell line (author's transl)]. Ann Microbiol (Paris) 126, 3-22.

Nie, S., Emory, S.R., 1997. Probing Single Molecules and Single Nanoparticles by Surface-Enhanced Raman Scattering. Science 275, 1102-1106.

Nie X, C.D., 2013. A New Approach to Solving the Inverse Frobenius-Perron Problem. 12th European Control Conference ECC 2013. Zurich, Switzerland.

Nie, X.K., Coca, D., 2013. A New Approach to Solving the Inverse Frobenius-Perron Problem. 2013 European Control Conference (Ecc), 2916-2920.

Nie, X.K., Coca, D., 2015. Reconstruction of one-dimensional chaotic maps from sequences of probability density functions. Nonlinear Dynam 80, 1373-1390.

Niwa, H., Burdon, T., Chambers, I., Smith, A., 1998. Self-renewal of pluripotent embryonic stem cells is mediated via activation of STAT3. Genes & development 12, 2048-2060.

Niwa, H., Ogawa, K., Shimosato, D., Adachi, K., 2009. A parallel circuit of LIF signalling pathways maintains pluripotency of mouse ES cells. Nature 460, 118-122.

Niwa, Y., Shimojo, H., Isomura, A., Gonzalez, A., Miyachi, H., Kageyama, R., 2011. Different types of oscillations in Notch and Fgf signaling regulate the spatiotemporal periodicity of somitogenesis. Genes & development 25, 1115-1120.

Notingher, I., Jell, G., Lohbauer, U., Salih, V., Hench, L.L., 2004a. In situ non-invasive spectral discrimination between bone cell phenotypes used in tissue engineering. J Cell Biochem 92, 1180-1192.

Notingher, I.N., I); Verrier, S (Verrier, S); Romanska, H (Romanska, H); Bishop, AE (Bishop, AE); Polak, JM (Polak, JM); Hench, LL (Hench, LL), 2002. In situ characterisation of living cells by Raman spectroscopy. SPECTROSCOPY-AN INTERNATIONAL JOURNAL 16, 43-51.

Notingher, L., Bisson, I., Polak, J.M., Hench, L.L., 2004b. In situ spectroscopic study of nucleic acids in differentiating embryonic stem cells. Vib Spectrosc 35, 199-203.

Oates, A.C., Morelli, L.G., Ares, S., 2012. Patterning embryos with oscillations: structure, function and dynamics of the vertebrate segmentation clock. Development 139, 625-639.

Olariu, V., Coca, D., Billings, S.A., Tonge, P., Gokhale, P., Andrews, P.W., Kadirkamanathan, V., 2009. Modified variational Bayes EM estimation of hidden Markov tree model of cell lineages. Bioinformatics 25, 2824-2830.

Ott, E., 1993. Chaos in dynamical systems. Cambridge University Press, Cambridge.

Palmer, T.N., 2000. Predicting uncertainty in forecasts of weather and climate. Rep Prog Phys 63, 71-116.

Pappenheim, A., 1896. Virchows Arch., pp. 587–643.

Peerani, R., Rao, B.M., Bauwens, C., Yin, T., Wood, G.A., Nagy, A., Kumacheva, E., Zandstra, P.W., 2007. Niche-mediated control of human embryonic stem cell self-renewal and differentiation. The EMBO journal 26, 4744-4755.

Pera, M.F., Andrade, J., Houssami, S., Reubinoff, B., Trounson, A., Stanley, E.G., Ward-van Oostwaard, D., Mummery, C., 2004. Regulation of human embryonic stem cell differentiation by BMP-2 and its antagonist noggin. J Cell Sci 117, 1269-1280.

Pierce, G.B., Jr., Verney, E.L., 1961. An in vitro and in vivo study of differentiation in teratocarcinomas. Cancer 14, 1017-1029.

Pina, C., Fugazza, C., Tipping, A.J., Brown, J., Soneji, S., Teles, J., Peterson, C., Enver, T., 2012. Inferring rules of lineage commitment in haematopoiesis. Nature cell biology 14, 287-294.

Placzek, G., 1934. Rayleigh-Streuung und Raman-Effekt. Akad. Verlag-Ges.

Qian, X.M., Nie, S.M., 2008. Single-molecule and single-nanoparticle SERS: from fundamental mechanisms to biomedical applications. Chem Soc Rev 37, 912-920.

Race, R.R., Sanger, R.j.a., 1975. Blood groups in man, 6th ed. ed. Blackwell Scientific Publications ; Philadelphia : distributed by J. B. Lippincott, Oxford.

Ramalho-Santos, M., Willenbring, H., 2007. On the origin of the term "stem cell". Cell stem cell 1, 35-38.

Rea, D.G., 1959. Study of the Experimental Factors Affecting Raman Band Intensities in Liquids. J Opt Soc Am 49, 90-101.

Riedel-Kruse, I.H., Muller, C., Oates, A.C., 2007. Synchrony dynamics during initiation, failure, and rescue of the segmentation clock. Science 317, 1911-1915.

Robey, P.G., 2000. Stem cells near the century mark. J Clin Invest 105, 1489-1491.

Rosenthal, M.D., Wishnow, R.M., Sato, G.H., 1970. In vitro growth and differetiation of clonal populations of multipotential mouse clls derived from a transplantable testicular teratocarcinoma. J Natl Cancer Inst 44, 1001-1014.

Ryder, A.G., 2005. Surface enhanced Raman scattering for narcotic detection and applications to chemical biology. Curr Opin Chem Biol 9, 489-493.

Sato-Berru, R.Y., Araiza-Reyna, E.A., Vazquez-Olmos, A.R., 2016. Moles quantification in liquid samples by Raman spectroscopy. Spectrochimica acta. Part A, Molecular and biomolecular spectroscopy 158, 56-59.

Schlucker, S., 2009. SERS microscopy: nanoparticle probes and biomedical applications. Chemphyschem 10, 1344-1354.

Schulze, H.G., Konorov, S.O., Caron, N.J., Piret, J.M., Blades, M.W., Turner, R.F., 2010a. Assessing differentiation status of human embryonic stem cells noninvasively using Raman microspectroscopy. Anal Chem 82, 5020-5027.

Schulze, H.G., Konorov, S.O., Caron, N.J., Piret, J.M., Blades, M.W., Turner, R.F.B., 2010b. Assessing Differentiation Status of Human Embryonic Stem Cells Noninvasively Using Raman Microspectroscopy. Anal Chem 82, 5020-5027.

Schuster, K.C., Reese, I., Urlaub, E., Gapes, J.R., Lendl, B., 2000. Multidimensional information on the chemical composition of single bacterial cells by confocal Raman microspectroscopy. Anal Chem 72, 5529-5534.

Sestan, N., Artavanis-Tsakonas, S., Rakic, P., 1999. Contact-dependent inhibition of cortical neurite growth mediated by notch signaling. Science 286, 741-746.

Shevinsky, L.H., Knowles, B.B., Damjanov, I., Solter, D., 1982. Monoclonal antibody to murine embryos defines a stage-specific embryonic antigen expressed on mouse embryos and human teratocarcinoma cells. Cell 30, 697-705.

Shi, W., Wang, H., Pan, G., Geng, Y., Guo, Y., Pei, D., 2006. Regulation of the pluripotency marker Rex-1 by Nanog and Sox2. The Journal of biological chemistry 281, 23319-23325.

Shimojo, H., Ohtsuka, T., Kageyama, R., 2008. Oscillations in notch signaling regulate maintenance of neural progenitors. Neuron 58, 52-64.

Shinbrot, T., Grebogi, C., Wisdom, J., Yorke, J.A., 1992. Chaos in a Double Pendulum. Am J Phys 60, 491-499.

Short, K.W., Carpenter, S., Freyer, J.P., Mourant, J.R., 2005. Raman spectroscopy detects biochemical changes due to proliferation in mammalian cell cultures. Biophys J 88, 4274-4288.

Shostak, S., 2006. (Re)defining stem cells. Bioessays 28, 301-308.

Smekal, 1923. Zur Quantentheorie der Dispersion. Die Naturwissenschaften.

Smith, A.G., 2001. Embryo-derived stem cells: of mice and men. Annu Rev Cell Dev Biol 17, 435-462.

Smith, A.G., Heath, J.K., Donaldson, D.D., Wong, G.G., Moreau, J., Stahl, M., Rogers, D., 1988. Inhibition of pluripotential embryonic stem cell differentiation by purified polypeptides. Nature 336, 688-690.

Smith, R., Wright, K.L., Ashton, L., 2016. Raman spectroscopy: an evolving technique for live cell studies. Analyst 141, 3590-3600.

Solter, D., Damjanov, I., 1979. Teratocarcinomas rarely develop from embryos transplanted into athymic mice. Nature 278, 554-555.

Solter, D., Knowles, B.B., 1978. Monoclonal antibody defining a stage-specific mouse embryonic antigen (SSEA-1). P Natl Acad Sci USA 75, 5565-5569.

Stevens, L.C., 1964. Experimental Production of Testicular Teratomas in Mice. P Natl Acad Sci USA 52, 654-661.

Stevens, L.C., 1967. Origin of testicular teratomas from primordial germ cells in mice. J Natl Cancer Inst 38, 549-552.

Stevens, L.C., 1970. Experimental production of testicular teratomas in mice of strains 129, A/He, and their F1 hybrids. J Natl Cancer Inst 44, 923-929.

Stevens, L.C., Hummel, K.P., 1957. A description of spontaneous congenital testicular teratomas in strain 129 mice. J Natl Cancer Inst 18, 719-747.

Stevens, L.C., Little, C.C., 1954. Spontaneous Testicular Teratomas in an Inbred Strain of Mice. P Natl Acad Sci USA 40, 1080-1087.

Strutt, J.W.B.R., On the light from the sky, its polarization and colour. Bedford.

Swain, R.J., Stevens, M.M., 2007. Raman microspectroscopy for non-invasive biochemical analysis of single cells. Biochem Soc Trans 35, 544-549.

Swiers, G., Patient, R., Loose, M., 2006. Genetic regulatory networks programming hematopoietic stem cells and erythroid lineage specification. Developmental biology 294, 525-540.

Takahashi, K., Yamanaka, S., 2006. Induction of pluripotent stem cells from mouse embryonic and adult fibroblast cultures by defined factors. Cell 126, 663-676.

Takashima, Y., Guo, G., Loos, R., Nichols, J., Ficz, G., Krueger, F., Oxley, D., Santos, F., Clarke, J., Mansfield, W., Reik, W., Bertone, P., Smith, A., 2014. Resetting transcription factor control circuitry toward ground-state pluripotency in human. Cell 158, 1254-1269.

Takehara, N., Tsutsumi, Y., Tateishi, K., Ogata, T., Tanaka, H., Ueyama, T., Takahashi, T., Takamatsu, T., Fukushima, M., Komeda, M., Yamagishi, M., Yaku, H., Tabata, Y., Matsubara, H., Oh, H., 2008. Controlled delivery of basic fibroblast growth factor promotes human cardiosphere-derived cell engraftment to enhance cardiac repair for chronic myocardial infarction. J Am Coll Cardiol 52, 1858-1865.

Tesar, P.J., Chenoweth, J.G., Brook, F.A., Davies, T.J., Evans, E.P., Mack, D.L., Gardner, R.L., McKay, R.D., 2007. New cell lines from mouse epiblast share defining features with human embryonic stem cells. Nature 448, 196-199.

Thietart, R.A., Forgues, B., 1993. Chaos theory and organization. CERESSEC, Cergy Pontoise.

Thomson, J.A., Itskovitz-Eldor, J., Shapiro, S.S., Waknitz, M.A., Swiergiel, J.J., Marshall, V.S., Jones, J.M., 1998. Embryonic stem cell lines derived from human blastocysts. Science 282, 1145-1147.

Thomson, J.A., Kalishman, J., Golos, T.G., Durning, M., Harris, C.P., Becker, R.A., Hearn, J.P., 1995. Isolation of a primate embryonic stem cell line. P Natl Acad Sci USA 92, 7844-7848.

Thomson, J.A., Marshall, V.S., 1998. Primate embryonic stem cells. Curr Top Dev Biol 38, 133-165.

Till, J.E., Mc, C.E., 1961. A direct measurement of the radiation sensitivity of normal mouse bone marrow cells. Radiat Res 14, 213-222.

Till, J.E., McCulloch, E.A., 1964. Repair Processes in Irradiated Mouse Hematopoietic Tissue. Ann N Y Acad Sci 114, 115-125.

Tippett, P., Andrews, P.W., Knowles, B.B., Solter, D., Goodfellow, P.N., 1986. Red cell antigens P (globoside) and Luke: identification by monoclonal antibodies defining the murine stage-specific embryonic antigens -3 and -4 (SSEA-3 and SSEA-4). Vox sanguinis 51, 53-56.

Tonge, P.D., Andrews, P.W., 2010. Retinoic acid directs neuronal differentiation of human pluripotent stem cell lines in a non-cell-autonomous manner. Differentiation 80, 20-30.

Tonge, P.D., Olariu, V., Coca, D., Kadirkamanathan, V., Burrell, K.E., Billings, S.A., Andrews, P.W., 2010. Prepatterning in the stem cell compartment. PloS one 5, e10901.

Tonge, P.D., Shigeta, M., Schroeder, T., Andrews, P.W., 2011. Functionally defined substates within the human embryonic stem cell compartment. Stem cell research 7, 145-153.

Tosolini, M., Jouneau, A., 2016. Acquiring Ground State Pluripotency: Switching Mouse Embryonic Stem Cells from Serum/LIF Medium to 2i/LIF Medium. Methods Mol Biol 1341, 41-48.

Toyooka, Y., Shimosato, D., Murakami, K., Takahashi, K., Niwa, H., 2008. Identification and characterization of subpopulations in undifferentiated ES cell culture. Development 135, 909-918.

Tsakiridis, A., Huang, Y., Blin, G., Skylaki, S., Wymeersch, F., Osorno, R., Economou, C., Karagianni, E., Zhao, S., Lowell, S., Wilson, V., 2015. Distinct Wnt-driven primitive streak-like populations reflect in vivo lineage precursors. Development 142, 809.

van Manen, H.J., Kraan, Y.M., Roos, D., Otto, C., 2005. Single-cell Raman and fluorescence microscopy reveal the association of lipid bodies with phagosomes in leukocytes. Proc Natl Acad Sci U S A 102, 10159-10164.

Varum, S., Rodrigues, A.S., Moura, M.B., Momcilovic, O., Easley, C.A.t., Ramalho-Santos, J., Van Houten, B., Schatten, G., 2011. Energy metabolism in human pluripotent stem cells and their differentiated counterparts. PloS one 6, e20914.

Weinberger, L., Ayyash, M., Novershtern, N., Hanna, J.H., 2016. Dynamic stem cell states: naive to primed pluripotency in rodents and humans. Nature reviews. Molecular cell biology 17, 155-169.

Weissman, A.W., 1885. Het Rijks-Museum te Amsterdam, etc. Arnhem.

Wichterle, H., Lieberam, I., Porter, J.A., Jessell, T.M., 2002. Directed differentiation of embryonic stem cells into motor neurons. Cell 110, 385-397.

Wilkinson, H.A., Fitzgerald, K., Greenwald, I., 1994. Reciprocal Changes in Expression of the Receptor Lin-12 and Its Ligand Lag-2 Prior to Commitment in a C-Elegans Cell Fate Decision. Cell 79, 1187-1198.

Williams, R.L., Hilton, D.J., Pease, S., Willson, T.A., Stewart, C.L., Gearing, D.P., Wagner, E.F., Metcalf, D., Nicola, N.A., Gough, N.M., 1988. Myeloid leukaemia inhibitory factor maintains the developmental potential of embryonic stem cells. Nature 336, 684-687.

Wilson, E.B., 1896. The Cell in Development and Inheritance. Macmillan, New York.

Wolf, D., 1996. Micro-Raman spectroscopy to study local mechanical stress in silicon integrated circuits. Semicond. Sci. Technol. 11 (1996) 139–154.

Wray, J., Kalkan, T., Smith, A.G., 2010. The ground state of pluripotency. Biochemical Society transactions 38, 1027-1032.

Wright, A.J., Andrews, P.W., 2009. Surface marker antigens in the characterization of human embryonic stem cells. Stem cell research 3, 3-11.

Xie, S.B., Iglesia, E., Bell, A.T., 2001. Effects of temperature on the Raman spectra and dispersed oxides. J Phys Chem B 105, 5144-5152.

Yamanaka, S., 2007. Strategies and new developments in the generation of patient-specific pluripotent stem cells. Cell stem cell 1, 39-49.

Ying, Q.L., Nichols, J., Chambers, I., Smith, A., 2003. BMP induction of Id proteins suppresses differentiation and sustains embryonic stem cell self-renewal in collaboration with STAT3. Cell 115, 281-292.

Ying, Q.L., Wray, J., Nichols, J., Batlle-Morera, L., Doble, B., Woodgett, J., Cohen, P., Smith, A., 2008. The ground state of embryonic stem cell self-renewal. Nature 453, 519-523.

Zhang, P., Ren, L., Zhang, X., Shan, Y., Wang, Y., Ji, Y., Yin, H., Huang, W.E., Xu, J., Ma, B., 2015. Raman-activated cell sorting based on dielectrophoretic single-cell trap and release. Anal Chem 87, 2282-2289.

Zhou, D., Henion, T.R., Jungalwala, F.B., Berger, E.G., Hennet, T., 2000. The beta 1,3-galactosyltransferase beta 3GalT-V is a stage-specific embryonic antigen-3 (SSEA-3) synthase. The Journal of biological chemistry 275, 22631-22634.